National Library of Canada
Acquisitions and Bibliographic Services Branch
395 Wellington Street
Ottawa Ontario
K1A 0N4

Bibliotheque nationale du Canada
Direction des acquisitions et des services bibliographiques
395 rue Wellington
Ottawa (Ontario)
K1A 0N4

## NOTICE

The quality of this microform is heavily dependent upon the quality of the original thesis submitted for microfilming. Every effort has been made to ensure the highest quality of reproduction possible.

If pages are missing, contact the university which granted the degree.

Some pages may have indistinct print especially if the original pages were typed with a poor typewriter ribbon or if the university sent us an inferior photocopy.

Reproduction in full or in part of this microform is governed by the Canadian Copyright Act, R.S.C. 1970, c. C-30, and subsequent amendments.

## AVIS

La qualité de cette microforme dépend grandement de la qualité de la thèse soumise au microfilmage. Nous avons tout fait pour assurer une qualité supérieure de reproduction.

S'il manque des pages, veuillez communiquer avec l'université qui a conféré le grade.

La qualité d'impression de certaines pages peut laisser à désirer, surtout si les pages originales ont été dactylographiées à l'aide d'un ruban usé ou si l'université nous a fait parvenir une photocopie de qualité inférieure.

La reproduction, même partielle, de cette microforme est soumise à la Loi canadienne sur le droit d'auteur, SRC 1970, c. C-30, et ses amendements subséquents.

Canada

# FUNDAMENTAL AND APPLIED STUDIES IN HETEROGENEOUS PHOTOCATALYSIS

## PRIMARY RADICAL INTERMEDIATES AND KINETICS OF PHOTO-OXIDATION OF CREOSOTE PHENOLICS

**Rita TERZIAN**

*A Thesis*
*in*
*the Department*
*of*
*Chemistry & Biochemistry*

*Presented in Partial Fulfilment of the Requirements for the*
***Degree of Doctor of Philosophy***
*at*
*Concordia University,*
*Montréal, Québec, Canada*

January 1993

© Rita Terzian, 1993

National Library of Canada
Acquisitions and Bibliographic Services Branch
395 Wellington Street
Ottawa, Ontario
K1A 0N4

Bibliothèque nationale du Canada
Direction des acquisitions et des services bibliographiques
395, rue Wellington
Ottawa (Ontario)
K1A 0N4

The author has granted an irrevocable non-exclusive licence allowing the National Library of Canada to reproduce, loan, distribute or sell copies of his/her thesis by any means and in any form or format, making this thesis available to interested persons.

L'auteur a accordé une licence irrévocable et non exclusive permettant à la Bibliothèque nationale du Canada de reproduire, prêter, distribuer ou vendre des copies de sa thèse de quelque manière et sous quelque forme que ce soit pour mettre des exemplaires de cette thèse à la disposition des personnes intéressées.

The author retains ownership of the copyright in his/her thesis. Neither the thesis nor substantial extracts from it may be printed or otherwise reproduced without his/her permission.

L'auteur conserve la propriété du droit d'auteur qui protège sa thèse. Ni la thèse ni des extraits substantiels de celle-ci ne doivent être imprimés ou autrement reproduits sans son autorisation.

ISBN 0-315-84674-7

Canada

# ABSTRACT

## FUNDAMENTAL AND APPLIED STUDIES IN HETEROGENEOUS PHOTOCATALYSIS
### PRIMARY RADICAL INTERMEDIATES AND KINETICS OF PHOTO-OXIDATION OF CREOSOTE PHENOLICS

*Rita Terzian, Ph.D.*
*Concordia University, 1993*

Titanium dioxide, irradiated by ultraviolet/visible light was used to mediate the photocatalyzed degradation of several methylated creosote phenolics: *ortho*-, *meta*-, and *para*-cresol, 2,3-, 2,4-, 2,5-, 2,6-, 3,4- and 3,5-xylenol as well as 2,3,5-trimethylphenol. Total mineralization of the phenols to $CO_2$ and $H_2O$ ensues as evidenced for *m*-cresol, 3,4-xylenol, and 2,3,5-trimethylphenol. The photo-oxidation of methylhydroquinone and 4-methylcatechol, two intermediates detected in the photodegradation of cresols, also leads to total mineralization to $CO_2$. The effect of such parameters as pH, initial phenol concentration, $TiO_2$ concentration, oxygen concentration and radiant power levels on the degradation of methylated phenols was examined in detail for *m*-cresol and 3,4-xylenol. The rates of photodegradation were found to increase as a function of pH and temperature. Concentration dependence experiments show the photo-oxidation process follows saturation-type behaviour. In ermediates were identified in these photo-oxidation reactions; these were typically methylated derivatives of dihydroxybenzenes or *p*-benzoquinone. Photochemical efficiencies (lower limits of quantum yields) were determined for the cresols and the xylenols; these were: 0.0096 (*o*-cresol), 0.0076 (*m*-cresol), 0.0104 (*p*-cresol), 0.0067 (2,3-xylenol), 0.012 (2,4-xylenol), 0.0074 (2,5-

xylenol), 0.015 (2,6-xylenol), 0.0060 (3,4-xylenol) and 0.0067 (3,5-xylenol).

A practical case study was carried out using aqueous mixtures of coal tar creosote; irradiation of the solutions in the presence of $TiO_2$ resulted in the complete mineralization of the organic components (75 wt % C) to $CO_2$.

The reactions of xylenols and pentahalogenated phenols with •OH radicals were examined in homogeneous solution using pulse radiolysis in order to identify the primary organic radicals formed. Reaction of •OH radicals with 2,3-, 2,4-, 2,5-, 2,6- and 3,5-xylenol yields exclusively the •OH-adducts (dihydroxydimethylcyclohexadienyl radicals) as the initial products. 3,4-Xylenol reacts with •OH to form both an •OH-adduct and a phenoxyl radical. At pH $\leq$ 8, the 3,4-phenoxyl radical is formed via $H_2O$ elimination from the •OH-adduct; by contrast, at pH $\geq$ 9, both radicals appear to form concurrently.

The principal products from the reaction of OH• with pentabromophenoxide and pentachlorophenoxide are the corresponding pentahalophenoxyl radicals; other products formed are the •OH-adducts (dihydroxypentahalocyclohexadienyl radical anions), and the semiquinone radicals. The reaction of OH• with pentafluorophenoxide anion yields exclusively the dihydroxypentafluorocyclohexadienyl radical.

The sonochemical oxidation of phenol was also examined in aerated solutions. Major intermediates detected were hydroquinone, catechol and *p*-benzoquinone. In contrast with photo-oxidation, complete mineralization to $CO_2$ did not occur.

**To**

***Darren***

# Acknowledgements

First and foremost, I would like to express my gratitude and sincere appreciation to Professor Nick Serpone, my research supervisor and mentor, for his guidance, patience, and active interest in my work. I owe him a great deal. I am also grateful to Dr. Enrico Borgarello, presently Director of Research & Development at the Ente Nazionale Idrocarburi in Milano, Italy, for stimulating discussions in photocatalysis and for sharing some of his laboratory skills during my senior undergraduate project (Summer 1985).

I am thankful to Professor Marye Anne Fox, University of Texas at Austin, for her kind hospitality and for truly making me feel like a member of her research group during my three fruitful and enjoyable periods in Austin. My thanks to her group for their hospitality in their lab, and particularly to Dr. Bart Draper for sharing with me some of his experience in carrying out the pulse radiolysis experiments on phenols. Finally, I would like to express my gratitude to Dr. Anthony Harriman, Director of the Center For Fast Kinetics Research at Austin, and the CFKR staff for sharing their expertise in the pulse radiolysis experiments, particularly Mr. Bill Naumann for his expert operation and maintenance of the Electron Accelerator.

My thanks to Mr. Robert Patterson of Science Industrial Research Unit at Concordia, Dr. Claudio Minero of Torino, and Miss Anne Marie Pelletier (COOP student from the Université de Sherbrooke) for their technical assistance in some of the measurements.

I would like to thank Mr. Pierre Kennepohl for proofreading some of the text, Profs. R. Zienius and A. English for serving on my Research Committee, and Prof. R.H. Pallen for substituting for Dr. English in her absence.

Lastly but not least, I am grateful to my parents for encouraging me to pursue my studies. I would be remiss if I didn't thank my husband and colleague, Darren Lawless, for his help, support, understanding and for putting up with me throughout our joint graduate studies. I could not have made it without him.

# TABLE OF CONTENTS

LIST OF FIGURES . . . . . xiii

LIST OF TABLES . . . . . xxviii

## CHAPTER 1

## INTRODUCTION

1.1 GENERAL INTRODUCTION . . . . . 2
1.2 HETEROGENEOUS PHOTOCATALYSIS . . . . . 4
1.3 SUCCESSES IN HETEROGENEOUS PHOTOCATALYSIS . . . . . 8
1.4 RESEARCH FOCUS . . . . . 10
REFERENCES . . . . . 13

## CHAPTER 2

## SEMICONDUCTORS IN HETEROGENEOUS PHOTOCATALYSIS

2.1 BRIEF INTRODUCTION TO SOME FUNDAMENTAL PROPERTIES OF N-TYPE SEMICONDUCTORS . . . . . 16
2.2 NATURE OF THE $TiO_2$ PARTICLE SURFACE . . . . . 19
2.3 NATURE OF THE OXIDIZING SPECIES . . . . . 26
2.4 SURFACE *VERSUS* SOLUTION REACTIONS . . . . . 31
2.5 RESEARCH FOCUS . . . . . 35
REFERENCES . . . . . 37

## CHAPTER 3

## EXPERIMENTAL

3.1 PHOTOCATALYSIS EXPERIMENTS . . . . . 43
3.1.1 Cresols . . . . . 43
3.1.2 Methylhydroquinone and 4-Methylcatechol . . . . . 45
3.1.3 Xylenols . . . . . 45
3.1.4 2,3,5-Trimethylphenol . . . . . 46
3.1.5 Coal Tar Creosote . . . . . 47

3.1.6 Instrumentation and Methodology . . . . . 48
3.1.6.1 Light Source . . . . . 48
3.1.6.2 Photochemical Efficiency Determinations . . . . . 49
3.1.6.3 High Performance Liquid Chromatography . . . . . 50
3.1.6.4 Determination of $CO_2$ by Gas Chromatography . . . . . 53
3.1.6.5 UV/Visible Spectrophotometer . . . . . 54
3.1.6.6 Carbon Content Analysis . . . . . 54
3.2 KINETIC CONSIDERATIONS IN HETEROGENEOUS PHOTOCATALYSIS . . . . . 55
3.3 PULSE RADIOLYSIS EXPERIMENTS . . . . . 61
3.3.1 Electron Accelerator . . . . . 61
3.3.2 Radical Production and Dosimetry . . . . . 62
3.3.3 Data Analysis . . . . . 66
3.3.3.1Kinetic Analysis . . . . . 66
3.3.3.2Calculation of Extinction Coefficients . . . . . 70
3.3.4 Pulse Radiolysis on Pentahalophenols . . . . . 70
3.3.5 Pulse Radiolysis on Xylenols . . . . . 72
3.4 SONOCHEMISTRY EXPERIMENTS . . . . . 73
3.4.1 Chemicals . . . . . 73
3.4.2 Ultrasonic Irradiation Procedure . . . . . 74
3.4.3 Analytical Procedures . . . . . 74
3.4.3.1 High Performance Liquid Chromatography . . . . . 74
3.4.3.2 Total Organic Carbon Analysis . . . . . 75
REFERENCES . . . . . 76

## CHAPTER 4

## THE PHOTOCATALYZEDMINERALIZATION OF CRESOLS IN AQUEOUS MEDIA WITH IRRADIATED TITANIA

4.1 INTRODUCTION . . . . . 79
4.2 PHOTOOXIDATIVE DEGRADATION OF CRESOLS . . . . . 80
4.2.1 Catalyst Loading . . . . . 80
4.2.2 Effect of pH . . . . . 83
4.2.3 Identification of Intermediates . . . . . 85
4.2.4 Rate Data for the Degradation of Cresols . . . . . 90
4.2.5 Effect of Oxygen . . . . . 96
4.2.6 pH Dependence . . . . . 96
4.2.7 Concentration Dependence . . . . . 98
4.2.8 Radiant Power Level Dependence . . . . . 101
4.2.9 Photochemical Efficiencies . . . . . 101
4.2.10 Mechanism of the Photodegradation of Cresols . . . . . 104
4.2.11 Kinetic Considerations . . . . . 105

4.3 CONCLUSIONS . . . . . 106
REFERENCES . . . . . 107

## CHAPTER 5

## THE PHOTOMINERALIZATION OF METHYLHYDROQUINONE AND 4-METHYLCATECHOL

5.1 INTRODUCTION . . . . . 110
5.2 PHOTOCATALYZED DEGRADATION OF MHQ AND 4-MCC . . . . . 110
5.2.1 Photomineralization of Methylhydroquinone . . . . . 110
5.2.2 Photomineralization of 4-Methylcatechol . . . . . 114
5.2.3 Kinetic Considerations . . . . . 116
5.2.3.1 Methylhydroquinone . . . . . 116
5.2.3.2 *4*-Methylcatechol . . . . . 118
5.3 CONCLUSIONS . . . . . 119
REFERENCES . . . . . 120

## CHAPTER 6

## THE PHOTOCATALYZEDMINERALIZATION OF XYLENOLS IN AQUEOUS MEDIA WITH IRRADIATED TITANIA

6.1 INTRODUCTION . . . . . 122
6.2 PHOTOOXIDATIVE DEGRADATION OF XYLENOLS . . . . . 123
6.2.1 Catalyst Loading . . . . . 123
6.2.2 Effect of pH . . . . . 123
6.2.3 Identification of Intermediates . . . . . 127
6.2.4 Rate Data for the Degradation of Xylenols . . . . . 131
6.2.5 Effect of Oxygen . . . . . 140
6.2.7 Concentration Dependence . . . . . 140
6.2.8 Radiant Power Level Dependence . . . . . 144
6.2.9 Photochemical Efficiencies . . . . . 147
6.2.10 Effect of Degussa P25 $TiO_2$ Batch Variation . . . . . 151
6.2.11 Mechanism of the Photodegradation of Xylenols . . . . . 153
6.2.12 Effect of Temperature . . . . . 153
6.2.13 Kinetic Considerations . . . . . 156
6.3 CONCLUSIONS . . . . . 157
REFERENCES . . . . . 158

## CHAPTER 7

## THE PHOTOMINERALIZATION OF 2,3,5-TRIMETHYLPHENOL


7.1 INTRODUCTION . . . . . 161
7.2 PHOTOCATALYZED DEGRADATION OF 2,3,5-TMP . . . . . 162
7.2.1 Identification of Intermediates . . . . . 162
7.2.2 Kinetics of the Photodegradation of 2,3,5-TMP . . . . . 162
7.2.3 Effect of Oxygen . . . . . 165
7.2.4 Mechanism of the Photodegradation of 2,3,5-TMP . . . . . 168
7.2.5 Kinetic Considerations . . . . . 169
7.3 CONCLUSIONS . . . . . 170
REFERENCES . . . . . 171


## CHAPTER 8

## THE PHOTOCATALYZEDMINERALIZATION OF *CREOSOTE* IN IRRADIATED $TiO_2$ MEDIA: *A PRACTICAL CASE STUDY*


8.1 INTRODUCTION . . . . . 172
8.2 PHOTOMINERALIZATION OF CREOSOTE . . . . . 174
8.3 CONCLUSIONS . . . . . 186
REFERENCES . . . . . 187


## CHAPTER 9

## PULSE RADIOLYTIC STUDIES OF THE REACTIONS OF PENTAHALOPHENOLS WITH •OH, $N_3$• AND $e_{(aq)}$: FORMATION OF PENTAHALOPHENOXYL,DIHYDROXYPENTAHALOCYCLOHEXADIENYL, AND SEMIQUINONE RADICALS


9.1 INTRODUCTION . . . . . 189
9.2 REACTIONS OF PENTAHALOPHENOLS WITH VARIOUS RADICALS . . 192
9.2.1 Pentabromophenol . . . . . 193
9.2.1.1 Pentabromophenoxyl Radical (PBP-O•) . . . . . 193
9.2.1.2 Pentabromophenol •OH Radical Adduct . . . . . 199
9.2.1.3 Dehalogenation to Phenyl Radical via Electron Attachment . . . . . 206
9.2.2 Pentachlorophenol . . . . . 210
9.2.2.1 Pentachlorophenoxyl Radicals (PCP-O•) . . . . . 210

9.2.2.2 Pentachlorophenol •OH Radical Adduct ..... 213
9.2.3 Pentafluorophenol ..... 220
9.2.3.1 Pentafluorophenol OH Adduct (HO•-PFP-O⁻) ..... 220
9.3 CONCLUSIONS ..... 223
REFERENCES ..... 225

## CHAPTER 10

## PULSE RADIOLYTIC STUDIES OF THE REACTION OF XYLENOLS WITH •OH, $N_3$•, AND H• RADICALS: FORMATION OF DIMETHYLPHENOXYL, DIHYDROXYDIMETHYLCYCLOHEXADIENYL AND HYDROXYDIMETHYL-CYCLOHEXADIENYL RADICALS

10.1 INTRODUCTION ..... 229
10.2 REACTIONS OF XYLENOLS WITH VARIOUS RADICAL SPECIES ..... 230
10.2.1 Reaction with $N_3$• ..... 230
10.2.1.1 *2,6*-Dimethylphenoxyl Radical ..... 231
10.2.1.2 *3,4*-Dimethylphenoxyl Radical ..... 235
10.2.2 Reaction of the Xylenols with •OH Radicals ..... 237
10.2.2.1 Dihydroxydimethylcyclohexadienyl Radicals ..... 237
10.2.2.2 Reaction of 3,4-Xylenol with •OH Radicals ..... 243
10.2.2.3 pH Dependence of the Reaction of 3,4-Xylenol with •OH Radicals ..... 243
10.2.3 Reaction with H• Radicals ..... 249
10.2.3.1 Hydroxy-2,6-dimethylcyclohexadienyl Radical ..... 255
10.3 CONCLUSIONS ..... 257
REFERENCES ..... 260

## CHAPTER 11

## SONOCHEMICAL OXIDATION OF PHENOL, HYDROQUINONE, CATECHOL, AND BENZOQUINONE IN AQUEOUS MEDIA: KINETIC AND MECHANISTIC ASPECTS

11.1 INTRODUCTION ..... 263
11.2 SONOCHEMICAL OXIDATION OF PHENOL ..... 265
11.3 SONOCHEMICAL OXIDATION OF INTERMEDIATES ..... 265
11.4 TOTAL ORGANIC CARBON DETERMINATION ..... 273
11.5 POWER DEPENDENCE ..... 273
11.5 SONO-OXIDATIVE DECOMPOSITION OF PHENOL - INTERPRETATION OF RESULTS ..... 275
11.6 KINETIC ASPECTS ..... 278

11.7 MECHANISTIC ASPECTS ..... 281
11.8 CONCLUDING REMARKS ..... 282
REFERENCES ..... 284

## CHAPTER 12

## KINETIC AND MECHANISTIC ASPECTS IN HETEROGENEOUS PHOTOCATALYSIS

12.1 KINETIC ASPECTS ..... 287
12.1.1 Reactions in Homogeneous *versus* Heterogeneous Media ..... 287
12.1.2 Effect of the Nature of the Substrate in Photocatalytic Reactions ..... 289
12.2 MECHANISTIC ASPECTS ..... 292
REFERENCES ..... 295

## CHAPTER 13

## FINAL CONCLUSIONS

13.1 CONCLUDING REMARKS ..... 297

## APPENDIX A

## KINETIC DATA OBTAINED IN THE PULSE RADIOLYTIC STUDY OF PENTAHALOPHENOLS

APPENDIX A ..... 305

## APPENDIX B

## KINETIC AND SPECTRAL DATA OBTAINED IN THE PULSE RADIOLYTIC STUDY OF XYLENOLS

APPENDIX B ..... 313

# LIST OF FIGURES

**Figure 1.1** Schematic representation of electron/hole formation in an irradiated semiconductor particle. . . . . 5

**Figure 1.2** Band edge position of several semiconductors in contact with aqueous electrolyte at pH 1. in relation to the electrode potential regions for the oxidation of organic functional groups. . . . . 6

**Figure 1.3** Predominant phenolic compounds in coal tar creosote. . . . . 11

**Figure 2.1** Charge transfer equilibration processes at a semiconductor-liquid interface. (a) Before charge flow. (b) After charge equilibration. . . . . 17

**Figure 2.2** Space charge layer formation at the n-type semiconductor-solution interface. a) Flat band situation; b) accumulation layer; c) depletion layer; d) inversion layer. . . . . 19

**Figure 2.3** Photoinduced charge carrier separation assisted by the electrostatic fields present in the depletion layer of a large semiconductor particle in contact with a redox system. . . . . 20

**Figure 2.4** Plot showing the effect of pH on the redox potentials of the conduction band (CB) of $TiO_2$ together with other redox couples in aqueous media. . . . . 22

**Figure 2.5** Hydrated surface of anatase $TiO_2$ showing both types of surface $OH^-$ groups: **(a)** acidic doubly coordinated $OH^-$ **(b)** singly coordinated basic $OH^-$. . . . . 23

**Figure 2.6** Saturation-type kinetic plot of initial rates versus [reactant]; the inset shows the linear transform of equation 2.25 from which the rate constant k and the equilibrium constant K can be estimated from the intercept and slope, respectively. . . . . 32

**Figure 3.1** Sample trace for the first order formation of a radical. . . . . 68

**Figure 3.2** Sample decay trace for the second order disappearance of a radical . . . . . 69

**Figure 3.3** Direct immersion ultasonic horn . . . . . 75

**Figure 4.1** Absorbance *versus* irradiation time plots at three monitoring wavelengths relevant to the HPLC technique employed in this work (214 nm, 254 nm, and 280 nm) in the mineralization of 20 mg/L of cresols in the presence of 2 g/L $TiO_2$ at pH 3: (a) *o*-cresol, (b) *m*-cresol, and (c) *p*-cresol. . . . . 81

**Figure 4.2** Plot showing the effect of the $TiO_2$ concentration on the initial rate of the photocatalyzed mineralization of 20 mg/L (169 $\mu$M) of *m*-cresol at pH 3. . . . . 82

**Figure 4.3** Plots of the normalized concentration as a function of irradiation time for the photomineralization of *m*-cresol (20 mg/L) at three different pH's: 3, natural ($\approx$ 6.5), and 12; concentration of $TiO_2$, 2 g/L. . . . . 84

**Figure 4.4** Sample chromatograms illustrating the retention times of the intermediates observed in the course of the mineralization of o-, m-, and p-cresol. Mobile phase: 25/75/0.1 methanol, $H_2O$, *o*-$H_3PO_4$. The feature at $\approx$1.5 min is due to the elution of the solvent (water) as well as any other compounds not retained on the column. . . . . 86

**Figure 4.5** Diffuse reflectance spectra of the catalyst powder from an air-equilibrated aqueous suspension of $TiO_2$ (2 g/L) and 500 mg/L of *m*-cresol after several hours of irradiation. . . . . 89

**Figure 4.6** Plots of normalized peak areas (or concentration) as a function of irradiation time showing the degradation of the three cresols (ca. 20 mg/L) and formation and decomposition of two intermediates in the photomineralization process with irradiated $TiO_2$ present (2g/L at pH 3). The behaviour of the cresols under dark conditions but in the presence of $TiO_2$, and under direct photolysis (no $TiO_2$ present), is also indicated: (a) *o*-cresol, (b) *p*-cresol, and (c) *m*-cresol. The curves are computer fits to equations noted in the text. . . . . 91

**Figure 4.7** Plots showing the temporal evolution of $CO_2$ from the photomineralization of 20 mg/L cresol in the presence of 2 g/L $TiO_2$ at an initial pH of 3; air-equilibrated suspensions. . . . . 95

**Figure 4.8** (a) Plots showing the photodegradation of 20 mg/L of *m*-cresol in the presence of 2 g/L $TiO_2$ in air-equilibrated suspensions and in oxygen-saturated suspensions; initial pH 3. (b) Plots showing the corresponding temporal evolution of $CO_2$ from the photomineralization of 20 mg/L of *m*-cresol in air-equilibrated and oxygen-saturated suspensions of $TiO_2$. . . . . 97

**Figure 4.9** Photodegradation of 164 $\mu$M *m*-cresol via direct photolysis and via the photocatalyzed process in the presence of $TiO_2$ at an initial pH of 12. Also shown are the formation and subsequent degradation of the four intermediate species detected by HPLC methods (see text). . . . . 99

**Figure 4.10** Zero-order plots of the photomineralization of *m*-cresol catalyzed by irradiated $TiO_2$ at various initial concentrations; initial pH 3. . . . . 100

**Figure 4.11** (a) Plot showing the effect of the initial concentration on the initial rate of the photodegradation of *m*-cresol under air-equilibrated conditions; initial pH 3. (b) Linear transform of the Langmuir type isotherm (see text). . . . . 102

**Figure 4.12** Effect of the radiant power levels of the light source (see text) on the initial rate of the photomineralization of m-cresol (20 mg/L); initial pH 3; $TiO_2$, 2 g/L; 100% radiant power corresponds to 36.2 mW/cm$^2$. . . . . 103

**Figure 5.1** HPLC chromatograms showing the decrease in concentration of MHQ as a function of irradiation time in irradiated aqueous $TiO_2$ dispersions; $[MHQ]_{ini}$ = 71.3 $\mu$M; $[TiO_2]$ = 2g/L; pH 3. The features between 1 and 2 min are attributed to the solvent and any other compounds not retained by the column. . . . . 112

**Figure 5.2** (A) Photodegradation of MHQ (71.3 $\mu$M) in air-equilibrated aqueous suspensions of $TiO_2$ irradiated by light at wavelengths > 300 nm; pH 3; $TiO_2$, 2 g/L; 50

mL samples. The asterisked points are those of an unknown intermediate(s) the quantity of which was estimated by mass balance. (B) Stoichiometric evolution of $CO_2$ with irradiation time; same conditions as in (A) but volume of sample was 25 mL. Dashed line denotes the amount of $CO_2$ expected upon total mineralization of MHQ ..... 113

**Figure 5.3** HPLC chromatograms showing the decrease in concentration of 4-MCC as a function of irradiation time in irradiated aqueous $TiO_2$ dispersions; $[4\text{-MCC}]_{ini} = 63.6\ \mu M$; $[TiO_2] = 2 g/L$; pH 3. The features between 1 and 2 min are attributed to the solvent and any intermediates not retained by the column. ..... 115

**Figure 5.4** Diffuse reflectance spectra of the catalyst powder after various irradiation periods for a suspension of $TiO_2$ and 4-MCC (see text). ..... 116

**Figure 5.5** (A) Photodegradation of 4-methylcatechol (63.6 $\mu$M); same conditions as for Figure 5.2 A. (B) Stoichiometric formation of carbon dioxide as a function of irradiation time; same conditions as in (A) but volume of sample was 25 mL. Dashed line denotes the amount of $CO_2$ expected upon total mineralization of 4-MCC. ..... 117

**Figure 6.1** (a) Plot showing the effect of the $TiO_2$ concentration on the initial rate of the photocatalyzed mineralization of 20 mg/L (160 $\mu$M) of 3,4-xylenol at pH 3. (b) Linear transform of the Langmuir type expression (see text). ..... 124

**Figure 6.2** Plots of the apparent first order rate constants for the photodegradation of 3,4-xylenol as a function of initial pH. (a) indicates the pzc ($\approx 5.6$) value for the $TiO_2$ material used in this work, (b) indicates the $pK_a$ of 3,4-xylenol (10.4). ..... 126

**Figure 6.3** Plots of normalized peak areas (or concentration) as a function of irradiation time showing the degradation of the six xylenols (ca. 20 mg/L) and formation and decomposition of major intermediates in the photomineralization process with irradiated $TiO_2$ present (2g/L at pH 3). (a) 2,3-xylenol, (b) 2,4-xylenol, (c) 2,5-xylenol, (d) 2,6-xylenol, (e) 3,4-xylenol and (f) 3,5-

Xylenol. The curves are computer fits to equations noted in Chapter 3. . . . . 133

**Figure 6.4** Plot showing the temporal evolution of $CO_2$ from the photomineralization of 165 $\mu$M xylenol in the presence of 2 g/L $TiO_2$ at an initial pH of 3 in an oxygen-saturated suspension. . . . . 139

**Figure 6.5** Plot showing the photodegradation of ≈ 20 mg/L of 3,4-xylenol in the presence of 2 g/L $TiO_2$ in air-equilibrated suspensions and in oxygen-saturated suspensions; initial pH 3. The apparent rate constants were, air *versus* O2, respectively, kapp: 0.085 $min^{-1}$ and 0.16 $min^{-1}$ . . . . . 141

**Figure 6.6** Plot showing the initial rates of the photomineralization of 3,4-xylenol catalyzed by irradiated $TiO_2$ at various initial concentrations; initial pH 3. . . . . 142

**Figure 6.7** (a) Plot showing the effect of the initial concentration on the initial rate of the photodegradation of 3,4-xylenol under air-equilibrated conditions; initial pH 3. (b) Linear transform of the Langmuir type expression (see text). . . . . 143

**Figure 6.8** Rate *versus* intensity plot showing the rate dependence on light intensity in the 3 operating regions. . . . . 146

**Figure 6.9** (a) Effect of the radiant power levels of the light source (see text) on the initial rate of the photomineralization of 3,4-xylenol (165 $\mu$M); initial pH 3; $TiO_2$, 2 g/L; 100% radiant power corresponds to 176 $mW/cm^2$. (b) Regions where the dependence of the initial rate on the radiant power level is a function of $I^1$ at low light fluxes and $I^0$ at high light fluxes. (c) Region where the initial rate is a function of the square root of the radiant power at intermediate light fluxes. . . . . 148

**Figure 6.10** Effect of the Intensity of the Photon Flux on the rates of Photo-oxidation in various systems: a) Phenol b) Isopropanol c) 3-Chlorophenol. . . . . 150

**Figure 6.11** Plot showing the effect of different lots of Degussa P25 $TiO_2$ on the rate of photodegradation of 3,4-xylenol. $[3,4\text{-xylenol}]_{in} = 160$ $\mu$M, pH 3, $[TiO_2] = 2$g/L. . . . . 152

**Figure 6.12** **(a)** Temperature dependence of the initial rate of photodegradation of 3,4-Xylenol; **(b)** Arrhenius (ln k *versus* 1/T) plot for the photodegradation of 3,4-xylenol **(c)** Eyring (ln (k/T) *versus* 1/T) plot for the photodegradation of 3,4-xylenol. . . . . 155

**Figure 7.1** Photodegradation of 2,3,5-TMP (159.3 $\mu$M) in air-equilibrated aqueous suspensions of $TiO_2$ irradiated by light of wavelengths > 300 nm; pH 3; $TiO_2$, 2 g/L; 50 mL samples. . . . . 164

**Figure 7.2** Plot showing the temporal evolution of $CO_2$ from the photomineralization of 146 $\mu$M 2,3,5-TMP in the presence of 2 g/L $TiO_2$ at an initial pH of 3 in an oxygen-saturated suspension. The dotted line indicates the amount of $CO_2$ expected upon total mineralization. . . . . 166

**Figure 7.3** Plot showing the photodegradation of ≈ 20 mg/L of 2,3,5-TMP in the presence of 2 g/L $TiO_2$ in air-equilibrated suspensions and in oxygen-saturated suspensions; initial pH 3. The apparent rate constants were, air *versus* O2, respectively: $k_{app}$, 0.143 $min^{-1}$ and 0.211 $min^{-1}$. . . . . 167

**Figure 8.1** Absorption spectra of the filtrates containing water-soluble components of creosote during the photocatalyzed degradation of 360 ppm of creosote under air-equilibrated conditions (see text). . . . . 177

**Figure 8.2** HPLC chromatograms of the initial water-soluble substances in creosote and intermediates following light irradiation of an aqueous suspension containing the photocatalyst $TiO_2$ and creosote under air-equilibrated conditions. The samples used were those used to record the absorption spectra (see Figure 8.1). [mobile phase, 50/50 water/methanol]; the features at r.t. 1-3 min are attributed to the elution of the solvent and any other compounds not retained by the column. . . . . 178

**Figure 8.3** Scanned image of the $TiO_2$ particle filtrates (on MSI Nylon filters) as a function of irradiation time in minutes. A $TiO_2$ blank is included for comparison purposes. . . . . 179

**Figure 8.4** Diffuse reflectance spectra of the $TiO_2$ particulates after filtration of the irradiated aliquots taken during the photocatalyzed degradation of creosote. . . . . 182

**Figure 8.5** Kinetic analyses of the changes in concentrations (as absorbance) from the data in Figures 8.1 and 8.4 at the wavelengths indicated. . . . . 183

**Figure 8.6** Plots showing the double exponential evolution of stoichiometric quantities of carbon dioxide formed from the total photomineralization of 100 ppm of creosote under a saturated oxygen atmosphere. See text for additional details. . . . . 185

**Figure 9.1** Transient absorption spectra of PBP-O• at 40, 90, 245, 475, and 745 $\mu$s after irradiation of 2 x $10^{-4}$ M pentabromophenoxide at pH 8 (buffered) in a 0.01 M $NaN_3$ aqueous solution; the solution was $N_2O$-saturated. [•OH]= 1.97 x $10^{-6}$ M. Insets show the decays of the optical density at 350 nm and 470 nm. . . . . 194

**Figure 9.2** Changes in the optical spectrum of PBP-O• in the presence of ascorbate. The spectra were recorded at 2.5, 7.75, 15.5, 23.25 and 52.25 $\mu$s following irradiation of 2 x $10^{-4}$ M pentabromophenoxide in an $N_2O$-saturated aqueous solution at pH 8 containing 0.01 M $NaN_3$ and 5 x $10^{-5}$ M ascorbate. [•OH]= 3.17 x $10^{-6}$ M. The right inset shows the decay of the 470-nm absorbance; [•OH]= 7.37 x $10^{-6}$ M. The left inset shows the growth observed at 390 nm; [•OH]= 2.85 x $10^{-6}$ M. . . . . 198

**Figure 9.3** Transient absorption spectra of the product(s) of the reaction between PBP-$O^-$ and •OH at 25, 75, 220, 615 and 1325 $\mu$s following irradiation of a $N_2O$-saturated aqueous solution of 2 x $10^{-4}$ M PBP-$O^-$ at pH 8 (buffered); [•OH] = 4 x $10^{-6}$ M. The inset shows the decay of optical density due to products of the (PBP-$O^-$ + •OH) reaction at 330 nm and at 460 nm. . . . . 200

**Figure 9.4** Changes in the optical spectrum of the products of the (PBP-$O^-$ + •OH) reaction in the presence of ascorbate. The spectra were recorded at 6, 11.5, 22, 41, and 91 $\mu$s following irradiation of a $N_2O$-saturated aqueous solution containing 2 x $10^{-4}$ M pentabromophenoxide and

5 x $10^{-5}$ M ascorbate at pH 8; [•OH]= 2.78 x $10^{-6}$ M. The left inset shows the growth observed at 380 nm; [•OH] = 3.38 x $10^{-6}$ M. The right inset shows the decay observed at 460 nm; [•OH] = 3.38 x $10^{-6}$ M. ..... 202

**Figure 9.5** Transient difference absorption spectrum of the dihydroxypentabromocyclohexadienyl radical HO•-PBP-O$^-$ (+ other species) (◇) as calculated from the transient absorption spectrum of the products of the reaction between PBP-O$^-$ solution and •OH (■) at 75 μs following irradiation of an aqueous solution 2 x $10^{-4}$ M PBP-O$^-$, buffered at pH 8. The solution was $N_2O$-saturated. [•OH] = 4 x $10^{-6}$ M. (●) represents the contribution to the product spectrum of the pentabromophenoxyl radical. ..... 203

**Figure 9.6** Transient absorption spectra of tetrabromophenoxyl radical(s) resulting from the reaction of PBP-OH with e at 15, 25, 55, 175 and 395 μs following irradiation of a 2 x $10^{-4}$ M PBP-OH and 0.2 M t-BuOH aqueous $N_2$-saturated solution at pH 8; [e]= 1.15 x $10^{-6}$ M. The left inset shows the decay at 330 nm and the right inset shows the decay at 460 nm. ..... 207

**Figure 9.7** Changes in the optical spectrum of tetrabromophenoxyl radical(s) resulting from the reaction of PBP-OH with e following the addition of ascorbate. The spectra were recorded at 7.5, 11.75, 18.5, 32 and 61.25 μs after the pulse following irradiation of a 2 x $10^{-4}$ M PBP-OH, 0.2 M t-BuOH, and 2.5 x $10^{-5}$ M ascorbate aqueous $N_2$-saturated solution at pH 8; [e$^-$] = 2 x $10^{-6}$ M. The left inset shows the growth at 380 nm, [e] = 2.6 x $10^{-6}$ M; the right inset shows the decay at 480 nm, [e] = 2.5 x $10^{-6}$ M. ..... 211

**Figure 9.8** Transient absorption spectra of PCP-O• at 25, 75, 190, 520, and 1270 μs after irradiation of 2.5 x $10^{-4}$ M pentachlorophenoxide at pH 8 (buffered) in a 0.01 M $NaN_3$ aqueous solution; the solution was $N_2O$-saturated. [•OH]= 2.95 x $10^{-6}$ M. Inset shows the decays of the optical density at 440 nm. ..... 212

**Figure 9.9** Changes in the optical spectrum of PCP-O• in the presence of ascorbate. The spectra were recorded at 1.5,

4.5, 10.5, 25, and 45 $\mu$s following irradiation of $2.5 \times 10^{-4}$ M pentachlorophenoxide in a $N_2O$-saturated aqueous solution at pH 8 containing 0.01 M $NaN_3$ and $5 \times 10^{-5}$ M ascorbate. [•OH]= $5.76 \times 10^{-6}$ M. The right inset shows the decay of the 440 nm absorbance of PCP-O• in the presence of ascorbate, [•OH]= $3.41 \times 10^{-6}$ M. The left inset shows the growth of the 360 nm absorbance, [•OH]= $3.21 \times 10^{-6}$ M. . . . . 214

**Figure 9.10** Transient absorption spectra of the product(s) of the reaction between PCP-O$^-$ and •OH at 24.5, 84, 189, 399 and 868 $\mu$s following irradiation of an aqueous $2.5 \times 10^{-4}$ M PCP-O$^-$, $N_2O$-saturated aqueous solution buffered at pH 8; [•OH]= $5.1 \times 10^{-6}$ M. The insets show the decays of the optical density at 340 nm and 450 nm. . . . . 216

**Figure 9.11** Changes in the optical spectrum of the products of the (PCP-O$^-$ + •OH) reaction in the presence of ascorbate. The spectra were recorded at 4, 11, 23, 48, and 118 $\mu$s following irradiation of a $N_2O$-saturated aqueous solution containing $2.5 \times 10^{-4}$ M pentachlorophenoxide and $2.5 \times 10^{-5}$ M ascorbate at pH 8; [•OH]= $4.78 \times 10^{-6}$ M. The left inset shows the growth observed at 360 nm; [•OH] = $4.38 \times 10^{-6}$ M. The right inset shows the decay observed at 450 nm; [•OH] = $3.38 \times 10^{-6}$ M. . . . . 217

**Figure 9.12** Transient absorption spectrum of the products of the (PCP-O$^-$ + •OH) reaction corrected (◇) for the absorbance due to PCP-O• based on the transient absorption spectrum of the total products of the reaction between PCP-O$^-$ and •OH (■) at 24.5 $\mu$s following irradiation of an aqueous solution $2.5 \times 10^{-4}$ M PCP-O$^-$ buffered at pH 8. The solution was saturated with $N_2O$. [•OH]= $5.2 \times 10^{-6}$ M. (●) represents the contribution of the pentachlorophenoxyl radical to the product spectrum. . . . . 219

**Figure 9.13** Transient absorption spectra of the HO•-PFP-O$^-$ radical monitored at 75, 215, 540, 1040, and 1530 $\mu$s following irradiation of a $5 \times 10^{-4}$ M aqueous PFP-O$^-$ solution buffered at pH 8. The solution was $N_2O$-saturated; [•OH]= $3.92 \times 10^{-6}$ M. The insets show the decay of the optical density at 300 nm and 430 nm. . . . . 221

**Figure 10.1** Transient absorption spectra of 2,6-dimethylphenoxyl radical at 0.026, 0.104, 0.206, 0.344 and 0.884 ms

following irradiation of 3 x $10^{-4}$ M 2,6-Xylenol at pH 5.8 in a 0.01 M $NaN_3$ aqueous solution; the solution was $N_2O$-saturated; [•OH]= 5.20 x $10^{-6}$ M. Insets show the decays of the optical density at 375 and 390 nm. ..... 232

**Figure 10.2** Transient absorption spectra of 3,4-dimethylphenoxyl radical at 0.008, 0.068, 0.158, 0.380 and 0.926 ms following irradiation of 3 x $10^{-4}$ M 3,4-Xylenol at pH 5.8 in a 0.01 M $NaN_3$ aqueous solution; the solution was $N_2O$-saturated; [•OH]= 4.78 x $10^{-6}$ M. Insets show the decays of the optical density at 400 and 415 nm. ..... 236

**Figure 10.3** Transient absorption spectra of the dihydroxy-2,6-dimethylcyclohexadienyl radical monitored at 0.013, 0.043, 0.085, 0.196 and 0.577 ms following irradiation of a 2.5 x $10^{-4}$ M aqueous 2,6-Xylenol solution buffered at pH 4. The solution was $N_2O$-saturated; [•OH]= 5.02 x $10^{-6}$ M. The inset shows the decay of the optical density at 320 nm. ..... 238

**Figure 10.4** Transient absorption spectra of the reaction product between 3,4-Xylenol and •OH monitored at 0.118, 0.236, 0.354, 0.768 and 1.124 ms following irradiation of a 3 x $10^{-4}$ M aqueous 3,4-Xylenol solution buffered at pH 4. The solution was $N_2O$-saturated; [•OH]= 6.01 x $10^{-6}$ M. Insets show the decay of the optical density at 300 and 400 nm. ..... 244

**Figure 10.5** Transient difference absorption spectrum of the dihydroxy-3,4-dimethylcyclohexadienyl radical (●) as calculated from the transient absorption spectrum of the products of the reaction between 3,4-Xylenol and •OH (■) at 118 $\mu$s following irradiation of a 2 x $10^{-4}$ M aqueous solution of 3,4-Xylenol, buffered at pH 4. The solution was $N_2O$ saturated. [•OH]= 6.01 x $10^{-6}$ M. The open squares (□) represent the contribution to the product spectrum of the 3,4-dimethylphenoxyl radical. ..... 245

**Figure 10.6** Transient absorption spectra of the reaction product(s) between 3,4-Xylenol and •OH monitored at 11.8, 23.6, 47.2, 76.6 and 111.8 $\mu$s following irradiation of a 3 x $10^{-4}$ M aqueous 3,4-Xylenol solution buffered at pH 4. The solution was $N_2O$-saturated; [•OH]= 2.99 x $10^{-6}$ M. Insets show the decay of the optical density at 300 nm and the increase in optical density at 400 nm. ..... 247

**Figure 10.7** [3,4-Xylenol] dependence of the observed rate constants (415 nm) for the formation of the 3,4-dimethylphenoxyl radical at pH 4 (inset) and pH 10, at constant [•OH]. The solutions were $N_2O$-saturated; [•OH]= $2.72 \times 10^{-6}$ M at pH 4; [•OH]= $1.42 \times 10^{-6}$ M at pH 10. . . . . 251

**Figure 10.8** Transient absorption spectra of the reaction product(s) between 3,4-Xylenol and •OH monitored at 0.120,0.240, 0.360, 0.600 and 0.956 ms following irradiation of a $3 \times 10^{-4}$ M aqueous 3,4-Xylenol solution buffered at pH 10. The solution was $N_2O$-saturated; [•OH]= $6.10 \times 10^{-6}$ M. Insets show the decay of the optical density at 300 and 400 nm. . . . . 253

**Figure 10.9** Transient absorption spectra of the reaction product(s) between 3,4-Xylenol and •OH monitored at 2.12, 3.18, 6.88, and 10.04 $\mu$s following irradiation of a $3 \times 10^{-4}$ M aqueous 3,4-Xylenol solution buffered at pH 10. The solution was $N_2O$-saturated; [•OH]= $5.97 \times 10^{-6}$ M. . . . . 254

**Figure 10.10** Transient absorption spectra of Hydroxy-2,6-dimethyl-cyclohexadienyl radical at 0.014, 0.074, 0.140, 0.230 and 0.806 ms following irradiation of $4 \times 10^{-4}$ M 2,6-Xylenol at pH 1 (buffered) in a 0.2 M *tert*-butyl alcohol aqueous solution. The solution was $N_2$-saturated; [H•]= $2.49 \times 10^{-6}$ M. The inset shows the decay of the optical density at 320 nm. . . . . 256

**Figure 11.1** a) Plot of concentrations as a function of sonoirradiation time showing the degradation of phenol, $[phenol]_{in}$ = 68.1 $\mu$M, and the formation and degradation of the three intermediates observed: hydroquinone, catechol and *p*-benzoquinone. Other conditions: air-equilibrated aqueous media, pH 3, 20 kHz, and 50 Watts power. (b) Similar observations but at pH 5.7; [phenol] = 50.8 $\mu$M. Note that BQ was not observed under these conditions. . . . . 266

**Figure 11.2** pH dependence of the sonolysis of phenol. The inset illustrates the linear dependence of the initial rates of disappearance of phenol on pH. Other conditions as in Figure 11.1; [phenol] = 68.5 $\mu$M. . . . . 267

**Figure 11.3** (a) Sonolysis of hydroquinone in air-equilibrated aqueous media at pH 3 and 50 Watts power; [HQ] =

43.7 $\mu$M. Plot also shows the formation and disappearance of BQ and the intermediate whose retention time was 5.1 min. under the HPLC conditions used. Other conditions as in Figure 11.1.(b) Sonolysis of *p*-benzoquinone (42.7 $\mu$M) as a function of irradiation time (50 Watts power). Other conditions as in Figure 11.1. . . . . 271

**Figure 11.4** (a) pH dependence of the sonolysis of catechol. Other conditions as in Figure 11.1 and in Tables 11.1 and 11.2. (b) pH dependence of the sonolysis of hydroquinone. Other conditions as in Figure 11.1 and in Tables 11.1 and 11.2. . . . . 272

**Figure 11.5** (a) Power dependence in the sonolysis of phenol, 100 $\mu$M, as a function of time in air-equilibrated aqueous media at pH 3. (b) Initial rates *versus* power in the sonodegradation of phenol. Other conditions as in Figure 11.5a. . . . . 274

**Figure 12.1** Comparison of the rates of degradation of xylenols in heterogeneous media (conditions as per Table 6.4, Chapter 6) with the rates of a) formation of •OH-adducts in homogeneous solution, and b) decay of •OH-adducts (conditions as per Table 10.4 and text, Chapter 10). . . . . 288

**Figure 12.2** Proposed mechanism for the photo-oxidation of methylated phenols. . . . . 293

**Figure A1** Plot of $k_{obs}$ *versus* [PBP-O$^-$] as measured at 350 nm for the $N_3$• oxidation of PBP-O$^-$ at constant [•OH] (=1.88 x $10^{-6}$ M). Inset shows the increase in the optical density at 350 nm upon irradiation of 2 x $10^{-4}$ M PBP-O in a $N_2O$-saturated solution at pH 8 and containing 0.01 M $NaN_3$. . . . . 306

**Figure A2** Plot of $k_{obs}$ *versus* [PBP-O$^-$] as measured at 470 nm for the $N_3$• oxidation of PBP-O$^-$ at constant [•OH] (=1.88 x $10^{-6}$ M). Inset shows the increase in the optical density at 470 nm upon irradiation of 2 x $10^{-4}$ M PBP-O in a $N_2O$-saturated solution at pH 8 and containing 0.01 M $NaN_3$. . . . . 307

**Figure A3** Plot of $k_{obs}$ *versus* [PBP-O$^-$] as measured at 715 nm for the $e^-_{(aq)}$ addition to PBP-O$^-$ at constant [$e^-_{(aq)}$] (=2.2 x $10^{-6}$ M). Inset shows the decay in the optical density at 715 nm upon irradiation of 2 x $10^{-4}$ M PBP-O$^-$, 0.2 M *t*-butanol, in a $N_2$-saturated aqueous solution at pH 8. . . . . 308

**Figure A4** Plot of $k_{obs}$ *versus* [PCP-O$^-$] as measured at 440 nm for the $N_3$• oxidation of PCP-O$^-$ at constant [•OH] (=1.14 x $10^{-6}$ M). Inset shows the increase in the optical density at 440 nm upon irradiation of 2.5 x $10^{-4}$ M PCP-O$^-$ in a $N_2O$-saturated solution at pH 8 and containing 0.01 M $NaN_3$. . . . . 309

**Figure A5** Plot of $k_{obs}$ *versus* [PFP-O$^-$] as measured at 300 nm for the •OH oxidation of PFP-O$^-$ at constant [•OH] (=1.52 x $10^{-6}$ M). Inset shows the increase in the optical density at 300 nm upon irradiation of 5 x $10^{-4}$ M PFP-O$^-$ in a $N_2O$-saturated solution at pH 8. . . . . 310

**Figure A6** Plot of $k_{obs}$ *versus* [PFP-O$^-$] as measured at 430 nm for the •OH oxidation of PFP-O$^-$ at constant [•OH] (=1.83 x $10^{-6}$ M). Inset shows the increase in the optical density at 430 nm upon irradiation of 5 x $10^{-4}$ M PFP-O$^-$ in a $N_2O$-saturated solution at pH 8. . . . . 311

**Figure B1** Plot of [2,6-Xylenol] *versus* $k_{obs}$ as measured at 375 nm for the $N_3$• oxidation of 2,6-Xylenol at constant dose ([OH•]= 3.34 x $10^{-6}$ M); Inset shows the increase in optical density at 375 nm upon irradiation of 2 x $10^{-4}$ M 2,6-Xylenol at pH 5.8 in a 0.01 M $NaN_3$ aqueous solution; the solution was $N_2O$-saturated. . . . . 314

**Figure B2** Plot of [3,4-Xylenol] *versus* $k_{obs}$ as measured at 415 nm for the $N_3$• oxidation of 3,4-Xylenol at constant dose ([OH•]= 1.68 x $10^{-6}$ M); Inset shows the increase in optical density at 415 nm upon irradiation of 3 x $10^{-4}$ M 3,4-Xylenol at pH 5.8 in a 0.01 M $NaN_3$ aqueous solution; the solution was $N_2O$-saturated. . . . . 315

**Figure B3** Plot of [2,6-Xylenol] *versus* $k_{obs}$ as measured at 320 nm for the OH• oxidation of 2,6-Xylenol at constant dose ([OH•]= 4.22 x $10^{-6}$ M); Inset shows the increase in optical density at 320 nm upon irradiation of a 1.5 x $10^{-4}$ M aqueous solution of 2,6-Xylenol buffered at pH 4. The

solution was $N_2O$-saturated. . . . . 316

**Figure B4** Transient absorption spectra of the reaction product between 2,3-Xylenol and OH• monitored at 0.6, 1.2, 2.4, 3.9 and 6.6 ms following irradiation of a $2.5 \times 10^{-4}$ M aqueous 2,3-Xylenol solution buffered at pH 4. The solution was $N_2O$-saturated; $[\bullet OH] = 4.87 \times 10^{-6}$ M. The inset shows the decay of the optical density at 300 nm. . . . . 317

**Figure B5** Plot of [2,3-Xylenol] *versus* $k_{obs}$ as measured at 300 nm for the OH• oxidation of 2,3-Xylenol at constant dose ($[OH\bullet] = 2.5 \times 10^{-6}$ M); Inset shows the increase in optical density at 300 nm upon irradiation of a $1.5 \times 10^{-4}$ M aqueous solution of 2,3-Xylenol buffered at pH 4. The solution was $N_2O$-saturated. . . . . 318

**Figure B6** Transient absorption spectra of the reaction product between 2,4-Xylenol and OH• monitored at 0.025, 0.082, 0.145, 0.256 and 0.571 ms following irradiation of a $2.5 \times 10^{-4}$ M aqueous 2,4-Xylenol solution buffered at pH 4. The solution was $N_2O$-saturated; $[\bullet OH] = 5.16 \times 10^{-6}$ M. The inset shows the decay of the optical density at 300 nm. . . . . 319

**Figure B7** Plot of [2,4-Xylenol] *versus* $k_{obs}$ as measured at 300 nm for the OH• oxidation of 2,4-Xylenol at constant dose ($[OH\bullet] = 2.69 \times 10^{-6}$ M); Inset shows the increase in optical density at 300 nm upon irradiation of a $2 \times 10^{-4}$ M aqueous solution of 2,4-Xylenol buffered at pH 4. The solution was $N_2O$-saturated. . . . . 320

**Figure B8** Transient absorption spectra of the reaction product between 2.5-Xylenol and OH• monitored at 0.014, 0.056, 0.11, 0.212 and 0.818 ms following irradiation of a $3 \times 10^{-4}$ M aqueous 2,5-Xylenol solution buffered at pH 4. The solution was $N_2O$-saturated; $[\bullet OH] = 5.45 \times 10^{-6}$ M. The inset shows the decay of the optical density at 330 nm. . . . . 321

**Figure B9** Plot of [2,5-Xylenol] *versus* $k_{obs}$ as measured at 330 nm for the OH• oxidation of 2,5-Xylenol at constant dose ($[OH\bullet] = 3 \times 10^{-6}$ M); Inset shows the increase in optical density at 330 nm upon irradiation of a $1.5 \times 10^{-4}$ M aqueous solution of 2,4-Xylenol buffered at pH 4. The solution was $N_2O$-saturated. . . . . 322

**Figure B10** Transient absorption spectra of the reaction product between 3,5-Xylenol and OH• monitored at 0.013,0.052, 0.094, 0.119 and 0.583 ms following irradiation of a 3 x $10^{-4}$ M aqueous 3,5-Xylenol solution buffered at pH 4. The solution was $N_2O$-saturated; [•OH]= 2.93 x $10^{-6}$ M. The inset shows the decay of the optical density at 310 nm. . . . . 323

**Figure B11** Plot of [3,5-Xylenol] *versus* $k_{obs}$ as measured at 310 nm for the OH• oxidation of 3,5-Xylenol at constant dose ([OH•]= 2.8 x $10^{-6}$ M); Inset shows the increase in optical density at 310 nm upon irradiation of a 1.5 x $10^{-4}$ M aqueous solution of 3,5-Xylenol buffered at pH 4. The solution was $N_2O$-saturated. . . . . 324

**Figure B12** Plot of [3,4-Xylenol] *versus* $k_{obs}$ as measured at 300 nm for the OH• oxidation of 3,4-Xylenol at constant dose ([OH•]= 2.72 x $10^{-6}$ M); Inset shows the increase in optical density at 300 nm upon irradiation of a 1 x $10^{-4}$ M aqueous solution of 3,4-Xylenol buffered at pH 4. The solution was $N_2O$-saturated. . . . . 325

**Figure B13** a) Plot of [3,4-Xylenol] *versus* $k_{obs}$ as measured at 300 nm for the OH• oxidation of 3,4-Xylenol at constant dose ([•OH]= 1.83 x $10^{-6}$ M) at pH 6; b) Plot of [3,4-Xylenol] vs $k_{obs}$ as measured at 300 nm for the •OH oxidation of 3,4-Xylenol at constant dose ([•OH]= 1.62 x $10^{-6}$ M) at pH 8. . . . . 326

**Figure B14** a) Plot of [3,4-Xylenol] *versus* $k_{obs}$ as measured at 300 nm for the OH• oxidation of 3,4-Xylenol at constant dose ([OH•]= 1.90 x $10^{-6}$ M) at pH 9; b) Plot of [3,4-Xylenol] vs $k_{obs}$ as measured at 300 nm for the OH• oxidation of 3,4-Xylenol at constant dose ([OH•]= 1.42 x $10^{-6}$ M) at pH 10. . . . . 327

**Figure B15** Plot of [2,6-Xylenol] *versus* $k_{obs}$ as measured at 320 nm for the reaction of 2,6-Xylenol with H• at constant dose ([H•]= 2.19 x $10^{-6}$ M); Inset shows the increase in optical density at 320 nm upon irradiation of 2 x $10^{-4}$ M 2,6-Xylenol at pH 1 (buffered) in a 0.2 M *tert*-butanol aqueous solution; the solution was $N_2$-saturated. . . . . 328

# LIST OF TABLES


**Table 1.1** List of US EPA Priority Pollutants. . . . . 3

**Table 1.2** Structural Formulas of Some Organic Pollutants Degraded Photocatalytically. . . . . 9

**Table 3.1** Experimental Conditions used for HPLC Analyses . . . . . 52

**Table 3.2** Optical Properties of Some Radical Species Generated by Pulse Radiolysis . . . . . 65

**Table 3.3** $pK_a$ values for Xylenols . . . . . 72

**Table 4.1** HPLC Retention Times of Intermediates Produced from the Photodegradation of Cresols in Air-Equilibrated $TiO_2$ Aqueous Suspensions ([Cresol]= 20 mg/L; pH 3). . . . . 85

**Table 4.2** Identification of Intermediates Produced in the Photomineralization of Cresols in Air-Equilibrated $TiO_2$ Aqueous Suspensions (pH 3; [Cresol]= 20 mg/L)- Values in Parentheses Denote Retention Times. . . . . 87

**Table 4.3** Apparent Kinetics of the Mineralization of Cresols Photocatalyzed by Irradiated $TiO_2$ in Air-Equilibrated Suspensions at pH 3. . . . . 93

**Table 4.4** Apparent Kinetics of Formation of Intermediates Produced at pH 3 in Air-Equilibrated Irradiated $TiO_2$ Suspensions. . . . . 94

**Table 6.1** HPLC Retention Times of Intermediates Produced from the Photodegradation of Xylenols in Air-Equilibrated $TiO_2$ Aqueous Suspensions ([Xylenol]≈ 20 mg/L; pH 3). . . . . 128

**Table 6.2** Possible Intermediates in the Photomineralization of Xylenols in Air-Equilibrated $TiO_2$ Aqueous Suspensions (pH 3; [Xylenol]≈ 20 mg/L)- Values in Parentheses Denote Retention Times. . . . . 130

**Table 6.3** Identification of Intermediates Detected in the Course of the Mineralization of Xylenols. . . . . 132

**Table 6.4** Apparent Kinetics of the Mineralization of Xylenols Photocatalyzed by Irradiated $TiO_2$ in Air-Equilibrated Suspensions at pH 3. . . . . 137

**Table 6.5** Apparent Kinetics of Formation of Intermediates Produced at pH 3 in Air-Equilibrated Irradiated $TiO_2$ Suspensions. . . . . 138

**Table 6.6** Kinetic Parameters for the disappearance of 3,4-xylenol obtained in the $TiO_2$ Batch Dependence Study. $[3,4\text{-Xylenol}]_{ini} = 160\ \mu M$, $[TiO_2]$ (Degussa P25) = 2g/L, pH 3. . . . . 151

**Table 7.1** Identification of Intermediates in the course of the photomineralization of 2,3,5-TMP. . . . . 163

**Table 8.1** Predominant Polycyclic Aromatic Compounds in coal tar creosote. . . . . 174

**Table 8.2** Predominant Heterocyclic Compounds in coal tar creosote. . . . . 175

**Table 8.3** Predominant Phenolic Compounds in coal tar creosote. . . . . 175

**Table 9.1** Comparison of the Optical and Kinetic Properties of PXP-O• with Values Published for Similar Radicals . . . . . 195

**Table 9.2** Observed Kinetics of Formation and Decay of Transients in Various PBP-$O^-$ Reaction Systems. . . . . 196

**Table 9.3** Comparison of the Optical and Kinetic Properties of HO•-PXP-$O^-$ with Values Published for Similar Radicals . . . . . 205

**Table 9.4** Comparison of the Rate of Reaction of PBP-$O^-$ with $e^-_{aq}$ with Published Values for Similar Compounds . . . . . 209

**Table 9.5** Observed Kinetics of Formation and Decay of Transients in Various PCP-$O^-$ Reaction Systems. . . . . 215

**Table 9.6** Observed Kinetics of Formation and Decay of Transients in Various PFP-O$^-$ Reaction Systems. . . . . 222

**Table 10.1** Comparison of the Optical and Kinetic Properties of Dimethylphenoxyl radicals with Values Published for Similar Radicals . . . . . 233

**Table 10.2** Observed Kinetics of Formation and Decay of Phenoxyl Radicals in Various Reaction Systems. . . . . 234

**Table 10.3** Observed Kinetics of Formation and Decay of OH-adducts of xylenols in Various Reaction Systems. . . . . 239

**Table 10.4** Comparison of the Optical and Kinetic Properties of dihydroxydimethylcyclohexadienyl radicals with Values Published for Similar Radicals. . . . . 240

**Table 10.5** Comparison of Rates of •OH Addition to Xylenols in Aqueous Solution and in the Gas Phase. . . . . 242

**Table 10.6** Data Obtained from the pH Dependence Study of the Reaction of 3,4-Xylenol with •OH. . . . . 250

**Table 10.7** Comparison of the Optical and Kinetic Properties of the hydroxy-2,6-dimethylcyclohexadienyl radical with values published for similar radicals. . . . . 258

**Table 11.1** Summary of Sonolysis Rate Data in Aqueous Media at pH 3 (power, 50 Watts). . . . . 268

**Table 11.2** Summary of Sonolysis Rate Data in Aqueous Media at other pH's (power, 50 Watts). . . . . 269

**Table 12.1** Comparison of Apparent Rate Constants of $TiO_2$-Photocatalyzed Degradation Reactions under Various Experimental Conditions . . . . . 290

# CHAPTER 1

# INTRODUCTION

## 1.1 GENERAL INTRODUCTION

Increased industrial and agricultural activity in this century has resulted in an increase of water pollution, a serious and pressing environmental problem. Several industries contribute significantly in discharging organic pollutants in the environment: petroleum refining, organic chemicals and synthetic industries, milling and coal conversion, pulp and paper, and textile processing industries.[1,2] Additional pollution emanates from the use of fuel for heating and transportation, from fertilizers and pesticides, and from detergents and aerosol sprays. Accidental spillage, misuse and improper disposal of chemicals, and effluents from wastewater treatment plants also contribute to the problem.[1] The United States Environmental Protection Agency (EPA) has identified several classes of *top priority pollutants*; these are listed in Table 1.1.[2,3]

A significant challenge facing the modern day chemist is to find alternative water treatment processes. Traditional methods have employed ultrafiltration, extraction, air stripping, carbon adsorption, incineration, and oxidation via ozonation or via hydrogen peroxide. The United States EPA considers only air stripping (removal of volatile components) and carbon adsorption (removal of both volatile and non-volatile contaminants) as effective treatment technologies.[4] A weakness of air stripping and

**Table 1.1** List of US EPA Priority Pollutants. (from refs. 2 and 3).

| Compounds | Number of Compounds |
|---|---|
| ***Organics*** | |
| Pesticides and metabolites | 21 |
| PCBs and related compounds | 7 |
| Halogenated aliphatics | 26 |
| Ethers | 7 |
| Monocyclic aromatics (excluding phenols, cresols and phthalates) | 12 |
| Phenols and Cresols | 11 |
| Phthalate esters | 6 |
| Polycyclic aromatics | 16 |
| Nitrosamines and other Nitrogen containing compounds | 7 |
| ***Inorganics*** | |
| Metals | 13 |
| Asbestos | |
| Cyanides | |

carbon adsorption processes is that they are *non-destructive*; they simply transfer the pollutant from one phase to another. Both these methods are being legislated and in particular air stripping has been banned in the state of California.

Photochemical processes provide an alternative route to water purification, since UV irradiation in combination with other processes (such as ozonation, peroxidation, or both) can remove bacterial substances from solution as well as dissolved organics. These photochemical oxidation reactions have become known as *Advanced Oxidation Processes* (AOPs). Presently, only three photochemical technologies, *viz.*, UV-ozonation, UV-peroxidation with $H_2O_2$, and heterogeneous photocatalytic methods, are known to result in relatively rapid and complete destruction of numerous organics, including

halogenated hydrocarbons. Heterogeneous photocatalysis uses air (or oxygen) rather than $O_3$ or $H_2O_2$ which renders it a very attractive method for water decontamination.[5] Another factor that has contributed to the attractiveness of heterogeneous photocatalysis as an alternative route to water detoxification is the fact that the process can be carried out under ambient conditions and results in the total mineralization of organic pollutants to $CO_2$, without the formation of significant photocyclized intermediate products. In addition, the photocatalyst ($TiO_2$) is inexpensive and can be supported on suitable materials[6-9] so that the process has great industrial potential.

## 1.2 HETEROGENEOUS PHOTOCATALYSIS

Heterogeneous photocatalysis is a technology based on the irradiation of a photocatalyst, usually a semiconductor such as $TiO_2$, ZnO or CdS. Semiconductors are materials whose electrical conductivity properties are between those of metals and insulators; they have narrow energy gaps (bandgap) between a filled valence band and a conduction band.[10] Irradiation of a semiconductor (SC) with light of energy equal to or greater than its bandgap ($E_{bg}$) will result in electronic transitions ($e^-$) from the valence band (VB) to the conduction band (CB) and the creation of holes ($h^+$) in the valence band (equation 1.1).

$$SC + h\nu \rightarrow h^+_{VB} + e^-_{VB} \qquad (1.1)$$

These charge carriers can then recombine in competition with their rapid migration to the particle surface where redox chemistry can take place as illustrated in Figure 1.1. A

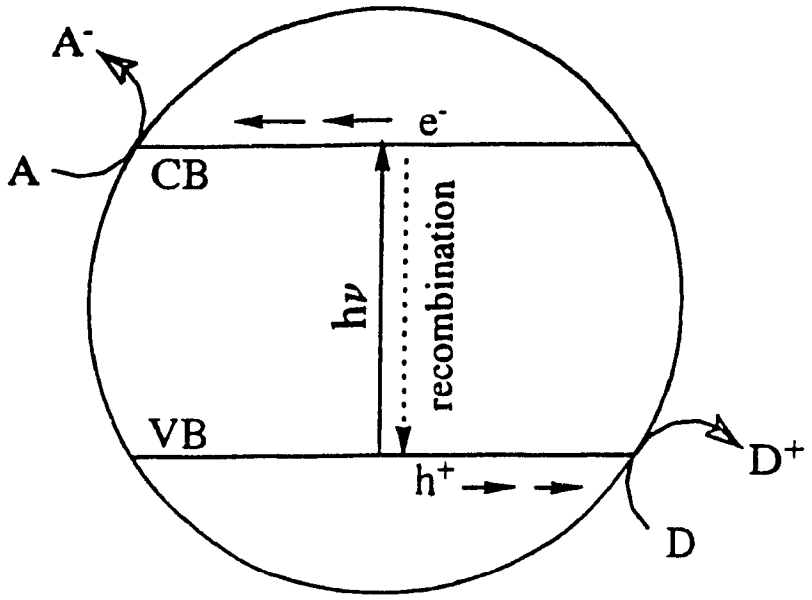


**Figure 1.1** Schematic representation of electron/hole formation in an irradiated semiconductor particle.

more detailed description of the processes taking place on semiconductor particle surfaces will be given in Chapter 2.

Figure 1.2 illustrates bandgaps and band edge positions in aqueous media (at pH 1) for a number of semiconductor materials ($TiO_2$, ZnO, CdS, and $WO_3$) which have been useful in heterogeneous photocatalysis. Also shown are the regions of redox potential for the oxidation of organic groups to illustrate the thermodynamic limitations of the type of photoreactions than can be carried out with the photogenerated electrons and holes. For example, if the reduction of a given species (A; Figure 1.1) is to be carried out, the conduction band level of the semiconductor must be positioned above the

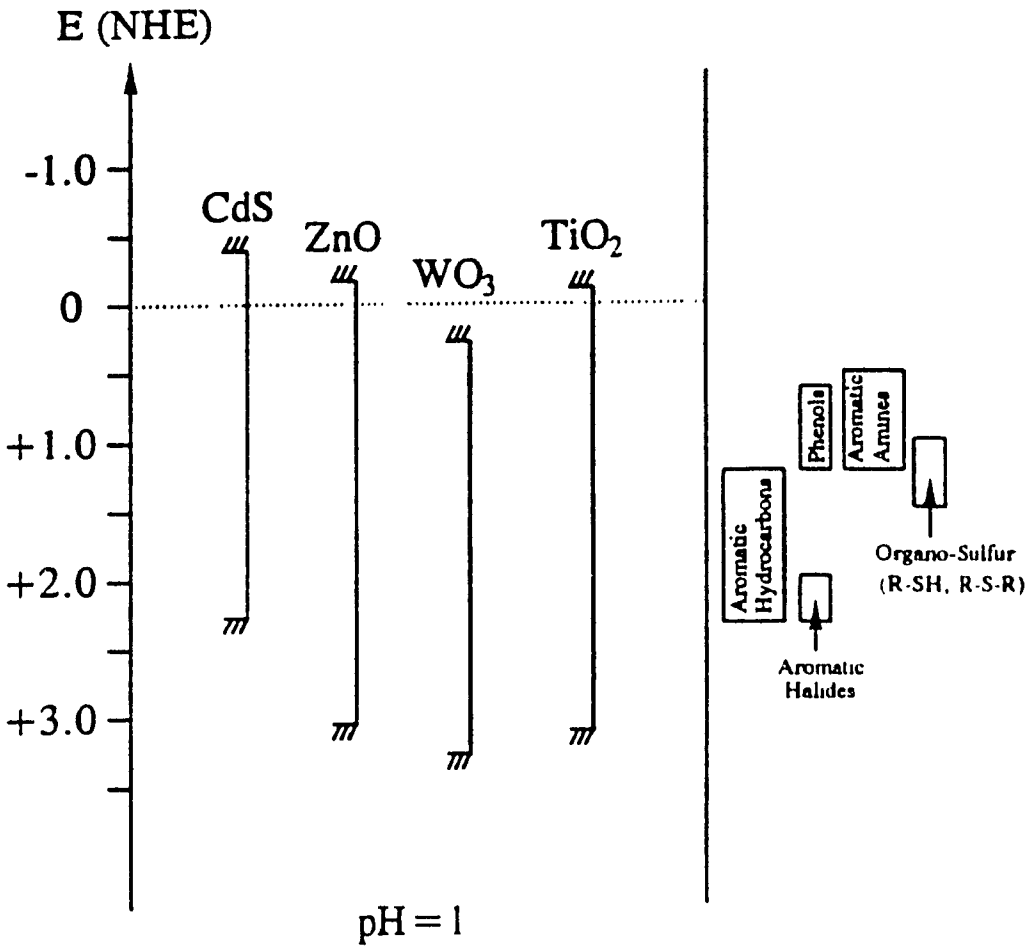


**Figure 1.2** Band edge position of several semiconductors in contact with aqueous electrolyte at pH 1. in relation to the electrode potential regions for the oxidation of organic functional groups (adapted from refs. 11 and 12).

redox level of A. Similarly, if the oxidation of D is to be carried out, its redox level must be positioned above the valence band of the semiconductor. If the redox level of A (or D) is located between the valence and conduction bands of the semiconductor, both reduction and oxidation processes can occur.

This work will deal solely with the use of titanium dioxide ($TiO_2$) as the photocatalyst in aqueous media. It has been used extensively to photocatalyze the mineralization of a large number of organics many of which have been listed as *top priority pollutants* (see Table 1.1). This photocatalyzed mineralization of organics in aqueous media will typically proceed via the formation of a series of intermediates of progressively higher oxygen to carbon ratios and which eventually will also be oxidized quantitatively to carbon dioxide (and $H_2O$). In the case of phenol, often taken as a model compound in heterogeneous photocatalytic studies, mineralization proceeds via the formation of several hydroxylated intermediates that includes predominantly catechol and hydroquinone, (scheme 1.2).[13]

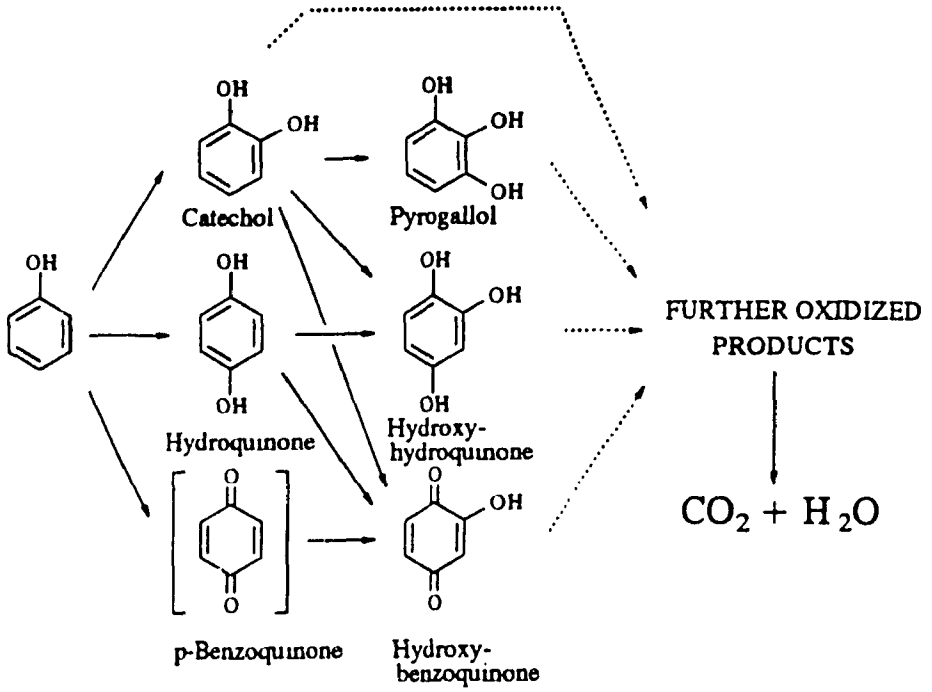


(1.2)

The intermediates detected during the course of the reaction are similar to the products observed for the reaction of phenol with •OH radicals in homogeneous solution.[14] The role of hydroxyl radicals in the photodegradation process will be discussed in greater detail in Chapter 2. Organic compounds containing phosphorus, sulfur, nitrogen, and halogen atoms may be oxidized quantitatively to produce phosphate ($PO_4^{3-}$), sulfate ($SO_4^{2-}$), ($NO_3^-$) and halide ($X^-$), respectively, in addition to $CO_2$.[15,16]

## 1.3 SUCCESSES IN HETEROGENEOUS PHOTOCATALYSIS

Significant progress has been made in recent years in the field of heterogeneous photocatalysis. A survey of the mineralization of several classes of compounds including chlorinated aromatics, surfactants, pesticides, and herbicides has been made. Table 1.2 shows a sample of some of the compounds which have been photocatalytically degraded. Pelizzetti *et al*[17] have demonstrated the total mineralization of long chain alkanes and such alkyl derivatives as dodecane, dodecyl sulfate, 1-bromododecane and decanoic acid. The photocatalyzed destruction of simple and complex chlorinated derivatives of alkanes, alkenes, carboxylic acids, and aromatics has also been achieved.[7] Examples include: 4-chlorophenol, 2,4,5-trichlorophenol, pentachlorophenol, chlorobenzene, 2,4,5-trichlorophenoxyacetic acid (2,4,5 T), 4,4'-dichlorodiphenyltrichloroethane (4,4'-DDT), 3,3'-dichlorobiphenyl (3,3'-DCB), 2,7-dichlorodibenzo-*p*-dioxin, and others.[18] Although chlorinated compounds have been more extensively studied, there are examples of brominated (bromoform)[19] and fluorinated (fluorophenols)[20] compounds as well as compounds containing phosphorus,[15] sulfur,[15] and nitrogen.[16] Such water insoluble

**Table 1.2** Structural Formulas of Some Organic Pollutants Degraded Photocatalytically.

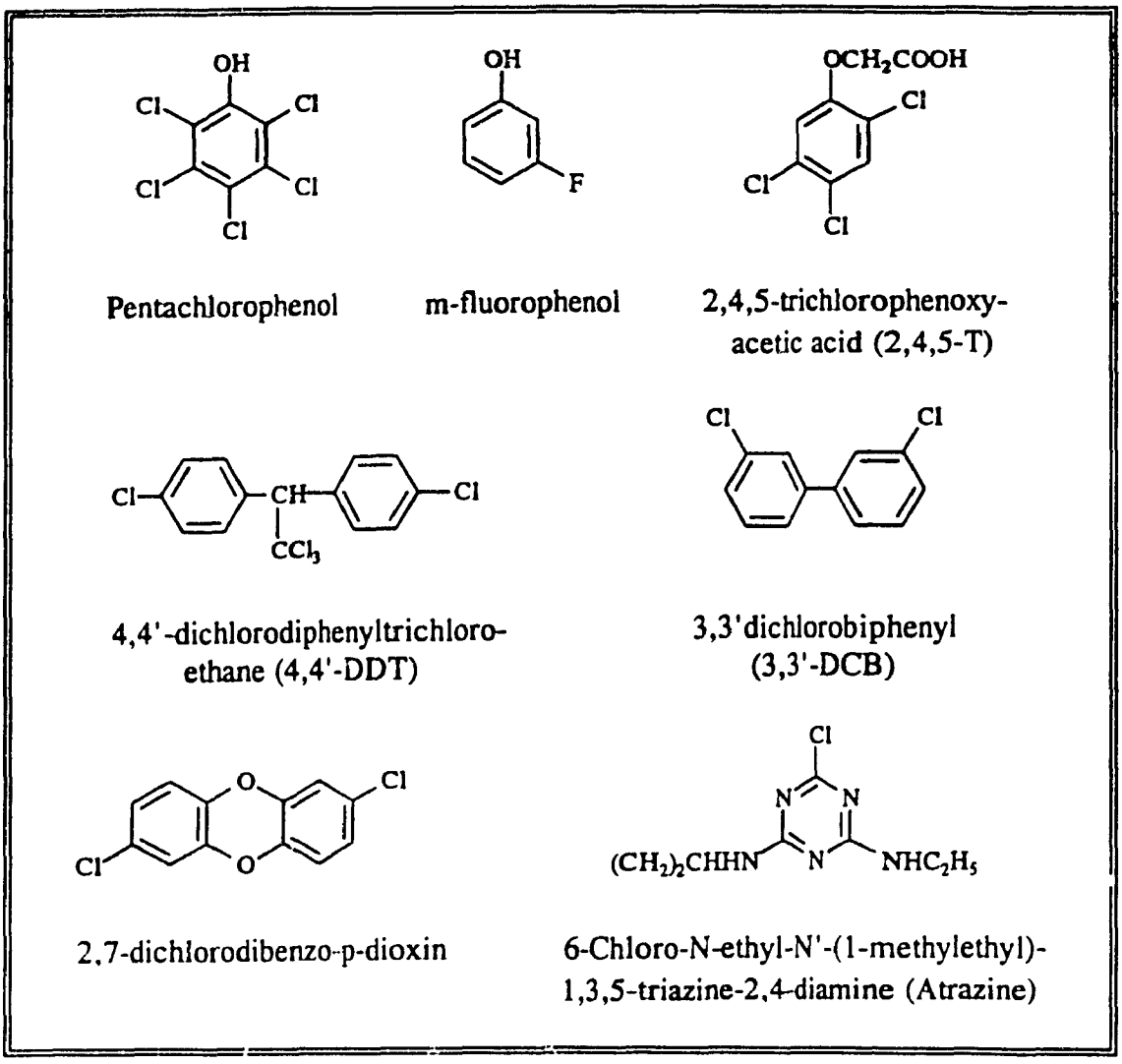


compounds as dioxins have been examined by loading them onto the photocatalyst via dissolution in hexane, solvent evaporation, followed by addition of water.

Studies carried out on anionic, cationic and non-ionic surfactants have shown that the aromatic and hydrophilic portions of the molecules are easily oxidized whereas the long hydrocarbon chains are converted at slower rates; surfactant activity did, however,

disappear with the loss of the aromatic portion, thereby reducing the nuisance of the reactants.[21-24] Total mineralization to $CO_2$ has been demonstrated for non-ionic polyethoxylated 4-nonylphenols with average numbers of 2, 5, and 12 ethoxy units.[25]

The herbicide bentazon (3-isopropyl-2,1,3-benzothiadiazin-4-one-2,2-dioxide) is nearly quantitatively mineralized to yield sulfate ions and $CO_2$.[26] The s-triazine herbicides (atrazine, simazine, trietazine, prometon, and prometryn) are rapidly degraded but are resistant to total mineralization; the final product in these cases, in addition to nitrate, sulfate and chloride ions, is cyanuric acid, a very stable 6-membered ring $(-N=C(OH)-)_3$.[27] Nevertheless, these results are encouraging due to the low toxicity of cyanuric acid.[28] The only compound to date that has been found to be resistant to initial photocatalyzed oxidative attack is carbon tetrachloride.[29]

## 1.4 RESEARCH FOCUS

The onslaught of research in photocatalysis in recent years has been driven by legislation in industrialized countries that encourages water decontamination and simultaneous contaminant destruction.[18] The ultimate goal of current research is to establish **heterogeneous photocatalysis** as a viable industrial water detoxification technology. In order to achieve this goal, the technology must be able to treat simultaneously several components in a multicomponent mixture, since most wastewater samples are multicomponent. Also, intermediates produced in the course of mineralization render even a single component process multicomponent. It is therefore imperative to monitor the formation and subsequent elimination of intermediates in the

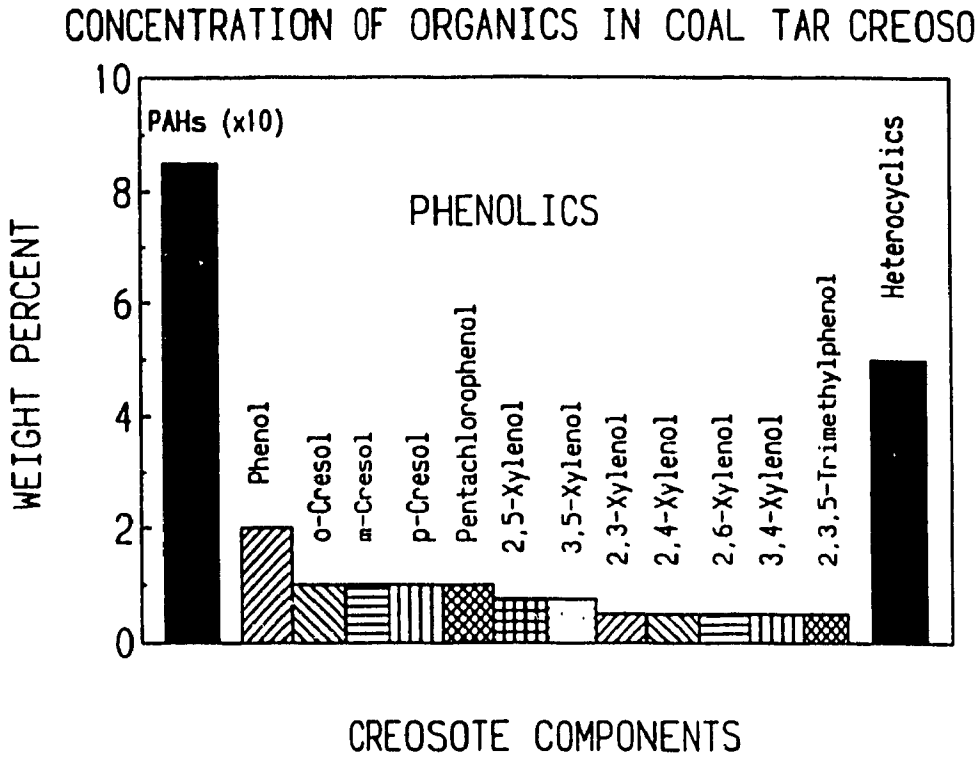


**Figure 1.3** Predominant phenolic compounds in coal tar creosote (adapted from ref. 31).

photo-oxidative process, in addition to demonstrating the applicability of photocatalysis using actual multicomponent waste samples. In all cases, the intermediates and final products must be identified.

The present work will address both areas of concern stated above. First, the $TiO_2$ photocatalyzed mineralization of methylated phenols has been surveyed; this class of compounds had not been investigated even though it contributes significantly to water pollution. Emphasis was placed on monitoring the formation and subsequent elimination of intermediates and on demonstrating that the process results in total mineralization of the phenols. Second, the practicality of heterogeneous photocatalysis is demonstrated by

decontaminating aqueous solutions of coal tar creosote. Contamination of groundwater by creosote, a wood preservative, is a recurring problem in the vicinity of wood-preserving facilities. For example, groundwater near the American Creosote Works Inc. facility in Pensacola, Florida, was found to be contaminated with pentachlorophenol and creosote 4 to 5 years after the facility was closed.[30] Creosote is a complex mixture of organic compounds: 85 wt % polycyclic aromatic hydrocarbons (PAHs), 10 wt % phenolic compounds (including methylated phenols, see Figure 1.3), and the remaining 5 wt % N-, S-, and O- heterocyclics.[31] Aqueous solutions of creosote are therefore, in many ways, typical multicomponent samples such as one is likely to encounter in polluted aquifers.

In addition to the practical aspects of heterogeneous photocatalysis, this thesis will also address some more fundamental issues, specifically regarding the mechanism of photodegradation. These aspects will be presented in Chapter 2.

# REFERENCES


1. *Water Quality Criteria Documents*, U.S. Environmental Protection Agency, Washington D.C., **1979**.

2. Ollis, D.F., Pelizzetti, E., Serpone, N. in *"Photocatalysis: Fundamentals and Applications"*; Serpone, N. and Pelizzetti, E., Eds., Wiley, New York, p. 603, **1989**.

3. Callahan, M.A., Slimak, M., Gbel, N., May, I., Fowler, C., Freed R., Jennings, P., Dupree, R., Whitmore, F., Maestri, B., Holt, B., Gould, C., *"Water Related Environmental Fate of 129 Priority Pollutants"*, Report EPA-44014-79-029a,b, NTIS.

4. Patterson, J.W., *"Industrial Wastewater Treatment Technology"*, 2nd ed., Butterworth Publishers, Boston, **1985**.

5. Ollis, D.F., in *"Photocatalysis and Environment: Trends and Applications"*, Schiavello, M., Ed., Kluwer Academic Publishers, p. 663, **1988** and references therein.

6. Al-Ekabi, H., Serpone, N., *J. Phys. Chem.*, **1988**, *92*, 5726.

7. Serpone, N., Borgarello, E., Harris, R., Cahill, P., Borgarello, M., Pelizzetti, E., *Sol. Energy Mater.*, **1986**, *14*, 121.

8. Matthews, R.W., *J. Catal.*, **1986**, *97*, 565.

9. Matthews, R.W., *Water Res.*, **1986**, *20*, 569.

10. Jolly, W.L., *"The Principles of Inorganic Chemistry"*, McGraw Hill, New York, **1976**.

11. Grätzel, M., *"Heterogeneous Photochemical Electron Transfer"*, CRC Press, Boca Raton, **1989**.

12. Rifi, M.R., Covitz, F.H., *"Introduction to Organic Electrochemistry"*, Marcel Dekker, New York, **1974**.

13. Okamoto, K., Yamamoto, Y., Tanaka, H., Tanaka, M., Itaya, A., *Bull. Chem. Soc. Jpn.*, **1985**, *58*, 2015.

14. Land, E.J., Ebert, M., *Trans. Faraday Soc.*, **1967**, *63*, 1181.

15. Low, G.K.-C., McEvoy, S.R., Matthews, R.W., *Environ. Sci. Technol.*, **1991**, *25*, 460.

16. Low, G.K.-C., McEvoy, S.R., Matthews, R.W., *Chemosphere*, **1989**, *19*, 611.

17. Pelizzetti, E., Minero, C., Maurino, V., Hidaka, H., Serpone, N., Terzian, R., *Ann. Chim.*, **1990**, *80*, 81.

18. Ollis, D.F., Pelizzetti, E., Serpone, N., *Environ. Sci. Technol.*, **1991**, *25*, 1522, and references therein.

19. Nguyen, T., Ollis, D.F., *J. Phys. Chem.*, **1984**, *88*, 96.

20. Minero, C., Aliberti, C., Pelizzetti, E., Terzian, R., Serpone, N., *Langmuir*, **1991**, *7*, 928.

21. Hidaka, H., Kubota, H., Grätzel, M., Serpone, N., Pelizzetti, E., *Nouv. J. Chim.*, **1985**, *9*, 67.

22. Hidaka, H., Kubota, H., Grätzel, M., Pelizzetti, E., Serpone, N., *J. Photochem.*, **1986**, *35*, 219.

23. Hidaka, H., Fujita, Y., Ihara, K., Yamada, S., Suzuki, K., Serpone, N., Pelizzetti, E., *J. Jpn. Oil Chem. Soc.*, **1987**, *36*, 386.

24. Hidaka, H., Ihara, K., Fujita, Y., Yamada, S., Pelizzetti, E., Serpone, N., *J. Photochem. Photobiol. A: Chem.*, **1988**, *42*, 375.

25. Pelizzetti, E., Minero, C., Maurino, V., Sclafani, A., Hidaka, H., Serpone, N., *Environ. Sci. Technol.*, **1989**, *23*, 1385.

26. Pelizzetti, E., Maurino, V., Minero, C., Zerbinati, O., Borgarello, E., *Chemosphere*, **1989**, *18*, 1437.

27. Pelizzetti, E., Maurino, V., Minero, C., Carlin, V., Pramauro, E., Zerbinati, O., Tosato M.L. , *Environ. Sci. Technol.*, **1990**, *24*, 1559.

28. Canelli, E., *Am. J. Public Health*, **1974**, *64*, 155.

29. Ollis, D.F., *Environ. Sci. Technol.*, **1985**, *19*, 480, and references therein.

30. Goerlitz, D.F., Troutman, D.E., Godsy, E.M., Franks, B.J., *Environ. Sci. Technol.*, **1985**, *19*, 955, and references therein.

31. Mueller, J.G., Chapman, P.J., Pritchard, P.H., *Environ. Sci. Technol.*, **1989**, *23*, 1197.

# CHAPTER 2

# SEMICONDUCTORS IN HETEROGENEOUS PHOTOCATALYSIS

## 2.1 BRIEF INTRODUCTION TO SOME FUNDAMENTAL PROPERTIES OF n-TYPE SEMICONDUCTORS

To the extent that heterogeneous photocatalysis implicates semiconductor materials (n-type $TiO_2$, CdS, ZnO, $WO_3$) it is instructive to consider some of the properties of these materials to illustrate those factors that will bear on the success/failure of photocatalysis. This section will treat specifically the n-type materials.

When an n-type semiconductor material comes in contact with an aqueous electrolyte system, as is the case in heterogeneous photocatalysis, a liquid-solid junction is formed. Considering this junction in greater detail, we find that the Fermi level of the solution (free energy of the electrons) is determined by the redox couple in solution (Figure 2.1).[1] If the Fermi level of the solid semiconductor ($E_F$) coincides with the equivalent Fermi level of the redox couple in solution [E(A/A)], there is no macroscopically observable charge transfer, i.e. an equilibrium situation exists.[2] If $E(A/A^-)$ is below $E_F$, when there is contact, electron transfer occurs from the higher energy level of the semiconductor into the lower energy redox level of the solution. The electrons leave behind positively charged donor ions at the semiconductor surface. This results in a potential drop across the junction. This region is known as the *space charge*

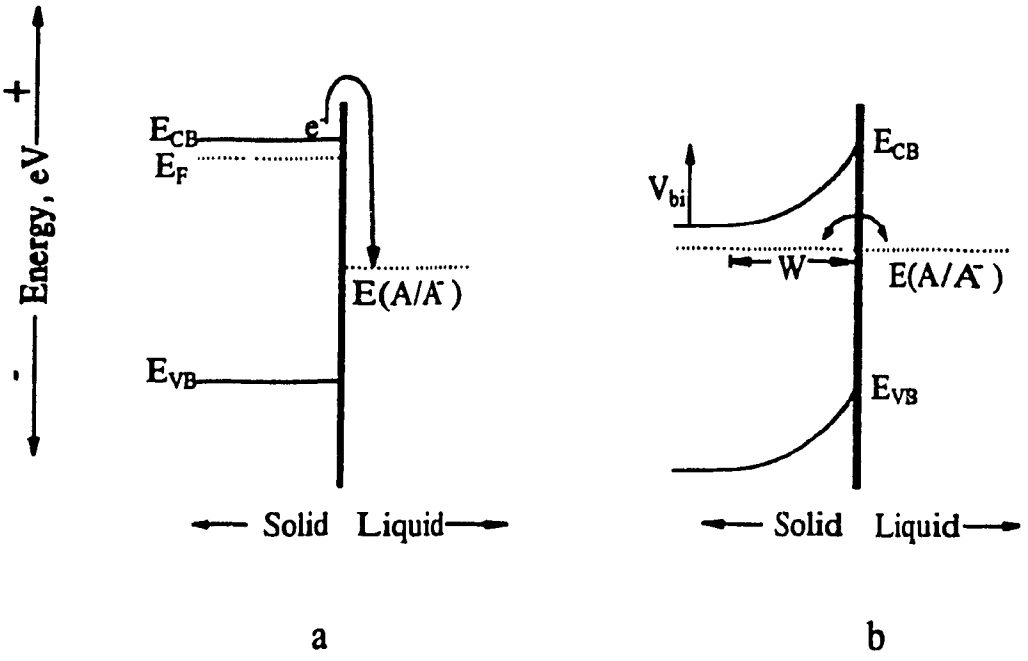


**Figure 2.1** Charge transfer equilibration processes at a semiconductor-liquid interface. (a) Before charge flow. (b) After charge equilibration. (Adapted from reference 3).

*region*. The positive charge build-up in this region is compensated by a counter charge in the electrolyte. At equilibrium, the Fermi level of the semiconductor will be equal to the redox potential level of the solution. Assuming there are no other sources of charge flow besides the semiconductor electrons and the redox system, almost all of the built-in potential drop, $V_{bi}$, will appear across the semiconductor. If surface states are present or if the electrolyte is adsorbed on the semiconductor surface, $V_{bi}$ can be either larger or smaller than the initial contact potential difference as illustrated in the simplified model of Figure 2.1.[3]

In practice, the position of the band edges (which reflect the energies of the free charge carriers) in solution is a function of various parameters in addition to the Fermi level of the redox couple in solution; these include surface states and the adsorption of adventitious ions and molecules on the semiconductor particle surface.[3] The various types of space charge layers and band bending will now be described for an n-type semiconductor.

The formation of a space charge layer requires interfacial electron transfer between the semiconductor and the electroactive species in the electrolyte medium. The valence and conduction bands are bent within this space charge layer. The four possible scenarios are depicted in Figure 2.2:[4] The *flatband condition* (case a) is the condition when there is no space charge layer. If electrons accumulate on the semiconductor side, an *accumulation layer* (case b) is obtained and the bands are bent downward. But if electrons accumulate on the electrolyte side (case c), a *depletion layer* is formed and the bands are bent upward. Depletion of the majority carriers (e) can continue to a point such that their concentration at the surface decreases below the intrinsic level.[4] With the electronic equilibrium maintained, the concentration of the minority carriers ($h^+$) in this region of the space charge layer will exceed that of the electrons, and an *inversion layer* is created (case d); as a result, the Fermi level is closer to the valence band than the conduction band, and the semiconductor then acquires p-type semiconductivity at the surface but remains n-type in the bulk.

The depletion layer, also referred to as a *Schottky barrier*, plays an important role in photocatalysis. The electrostatic field generated in the space charge layer leads to the

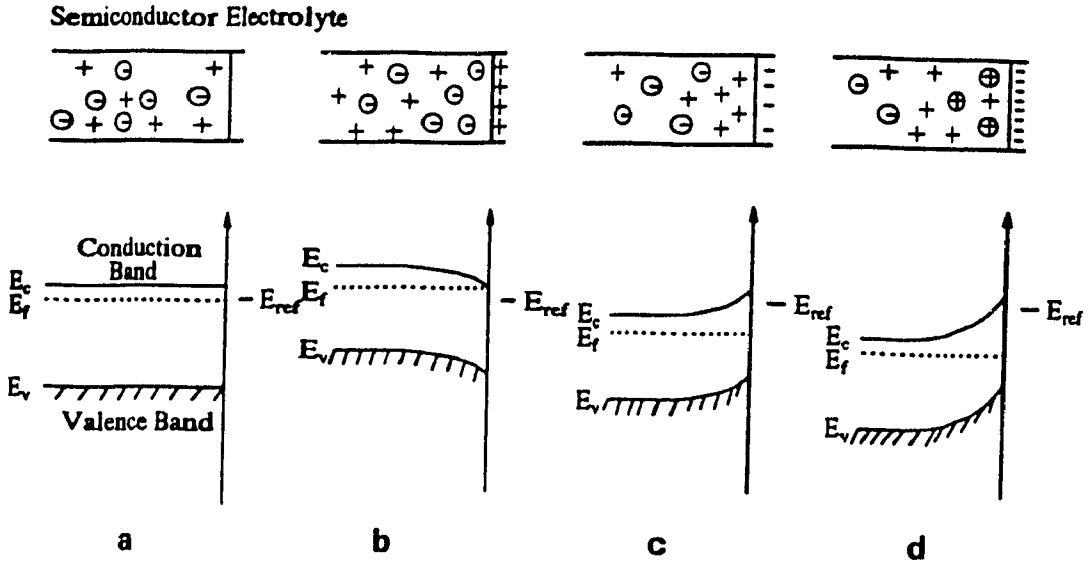


**Figure 2.2** Space charge layer formation at the n-type semiconductor-solution interface. a) Flat band situation; b) accumulation layer; c) depletion layer; d) inversion layer (Ref. 4)

separation of the photogenerated electrons and holes following light absorption. The direction of the field in a large particle of an n-type semiconductor is such that holes migrate to the irradiated side of the particle, while electrons migrate into the particle bulk, that is, to the dark side of the particle as illustrated in Figure 2.3. Both charge carriers can then undergo redox reactions at the surface as alluded to in Chapter 1.

## 2.2 NATURE OF THE $TiO_2$ PARTICLE SURFACE

Most $TiO_2$ photocatalyzed degradation reactions have been carried out with $TiO_2$ powders which are either dispersed in aqueous media or supported[5-8] on suitable

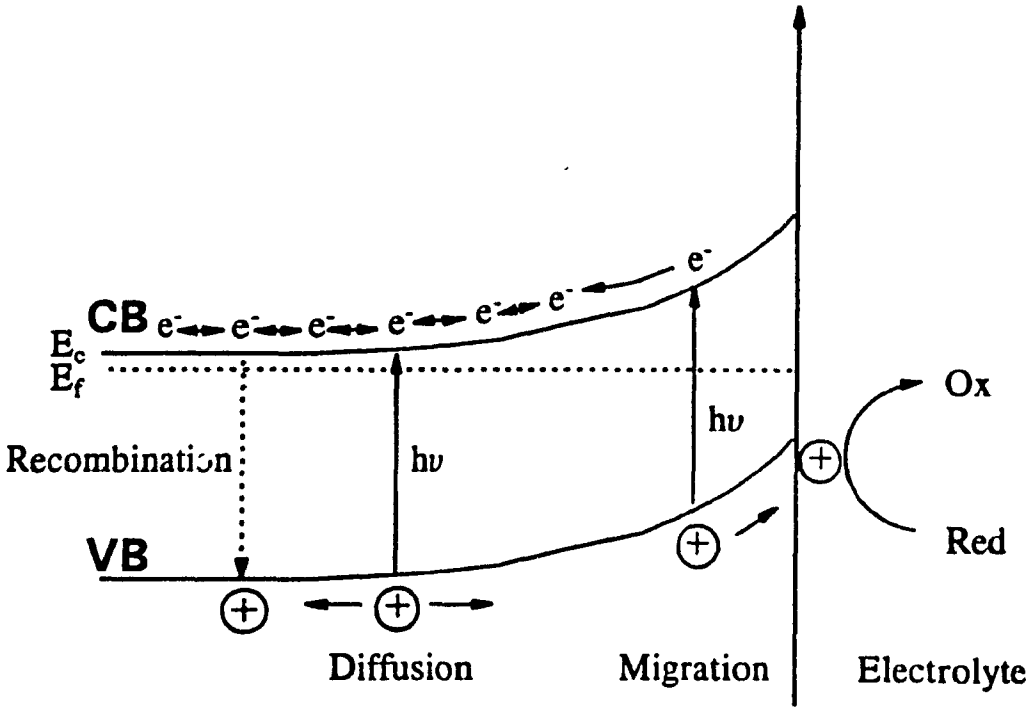


**Figure 2.3** Photoinduced charge carrier separation assisted by the electrostatic fields present in the depletion layer of a large semiconductor particle in contact with a redox system. (Adapted from reference 4).

materials. The origin and/or method of preparation of the $TiO_2$ powder has been found to greatly influence its photocatalytic properties.[9] Commercially available titania usually consists of either the *rutile* or *anatase* crystalline phases of $TiO_2$ or a mixture of both. $TiO_2$ in the anatase phase is a highly active photocatalyst in the degradation of organic pollutants (note the examples in Chapter 1). By contrast, $TiO_2$ in the rutile phase is either inactive, active, or shows negligible activity depending on the probe molecule. The inactivity of the rutile phase has been attributed partly to a higher electron/hole recombination rate.[10-12] However, this is unlikely to be the sole factor responsible as there

are a variety of physicochemical factors than can affect the photocatalytic activity: particle size distribution, texture, adsorption/desorption phenomena, nature of the interface, etc.[9] Presently, the most commonly used type of titania in heterogeneous catalysis is *Degussa P25* $TiO_2$ ($\approx$80% anatase, $\approx$20% rutile).

For semiconductor oxides in general, and $TiO_2$ in particular, the particle surface is amphoteric with sites that can be charged positively (protonated) or negatively (deprotonated) depending upon the point of zero charge (pzc is the pH at which the surface charge is zero), equations 2.1 and 2.2.[4]

$$\equiv Ti-O^- + H_2O \rightleftarrows \equiv Ti-OH + OH^- \qquad (2.1)$$

$$\equiv Ti-OH + H^+ \rightleftarrows Ti-OH_2^+ \qquad (2.2)$$

Flatband potential measurements have shown that for $TiO_2$ electrodes and colloidal particles, the redox potential of the conduction band changes by 0.059 V per pH unit, equation 2.3.[13]

$$E_{CB} = -0.1 - 0.059pH \qquad (2.3)$$

Figure 2.4 illustrates the redox potentials of the conduction and valence bands of $TiO_2$ as a function of pH; also shown are the positions of the redox potentials of the reduction and oxidation of water. Light-assisted redox reactions occurring on $TiO_2$ particles can be fine-tuned by simply varying the pH of the solution. In the case of water, both reduction and oxidation occur over the entire pH range.

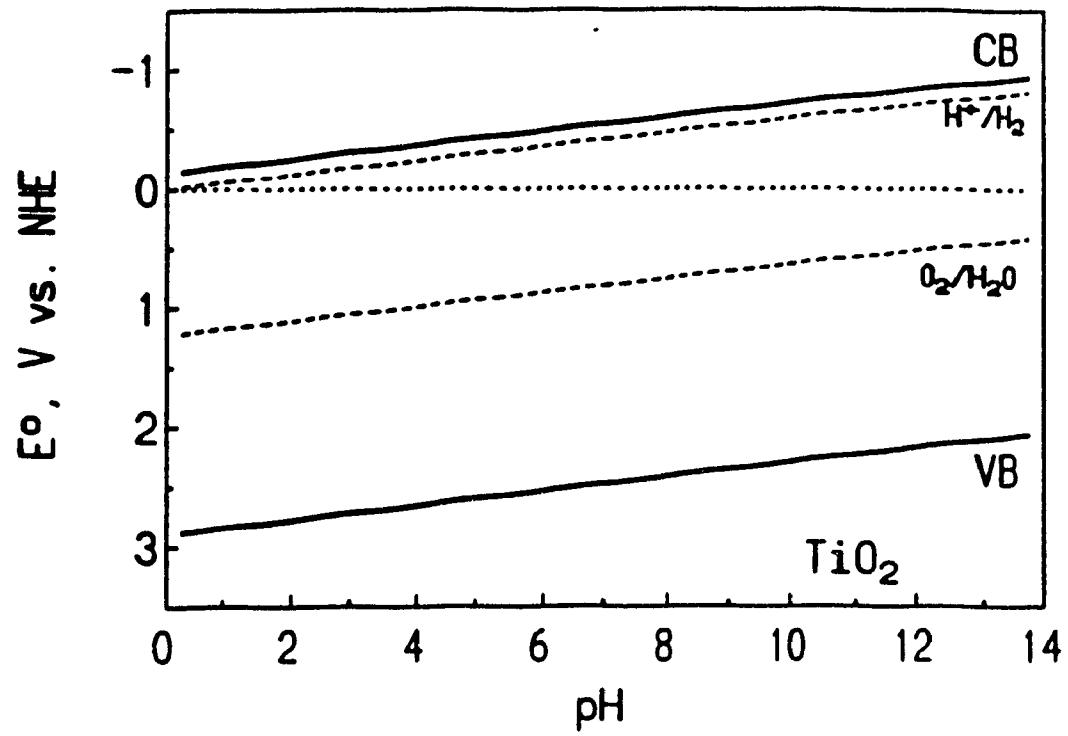


**Figure 2.4** Plot showing the effect of pH on the redox potentials of the conduction band (CB) of $TiO_2$ together with other redox couples in aqueous media.

In the dark, the surface of a $TiO_2$ particle exposed to water is partially covered (< 50%) with $OH^-$ groups.[14] The process of surface hydroxylation is believed to proceed through the chemisorption and subsequent dissociation of molecular water on coordinatively unsaturated surface $Ti^{IV}$ ions. The number of OH groups on the surface of $TiO_2$ at ambient temperature has been estimated at 7-10 OH /nm$^2$. [15-19] There are two types of surface $OH^-$ groups; both are shown in Figure 2.5. The first type bridges two surface vicinal $Ti^{IV}$ ions and has acidic character, the other is a terminal $Ti^{IV}$-OH group of basic character.[20] Other species present in the medium can also adsorb on the surface

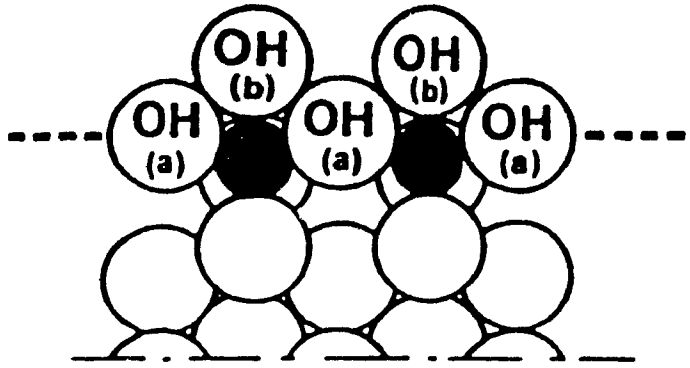


**Figure 2.5** Hydrated surface of anatase $TiO_2$ showing both types of surface $OH^-$ groups: (a) acidic doubly coordinated $OH^-$ (b) singly coordinated basic $OH^-$. (ref. 14).

either reversibly ($Cl^-$, $I^-$, and $SO_4^{2-}$) or irreversibly ($H_2PO_4^-$, $F^-$, and $NO_3^-$),[14,21-24] and can thus have an important influence on photo-redox processes.

Upon irradiation, the surface properties may change drastically thereby altering such phenomena as adsorption and desorption. The first event upon light absorption ($\lambda < 400$ nm) is the formation followed by the separation of electron/hole pairs, equation 2.4:

$$TiO_2 + h \rightarrow e^-_{CB} + h^+_{VB} \qquad (2.4)$$

In competition with recombination in the bulk, both charge carriers rapidly migrate to the surface where they are both ultimately trapped by intrinsic traps [($Ti^{IV}$ $O^{2-}$-$Ti^{IV}$) for the hole and (-$Ti^{IV}$-) for the electron] and extrinsic traps [surface adsorbed electron

donors ($D_{ads}$) and acceptors ($A_{ads}$)], equations 2.5-2.8.[25-26]

$$(Ti^{IV}-O^{2-}-Ti^{IV})_{subsurface} + h^{+}_{VB} \rightarrow (Ti^{IV}-O^{-}\bullet-Ti^{IV})_{subsurface} \quad (2.5)$$

$$(-Ti^{IV})_{surface} + e^{-}_{CB} \rightarrow (-Ti^{III})_{surface} \quad (2.6)$$

$$h^{+}_{VB} + D_{ads} \rightarrow D^{+}_{ads} \quad (2.7)$$

$$e^{-}_{CB} + A_{ads} \rightarrow A^{-}_{ads} \quad (2.8)$$

Hole trapping on the surface may occur via equations 2.9 or 2.10 for hydroxylated and hydrated anatase $TiO_2$ particles, respectively, to yield surface-bound •OH radicals.[25,26]

$$(Ti^{IV}-O^{2-}-Ti^{IV})-OH^{-} + h^{+}_{VB} \rightarrow (Ti^{IV}-O^{2-}-Ti^{IV})-OH\bullet \quad (2.9)$$

$$(Ti^{IV}-O^{2-}-Ti^{IV})-OH_2 + h^{+}_{VB} \rightarrow (Ti^{IV}-O^{2-}-Ti^{IV})-OH\bullet + H^{+} \quad (2.10)$$

To prevent rapid electron/hole recombination on the surface, electrons can be scavenged by pre-adsorbed molecular oxygen to give the superoxide radical anion $(O_2^{-}\bullet)_{ads}$ (equation 2.11) which can be reduced further to the peroxide dianion $(O_2^{2-})_{ads}$ (equation 2.12). Alternatively, surface peroxo species can be formed[27-32] either by hydroxyl radical pairing (equation 2.13) or by sequential two hole capture by the same OH group (equations 2.9 and 2.15) or by dismutation of $O_2^{-}\bullet$ via equation 2.16.

$$O_{2\ (ads)} + e^-_{CB} \rightarrow O_2^{-}\bullet_{(ads)} \quad (2.11)$$

$$O_2^{-}\bullet_{(ads)} + e^-_{CB} \rightarrow (O_2^{2-})_{surface} \quad (2.12)$$

$$2(\bullet OH)_{surface} \rightarrow (H_2O_2)_{surface} \quad (2.13)$$

$$(H_2O_2)_{surface} \rightarrow (O_2^{2-})_{surface} + 2H^+ \quad (2.14)$$

$$(Ti^{IV}\text{-}O^{2-}\text{-}Ti^{IV})\text{-}OH\bullet + h^+_{VB} \xrightarrow{-H^+} (O)_{surface} \rightarrow \tfrac{1}{2}\, O_{2\ (ads)} \quad (2.15)$$

$$2O_2^{-}\bullet_{(ads)} \rightarrow O_{2\ (ads)} + O^{2-}_{2\ (ads)} \quad (2.16)$$

Most photocatalyzed degradation reactions using $TiO_2$ have historically been carried out in acidic media (pH 3). At this pH, many other reactions are presumed to occur on the particle surface; these are summarized below:[26]

$$O_2^{-}\bullet_{(ads)} + H^+ \rightarrow HO_2\bullet_{(ads)} \quad (2.17)$$

$$2HO_2\bullet \rightarrow H_2O_2 + O_2 \quad (2.18)$$

$$H_2O_2 + O_2^{-}\bullet \rightarrow OH\bullet + OH^- + O_2 \quad (2.19)$$

$$H_2O_2 + e^-_{CB} \rightarrow OH\bullet + OH^- \quad (2.20)$$

$$H_2O_2 + h^+_{VB} \rightarrow O_2 + 2H^+ \quad (2.21)$$

$$O_2^-\bullet + HO_2\bullet \rightarrow O_2 + HO_2^- \xrightarrow{H^+} H_2O_2 \quad (2.22)$$

Clearly, illumination of the $TiO_2$ particle surface in the presence of organics results in a chain of events that ultimately leads to the photo-oxidative mineralization of these organic pollutants.

## 2.3 NATURE OF THE OXIDIZING SPECIES

The chemical evidence to date supports the notion that the •OH radical is the principal oxidizing species involved in the photomineralization of most organic compounds examined. One piece of evidence is the detection of hydroquinone, catechol and other hydroxylated intermediates in the photodegradation of phenol[11] (Chapter 1; equation 1.2). Similar hydroxylated species (3-fluorocatechol, fluorohydroquinone, 4-fluorocatechol, and 1,2,4-trihydroxybenzene) have been identified in the photo-oxidation of 3-fluorophenol.[33] Additional support for •OH being the primary oxidant in aqueous media comes from kinetic deuterium isotope studies[34] which showed the rate limiting step in the photo-oxidation of isopropanol on $TiO_2$ to be the formation of active oxygen species through a reaction involving water.

Two mechanisms have traditionally been proposed for the photodegradation of organic substrates. The *first mechanism* postulates that the photogenerated holes react primarily with $H_2O$ or $OH^-$ on the surface of $TiO_2$ (equations 2.9 and 2.10) to produce surface bound •OH radicals which may subsequently react with the organic substrates either from their adsorbed state or following desorption to the solution. The *second mechanism* proposes a direct reaction between the hole and the organic substrate. The two mechanisms cannot be differentiated on the basis of product analysis alone since both pathways lead to the formation of the same products. For example, in the oxidation of phenol, •OH addition to the ring directly results in the formation of the dihydroxy-cyclohexadienyl radical (equation 2.23) and subsequently in the formation of hydroxylation products. Direct hole oxidation of phenol would produce a cation radical which can subsequently undergo hydration, followed by the formation of the dihydroxy-cyclohexadienyl radical, and ultimately hydroxylation products (equation 2.24).[26]

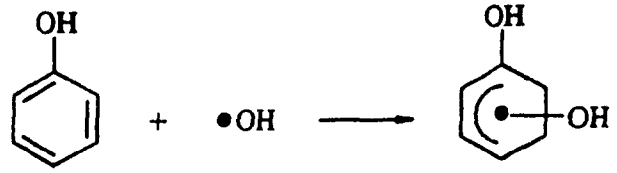


(2.23)

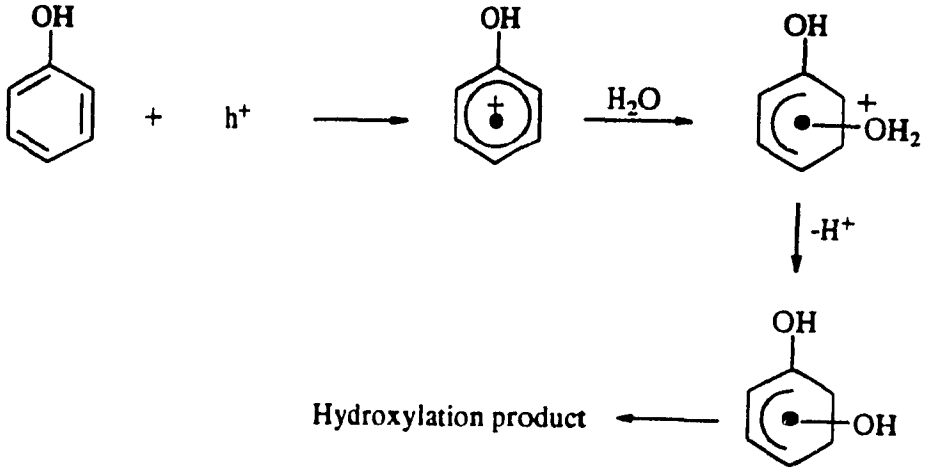


(2.24)

The nature of the intermediates implicated in the photo-oxidation of water with $TiO_2$ has been identified in several reports using spin traps by the electron spin resonance (ESR) technique. Using a prereduced anatase powder in aqueous solutions (pH 4 and 7) at ambient conditions, Jaeger and Bard[35] and Harbour *et al.*[36] identified only the anodically formed •OH radical; these results have since been confirmed by other workers.[37-46] A low-temperature (77 K) ESR study identified the •OH radical (no spin traps);[43] however, this was recently disputed by Howe and Grätzel[37] who found no evidence for •OH species, even at 4.2 K, but inferred that the ESR signal seen by Anpo *et al.*[43] is attributable to the $O^{-}$• radical anion resulting from trapping positive holes at lattice oxide ions (equation 2.5). They further postulated[37] that the •OH radical identified by spin trapping methods is not the primary product of hole trapping, but originates as a transient intermediate of photo-oxidation.

Unfortunately, ESR investigations have provided no conclusive evidence as to the nature of the primary radical intermediate(s) in the $TiO_2$ photo-oxidation of water. The nature of the observed radical species appears to depend on the origin and pretreatment of the $TiO_2$ sample, on the conditions and extent of its reduction, on the extent of surface hydroxylation, and on the presence of molecular oxygen, among other conditions.[14]

Competition experiments which have been carried out in the presence of inhibitors (•OH radical scavengers) as well as the identification of intermediate products and their relative ratios has led some authors to infer that photo-oxidation of organics over light-activated $TiO_2$ (and ZnO) implicates both •OH radicals and $h^+$.[47-51] Oxidation of acetate at illuminated $TiO_2$/water interfaces produced both the hole oxidation products ($CO_2$ and

methyl radicals), and •OH radical oxidation products (glycolate and glyoxylate).[49] The quantitative inhibition by ethanol (a •OH scavenger) of the photo-oxidation of dichlorobenzene over aqueous ZnO dispersions has led to various hydroxylated intermediates. This was taken[51] as evidence that the •OH species is the sole oxidant. By contrast, the photo-oxidation of furfuryl alcohol[50] and monochlorophenols[48] has been suggested to proceed by both pathways. For the phenols, the major pathway ($\approx$ 65%) was oxidation via •OH radicals and the remainder via direct hole oxidation.[48]

Some years ago, it was established that complete degradation of organics over light-activated $TiO_2$ suspensions does not occur if either $H_2O$ and/or molecular $O_2$ are absent.[52] When photooxidations are carried out in redox inert solvents such as acetonitrile and dichloromethane, only partial oxidation ensues.[53,54] In the absence of water, mineralization of the organic substrate ***does not occur***; only partially oxidized products, often involving photo-oxygenation, have been isolated.[53] The principal oxidizing species in these cases has been described as $h^+$.

Early evidence for direct $h^+$ oxidation, as the principal step was reported in a study by Boonstra and Mutsaers[17] who noted that •OH is unlikely to participate in reactions involving $TiO_2$. Modification of the $TiO_2$ surface with chlorosilicon compounds led to a decrease in the activity for several photocatalyzed reactions, yet the effect was smaller than expected based on the extent of the eliminated hydroxyl groups. The enhanced yield of phenol photo-oxidation in de-oxygenated suspensions of ZnO, containing $Hg^{2+}$ ions as e scavengers, has been taken by Domenech *et al.*[55] as "conclusive" evidence for a direct hole oxidation pathway.

Additional evidence for direct hole oxidation comes from a recent study[56] which failed to detect any of the expected •OH-adducts following diffuse reflectance flash photolysis of several $TiO_2$/substrate combinations. Unfortunately, experimental difficulties together with the fact that the •OH-adduct of 2,4,5-trichlorophenol possesses absorption bands in the UV region where $TiO_2$ absorption interferes, thereby obstructing observation of such species, do not rule out the participation of OH• radicals in photo-oxidations, possibly by an electron transfer process via an inner sphere pathway. As noted recently by Fox,[53] the possibility that such single electron redox reactions could be mediated by trapped hole equivalents either on the metal oxide surface (as, for example, by a surface bound •OH radical) or by a sub-surface lattice oxygen situated directly beneath an adsorbed hydroxide ion cannot be ruled out.

It must be noted that assigning either the $h^+$ or the •OH radical as the oxidant in specific photo-oxidations must be based on strong, direct experimental evidence. Many of the previous studies have been inconclusive on this issue, despite the various claims to the contrary.

A recent pulse radiolytic study[57] established that •OH reacts with $TiO_2$ in aqueous media at a diffusion controlled rate ($\approx 6 \times 10^{11}$ $M^{-1}s^{-1}$); desorption of •OH to the solution was thought unlikely. The surface trapped hole is indistinguishable from a surface bound •OH radical, $(Ti^{IV}\text{-}O^{2-}\text{-}Ti^{IV})\text{-}OH•$, equation 2.9. The debate between $h^+$ versus •OH oxidation then becomes moot. In light of this study, no distinction is made in this thesis between a trapped hole and a surface bound •OH radical.

## 2.4 SURFACE VERSUS SOLUTION REACTIONS

Another point of contention, often raised in discussions of heterogeneous photocatalytic processes, is whether the initial oxidation of the organic substrate occurs on the photocatalyst's surface or in solution.

In analyzing the kinetic data of photocatalyzed oxidations (and reductions), mediated by photo-activated semiconductor particles, several studies in the 1980's literature have fitted the results to the simple rate expression of the form of equation 2.25.[5,58,59]

$$r_{initial} = \frac{kKC}{(1 + KC)} \qquad (2.25)$$

(where $k$ is the observed rate constant, $K$ is the adsorption coefficient of a given substrate and $C$ is the initial concentration of substrate)

Determination of initial rates of oxidation as a function of increased concentration of organic substrate, for a given photocatalyst loading, commonly yields the type of plots illustrated in Figure 2.6. The similarities of equation 2.25 to a Langmuir adsorption isotherm,[60] have led to inferences that the mineralization process takes place on the photocatalyst's surface.[61] Similar plots are also obtained in homogeneous media if one considers a bimolecular reaction between reactants X and Y. The initial rate will at first increase with increases in the concentration of the Y (or X) substrate; however, the kinetics eventually become pseudo first order, and will yield the same type of plot. Thus, a Langmuirian type behaviour does not guarantee a surface occurring process. In fact, the behaviour may have nothing to do with the Langmuir-Hinshelwood model so often

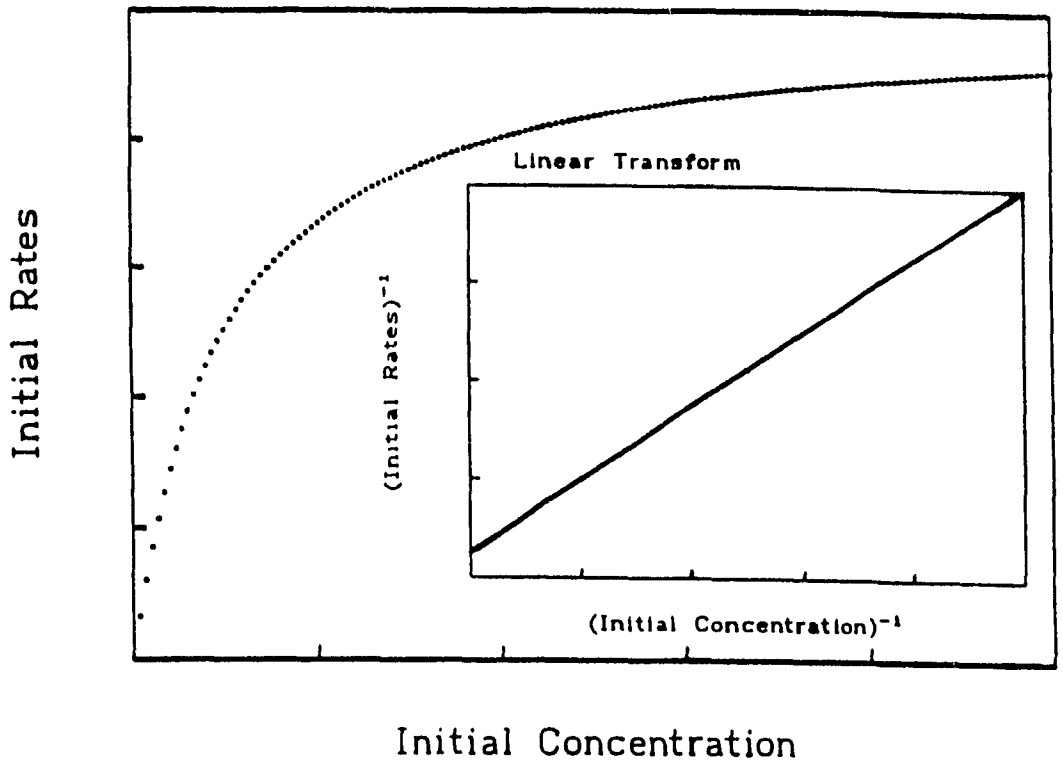


**Figure 2.6** Saturation-type kinetic plot of initial rates versus [reactant]; the inset shows the linear transform of equation 2.25 from which the rate constant k and the equilibrium constant K can be estimated from the intercept and slope, respectively.

invoked in the past literature (see below).

An extensive treatment[62] of the kinetics involved in the photocatalyzed oxidations of organic substrates on an irradiated semiconductor, under a variety of conditions, has recently examined whether it was possible to differentiate surface reactions from solution bulk reactions on the basis of observed kinetics. The derived kinetic model which considered four cases implicating •OH radical attack of the organic substrate, namely (i) reaction occurs while both species are adsorbed, (ii) reaction occurs between the adsorbed substrate and the *free* •OH radical, (iii) reaction occurs between surface bound •OH radical and the substrate in solution, and (iv) reaction occurs while both species are

in solution, showed that the analytical form of the derived complex rate expressions was identical for all four cases and was similar to that of the Langmuir model (equation 2.25). Clearly, kinetic studies alone are silent as to whether photo-oxidations are surface processes or solution processes. Other studies have since confirmed this difficulty.[33,63]

In their elegant study, Turchi and Ollis[62] inferred that the photo-oxidative process need not occur at the catalyst's surface, as the reactive •OH species can in principle diffuse several hundred angstroms in the solution. A recent photoelectrochemical study[64] is strongly supportive of a solution •OH reactive species in photocatalyzed oxidations. By contrast, an ESR study[65] concludes that the •OH radical does all its work on the catalyst's surface, and that photo-oxidation is a surface process.

It is clear that one technique alone cannot provide unambiguous conclusions but rather gives one piece of the puzzle which together with other results might lead to a reasonable understanding of the complex events in heterogeneous photocatalysis. To date, the most convincing results are those of the pulse radiolytic study[57] which established that •OH reacts with $TiO_2$ in aqueous media at a diffusion controlled rate and that desorption of these radicals is highly unlikely. Surface bound hydroxyl radicals can account for all the oxidations which have previously been attributed to free OH• radicals in solution. The formation of $H_2O_2$ and hydroxylated intermediate products can all occur on the surface via reactions of this •OH species. Free hydroxyl radicals are believed to play only a minor role, if any.

Further evidence that the •OH radical is surface bound, and is unlikely to desorb

into the solution, stems from a recent study[66] which noted that decafluorobiphenyl (DFBP) is strongly adsorbed (> 99%) on metal oxide particle surfaces ($Al_2O_3$ and $TiO_2$) and does not easily exchange between the two metal oxides (< 5%). When adsorbed on the alumina surface in dispersions into which $H_2O_2$ or a $TiO_2$ colloidal sol (particle size ca. 0.05 $\mu$m) was added, followed by uv irradiation, the DFBP photodegraded. This indicates that the •OH radical from $H_2O_2$ and $TiO_2$ sols (particles adsorbed on alumina) migrate to the reaction site on the DFBP/$Al_2O_3$ system to initiate the photo-oxidative events. By contrast, if $TiO_2$ beads (size ca. 1000 $\mu$m) were used instead of $H_2O_2$ or the $TiO_2$ sol to generate the oxidizing species, the photodegradation was nearly suppressed and the behaviour of the system was identical to the behaviour of the DFBP/$Al_2O_3$ system alone, irradiated with uv light under otherwise identical conditions. Pentafluorophenol, which readily exchanges between the two metal oxide surfaces, easily undergoes photodegradation under the same conditions. Thus, the photogenerated oxidizing species (•OH radical) does not migrate far from the photogenerated active sites on $TiO_2$, and the degradation process must occur at the photocatalyst surface or within a few atomic distances from the surface.[66]

Additional evidence that the photodegradation reactions are surface reactions comes from a recent work by Pelizzetti *et al.*[67] When atrazine was used as the probe molecule in comparing the activity and selectivity between a "virgin" sample of $TiO_2$ used for the first time and then used in several consecutive cycles, a significant change in selectivity was noticed as significant variations occurred in the temporal distributions of the intermediate species and products formed.[67] However, if the $TiO_2$ material was

initially treated by irradiating it in aqueous media for several hours and subsequently filtering and drying it, the product distribution no longer showed these variations from cycle to cycle.[67] This is supportive of the fact that the surface is implicated in the photo-oxidative process. One would not expect a reaction occurring in solution to be sensitive to changes taking place on the surface since the •OH radical is always the same irrespective of its formation history.

A general consensus is thus emerging, based on the evidence presented, that the degradation process is a surface process, with both the oxidizing species and the organic substrate present on the surface.

## 2.5 RESEARCH FOCUS

Based on the discussions above, it appears that surface-bound •OH radicals (trapped holes) play a major role in the photodegradation of the organic compounds examined. The role of the electrons concurrently photoproduced with the holes has not been established. The present view is that electrons are consumed via reaction 2.11 to produce the superoxide radical anion, $O_2^{-}$•. This is supported by the following facts: (a) the degradation reaction does not proceed in the absence of oxygen[52], and (b) $O_2^{-}$• radicals have been observed upon irradiation of $TiO_2$ in the presence of oxygen.[68] It is, however, not inconceivable that the electrons react via a parallel process with the organic substrates. Reductive dehalogenation of halo-aromatics is known to occur.[69]

In order to acquire a better understanding of the photocatalytic process, it is necessary to examine the reactions of both the oxidizing and reducing species with

various substrates. This is a difficult task in heterogeneous media due to the large number of processes that may take place within the particle (electron/hole recombination, diffusion to the surface), on the particle surface (equations 2.5-2.16), and in solution (equations 2.17-2.22); it is therefore unrealistic to attempt to isolate one process and examine it in detail under these conditions. Pulse radiolysis of water yields the quantitative production of both •OH and $e_{aq}^-$ in homogeneous media and affords a controlled means of examining separately the actions of each on organic substrates. Two pulse radiolytic studies were undertaken in this work; the aim of these studies was to examine the kinetic and spectroscopic properties of the organic radical species formed upon reaction of organic substrates with the primary radicals (•OH, $e_{aq}^-$). The first study examined the reaction pathways of a series of pentahalophenols with both •OH and $e_{aq}^-$. The second study examined the reaction of a series of dimethyl phenols with •OH radicals. It is hoped that examination of these reactions in homogeneous solution will shed some light on the pathways of photocatalytic degradation in heterogeneous media.

The sonication of water also allows for the production of •OH radicals in a homogeneous medium; the two principal products resulting from the sonication of water are $H_2O_2$ and $H_2$ with •OH radicals and H• atoms as the intermediates.[70,71] Because •OH radicals play a role in photodegradation reactions, and the fact that the •OH radical can also be generated sonochemically, the sonochemical oxidation of phenol, first reported by Zechmeister *et al*[72], Lur'e[73] and subsequently, by Chen and co-workers[74], has been reexamined under conditions different from those reported earlier. Special emphasis is placed on intermediate identification and mechanistic aspects of the sono-induced process.

# REFERENCES


1. Reiss, H., *J. Phys. Chem.*, **1985**, *89*, 3783.

2. Gerischer, H., *Pure & Appl. Chem.*, **1980**, *52*, 2649.

3. Lewis, N.S., Rosenbluth, M.L., in: *"Photocatalysis: Fundamentals and Applications"*; Serpone, N. and Pelizzetti, E., Eds., Wiley, New York, **1989**.

4. Grätzel, M., *"Heterogeneous Photochemical Electror Transfer"*, CRC Press, Boca Raton, **1989**.

5. Al-Ekabi, H., Serpone, N., *J. Phys. Chem.*, **1988**, *92*, 5726.

6. Serpone, N., Borgarello, E., Harris, R., Cahill, P., Borgarello, M., Pelizzetti, E., *Sol. Energy Mater.*, **1986**, *14*, 121.

7. Matthews, R.W., *J. Catal.*, **1986**, *97*, 565

8. Matthews, R.W., *Water Res.*, **1986**, *20*, 569.

9. Sclafani, A., Palmisano, L., Schiavello, M., *J. Phys. Chem.*, **1990**, *94*, 829.

10. Kawagushi, H., *Environ. Technol. Lett.*, **1984**, *5*, 471.

11. Okamoto, K., Yamamoto, Y., Tanaka, H., Tanaka, M., Itaya, A., *Bull. Chem. Soc. Jpn.*, **1985**, *58*, 2015.

12. Augugliaro, V., Palmisano, L., Sclafani, A., Minero, C., Pelizzetti, E., *Toxicol. Environ. Chem.*, **1988**, *16*, 89.

13. Duonghong, D., Ramsden, J.J., Grätzel, M., *J. Am. Chem. Soc.*, **1982**, *104*, 2977.

14. Augustynski, J., *Structure and Bonding*, **1988**, *69*, 1.

15. Suda, Y., Morimoto, T., *Langmuir*, **1987**, *3*, 786.

16. Morishige, K., Kanno, F., Ogawara, S., Sasaki, S., *J. Phys. Chem.*, **1985**, *89*, 4404.

17. Boonstra, A.H., Mustaers, C., *J. Phys. Chem.*, **1975**, *79*, 1694.

18. Munuera, G., Rives-Arnau, V., Saucedo, A., *J. Chem. Soc. Faraday Soc. 1*, **1979**, *75*, 736.

19. Doremieux-Morin, C., Enriquez, M.A., Sanz, J., Fraissard, J., *J. Colloid Interfac. Sci.*, **1983**, *95*, 502.

20. Sham, T.K., Lazarus, M.S., *Chem. Phys. Lett.*, **1979**, *68*, 426.

21. Flaig-Baumann, R., Herrmann, M., Boehm, H.P., *Z. Anorg. Chem.*, **1970**, *372*, 296.

22. Herrmann, M., Kaluza, U., Boehm, H.P., *Z. Anorg. Chem.*, **1970**, *372*, 308.

23. Munuera, G., Navio, J.A., Rives-Arnau, V., in: *"Fourth International Conference on Photochemical Conversion and Storage of Solar Energy"*, Rabani, J., Ed., Jerusalem, p. 141, **1982**.

24. Munuera, G., Gonzales-Elipe, A.R., Rives-Arnau, V., Navio, J.A., Malet, P., Soria, J., Conesa, J.C., Sanz, J., in *"Studies in Surface Science and Catalysis"*, Che M., Bond, G.C., Eds., Amsterdam, p. 113, vol. 21, **1985**.

25. Howe, R.F., Grätzel, M., *J. Phys. Chem.*, **1987**, *91*, 3906.

26. Serpone, N., Pelizzetti, E., Hidaka, H., in: *Proceedings of the Solar Energy Meeting IPS-9*, Beijing, China, *In press 1992*, and references therein.

27. Markham, M.C., Laidler, J.K., *J. Phys. Chem.*, **1953**, *57*, 363.

28. Oosawa, Y.O., Grätzel, M., *J. Chem. Soc. Faraday Trans. 1*, **1988**, *84*, 197.

29. Thampi, K.R., Rao, M.S., Schwartz, W., Gratzel, M., Kiwi, J., *J. Chem. Soc. Faraday Trans. 1*, **1988**, *84*, 1703.

30. Gu, B., Kiwi, J., Grätzel, M., *Nouv. J. Chim.*, **1985**, *9*, 539

31. Muraki, H., Saji, T., Fujihira, M., Aoyagui, S., *J. Electroanal Chem.*, **1984**, *169*, 319.

32. Grätzel, C.K., Jirousek, M., Grätzel, M., *J. Mol. Catal.*, **1990**, *60*, 375.

33. Minero, C., Aliberti, C., Pelizzetti, E., Terzian, R., Serpone, N., *Langmuir*, **1991**, *7*, 928.

34. Cunningham, J., Srijaranai, S., *J. Photochem. Photobiol. A: Chem.*, **1988**, *43*, 329.

35. Jaeger, C.D., Bard, A.J., *J. Phys. Chem.*, **1979**, *83*, 3146.

36. Harbour, J.R., Tromp, J., Hair, M.L., *Can. J. Chem.*, **1985**, *63*, 204.

37. Howe, R.F., Grätzel, M., *J. Phys. Chem.*, **1987**, *91*, 3906.

38. Avudaithai, M., Kutty, T.R.N., *Mat. Res. Bull.*, **1988**, *23*, 1675.

39. Volz, H.G., Kaempf, G., Fitzky, H.G., Klaeren, A., *ACS Symp. Ser.*, **1981**, *151*, 163.

40. Grätzel, M., Howe, R.F., *J. Phys. Chem.*, **1990**, *94*, 2566.

41. Maldotti, A., Amadelli, R., Bartocci, C., Carassiti, V., *J. Photochem. Photobiol. A: Chem.*, **1990**, *53*, 263.

42. Howe, R.F., *Adv. Coll. Interfac. Sci.*, **1982**, *18*, 1.

43. Anpo, M., Shima, T., Kubokawa, Y., *Chem. Lett.*, **1985**, 1799.

44. Jaeger, C.D., Bard, A.J., *J. Phys. Chem.*, **1979**, *83*, 3146.

45. Ceresa, E.M., Burlamacchi, L., Visca, M., *J. Mater. Sci.*, **1983**, *18*, 289.

46. Bahnemann, D.W., Henglein, A., Spanhel, L., *Faraday Discuss. Chem. Soc.*, **1984**, *78*, 151.

47. Matthews, R.W., *J. Chem. Soc. Faraday Trans. 1*, **1984**, *80*, 457.

48. Sehili, T., Boule, P., Lemaire, J., *J. Photochem. Photobiol. A: Chem.*, **1989**, *50*, 117.

49. Bahnemann, D.W., in *"Proc. Symp. Semiconductor Photoelectrochemistry"*, C. Koval, Ed., The Electrochemical Society, Inc., Pennington, N.J., **1991**.

50. Richard, C., Lemaire, J., *J. Photochem. Photobiol. A: Chem.*, **1990**, *55*, 127.

51. Sehili, T., Boule, P., Lemaire, J., *J. Photochem. Photobiol. A: Chem.*, **1989**, *50*, 103.

52. Barbeni, M., Pramauro, E., Pelizzetti, E., Borgarello, E., Grätzel, M., Serpone, N., *Nouv. J. Chim.*, **1984**, *8*, 547.

53. Fox, M.A., Draper, R.B., Dulay, M., O'Shea, K., in *"Photochemical Conversion and Storage of Solar Energy"*, Pelizzetti, E., Schiavello, M., Eds., Kluwer Academic Publishers, Dordrecht, **1991**.

54. Fox, M.A., in *"Photocatalysis - Fundamentals and Applications"*, Serpone, N. and Pelizzetti, E., Eds., Wiley-Interscience, New York, **1989**, ch. 13, pp.421-455.

55. Peral, J., Casado, J., Domenech, J., *J. Photochem. Photobiol. A: Chem.*, **1988**, *44*, 209.

56. Draper, R.B., Fox, M.A., *Langmuir*, **1990**, *6*, 1396.

57. Lawless, D., Serpone, N., and Meisel, D., *J. Phys. Chem.*, **1991**, *95*, 5166.

58. Ollis, D.F., Pelizzetti, E., Serpone, N., in *"Photocatalysis - Fundamentals and Applications"*, Serpone, N., Pelizzetti, E., Eds., Wiley-Interscience **1989**, pp. 603-637.

59. Al-Ekabi, H., Serpone, N., Pelizzetti, E., Minero, C., Fox, M.A., Draper, A.B., *Langmuir*, **1989**, *5*, 250.

60. Pichat, P., Herrmann, J.M., in *"Photocatalysis - Fundamentals and Applications"*, Serpone, N., Pelizzetti, E., Eds., Wiley-Interscience **1989**, pp. 218-250.

61. Matthews, R.W., *Water Res.*, **1990**, *24*, 653.

62. Turchi C.S., Ollis, D.F., *J. Catal.*, **1990**, *122*, 178.

63. Terzian, R., Serpone, N., Minero, C., Pelizzetti, E., *J. Catal.*, **1991**, *128*, 352.

64. Peterson, M.W., Turner, J.A., Nozik, A.J., *J. Phys. Chem.*, **1991**, *95*, 221.

65. a) Bolton, J.R., *Proc. 13th. D.O.E. Solar Energy Conference*, U.S. Department of Energy, Argonne National Laboratory, Argonne, Illinois, **1989**, vol. 13.
b) Bolton, J.R., *Advanced Oxidation Symposium*, Toronto, Canada, June 4-5, **1990**.
c) Sun, L., Schindler, K.-M., Hoy, A.R., Bolton, J.R., *Proc. Symp. Environmental Aspects of Surface and Aquatic Photochemistry*, American Chemical Society Meeting, April 5-10, **1992**, San Francisco, CA., p. 259.

66. Minero, C., Catozzo, F., Pelizzetti, E., *Langmuir*, **1992**, *7*, 481.

67. Pelizzetti, E., Minero, C., Borgarello, E., Tinucci, L., Serpone, N., *submitted*, **1992**.

68. Anpo, M., Kubokawa, Y., *Rev. Chem. Int.*, **1987**, *8*, 105, and references therein.

69. Getoff, N., Solar, S., *Radiat. Phys. Chem. (Int. J. Radiat. Appl. Instrum. Part C)*, **1986**, *28*, 443.

70. Suslick, K.S., in: *"Ultrasound: Its Chemical, Physical, and Biological Effects"*, Suslick, K.S., ed., VCH Publishers, New York, **1988**, p. 123, and references therein.

71. Riesz, P., Berdahl, D., Christman, C.L., Environ. Health Perspect., **1985**, *64*, 233.

72. (a) Zechmeister, L., Wallcave, L., *J. Am. Chem. Soc.*, **1955**, *77*, 2953.
(b) Zechmeister, L., Magoon, E.F., *J. Am. Chem. Soc.*, **1956**, *78*, 2149.
(c) Currell, D.L., Zechmeister, L., *J. Am. Chem. Soc.*, **1958**, *80*, 207.

73. Lur'e, Y.Y., *Russ. J. Phys. Chem.*, **1963**, *37*, 1264.

74. Chen, J.W., Smith, G.V., *"Feasibility Studies of Applications of Catalytic Oxidation in Wastewater"*, United States Environmental Protection Agency, Report No. 17020 ECI 11/**1971**.

# CHAPTER 3

# EXPERIMENTAL

## 3.1 PHOTOCATALYSIS EXPERIMENTS

### 3.1.1 Cresols

**Chemicals:** *o*-, *m*- and *p*-Cresol, methylhydroquinone, 4- and 3-methylcatechol, 2-methylresorcinol, and orcinol monohydrate (3-methylresorcinol) (Aldrich, ≥ 99%) were used as supplied without further treatment. Titanium dioxide was Degussa P-25 (BET surface area, 55 $m^2/g$; mostly in the anatase form (≈ 80% anatase, 20 % rutile) and consisting of 99.5% $TiO_2$, and < 0.3% $Al_2O_3$, < 0.3% HCl, < 0.2% $SiO_2$ and < 0.01% $Fe_2O_3$ as impurities some of which are probably segregated on the particle surface).[1] Water was doubly distilled throughout. The mobile phase used for the HPLC analyses consisted of a mixture of methanol/water/*o*-phosphoric acid in either a 40/59.9/0.1 or 25/75/0.1 ratio. Methanol (BDH, omnisolv grade), and *o*-$H_3PO_4$ (Fisher, HPLC grade) were used as received.

**Procedures:** Irradiation (see below for description of lamp) was carried out at wavelengths above 220 nm on 50 mL samples (unless otherwise noted) exposed to air and efficiently stirred. The appropriate quantity of a stock solution of the cresol was added to a previously weighed amount of $TiO_2$ (unless otherwise stated: 100 mg to give

a 2 g/L catalyst loading. The pH of the stock solutions was adjusted with HCl (pH 3) or with NaOH (pH 12) as required. Aliquots were taken at various time intervals, filtered to remove suspended particles of $TiO_2$, and then analyzed by HPLC or used to record absorbance spectra as required; the diffuse reflectance spectra of the catalyst powder remaining on filtration of the aliquots were also recorded when colour changes were observed on the suspended particles. For studies at pH 12, the aliquots were acidified prior to HPLC analysis (to prevent deterioration of the column).

Typically, two control experiments were carried out for each set of experiments. The first one consisted of monitoring the changes in concentration of an identical solution to the one being irradiated (i.e. with catalyst present); this solution was however stirred in the dark. This was done to take into account the thermal component (if any) of the photodegradation reactions. The second experiment consisted of irradiating the cresol solution in the absence of catalyst to account for any direct photolysis.

For *m*-cresol, the degradation was also carried out in an oxygen-saturated atmosphere; the flask was oxygen purged for about 10 min. Typically, the temporal course of the mineralization was sampled at ca. 30 min. intervals. The flask was removed from the irradiation source, and a suitable aliquot (about 2 mL) was taken; subsequently, the flask was once again purged with oxygen for 5 min. followed by continued irradiation.

Where $CO_2$ evolution was monitored, 25 mL solutions were used; the flasks were sealed with rubber septa and aluminum seals. When the experiment was carried out in an oxygen atmosphere, the samples were purged for about 15 min with oxygen prior to

irradiation. At the indicated time intervals, samples of gas were taken from the headspace volume and analyzed by gas chromatography (see below).

### 3.1.2 Methylhydroquinone and 4-Methylcatechol

**Chemicals:** Methylhydroquinone (MHQ, > 99 %) and 4-methylcatechol (4-MCC, > 99%) were purchased from Aldrich and were used as received. $TiO_2$ (Degussa P25) was described earlier. Doubly distilled water was used throughout. The mobile phase used for the HPLC analyses consisted of a mixture of methanol/water/*o*-phosphoric acid in a 25/75/0.1 ratio. Methanol (BDH, omnisolv grade) and *o*-$H_3PO_4$ (Fisher, HPLC grade) were used as received.

**Procedures:** Unless otherwise noted, uv/visible irradiation was carried out on aerated 50 mL samples which were efficiently stirred. The appropriate quantity of a stock solution of MHQ or 4-MCC was added to a previously weighed amount of $TiO_2$ powder (100 mg/50 mL to give a concentration of $TiO_2$ of 2g/L). The pH of the sample was adjusted with HCl. Where the evolution of $CO_2$ was monitored, 25 mL samples were used in a procedure identical to the one used for cresols. The same control experiments as for cresols were also carried out.

### 3.1.3 Xylenols

**Chemicals:** 2,3-Xylenol (99%), 2,4-Xylenol (97%), 2,5-Xylenol (99+%), 2,6-Xylenol (99.8+%), 3,4-Xylenol (99%), and 3,5-Xylenol (99+%) were purchased

from Aldrich and were used as received. $TiO_2$ (Degussa P25) was described earlier. Doubly distilled water was used throughout. The mobile phase used for HPLC analyses consisted of a 50/50 mixture of methanol (BDH, Omnisolv grade) and doubly distilled water.

**Procedure:** Unless otherwise noted, uv/visible irradiation was carried out on aerated, efficiently stirred 50 mL samples. The appropriate quantity of a stock solution of xylenol was added to a previously weighed amount of $TiO_2$ powder to give the required concentration of $TiO_2$ (2g/L). The pH of the samples was adjusted with HCl or NaOH when required. Where the evolution of $CO_2$ was monitored, 25 mL samples were used; the procedure followed was identical to the one used for cresols. Experiments in an oxygen atmosphere were carried out as described for *m*-cresol. The same control experiments as for cresols were also carried out.

### 3.1.4 *2,3,5*-Trimethylphenol

**Chemicals:** 2,3,5-trimethylphenol (99%) was purchased from Aldrich and was used as received. $TiO_2$ (Degussa P25) was described earlier. Doubly distilled water was used throughout. The mobile phase used for HPLC analyses consisted of a 50/50 mixture of methanol (BDH, Omnisolv grade) and water.

**Procedure:** Unless otherwise noted, uv/visible irradiation was also carried out on aerated, efficiently stirred 50 mL samples. The appropriate quantity of a stock solution

of 2,3,5-trimethylphenol was added to a previously weighed amount of $TiO_2$ powder (catalyst loading, 2g/L). The pH of the samples was adjusted with HCl. Where the evolution of $CO_2$ was monitored, 25 mL samples were used; the procedure followed was identical to the one used for cresols. Experiments in an oxygen atmosphere were carried out as described for *m*-cresol. The same control experiments as for cresols were also carried out.

### 3.1.5 Coal Tar Creosote

**Chemicals:** Creosote was Armor Coat commercial domestic grade purchased from a hardware store (wood preservative liquid, 100% creosote guaranteed). $TiO_2$ (Degussa P25) was described earlier. Water was doubly distilled throughout. The mobile phase used for HPLC analyses consisted of a 50/50 mixture of methanol (BDH, Omnisolv grade) and doubly distilled water.

**Procedure:** Aqueous solutions of creosote were prepared by adding the required amount of creosote to water. The process was accelerated by gently heating the solution and sonicating it. Irradiation was carried out on 50 mL samples exposed to air and efficiently stirred. The appropriate quantity of a stock solution of creosote was added to a previously weighed amount of $TiO_2$ powder to give the required concentration of $TiO_2$ (unless otherwise stated: 100 mg to give a 2 g/L catalyst loading). Aliquots were taken at various time intervals, filtered to remove suspended solids and then analyzed by HPLC or used to record absorbance spectra as required; the diffuse reflectance spectra of the

catalyst powder remaining on filtration of the aliquots were also recorded. Control experiments were also carried out as previously described for cresols.

The degradation was also carried out in an oxygen-saturated atmosphere; the flask was oxygen purged for about 10 min and then sealed. For sampling, the flask was removed from the irradiation source, and a suitable aliquot (about 2 mL) was taken, filtered and analyzed; subsequently, the flask was once again purged with oxygen for 5 min. followed by continued irradiation.

Where $CO_2$ evolution was monitored, 25 mL solutions were used; the flasks were sealed with rubber septa and aluminum seals. When the experiment was carried out in an oxygen atmosphere, the samples were degassed for about 15 min with oxygen prior to irradiation. At various time intervals, samples of gas were taken from the headspace volume and analyzed by gas chromatography.

## 3.1.6 Instrumentation and Methodology

### 3.1.6.1 Light Source

The light source used in all the photocatalysis experiments was a 1000 Watt Hg/Xe lamp operated at ca. 900 Watts; it was equipped with a water jacket to filter out infrared radiation. The output spectrum (> 220 nm) of the lamp is characterized by strong mercury lines over the Xenon continuum through the visible and the ultraviolet regions.

The radiant power level dependence of the mineralization process was performed using appropriate neutral density filters in the light path. The filters consisted of a thin

vacuum deposited layer of a metal alloy applied to a ground and polished fused silica substrate which attenuated the photon flux by absorption when placed in the light path.[2] The radiant power ($mW/cm^2$) of the light source was ascertained with a calibrated power meter (Coherent, Model 210 power meter in the experiment with cresols and a Laser Instrumentation Ltd., Model 154BT power meter in the xylenol study).

### 3.1.6.2 Photochemical Efficiency Determinations

Photochemical efficiencies for the disappearance of cresols were determined at 365 nm (Bausch & Lomb monochromator; bandpass, $\pm$ 10 nm). Photochemical efficiencies for the disappearance of xylenols were also determined at 365 nm (Corning 365 nm interference filter). In both cases a specially designed quartz cell having a flat face with a surface area of 7.07 $cm^2$ was used.

The photochemical efficiencies were determined as follows:

1. The measurement of the radiant power ($mW/cm^2$) and the surface area of the cell ($cm^2$) allow the calculation of the total radiant power (mW) a given sample is exposed to. This value was then converted to Joules/min (1 Joule = 1 Watt x sec).

2. The light energy at 365 nm was calculated using $E = Nhc/\lambda$, giving the energy in Joules/Einstein (1 Einstein = 1 mole of photons).

3. Steps 1 and 2 allow the calculation of the number of Einsteins per minute the sample is exposed to. The photochemical efficiency was obtained using equation 3.1 where the rate of change of the substrate is in units of moles/min.

$$\textit{Photochemical Efficiency} = \frac{\textit{Rate of loss of substrate}}{\textit{Rate of Einsteins of light falling on the external reactor walls}} \qquad (3.1)$$

It should be noted that values of photochemical efficiencies are actually lower limits of the true quantum yield since the calculations were done based on the number of photons falling on the external reactor walls and not the actual number of photons absorbed by the sample. There are inherent difficulties in the area of heterogeneous photocatalysis in determining the amount of light **absorbed** by the catalysts. The usage of "quantum yield", as described in homogeneous photochemistry and used in heterogeneous photochemistry, has been seriously questioned.[3] Work is being carried out in this area in order to define a standard system that could be used as an "actinometer" in heterogeneous photochemistry so that efficiencies of various photocatalytic systems can be compared.[3]

### 3.1.6.3 High Performance Liquid Chromatography

The temporal evolution of the mineralization of the various substrates examined in this work and identification of the respective reaction intermediates were monitored by high performance liquid chromatographic (HPLC) techniques using a Waters Associates Liquid Chromatograph, equipped with a 501 HPLC Pump, a 441 Absorbance Detector, a Rheodyne 20 $\mu$L sample injection loop together with a Hewlett-Packard 3396A Integrator. The detection wavelengths available were 214 nm (Zn lamp) 254 nm and 280 nm (Hg lamp). The column was a Whatman reverse phase C-18 (Partisil-10, ODS-3) for the cresol, methylhydroquinone and methylcatechol studies. The column used for the xylenol and creosote work was a Waters reverse phase C-18 ($\mu$-Bondapack). The packing material in both columns is produced by chemically bonding hydrocarbon chains

($C_{18}$) onto a silica support.[4,5] Polar solvents, such as aqueous methanol, can be used with these columns to separate molecules containing polar functional groups such as alcohols: the less polar a component of a mixture is, the more it will interact with the non-polar hydrocarbon chains and the longer it will be retained by the column.

The mobile phases used in this work consisted of either a methanol/water/o-phosphoric acid mixture or a water/methanol mixture. All samples were filtered through MSI nylon 66 filters (pore size, 0.22 $\mu$m) prior to analysis. The details of the experimental conditions used are given in Table 3.1.

The instrument was typically calibrated by injecting known concentrations of the compound to be examined (typically 4 data points in the concentration range of interest); for example, when the photodegradation of a 20 ppm solution of cresol was examined, the standard solutions had concentrations of 5, 10, 15, and 20 ppm. Calibration curves of concentration *versus* chromatogram peak area (proportional to absorbance) were linear. The concentration of this compound in a sample was then easily deduced by matching the peak area obtained with a concentration using the calibration curve. When the integrator was used, the calibration curve data were entered so that peak areas were automatically converted into concentration by the instrument. Unknown compounds were identified by comparing their retention times and spectral characteristics with those of known compounds.

**Table 3.1** Experimental Conditions Used For HPLC Analyses.

| Compound(s) Examined | Composition of Mobile Phase (Volume ratios) | | | Detection Wavelength (nm) | Flow Rate (mL/min) |
|---|---|---|---|---|---|
| | $CH_3OH$ | $H_2O$ | o-$H_3PO_4$ | | |
| Cresols | 40 | 59.9 | 0.1 | 214, 280 | 2 |
| | 25[a] | 75[a] | 0.1[a] | 214, 280 | 2 |
| MHQ and 4-MCC | 25 | 75 | 0.1 | 214 | 2 |
| Xylenols | 50 | 50 | - | 214, 254 | 2 |
| 2,3,5-Trimethylphenol | 50 | 50 | - | 214, 254 | 2 |
| Creosote | 50 | 50 | - | 214 | 2 |

a) This mobile phase afforded a better separation of the HPLC signals and facilitated identification of the intermediates.

### 3.1.6.4 Determination of $CO_2$ by Gas Chromatography

Carbon dioxide evolution was monitored by gas chromatographic methods using a GOW-MAC Gas Chromatograph equipped with a Porapak-N (molecular sieve) column and a thermal conductivity detector. Helium was the carrier gas. Other experimental conditions were as follows: flow rate, 60 mL/min; column temperature, 160°C; detector temperature, 200°C; injection port temperature, 200°C; bridge current, 200 mA. The instrument was calibrated by one of the following two methods:

1. A known quantity of $CO_2$ was injected into a nitrogen-purged flask containing a 25 mL aqueous slurry at the desired pH (usually 3) of 2 g/L $TiO_2$. The flask was subsequently irradiated for 30 min to allow its contents to equilibrate, following which samples of the gas in the headspace were injected into the GC.

2. Known amounts of $Na_2CO_3$ were added to a 2 g/L suspension of $TiO_2$ in water; the flask was sealed and an appropriate quantity of HCl was added to bring the pH to 3. Subsequently, the sample was irradiated for 1 hour following which the gases in the headspace volume were sampled and injected into the chromatograph.

Sampling of the gases in the headspace for both of these methods affords the production of a calibration curve of $[CO_2]$ *versus* peak area from which the quantity of $CO_2$ produced in the photodegradation could be deduced. These methods were used throughout because they take into account any $CO_2$ that remains in solution and thus not present in the headspace; the method also takes into account any photoadsorption of $CO_2$ on $TiO_2$ that may take place upon irradiation of the samples.

For *p*-cresol, the complete mineralization was also verified by the quantitative determination of $CO_2$ using the $BaCO_3$ test after the complete disappearance of the initial reactant substrate. The photodegradation reaction was allowed to go to completion (ca.

9 hrs irradiation) in an oxygen atmosphere. Any gases produced were then flushed out with nitrogen into 3 flasks hooked up in series. The flasks contained known amounts of a standardized $Ba(OH)_2$ solution. These solutions were then titrated with HCl to determine the amount of $Ba(OH)_2$ remaining and, from there, the amount of $CO_2$ produced. Bromothymol blue was used as the indicator in the titration. A "blank" experiment was also carried out to correct for any $CO_2$ dissolved in the solutions; this was done by flushing nitrogen through a reaction vessel containing only water and $TiO_2$ into the 3 flasks as described above and titrating the $Ba(OH)_2$ solutions.

### 3.1.6.5 UV/Visible Spectrophotometer

When needed, UV/visible absorption spectra were recorded on a Shimadzu 265 SP uv/vis spectrophotometer. All samples were filtered through a MSI nylon 66 filter (pore size, 0.22 $\mu$m) prior to recording the spectra. The diffuse reflectance spectra of the catalyst powder remaining on filtration of the aliquots were recorded when desired on the same Shimadzu spectrophotometer; it was then equipped with an integrating sphere and $BaSO_4$ was used as the reference.

### 3.1.6.6 Carbon Content Analysis

The percent carbon content of the commercial coal tar creosote used in this study was kindly determined by Mr Robert Patterson of the Science Industrial Research Unit (S.I.R.U.) at Concordia University. A previously weighed sample of creosote was incinerated under a stream of oxygen in an induction furnace. All gases evolved were

passed through an absorption bulb containing ascarate (mainly sodium hydroxyde + magnesium perchlorate). Any $CO_2$ evolved was absorbed by the ascarate and resulted in a net increase in the weight of the bulb. The percent carbon content of the sample was then calculated.

## 3.2 KINETIC CONSIDERATIONS IN HETEROGENEOUS PHOTOCATALYSIS

Describing the kinetics of heterogeneous photocatalytic systems is not an easy task. The difficulty originates with the complex nature of the catalyst's surface which interacts to different extents with the solvent, initial substrate, intermediate species, and other species involved. The picture is further complicated by the effect photons have on the surface properties such as adsorption/desorption equilibria and the nature of the catalytic sites, among several others. Process kinetics in heterogeneous photocatalysis must therefore be considered as *apparent kinetics*, at least for the time being.

The photo-oxidation process of various aromatic substrates will typically proceed via consecutive and parallel stages; one example is the photocatalyzed mineralization of phenol (see Chapter 1; scheme 1.2).[6] The products formed upon primary hydroxylation of the phenol are catechol, hydroquinone and p-benzoquinone. Upon subsequent •OH radical attack, these primary hydroxylation products form pyrogallol, hydroxyhydroquinone, and hydroxybenzoquinone. These products in turn are subjected to further attack by •OH which eventually causes the benzene ring to open and leads to the formation of a series of intermediates of progressively higher oxygen-to-carbon ratios The species

eventually also oxidize quantitatively to carbon dioxide (and $H_2O$). The exact number of intermediates and the extent of interaction of each one with the surface of the catalyst remains unknown. The photocatalytic process for the oxidation of various aromatic substrates, on the basis of the above constraints, has been modelled in its most simplistic form by the consecutive and parallel reactions in scheme 3.2 , where $B_i$ and $C_{i,j}$ are the intermediates formed after •OH attack on A and $B_i$, respectively.

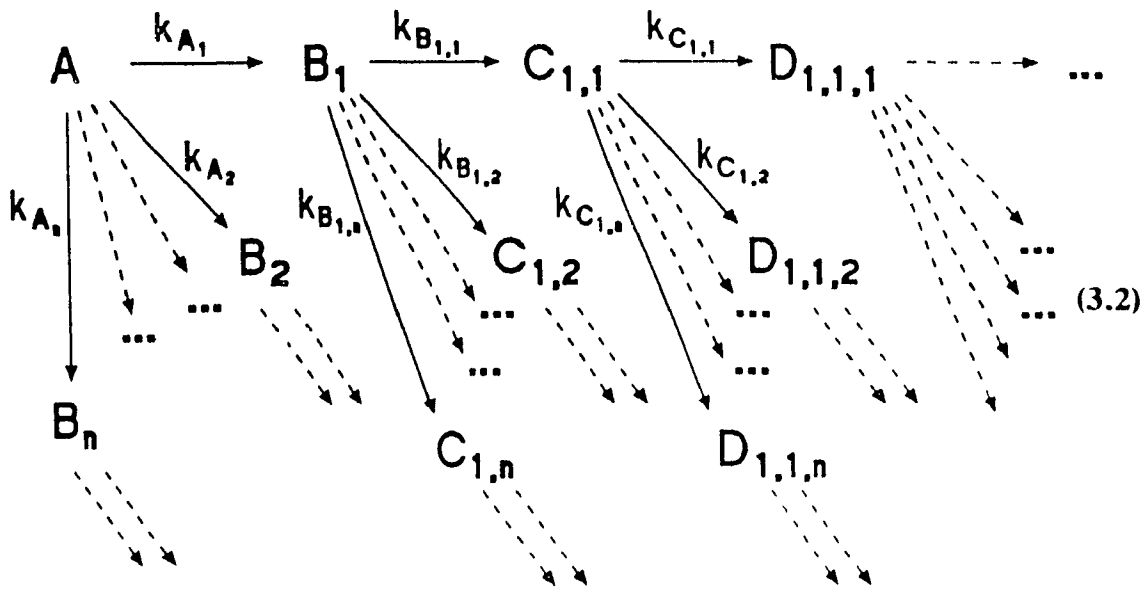


Taking $k_A$ and $k_B$ to represent the sum of microrate constants $\Sigma_i\ k_{A_i}$ and $\Sigma_j\ k_{B_{1,j}}$, respectively, the concentrations of A, $B_i$, and $C_{i,j}$ at some time $t$ will be given by the following equations[7] for first order processes:

$$[A]_t = [A]_0 e^{-k_A t} \qquad (3.3)$$

$$[B_i]_t = \frac{k_A[A]_0}{(k_B - k_A)}(e^{-k_A t} - e^{-k_B t}) \quad (3.4)$$

$$[C_{i,j}]_t = \frac{[A]_0}{(k_B - k_A)}[k_B(1 - e^{-k_A t}) - k_A(1 - e^{-k_B t})] \quad (3.5)$$

In this work, the actual data analysis was carried out using curve-fitting software (least squares method) that fits user-defined kinetic expressions to the data. For example, for equation 3.3, the expression used was:

$$Y = ae^{-bx} \quad (3.6)$$

which is analogous to equation 3.3. For equation 3.4, the expression used was:

$$Y = be^{-cx} - be^{-dx} \quad (3.7)$$

which is analogous to equation 3.4, taking $b = k_A[A]_0/(k_B - k_A)$. Where the disappearance of A is zero order, the rate expression is:

$$[A]_t - [A]_0 = -k_A t \quad (3.8)$$

The rate constant $k_A$ may be obtained from the slope of a plot of $[A]_t$ *versus* time.

The formation of $CO_2$ follows in nearly all cases simple exponential growth kinetics and was fitted to an equation of the form:

$$[CO_2] = f[1 - e^{k_P t}] \quad (3.9)$$

Assigning an operational mechanism for reactions taking place in heterogeneous

media to a Langmuir type process or to an equivalent type process is not possible on the basis of observed kinetics alone (see Chapter 2).[8] Therefore, although the analytical expression obtained for the rate of photo-oxidation may be analogous to the Langmuir-Hinshelwood relationship, **nothing can be concluded** about the operational mechanism in a heterogeneous photocatalysis experiment. In fact, many models that follow Langmuirian-type behaviour are simply various manifestations of saturation-type kinetics that are general in chemical kinetics (such as enzymatic reactions). It has therefore been suggested[3] that in heterogeneous photocatalysis involving solution/solid interfaces the events be described by a model described below. Most of the evidence being generated in various laboratories indicates that many, if not all, of the events are surface-occurring events. The expression(s) describing these will likely parallel those of saturation-type kinetics. However, no prior assumptions are made in the model as to the exact nature of the kinetic expressions which define the events. A few additional points should be noted. Although some of the compounds examined are only slightly adsorbed to the particle surface in the dark, the extent of *photoadsorption* is unknown. In developing rate expressions for the photo-oxidation process, the implicit assumption has often been made that there is a constant fraction, however small, of the organic substrate on the catalyst's oxidative active surface sites.[5] Following •OH attack on the aromatic ring of the substrate $S_{ads}$, one or more intermediates ($I_{ads}$ and or $I_{sol}$) form which subsequently or nearly simultaneously undergo fragmentation to aliphatic species which ultimately also degrade to produce stoichiometric amounts of $CO_2$ (equation 3.10)

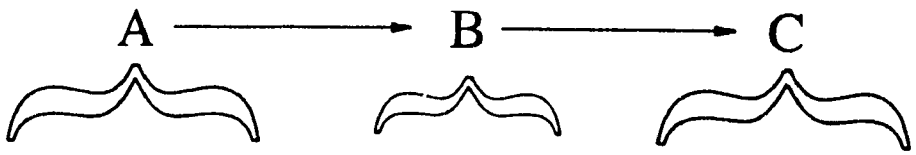


(3.10)

$$(\text{site}) + S \underset{k_d}{\overset{k_a}{\rightleftharpoons}} S_{ads} \xrightarrow{k_S} \{I_{ads} + I_{sol}\} \xrightarrow{k_I} \ldots \rightarrow \rightarrow \rightarrow CO_2$$

where $k_s$ denotes a sum of rate constants in the formation of various intermediate species and $k_I$ represents a sum of rate constants in the fragmentation of these intermediates. The rate of product formation is then given by equation 3.11,[7] where $K_S$ [$= k_a/(k_d + k_s)$] is the photoadsorption coefficient for the substrate and $N_s$ is the number of oxidative sites:

$$Rate = \frac{k_s K_S N_s [S]}{1 + \dfrac{k_S + k_I}{k_I} K_S [S]} \qquad (3.11)$$

Note the similarity of equation 3.11 to the Langmuir-Hinshelwood kinetic rate law. Considering that •OH radicals are formed from a light-assisted process, their formation and disappearance through back reactions also need to be accounted for in the expression for the overall rate of product formation.

The quantum yield of formation of •OH species is $\Phi_{\bullet OH} = \phi I_a^n k_{trap} \tau$ (at low light fluxes, n = 1), where $\tau$ is the lifetime of the valence band holes of the photocatalyst [$\tau = 1/(k_{rec} + k_{trap})$]. $k_{trap}$ and $k_{rec}$ are, respectively, the rate constant for the formation of

trapped holes (Chapter 2; equation 2.9) and the rate constant for the recombination of electron/hole pairs. Taking $k_{rec} > k_{trap}$,[9] $\Phi_{\bullet OH} = \phi I_a \beta A_p k_{trap}/k_{rec}$, where $\beta A_p$ represents the fraction of the particle surface that is irradiated and $A_p$ is the particle surface area. The overall rate will also depend on the lifetime of the surface bound •OH radicals $\tau_{\bullet OH}$. Water, intermediates, ions and other species present can, in principle, compete for the same adsorption sites as the cresols; these will act as inhibitors. It has also been noted that molecular $O_2$ affects the rate of degradation. Thus, the rate of formation of the products becomes:

$$Rate = \frac{\frac{\phi I_a \beta A_p k_{trap} \tau_{\bullet OH}}{k_{rec}} k_S K_S N_s [S]_0}{1 + \frac{k_S + k_I}{k_I} K_S[S] + K_W[H_2O] + K_I[I] + K_{ions}[Ions]} \bullet \frac{K_{O_2}[O_2]}{(1 + K_{O_2}[O_2])} \quad (3.12)$$

The above expression (equation 3.12) is similar to the one proposed by Okamoto *et al.*[10] and more recently by Turchi and Ollis[8] but is more global as it takes into account many of the properties of the systems looked at including absorption of light by the catalyst, formation and recombination of electrons and holes in the semiconductor, formation of the oxidizing species, the lifetime of the active species, and the adsorption properties of all the species involved including any intermediates produced, together with the effect oxygen has on the photo-oxidation process. The above expression (equation 3.12) for the rate of photodegradation of organic substrates on irradiated $TiO_2$ presents the same kinetic behaviour (with minor variations) as portrayed by the Langmuir Hinshelwood rate law.

## 3.3 PULSE RADIOLYSIS EXPERIMENTS

### 3.3.1 Electron Accelerator

All pulse radiolysis experiments were performed using a high-voltage Engineering Corp. Van de Graaff accelerator [4 MeV (1-3 Amps)] at the Center for Fast Kinetics Research (CFKR) of the University of Texas at Austin.# The instrument had been modified by the CFKR personnel to produce a pulsed beam of electrons with pulse durations of 50, 100, 250, and 500 ns.[11] In a Van de Graaff generator, the electrons to be accelerated are generated by an electron gun. They are extracted from the source and injected into an acceleration tube by an electrode. Subsequently, they are accelerated in this tube by a high voltage electric field. To produce this high voltage, electric charge was produced by a dc power supply and continuously sprayed onto a rapidly moving belt. This belt carried the charge to a high voltage terminal where it was removed. The high voltage attained at the terminal was uniformly distributed along the generator column by the electric charges flowing back to ground through a voltage dividing network and a series of equipotential planes. This potential applied to the evacuated accelerating tube provided for a uniform acceleration of the generated electrons.[12]

The design of the kinetic spectrometry apparatus was conventional, consisting of a xenon lamp (450 W), a grating monochromator, and a photomultiplier tube [Hamamatsu Corp. R928 (multi-alkali cathode)] arrangement, with all the optical elements being confined to a 1.5 m optical bench centred beneath the exit window of the

---

# The author is grateful to Professor Marye Anne Fox and Dr Anthony Harriman for their kind hospitality during the course of these studies.

vertically mounted accelerator. A fast shutter located between the sample and the lamp housing protected the sample from photolysis by continuous exposure to the analyzing light; this shutter was open only for a few microseconds during data collection. Another slower shutter, that opened before the fast shutter and closed after it, protected the fast shutter from excessive heating by the xenon lamp. Signals were transmitted from the photomultiplier tube in the radiation room to an external console via a coaxial cable. All operations such as wavelength changes, light attenuation, fresh sample injection, and others were performed from a remote position on the control console.

The electrical signal, produced in the detector circuit by changes in the optical absorption in the target medium following an electron pulse, was converted to intensity *versus* time coordinates using a Biomation 8100 digitizer interfaced with a PDP 11/70 computer for data analysis in the case where pentahalophenols were examined; in the study of the xylenols, the signal was converted by a Lacroix 8818 digitizer interfaced with an IBM compatible 386 computer. Data analysis could then be carried out using appropriate software. The dose, i.e. the amount of radiation the solution was exposed to, was measured by an energy meter. These meter readings were converted into radical concentrations using dosimetry.

## 3.3.2 Radical Production and Dosimetry

Radiolysis of water by high energy electrons produces a variety of radical and molecular species (equation 3.13).[11]

$$H_2O \rightarrow\rightarrow\rightarrow \bullet OH,\ e^-_{(aq)},\ H\bullet,\ H_2,\ H_2O_2,\ H^+,\ OH^- \qquad (3.13)$$

Hydroxyl radicals, hydrated electrons and hydrogen atoms are highly reactive species and may react with organic compounds to produce organic free radicals. When the desired primary radical is •OH, aqueous solutions are saturated with nitrous oxide ($[N_2O]$= 25 mM) to ensure scavenging of the other species; in addition to eliminating oxygen, $N_2O$ converts $e^-_{(aq)}$ to •OH via equation 3.14. The quantity of H• atoms produced may be controlled by varying the pH of the solution; the quantity of H• radicals produced at pH > 3 via equation 3.15 is negligible (< 10% of radicals produced[14,15]).

$$N_2O + e^-_{(aq)} + H_2O \rightarrow OH\bullet + N_2 + OH^- \qquad (3.14)$$

$$k = 9.1 \times 10^9\ M^{-1}s^{-1} \quad \textbf{[Ref. 14]}$$

$$H_3O^+ + e^-_{(aq)} \rightarrow H\bullet + H_2O \qquad (3.15)$$

$$k = 2.3 \times 10^{10}\ M^{-1}s^{-1} \quad \textbf{[Ref. 14]}$$

Hydroxyl radicals can be used to prepare less reactive oxidizing radicals such as the azide radical ($N_3\bullet$) via reaction with $NaN_3$ (equation 3.16).

$$OH\bullet + N_3^- \rightarrow OH^- + N_3\bullet \qquad (3.16)$$

$$k = 1.2 \times 10^{10}\ M^{-1}s^{-1} \quad \textbf{[Ref. 14]}$$

Azide radicals tend to be more selective and normally react with aromatic compounds via electron transfer, unlike OH• radicals where addition to the ring is usually the

predominant path.[16]

Electrons and H• atoms can be used as reducing radicals (an H• atom is simply the conjugate acid of $e^-_{(aq)}$).[14] Addition of *t*-butanol scavenges OH• radicals to produce a relatively inert radical (equation 3.17).

$$\bullet OH + (CH_3)_3COH \rightarrow H_2O + (CH_3)_2(\bullet CH_2)COH \qquad (3.17)$$

$$k = 6.0 \times 10^8\ M^{-1}s^{-1} \quad \text{[Ref. 14]}$$

The species H• and $e^-_{(aq)}$, react much more slowly with *t*-butanol: k = 1 x $10^5$ $M^{-1}s^{-1}$, [11] and 4 x $10^5$ $M^{-1}s^{-1}$, [17] respectively. Aqueous solutions of *t*-butanol, therefore, provide a medium in which either H• or $e^-_{(aq)}$, depending on pH, is the principal radical reacting with the organic substrate.

Table 3.2 summarizes the optical properties of the radicals generated in this work to react with the various organic substrates examined. In most cases, the amount of a given radical in solution was calculated by using dosimetry (see below) since $\lambda_{max}$ is not an easily accessible wavelength (e.g. for H•, •OH); this does, however, present an advantage as the absorption bands of these radicals do not interfere with the absorption bands of many of the organic radicals produced. Their spectral features occur in the UV and visible region of the spectrum. The hydrated electron can be monitored directly at about 720 nm and any reaction with an organic substrate can be observed by monitoring changes in the optical density at this wavelength.

The absorbed radiation dose, and thereby the amount of a given radical in solution, was determined by thiocyanate dosimetry using 0.01 M KSCN in $N_2O$-saturated

**Table 3.2** Optical Properties of Some Radical Species Generated by Pulse Radiolysis.

| Radical | $\lambda_{max}$, nm | $\epsilon_{max}$, $M^{-1} cm^{-1}$ |
|---|---|---|
| •OH | ≈ 225[a] | 540 (188 nm)[a] |
| $N_3$• | 274[b] | 2025[b] |
| $e^-_{(aq)}$ | 720[a] | 19000[a] |
| H• | <200[a] | 1620 (188 nm)[a] |

a) Ref. 14; b) Ref. 15

water. In the presence of excess $SCN^-$, any OH• produced reacts according to equation 3.18, to produce the dimeric radical anion $(SCN)_2^{-}$• via equation 3.19.[18,19]

$$OH\bullet + SCN^- \rightarrow OH^- + (SCN)\bullet \qquad (3.18)$$

$$(SCN)\bullet + SCN^- \rightarrow (SCN)_2^{-\bullet} \qquad (3.19)$$

The radical dimer $(SCN)_2^-$• has an extinction coefficient of 7600 $M^{-1}cm^{-1}$ at 480 nm and is known to disappear via second order kinetics.[18,19] The concentration of $(SCN)_2$• formed following the electron pulse can be calculated by recording the optical decay traces of the radical at 480 nm, fitting these traces to second order kinetics, and then extrapolating to time zero to obtain the optical density value ($OD_0$). The concentration was calculated using this $OD_0$ value, the extinction coefficient and the path length of the cell. If this procedure is carried out at several different doses (meter readings), the meter can be calibrated such that a given reading can be taken to correspond to a given concentration of •OH, since the G value (number of molecules formed / 100 eV absorbed

dose) of $(SCN)_2^{-\bullet}$ is equal to the yield of OH•: $[G(OH\bullet)] = [G(SCN)_2^{-\bullet}] = 6.0$ molecules/100 eV. The concentrations of any other radicals being examined can also be deduced from thiocyanate dosimetry by looking at their relative G values: $[G(N_3\bullet)] = [G(OH\bullet)]$ in the presence of sufficient $NaN_3$; $[G(H\bullet)] = 3.0$ molecules/100 eV [14] in acidic solutions containing sufficient *t*-butanol.

## 3.3.3 Data Analysis

### 3.3.3.1 Kinetic Analysis

The digitized data were analyzed according to the types of kinetics described below.

The first order disappearance of a radical S• follows the rate equation:

$$-\frac{d[S\bullet]}{dt} = k[S\bullet] \tag{3.20}$$

which upon integration, yields:

$$\ln\frac{[S\bullet]_t}{[S\bullet]_0} = -kt \tag{3.21}$$

$$\ln[S\bullet]_t = \ln[S\bullet]_0 - kt \tag{3.22}$$

where the subscript zero refers to time zero when the reaction starts and the subscript t to some time later. Assuming that Beer's law applies, the concentration of $S\bullet$ can be substituted in terms of the measured optical density; the term $\epsilon\ell$ ($\epsilon$ is the extinction

coefficient and $\ell$ the path length of the optical cell) cancels out in equation 3.23. Thus,

$$\ln\frac{(OD_t/\epsilon\ell)}{(OD_0/\epsilon\ell)} = -kt \qquad (3.23)$$

or

$$\ln OD_t = \ln OD_0 - kt \qquad (3.24)$$

The rate constant is obtained from the slope of a plot of **ln** $OD_t$ *versus* $t$ and the optical density at $t=0$, $OD_0$ is obtained from the y intercept. The same argument can also be used for the first order formation of a radical, and the rate constant calculated in the same manner. In this study, the actual data analysis was carried out using curve-fitting software (least squares method) that fits user-defined kinetic expressions to the data. Figure 3.1 shows a typical trace sample of a first order growth.

Where the disappearance of $S\bullet$ through reaction with itself follows second order kinetics ($2S\bullet \rightarrow S\text{-}S$), the rate equation is given by:

$$-\frac{1}{2}\frac{d[S\bullet]}{dt} = k[S\bullet]^2 \qquad (3.25)$$

which upon integration yields:

$$\frac{1}{[S\bullet]_t} = \frac{1}{[S\bullet]_0} + 2kt \qquad (3.26)$$

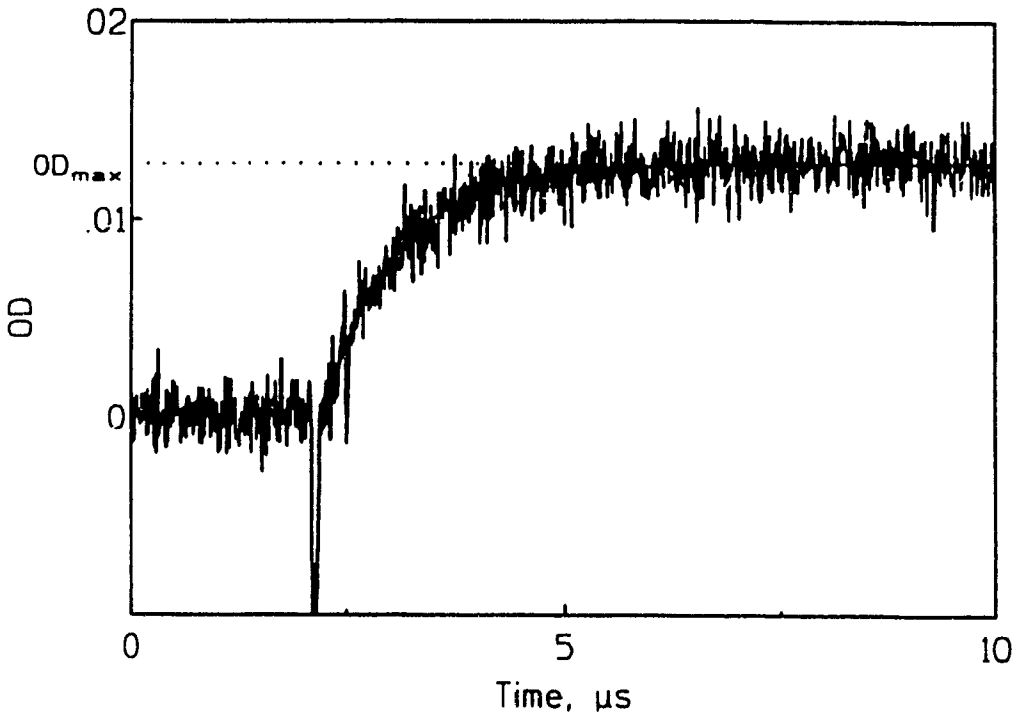


**Figure 3.1** Sample trace for the first order formation of a radical.

Substituting [$S\bullet$] by OD/$\epsilon\ell$ according to Beer's law yields:

$$\frac{1}{OD_t} = \frac{1}{OD_0} + \frac{2k}{\epsilon\ell}t \qquad (3.27)$$

The rate constant is obtained from the slope of a plot of $\mathbf{1/OD_t}$ *versus* time and $\mathbf{OD_0}$ from the y intercept. The slope has a value of $2k/\epsilon\ell$ which is the observed rate constant $k_{obs}$ in units of time$^{-1}$. The extinction coefficient of the observed species must be known in order to calculate the rate constant $k$. This explains why observed rate constants for second order reactions are often reported as $2k/\epsilon\ell$, $k/\epsilon\ell$, or $2k/\epsilon$. The reaction of $S\bullet$ with another species results in the same kinetic expression if the initial concentrations of

the two substrates are the same, except that the observed rate constant will be $k_{obs} = k/\epsilon\ell$ and not $2k/\epsilon\ell$. As for first order reactions, the actual data analysis was carried out using curve-fitting software (least squares method) that fits user-defined kinetic expressions to the data. Figure 3.2 shows a typical example of a second order decay.

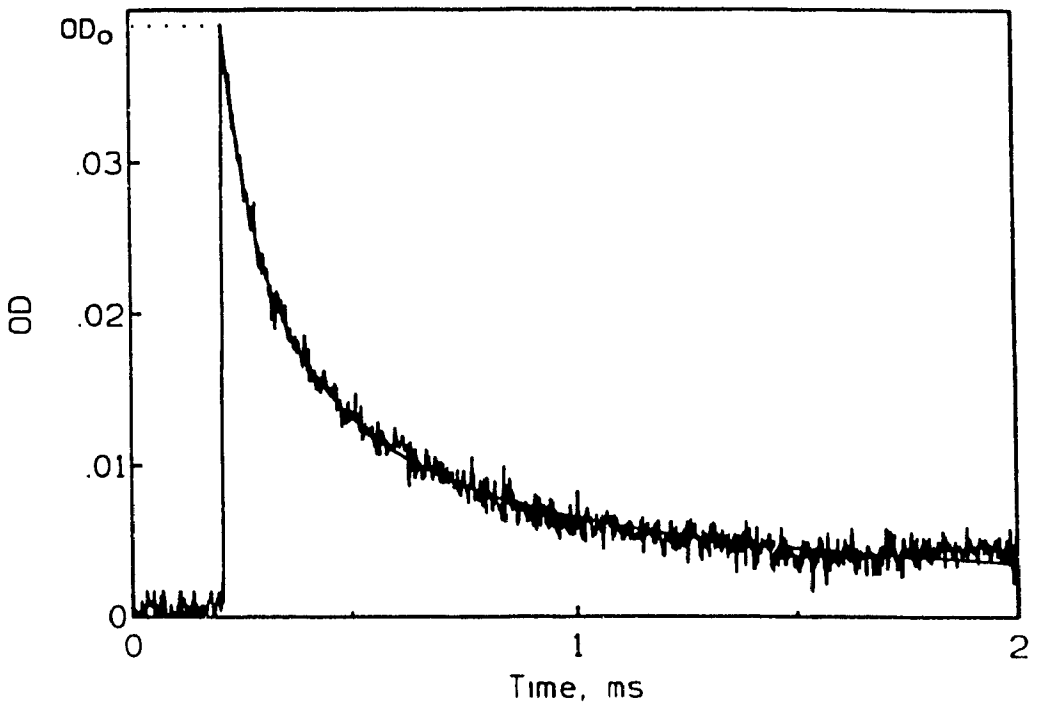


**Figure 3.2** Sample decay trace for the second order disappearance of a radical.

A special case of second order kinetics arises for reactions of the type: $A + B \rightarrow P$, when $[B]_0 >>> [A]_0$. In this case, the rate equation reduces to:

$$-\frac{d[A]}{dt} = k_{obs}[A] \qquad (3.28)$$

The disappearance of $A$ now follows pseudo first order kinetics with $k_{obs} = k[B]$. If $k_{obs}$

is measured for several different $[B]_0$, $k$ can be obtained by plotting $k_{obs}$ *versus* $[B]_0$.

In pulse radiolytic studies, it is important to remember that the optical density measured at any wavelength may be due to a number of species, so that the observed kinetics may well represent a combination of several of the kinetic processes described above.

#### 3.3.3.2 Calculation of Extinction Coefficients

Extinction coefficients for the organic radicals produced in this work were determined via both of the following two methods (unless otherwise stated):

1. Using second order decay data (as per Figure 3.2) at four radiation doses, the optical density at time zero ($OD_0$) was obtained by extrapolation. $OD_0$ was then divided by the concentration of the radical produced and by the optical path length.

2. The maximum optical density ($OD_{max}$) attained while measuring the rate of formation of the organic radical (as per Figure 3.1) was measured. $OD_{max}$ was then divided by the concentration of the radical produced and by the optical path length.

Typically, both sets of calculations were in agreement.

### 3.3.4 Pulse Radiolysis on Pentahalophenols

**Chemicals:** Pentafluorophenol (PFP-OH; 99+ %), pentachlorophenol (PCP-OH; 99%) and pentabromophenol (PBP-OH; 96%) were purchased from Aldrich. PFP-OH was used as received, while PBP-OH and PCP-OH were further purified by two successive sublimations. Nitrogen and Nitrous oxide (prepurified) were supplied by Linde and used as received. Sodium azide, potassium phosphate (MCB), *t*-butanol (Fisher

Scientific), potassium thiocyanate, L-ascorbic acid, and other chemicals were reagent grade and were used as received. Millipore filtered water was used for all solutions.

**Solutions:** Hydroxyl radicals (•OH) were generated in buffered pH 8 solutions of pentahalophenols ($10^{-3}$ M phosphate buffer) owing to the low solubility of PCP-OH (8 mg/100 mL) and PBP-OH (insoluble) in water.[20,21] The three pentahalophenols examined in this work exist as the phenoxides at pH 8 ($pKa_{PCP\,OH}$ = 4.5, $pKa_{PFP\,OH}$ = 5.53).[21,*] Deoxygenation was accomplished by bubbling with $N_2O$. Azide radicals ($N_3$•) were generated in $NaN_3$ (0.01 M) aqueous solutions, buffered at pH 8 ($10^{-1}$ M phosphate buffer) and purged with $N_2O$. In studies involving the hydrated electron $e_{(aq)}^-$, *t*-butanol (0.2 M) was added to buffered aqueous solutions (pH 8) to scavenge any •OH radicals formed. These solutions were deoxygenated using nitrogen gas.

Solutions (20 ± 2 °C) were irradiated in a single pass flow cell with a 3.3 cm analyzing path length (unless otherwise indicated) with fresh sample being injected into the cell after each pulse. The concentrations of solutes were chosen to ensure 90-100% capture of the desired primary radicals. Additional details of the experimental conditions are reported in Tables and Figure captions as required in the appropriate chapters to follow.

---

* The pKa of PBP-OH in aqueous solution could not be located, no doubt due to the insolubility of the protonated form of the compound in water. The pKa value is likely to be very close and slightly lower than that of PCP-OH [In methanol, pKa (PCP-OH) = 8.2; pKa (PBP-OH) = 8.0].[23]

### 3.3.5 Pulse Radiolysis on Xylenols

**Chemicals:** 2,3-Xylenol (99%), 2,4-Xylenol (97%), 2,5-Xylenol (99+%), 2,6-Xylenol (99.8+%), 3,4-Xylenol (99%), and 3,5-Xylenol (99+%) were purchased from Aldrich and were used as received. Nitrogen and Nitrous oxide (prepurified) were supplied by Linde and used as received. Sodium azide, potassium phosphate (MCB), potassium thiocyanate, *t*-Butanol (Fisher Scientific), and other chemicals were reagent grade and were used as received. Millipore filtered water was used for all solutions.

**Solutions:** Hydroxyl radicals were generated in buffered (pH 4; $10^{-3}$ M phosphate buffer) aqueous solutions of xylenols except during the pH dependence study. The six xylenols examined in this work exist in their protonated form at pH 4 (Table 3.3).[22]

**Table 3.3** pKa values for Xylenols. (From ref. 22)

| Phenol | $pK_a$ |
|---|---|
| 2,3-Xylenol | 10.54 |
| 2,4-Xylenol | 10.36 |
| 2,5-Xylenol | 10.65 |
| 2,6-Xylenol | 10.19 |
| 3,4-Xylenol | 10.4 |
| 3,5-Xylenol | 10.6 |

Deoxygenation was accomplished by bubbling the solution with $N_2O$. Azide radicals were generated in aqueous solutions of $NaN_3$ (0.01 M). The pH of the sodium azide $N_2O$-purged solutions was adjusted to pH 5.8 in order to compare the values obtained for the rate constants with the corresponding values from the literature. Hydrogen atoms were generated in buffered (pH 1) aqueous solutions of xylenol containing 0.2 M *t*-butanol. In this case, oxygen was removed by purging the solution with nitrogen.

Solutions (20 $\pm$ 2 °C) were irradiated in a single pass flow cell with a 2.5 cm analyzing path length with fresh sample being injected into the cell after each pulse. The concentrations of solutes were also chosen to ensure 90-100% capture of the desired primary radicals. Additional details of the experimental conditions are summarized in the Tables and Figure captions where useful in the appropriate chapters.

## 3.4 SONOCHEMISTRY EXPERIMENTS

### 3.4.1 Chemicals

Phenol (Aldrich, 99+ %), methanol (BDH, omnisolv grade), *o*-phosphoric acid (Fisher, HPLC grade) were used as received. Hydroquinone, catechol, *p*-benzoquinone, and other chemicals were reagent grade and were used without further purification. Doubly distilled water was used throughout. When required, the pH of the solutions was adjusted using either HCl or NaOH.

## 3.4.2 Ultrasonic Irradiation Procedure

The ultrasonic irradiation of aqueous solutions of phenol, hydroquinone (HQ), catechol (CC) and p-benzoquinone (BQ) was carried out with a Vibracell model VC-250 direct immersion ultrasonic horn (Sonics & Materials) that was operated at 20 kHz with a power output of 25, 50 or 75 Watts/cm$^2$, as indicated. Reactions were carried out in a glass sonication cell similar to the one described by Suslick[24] (see Figure 3.3). The upper part of the cell was left open to allow constant exposure of the solutions to air. The cell was encased in a water jacket and was cooled with a mixture of water and ethylene glycol at 15°C; the temperature inside the cell was fairly constant at 30 $\pm$ 2°C. The reaction volume was 100 mL in all cases. The titanium tips of the sonication horn were replaced every 4 hrs to compensate for any erosion.

## 3.4.3 Analytical Procedures

### 3.4.3.1 High Performance Liquid Chromatography

The temporal course of the sonodegradations was monitored by HPLC using the instrument described in section 3.1.6.3. The detection wavelengths were 214 and 254 nm; the column was a Whatman reverse phase C-18 (Partisil-10, ODS-3). The mobile phase was a methanol/water/*o*-phosphoric acid mixture (35:65:0.1). The intermediates were identified by comparing their retention times with those of known standards. The flow rate was 1 mL/min. All aliquots taken from the reaction vessel were filtered through MSI Nylon 66 filters (0.2 $\mu$m pore size) prior to analysis to remove some titanium metal particles produced during sonication by erosion of the titanium tip

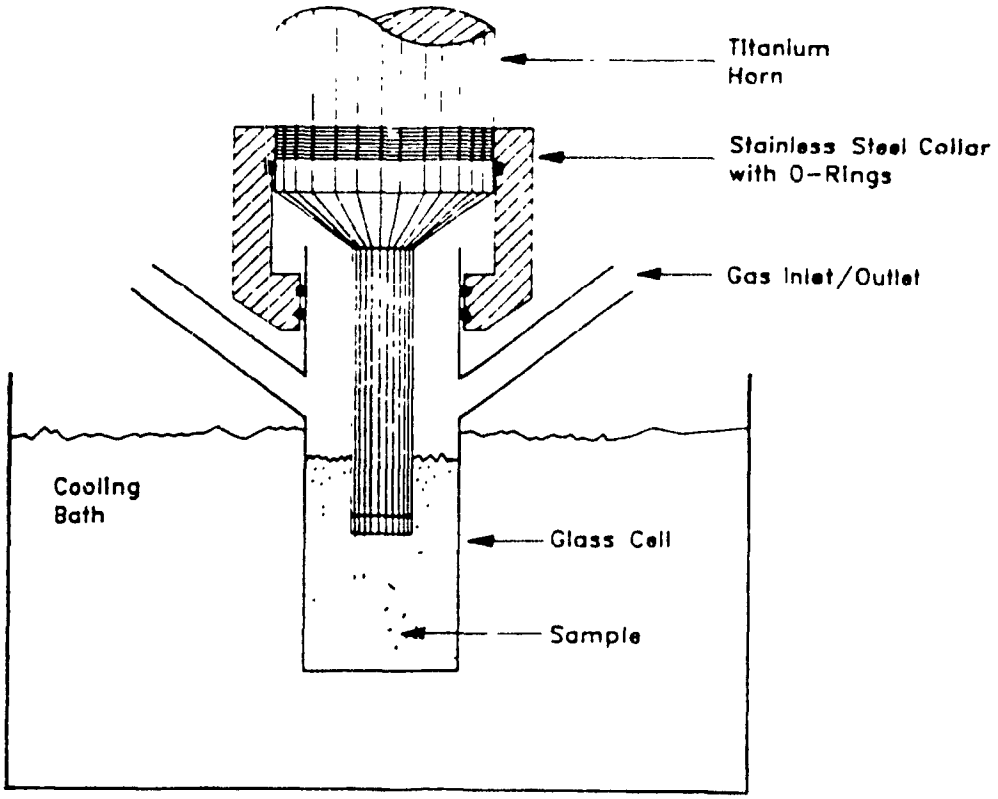


**Figure 3.3** Direct immersion ultrasonic horn (ref. 24).

of the sonication horn.

### 3.4.3.2 Total Organic Carbon Analysis

The temporal variations in total organic carbon (TOC) were followed using a Schimadzu 5000 instrument after filtration of the phenolic aqueous solution (75 $\mu$M phenol; pH 12); the insonation was carried out for 12 hr with a Branson Sonifier B-15 operated at 80 Watts/cm$^2$.*

---

* The author thanks Dr. C. Minero of the Dipartimento di Chimica Analitica, Università di Torino, Italy, for carrying out these analyses.

# REFERENCES


1. *Technical Bulletin No. 56,* Degussa Canada Ltd, 4261 Mainway Drive, Burlington, Ontario, **1982**.

2. *Oriel Corporation Catalogue, vol III, Optics and Filters*, Stratford, Connecticut, **1990**.

3. Serpone, N., Pelizzetti, E., Hidaka, H., in *"Proceedings of the Solar Energy Meeting IPS-9"*, Beijing, China, **1993**, in press.

4. *Chromatographic Specialties Inc. Catalogue*, Brockville, Ontario, **1992**, p. 110.

5. *Une Introduction à la Chromatographie Liquide*, Waters Chromatography division, Montréal, **1988**.

6. Okamoto, K., Yamamoto, Y., Tanaka, H., Tanaka, M., Itaya, A., *Bull. Chem. Soc. Jpn.*, **1985**, *58*, 2015.

7. Laidler, K.J., *"Chemical Kinetics"*, 3rd. Edn., Harper & Row Publ., New York, **1987**, pp. 278-281.

8. Turchi, C.S., Ollis, D.F., *J. Catal.*, **1990**, *122*, 178.

9. Rothenberger, G., Möser, J., Grätzel, M., Serpone, N., Sharma, D.K., *J. Am. Chem. Soc.*, **1985**, *107*, 8054.

10. Okamoto, K., Yamamoto, Y., Tanaka, H., Itaya, A., *Bull. Chem Soc. Jpn.*, **1985**, *58*, 2023.

11. Rodgers, M.A.J., Foyt, D.C., Zimek, Z.A., *Radiat. Res.*, *75*, 296, **1977**.

12. Matheson, M.S., Dorfman, L.M., *"Pulse Radiolysis"*, The Massachusetts Institute of Technology, Boston, **1969**.

13. Swallow, A.J., in *"The Study of Fast Processes and Transient Species by Electron Pulse Radiolysis"*, Baxendale, J.H., Busi, F., Eds., D. Reidel Publishing Company, Boston, **1982**, pp. 289-315.

14. Buxton, G.V., Greenstock, C.L., Helman, W.P., Ross, A.B. *J. Phys. Chem. Ref. Data* **1988**, *17(2)*, 513.

15. Buxton, G.V., *Radiat. Res. Rev.*, **1968**, *1*, 209.

16. Alfassi, Z.B., Schuler, R.H. *J. Phys. Chem.* **1985**, *89*, 3359.

17. Anbar, M., Ross, A.B., Ross, F., *Natl. Stand. Ref. Data Ser. (U.S., Natl. Bur. Stand.)*, **1973**, No 46.

18. Baxendale, J.H., Bevan, P.L.T., Stott, D.A. *Trans. Faraday Soc.* **1968**, *64*, 2389.

19. Schuler, R.H., Patterson, L.K., Janata, E., *J. Phys. Chem.*, **1980**, *84*, 2088.

20. *The Merck Index*, 10th ed., Windholz, M., Ed., Merck & Co. Inc., Rathway, N.J., **1983**, p. 6974.

21. *CRC Handbook of Chemistry and Physics*, 51st ed., Weast, R.C., Ed., The Chemical Rubber Co., Cleveland, **1970**.

22. Serjeant, E.P., Dempsey, B. *"Ionization Constants of Organic Acids in Aqueous Solution"* - IUPAC Chemical Data Series No. 23, Pergamon Press, Oxford, **1979**.

23. *Dictionary of Organic Compounds*, 5th ed., vol. 4, Buckingham, J., ed., Chapman and Hall, New York, **1982**.

24. Suslick, K.S., in *"Ultrasound: Its Chemical, Physical, and Biological Effects"*, Suslick, K.S., Ed., VCH Publishers, New York, **1988**, p. 123.

# CHAPTER 4

# THE PHOTOCATALYZED MINERALIZATION OF CRESOLS IN AQUEOUS MEDIA WITH IRRADIATED TITANIA

## 4.1 INTRODUCTION

Cresols figure prominently in the list of priority pollutants put forth by the United States Environmental Protection Agency (See Table 1.1).[1] Common uses of phenolic substrates such as cresols range from fumigants and insecticides to wood preservatives and disinfectants[2,3].

In the past several years, the photocatalyzed destruction (mineralization) of a number of organics appearing on the US EPA list of top priority pollutants has been carried out using titania (Degussa P-25 $TiO_2$) under ultraviolet/visible or simulated sunlight irradiation.[4,5] In each instance, total mineralization was demonstrated by following the temporal evolution of the products $CO_2$ and $H_2O$ (or HCl for chloroorganics) along with the concomitant disappearance of the original substrate. Systematic kinetic and mechanistic studies on $TiO_2$ mediated photooxidations on some of the environmental organic and inorganic pollutants have been forthcoming.[6-8] Herein, the mineralization of three cresols (*ortho-*, *meta-*, *and para*-cresol) in air-equilibrated (or oxygen saturated) $TiO_2$ suspensions is surveyed. The effects of such parameters as pH, initial cresol concentration, catalyst loading, and radiant power levels of the light source are also examined. Hydroxylated aromatic intermediates formed have been identified and

rate data are examined in the context of the kinetic principles described in Chapter 3. Photochemical efficiencies for the disappearance of the cresol(s) at 365 nm have also been determined.

## 4.2 PHOTOOXIDATIVE DEGRADATION OF CRESOLS

The photodegradation of *o*-, *m*-, and *p*-cresol was monitored by UV spectral methods at various wavelengths (214, 254, and 280 nm). Figures 4.1-a-c, show plots of absorbance *versus* irradiation time. For *m*- and *p*-cresol, the absorbance tends to zero after about 2.5-3.5 hr of irradiating the aerated $TiO_2$ suspensions. This was not the case for *o*-cresol (Figure 4.1 a). There probably exists some longer lived intermediate for this species even after ca. 3 hr of irradiation at the monitored wavelengths. The erratic behaviour of the plots, which arises from the evolution and disappearance of intermediates with similar but not identical spectral properties at different times along the course of the reaction precluded the spectral method as an analytical tool. HPLC was therefore used as the analytical method of choice in this thesis.

### 4.2.1 Catalyst Loading

Catalyst loading in the light-induced splitting of $H_2S$,[9] in the photooxidation of organics,[10] or in the photoreduction of trace metals from dilute solutions[11] has often been 2 g/L of the semiconductor material ($TiO_2$, CdS, ZnO, and others). In this case, the initial rate of degradation of *m*-cresol (169 $\mu$M; ca. 20 mg/L) showed little change upon varying the concentration of $TiO_2$ between 0.5 and 2 g/L as illustrated in Figure 4.2. A

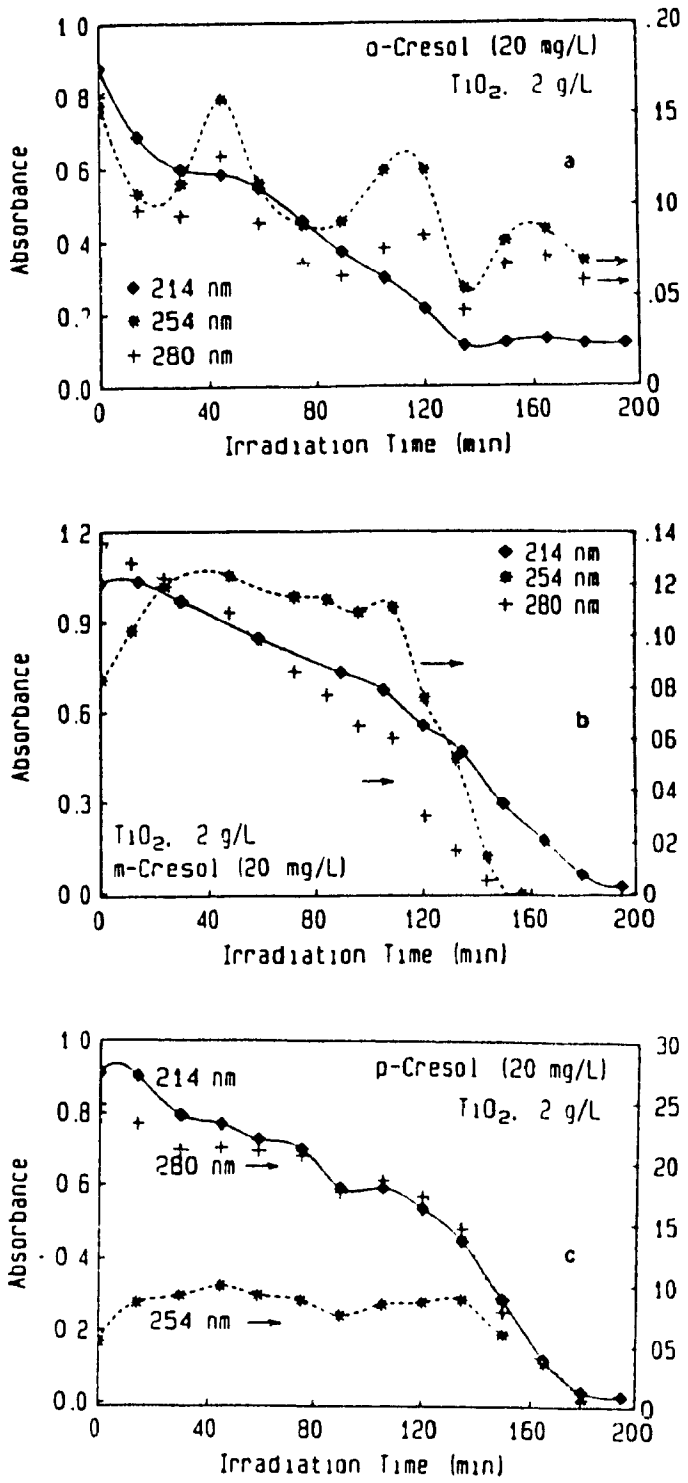


**Figure 4.1** Absorbance *versus* irradiation time plots at three monitoring wavelengths relevant to the HPLC technique employed in this work (214 nm, 254 nm, and 280 nm) in the mineralization of 20 mg/L of cresols in the presence of 2 g/L $TiO_2$ at pH 3: (a) *o*-cresol, (b) *m*-cresol, and (c) *p*-cresol.

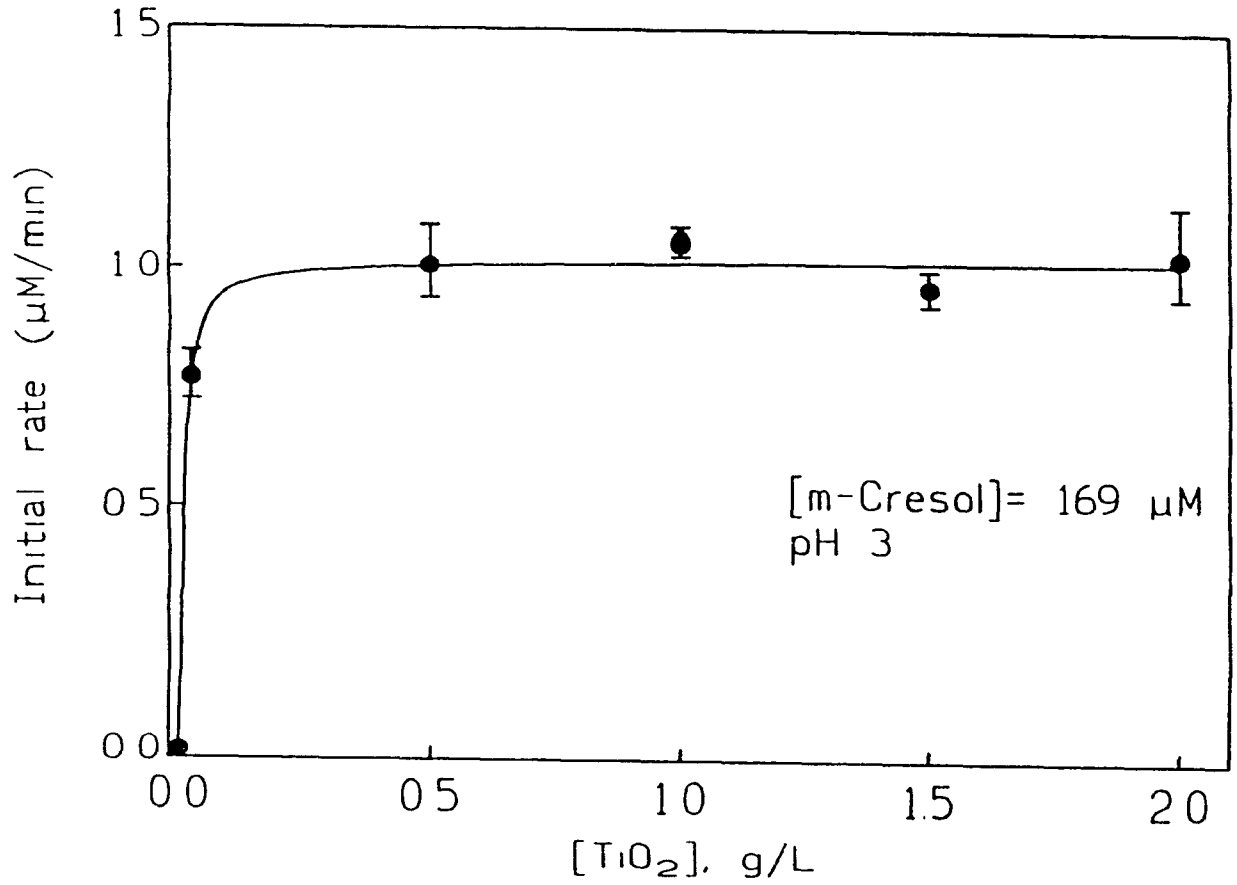


**Figure 4.2** Plot showing the effect of the $TiO_2$ concentration on the initial rate of the photocatalyzed mineralization of 20 mg/L (169 $\mu$M) of *m*-cresol at pH 3.

catalyst loading of 2 g/L is therefore equally appropriate under our conditions and was used throughout.

### 4.2.2 Effect of pH

Another parameter of some importance in reactions taking place on or involving semiconductor particle surfaces in heterogeneous media is the pH of the suspensions, as it often dictates the surface characteristics of the catalyst. For the $TiO_2$ material used in this work, the zero zeta potential occurs at pH $\approx$ 5.6. Thus, at more acidic pH the semiconductor particle surface is positively charged, while at pH $>$ 5.6 the surface is negatively charged (equations 4.1-4.2).

$$Ti^{IV}-OH + H^+ \rightleftarrows Ti^{IV}-OH_2^+ \quad (4.1)$$

$$Ti^{IV}-OH + OH^- \rightleftarrows Ti^{IV}-O^- + H_2O \quad (4.2)$$

This bears important consequences on the adsorption/desorption properties of the catalyst's particle surface, as well, no doubt, on the photoadsorption/photodesorption features of such surfaces. The influence, therefore, that pH changes will have on interfacial electron transfer kinetics (photoreductions and photooxidations) is evident.[12] Figure 4.3 illustrates the temporal course of the photodegradation of *m*-cresol (20 mg/L) at three pH's (pH 3, natural pH of $\approx$ 6.5, and pH 12). Clearly, degradation is most rapid in alkaline media where the phenoxide species is present ($pK_a$ of cresols $\approx$ 10)[13]

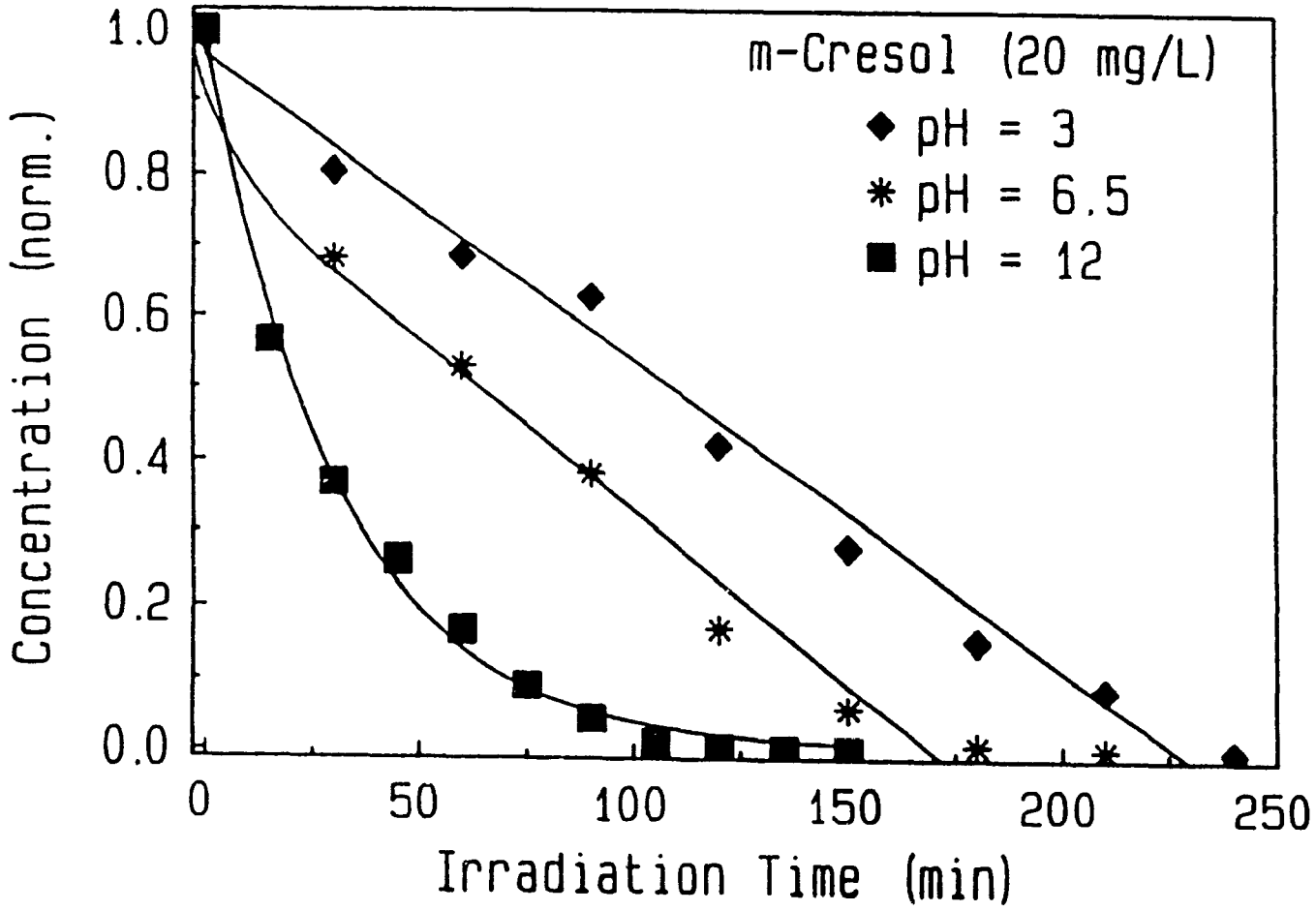


**Figure 4.3** Plots of the normalized concentration as a function of irradiation time for the photomineralization of *m*-cresol (20 mg/L) at three different pH's: 3, natural ($\approx$ 6.5), and 12; concentration of $TiO_2$, 2 g/L.

and slowest at pH 3. The quantitative aspects of the photodegradation process are treated later.

While alkaline media might seem most suited to carry out the photomineralization of organic contaminants, a deliberate choice was made to investigate the process in acidic media (henceforth, pH 3) to avoid the possible occurrence of direct photolysis, as witnessed in an earlier study on the photocatalyzed mineralization of 4-chlorophenol[14] and pentachlorophenol.[15]

## 4.2.3 Identification of Intermediates

At an initial pH of 3 and with the mobile phase used (25/75/0.1 in methanol/water/*o*-phosphoric acid), the HPLC chromatograms showed only two clearly detectable intermediates formed for each of the three cresols examined. A sample chromatogram for each cresol examined is shown in Figure 4.4. Table 4.1 summarizes the retention times (r.t., min) of the cresols and the intermediates **1**, **2**, **A** and **B**.

**Table 4.1** HPLC Retention Times of Intermediates Produced from the Photodegradation of Cresols in Air-Equilibrated $TiO_2$ Aqueous Suspensions ([Cresol] = 20 mg/L; pH = 3).[a]

| Intermediate:<br>Retention times: | **1**<br>3.8 min. | **2**<br>7.3 min. | **A**<br>4.6 min. | **B**<br>3.45 min. |
|---|---|---|---|---|
| *o*-cresol (14.1 min.) | ✓ | - | ✓ | - |
| *p*-cresol (14.1 min.) | - | ✓ | - | ✓ |
| *m*-cresol (14.5 min.) | ✓ | ✓ | - | - |

a) Mobile phase: 25: 75: 0.1; methanol, water, *o*-$H_3PO_4$.

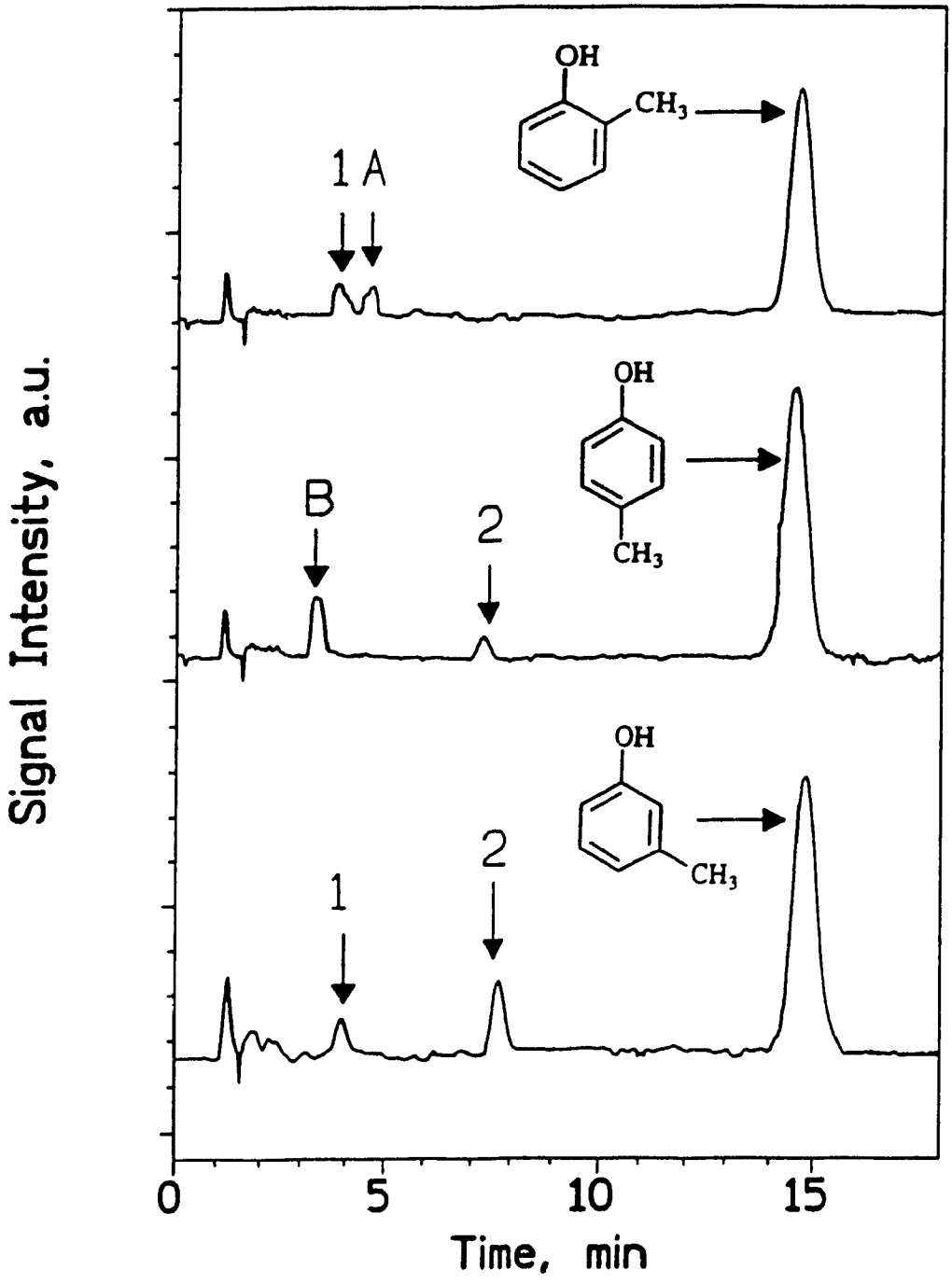


**Figure 4.4** Sample chromatograms illustrating the retention times of the intermediates observed in the course of the mineralization of o-, m-, and p-cresol. Mobile phase: 25/75/0.1 methanol, $H_2O$, $o$-$H_3PO_4$. The feature at $\approx$ 1.5 min is due to the elution of the solvent (water) as well as any other compounds not retained on the column.

The species that can form by monohydroxylation of cresols (see below), as well as the corresponding retention time (r.t.) of each species, determined from originally pure substrates (except for the 4-methylresorcinol which was not commercially available), under identical experimental conditions, are shown in Table 4.2. Comparison of these r.t. aided considerably in identifying the intermediates formed.

**Table 4.2** Identification of Intermediates Produced in the Photomineralization of Cresols in Air-Equilibrated $TiO_2$ Aqueous Suspensions (pH 3; [Cresol]= 20 mg/L)- Values in Parentheses Denote Retention Times.

| Cresol | Potential Intermediates | | | |
|---|---|---|---|---|
| 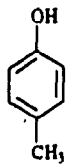 p-Cresol (14.1 min) | 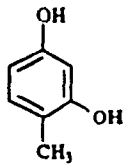 4-Methylresorcinol *(3.45 min)*[a] | 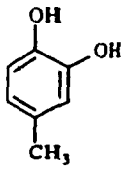 4-Methylcatechol (7.3 min) | | |
| 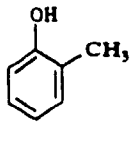 o-Cresol (14.1 min) | 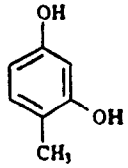 4-Methylresorcinol *(3.45 min)*[a] | 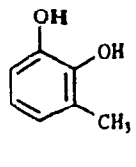 3-Methylcatechol (7.9 min) | 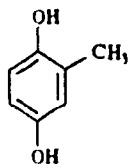 Methylhydroquinone (3.8 min) | 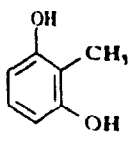 2 Methylresorcinol (4.0 min) |
| 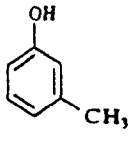 m-Cresol (14.5 min) | 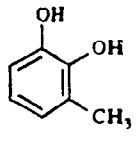 3-Methylcatechol (7.9 min) | 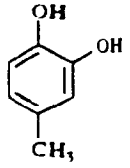 4-Methylcatechol (7.3 min) | 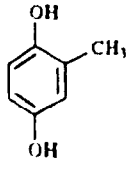 Methylhydroquinone (3.8 min) | 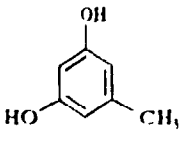 Orcinol (5.6 min) |

a) Retention times in italics were not obtained from pure samples but were "deduced" from the the data presented.

Hydroxylation of *p*-cresol yields two intermediates: 4-methylresorcinol and 4-methylcatechol. By contrast, both *o*- and *m*-cresol can in principle yield four isomeric species (see Table 4.2). Comparing the retention times of Table 4.2 with those from the liquid chromatograms indicates that species **2** (r.t. 7.3 min), common to both the *p*- and *m*-cresol is 4-methylcatechol (4-MCC). The common intermediate **1** with r.t. at 3.8 min in *o*- and *m*-cresol is identified as methylhydroquinone (MHQ). The intermediate **B** with r.t. 3.45 min, seen in the reaction of *p*-cresol, is tentatively assigned as 4-methylresorcinol; understandably, this species does not appear in the degradation of *o*-cresol as hydroxylation would have to occur at the position *meta* to the OH substituent. The identity of species **A** (Table 4.1 for *o*-cresol) with r.t. of 4.6 min is enigmatic. It is neither 2-methylresorcinol (r.t. 4.0 min), nor 3-methylcatechol (r.t. 7.9 min) which also does not form from *m*-cresol. It is possible that the quantities of these species are such that they were undetectable under our conditions. A trihydroxytoluene species cannot be ruled out for **A**; trihydroxylated benzene intermediates have been reported in the photomineralization of phenol but in very small quantities (0.3% pyrogallol and 2.1% hydroxyhydroquinone)[16,17].

Formation of 4-methylcatechol in the degradation of the cresols is confirmed by the diffuse reflectance spectra (Figure 4.5) of the catalytic powder recorded after filtration of the samples ($TiO_2$ and 500 mg/L *m*-cresol) taken at various time intervals from the irradiated flask. Before irradiation but after equilibration of the suspension in the dark, comparison of the spectral features at $\approx$ 420-500 nm with those for $TiO_2$ alone shows that some of the *m*-cresol is either physi- or chemisorbed on the semiconductor

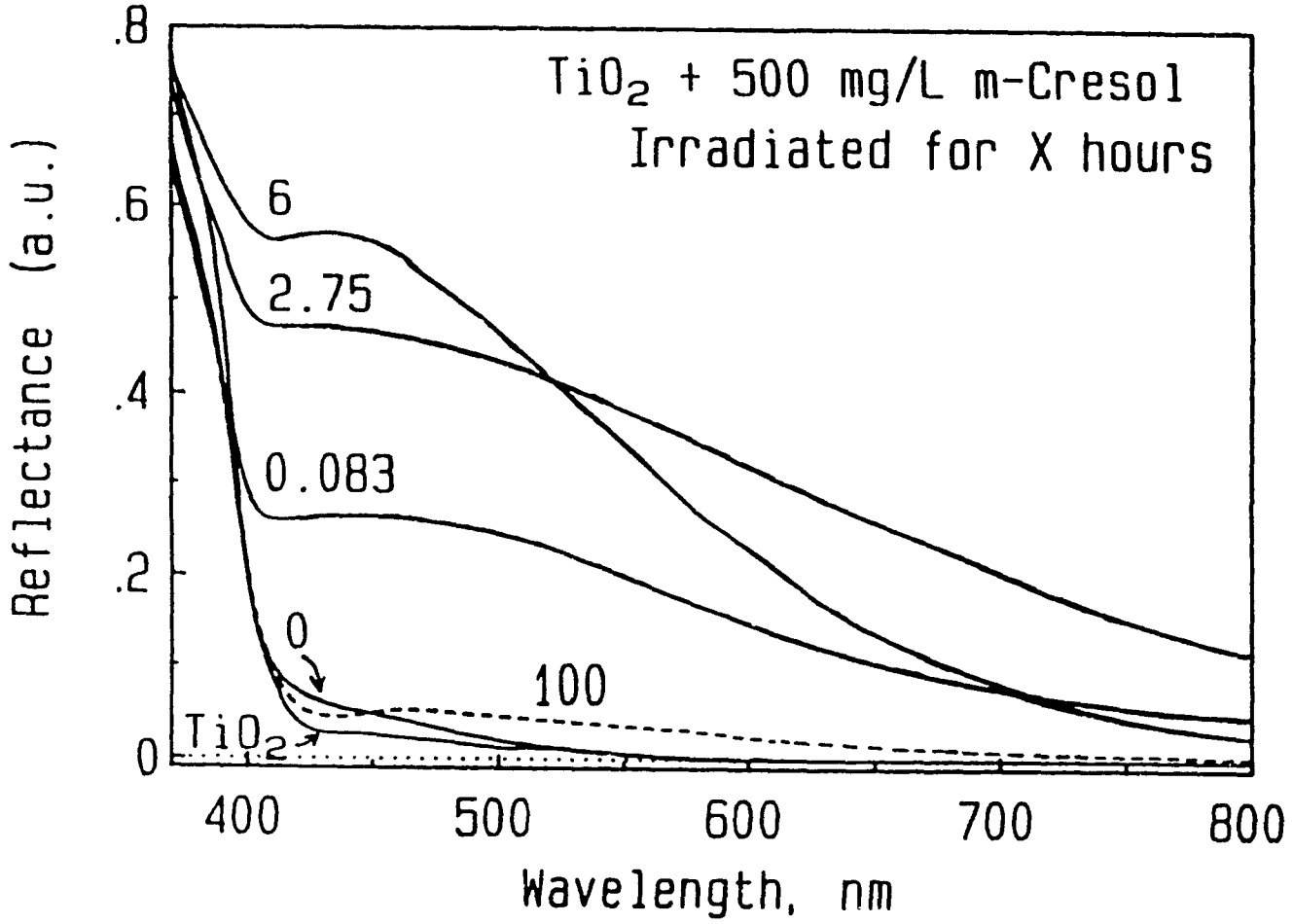


**Figure 4.5** Diffuse reflectance spectra of the catalyst powder from an air-equilibrated aqueous suspension of $TiO_2$ (2 g/L) and 500 mg/L of *m*-cresol after several hours of irradiation.

particle surface. After 5 min of irradiation, the spectra show a strong feature over the whole spectral range examined (400-800 nm); the feature grows for the first 6 hr. of irradiation. The $TiO_2$ catalyst powder appears greyish-pink coloured at this point. Identical spectral features were observed from reflectance spectra of the $TiO_2$ powder originating from a suspension consisting of $TiO_2$ and pure 4-methylcatechol.[18] Continued irradiation leads to a significant decrease in the intensity of the reflectance spectrum (100 hr) of Figure 4.5 which approaches that of $TiO_2$; it is also accompanied by a significant discoloration of the catalytic powder.

## 4.2.4 Rate Data for the Degradation of Cresols

None of the cresols investigated here undergo detectable changes in the dark in the presence of $TiO_2$. Any degradation of these substrates is therefore attributed to light-induced processes. Direct irradiation of aqueous solutions of the cresols with ultraviolet/visible light, in the absence of the semiconductor photocatalyst, leads to very small decreases in cresol concentration: 3 to 5% after $\approx$ 6 hr of irradiation (see Figures 4.6 a-c). For 20 mg/L of the cresols, the apparent rate constants are $6.3 \times 10^{-5}$ $min^{-1}$ (*o*-cresol), $18 \times 10^{-5}$ $min^{-1}$ (*m*-cresol) and $9.9 \times 10^{-5}$ $min^{-1}$ (*p*-cresol); thus, the apparent rate constants for direct photolysis are about 1 to 2 orders of magnitude smaller than those for catalyzed processes ($0.4 \times 10^{-2}$ to $1.3 \times 10^{-2}$ $min^{-1}$; see below).

The photocatalyzed decomposition of the three cresols in the presence of $TiO_2$ is presented in Figures 4.6 a-c. Both *o*- and *p*-cresol (20 mg/L) degrade via first-order kinetics. Curiously, *m*-cresol (also 20 mg/L) appears to decompose by zero-order kinetics

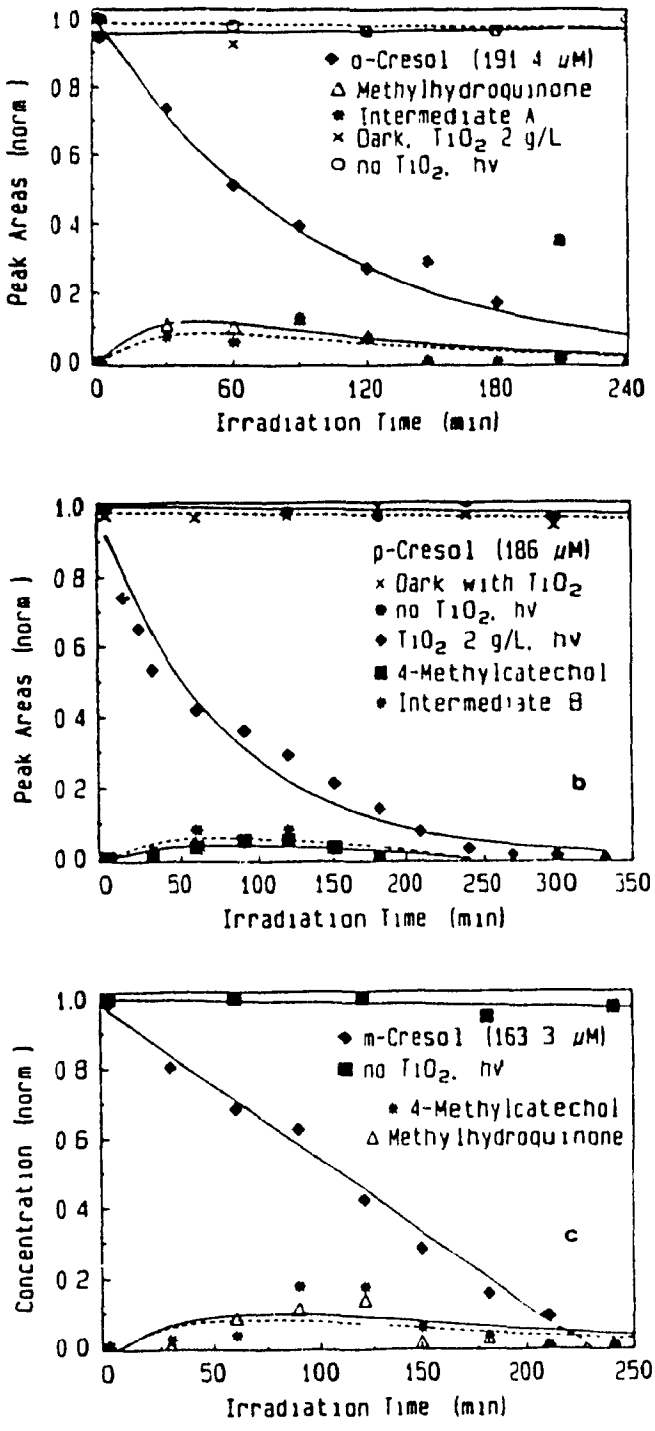


**Figure 4.6** Plots of normalized peak areas (or concentration) as a function of irradiation time showing the degradation of the three cresols (ca. 20 mg/L) and formation and decomposition of two intermediates in the photomineralization process with irradiated $TiO_2$ present (2g/L at pH 3). The behaviour of the cresols under dark conditions but in the presence of $TiO_2$, and under direct photolysis (no $TiO_2$ present), is also indicated: (a) *o*-cresol, (b) *p*-cresol, and (c) *m*-cresol. The curves are computer fits to equations noted in the text.

under identical experimental conditions of light source and initial pH. The formation and subsequent degradation of the two intermediates detected in each case are also indicated. In each case, total disappearance of the original cresol and decomposition of the intermediate species occur in $\leq$ 4 hr of irradiation. The corresponding apparent rate constants (first-order or pseudo first-order), initial rates, and half-lives for the degradation of the three cresols as a function of initial cresol concentration are summarized in Table 4.3. For *m*-cresol, data obtained at pH $\approx$ 6.5, pH 12, and in the presence of excess oxygen are also presented.

The ***apparent*** kinetic parameters for the formation and subsequent degradation of the intermediates produced in the course of mineralization for the three cresols were estimated as described in Chapter 3, section 3.2; they are presented in Table 4.4.

The photocatalyzed mineralization process for the three cresols follows the stoichiometric reaction 4.3, as evidenced by a quantitative product analysis:

$$CH_3C_6H_4OH + \frac{17}{2} O_2 \xrightarrow[TiO_2]{h\nu} 7\ CO_2 + 4\ H_2O \qquad (4.3)$$

The quantity of $CO_2$ evolved as a function of irradiation time is illustrated in Figure 4.7 for the three cresols. Approximately 32.5 $\mu$mols of $CO_2$ were expected from reaction 4.3 for $[cresol]_{in}$ = 20 mg/L. It is evident that after $\approx$ 4 hr of irradiation, when all the cresols and the aromatic intermediate species have decomposed, only about 65-70% of $CO_2$ is produced; 80-85% of $CO_2$ is evolved after about 7 hr of irradiation. We infer that

**Table 4.3** Apparent Kinetics of the Mineralization of Cresols Photocatalyzed by Irradiated $TiO_2$ in Air-Equilibrated Suspensions at pH 3.

| Cresol | [Cresol] ($\mu$M) | $k_{app}$ ($10^{-3}$ $min^{-1}$)[a] | Initial Rate ($\mu$M/min) | $t_{1/2}$(app) (min) |
|---|---|---|---|---|
| *o*-Cresol | 185 | 11.2 ± 1.0 | 2.07 ± 0.18 | 62 ± 6 |
| | 191 | 10.5 ± 0.8 | 2.01 ± 0.16 | 66 ± 5 |
| *p*-Cresol | 186 | 12.0 ± 1.1 | 2.23 ± 0.20 | 58 ± 5 |
| | 194 | 13.9 ± 1.0 | 2.69 ± 0.20 | 50 ± 4 |
| *m*-Cresol | 2.03 | 86.2 ± 7.7 | 0.175 ± 0.016 | 8.0 ± 0.7 |
| | 17.1 | 22.8 ± 2.8 | 0.390 ± 0.047 | 30 ± 4 |
| | 185 | 3.98 ± 0.17 | 0.736 ± 0.031 | 174 ± 7 |
| | 163 | 4.25 ± 0.16 | 0.694 ± 0.026 | 163 ± 6 |
| | 443 | 2.12 ± 0.08 | 0.993 ± 0.035 | 327 ± 12 |
| | 905 | 1.10 ± 0.05 | 0.996 ± 0.048 | 630 ± 29 |
| | 4966 | 0.154 ± 0.008 | 0.765 ± 0.040 | 4500 ± 234 |
| | 186[b] | 11.8 ± 0.6 | 2.19 ± 0.11 | 59 ± 3 |
| | 176[c] | 4.76 ± 0.38 | 0.836 ± 0.067 | 146 ± 12 |
| | 164[d] | 31.3 ± 1.2 | 5.13 ± 0.19 | 22 ± 1 |

a) Zero order rate constants for the photodegradation of *m*-cresol ($\mu$M $min^{-1}$) were converted to first order ($min^{-1}$) by dividing them by $[cresol]_{initial}$

b) In oxygen saturated suspensions

c) pH = 6.5

d) pH 12

**Table 4.4** Apparent Kinetics of Formation of Intermediates Produced at pH 3 in Air-Equilibrated Irradiated $TiO_2$ Suspensions.

| Parameter | Source | | |
|---|---|---|---|
| | *o*-Cresol | *p*-Cresol | *m*-Cresol |
| [Cresol], $\mu M$ | 191 | 186 | 163 |
| $k_{app}$ (degradation), $min^{-1}$ | 0.0105 | 0.012 | 0.0043 (0.0118)[a] |
| $k_{app}$ (formation), $min^{-1}$ | | | |
| 4-MCC | - | 0.014 | 0.0043 |
| MHQ | 0.011 | - | 0.0043 |
| Intermediate | 0.011 (A) | 0.014 (B) | - |
| $k_{app}$ (degradation), $min^{-1}$ | | | |
| 4-MCC | - | 0.014 | 0.02 |
| MHQ | 0.04 | - | 0.03 |
| Intermediate | 0.03 (A) | 0.014 (B) | - |
| $k_{app}$ ($CO_2$ formation), $min^{-1}$ | ≈0.0076 | ≈0.012 | ≈0.0095 (0.032)[a] |

a) In an oxygen-saturated suspension

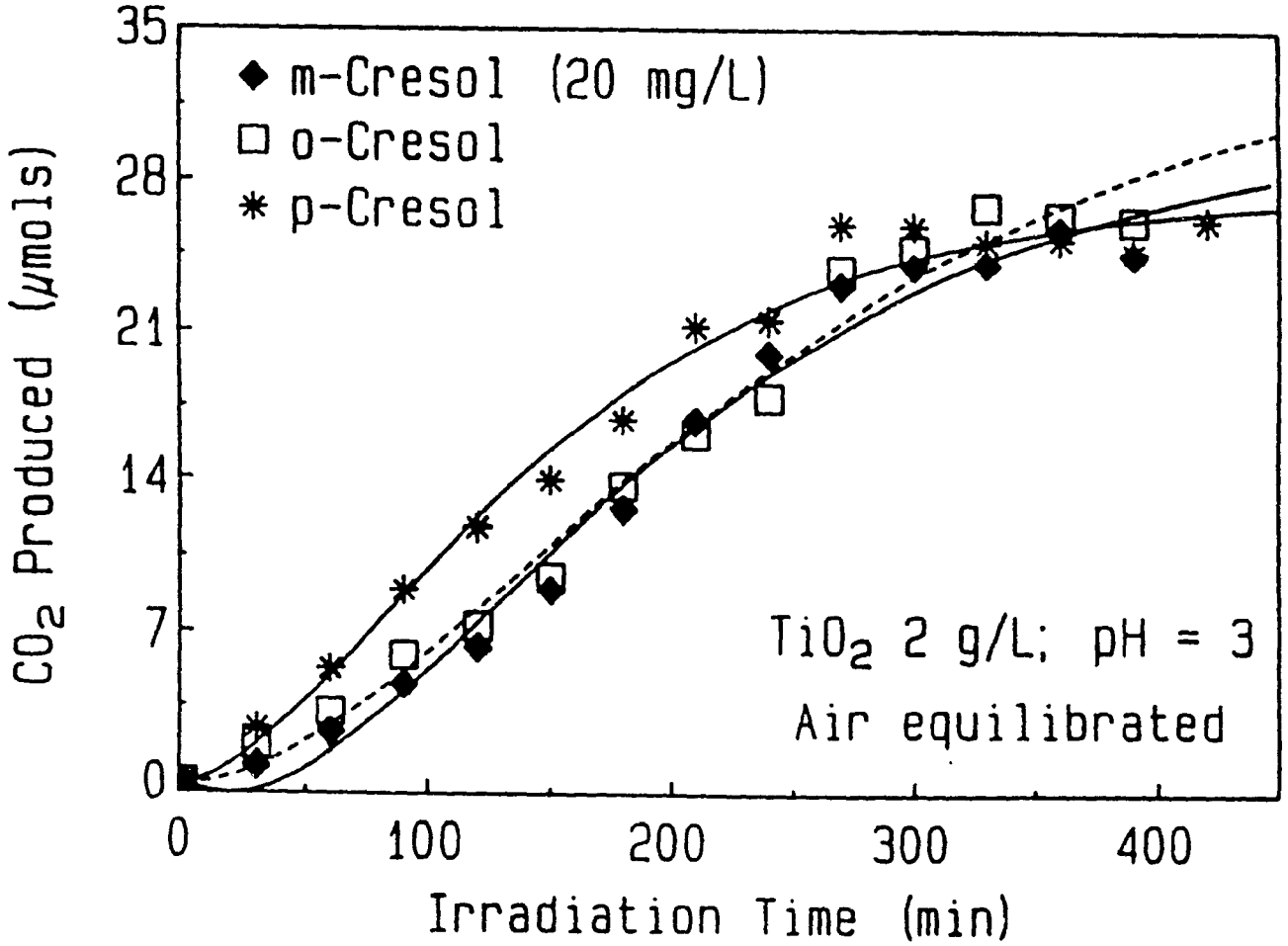


**Figure 4.7** Plots showing the temporal evolution of $CO_2$ from the photomineralization of 20 mg/L cresol in the presence of 2 g/L $TiO_2$ at an initial pH of 3; air-equilibrated suspensions.

other intermediates (aliphatic) are formed which are slow to degrade. Alternatively, the suspension may be starved of needed oxygen[15] or it could be a bit of both.

## 4.2.5 Effect of Oxygen

The effect of the concentration of oxygen on the kinetics of decomposition of *m*-cresol was determined by carrying out the mineralization process under conditions where the suspension was always saturated with molecular $O_2$. The decomposition of this cresol in air-equilibrated and in oxygen-saturated suspensions is compared in Figure 4.8 a. Apparent zero-order kinetics are also evident for the latter. The corresponding parameters are, air *versus* $O_2$, respectively: $k_{app}$, 3.98 x $10^{-3}$ $min^{-1}$ and 11.8 x $10^{-3}$ $min^{-1}$; initial rates, 0.74 $\mu$M/min and 2.2 $\mu$M/min; $t_{1/2}$(app), 174 min and 59 min. Note that in the presence of excess oxygen, decomposition of *m*-cresol occurs in < 1.5 hr. Comparison of the evolution of carbon dioxide from air-equilibrated and oxygen-saturated suspensions is made in Figure 4.8 b. For the latter suspensions, approximately 60% of $CO_2$ evolved after the cresol had decomposed. Near quantitative formation of $CO_2$ occurred in ca. 2.5 hr; $k_{app} \approx$ 9.5 x $10^{-3}$ $min^{-1}$ (air) and 32 x $10^{-3}$ $min^{-1}$ ($O_2$). The slower evolution of products cannot be due solely to the lack of oxygen, but rather to the intermediacy of the aliphatic intermediates.

## 4.2.6 pH Dependence

*m*-Cresol was chosen for more detailed investigation into the effect of pH on the total degradation to $CO_2$ and water. Air-equilibrated aqueous $TiO_2$ suspensions of

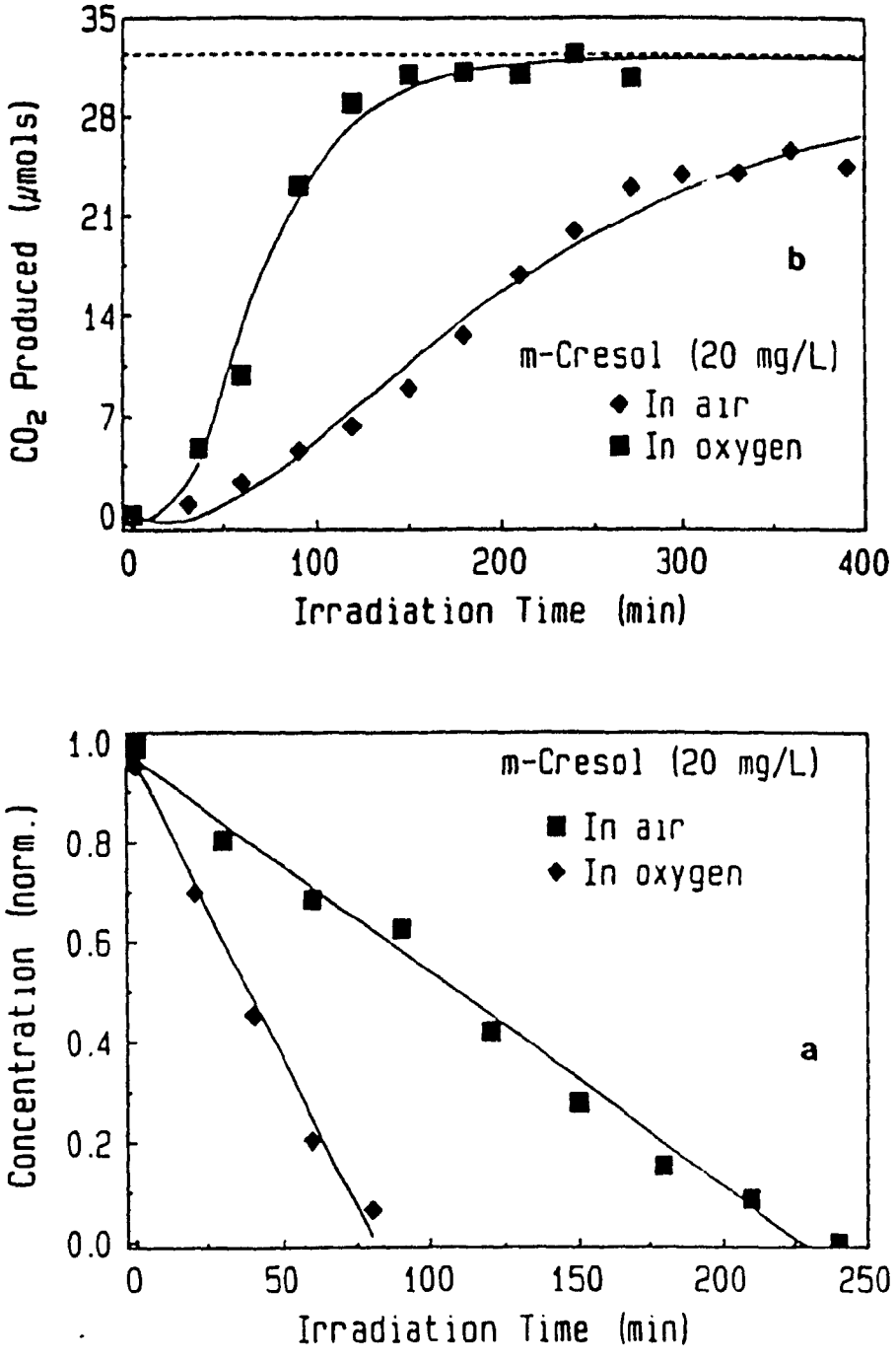


**Figure 4.8** (a) Plots showing the photodegradation of 20 mg/L of *m*-cresol in the presence of 2 g/L $TiO_2$ in air-equilibrated suspensions and in oxygen-saturated suspensions; initial pH 3. (b) Plots showing the corresponding temporal evolution of $CO_2$ from the photomineralization of 20 mg/L of *m*-cresol in air-equilibrated and oxygen-saturated suspensions of $TiO_2$.

20 mg/L of this substrate were examined at pH 3, at natural pH ($\approx$ 6.5), and at pH 12 (see Figure 4.3). The respective $k_{app}$ are 3.98 x $10^{-3}$ $min^{-1}$, 4.76 x $10^{-3}$ $min^{-1}$, and 31.3 x $10^{-3}$ $min^{-1}$. The photomineralization in alkaline media follows first-order kinetics unlike that in acidic media. This results because adsorption requires interaction between two negatively charged entities at pH 12 (the negative particle surface and the phenoxide), thereby leading to low surface coverage at this pH and concentration of *m*-cresol. Figure 4.9 depicts, as normalized peak heights *versus* irradiation time, the temporal course of the degradation of *m*-cresol at pH 12 in the absence (direct photolysis) and presence of $TiO_2$. Direct photolysis proceeds via zero-order kinetics; the pseudo first-order $k_{app}$ (17 x $10^{-5}$ $min^{-1}$) is similar to that from the direct photolysis at pH 3, but is about 20 times slower than for the catalyzed process.

Four intermediates were detected at pH 12: 4-methylcatechol, methylhydroquinone, and two unidentified intermediates (**I** and **II**). The corresponding apparent first order rate constants for both the formation and degradation of these species are: 0.029 $min^{-1}$ and 0.030 $min^{-1}$ (**MHQ**), 0.086 $min^{-1}$ and 0.087 $min^{-1}$ (**I**), and 0.113 $min^{-1}$ and 0.114 $min^{-1}$ (**II**). **4-Methylcatechol** forms via first-order kinetics (4.7 x $10^{-4}$ $min^{-1}$); it degrades via a zero-order process (pseudo first-order $k_{app} \approx 0.41$ $min^{-1}$).

## 4.2.7 Concentration Dependence

The photomineralization of *m*-cresol occurs via zero order kinetics (Figure 4.10 a, b, and Table 4.3) for all concentrations examined [$\approx$0.2 mg/L (2.03 $\mu$M) to $\approx$500 mg/L (4966 $\mu$M)]; the rate constants vary from 0.175 $\mu$M/min to 0.996 $\mu$M/min.

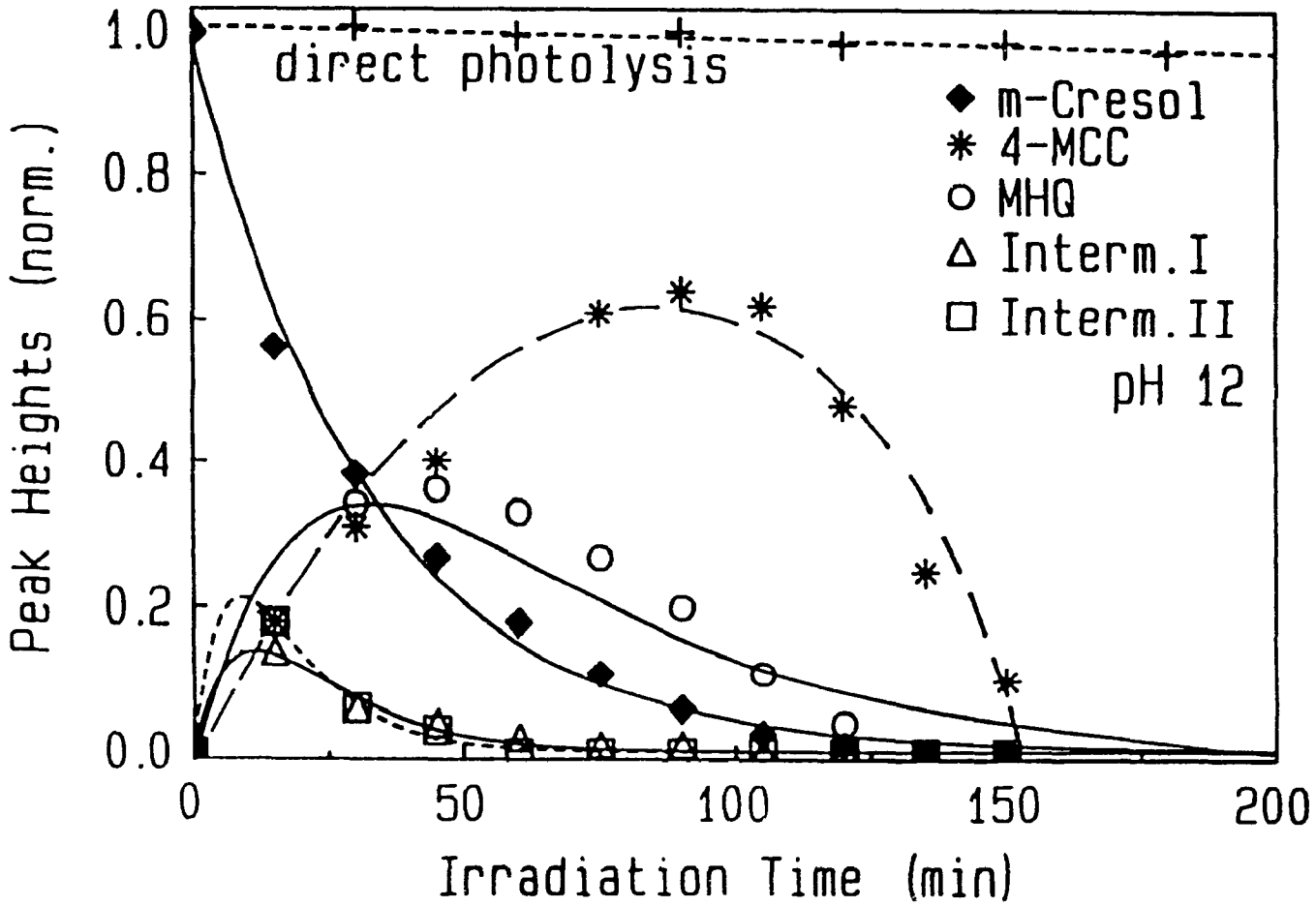


**Figure 4.9** Photodegradation of 164 $\mu$M *m*-cresol via direct photolysis and via the photocatalyzed process in the presence of $TiO_2$ at an initial pH of 12. Also shown are the formation and subsequent degradation of the four intermediate species detected by HPLC methods (see text).

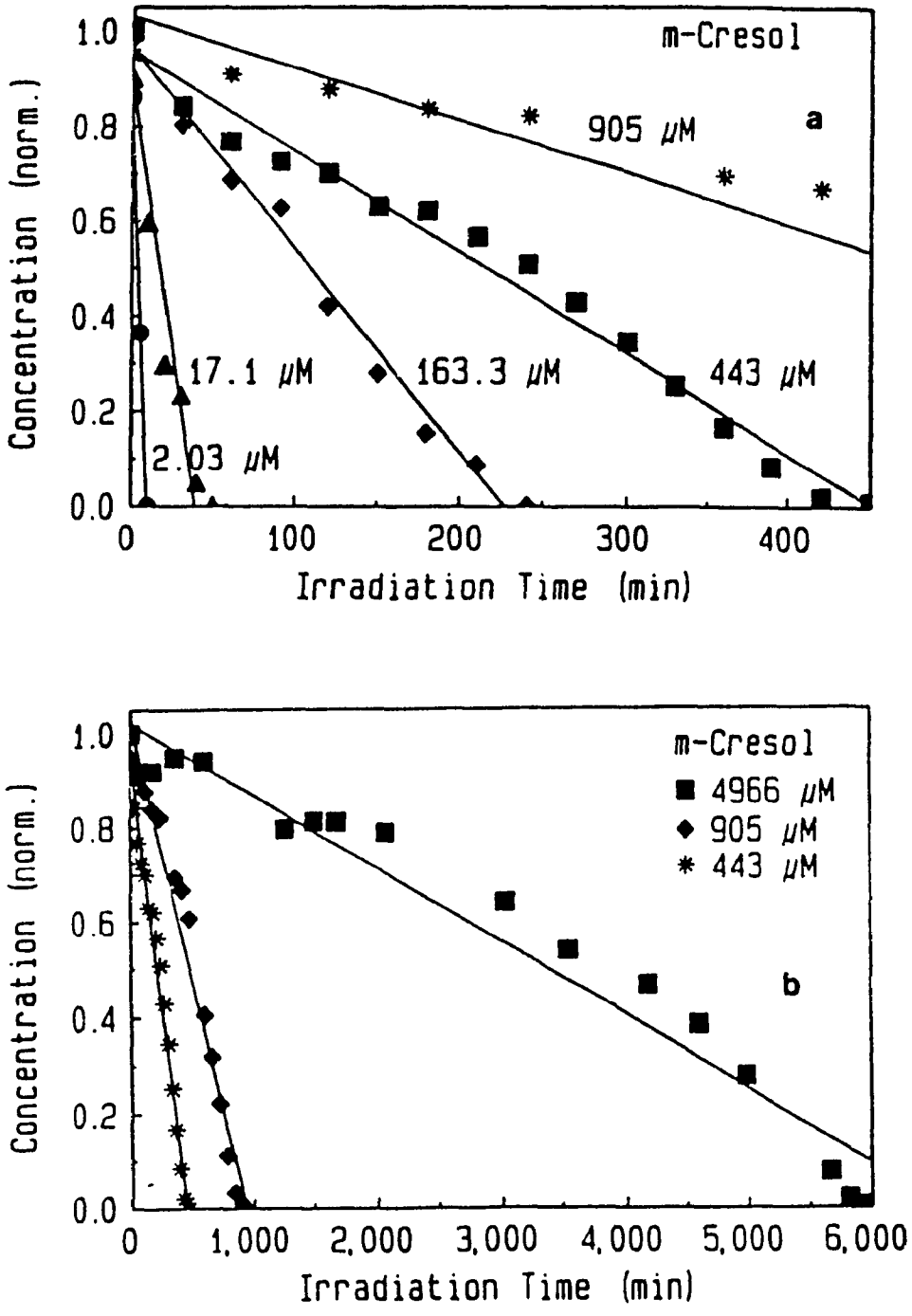


**Figure 4.10** Zero-order plots of the photomineralization of *m*-cresol catalyzed by irradiated $TiO_2$ at various initial concentrations; initial pH 3.

A plot of initial rates ($R_{in}$) *versus* initial [*m*-cresol] reveals similarities with Langmuir-Hinshelwood (LH) type behaviour (Figure 4.11 a): $R_{in} = k'_{app}K[m\text{-cresol}]/(1 + K[m\text{-cresol}])$.[19] The linear transform of this expression (Figure 4.11 b) yields the zero-order $k'_{app} = 0.86 \pm 0.06\ \mu M/min$ and the apparent adsorption coefficient $K = 4.8 \pm 0.6 \times 10^{-4}\ M^{-1}$.

## 4.2.8 Radiant Power Level Dependence

The dependence of the rate of photodegradation of *m*-cresol (20 mg/L) on the radiant power level of the light source is illustrated in Figure 4.12. The initial rate increases linearly (slope = $0.029 \pm 0.002\ \mu M\ cm^2/mW\ min$) with power level (low light fluxes), suggesting that electron/hole recombination is not the sole major deactivating pathway for photogenerated electrons and holes; the photooxidative step(s) on the semiconductor catalyst can also compete effectively as demonstrated by the very fact that photodegradation of the substrates does occur, albeit at low photochemical efficiencies (see below).

## 4.2.9 Photochemical Efficiencies

Owing to the bandgap of 3.2 eV of the semiconductor used ($TiO_2$), only light of wavelengths below 400 nm can drive the photocatalyzed process. The photochemical efficiencies for the decomposition of the cresols were determined at 365 nm and *reflect the number of molecules of the cresol that degraded per incident photon* (see Chapter 3, Experimental): 0.0096 (*o*-cresol), 0.0076 (*m*-cresol), and 0.010 (*p*-cresol).

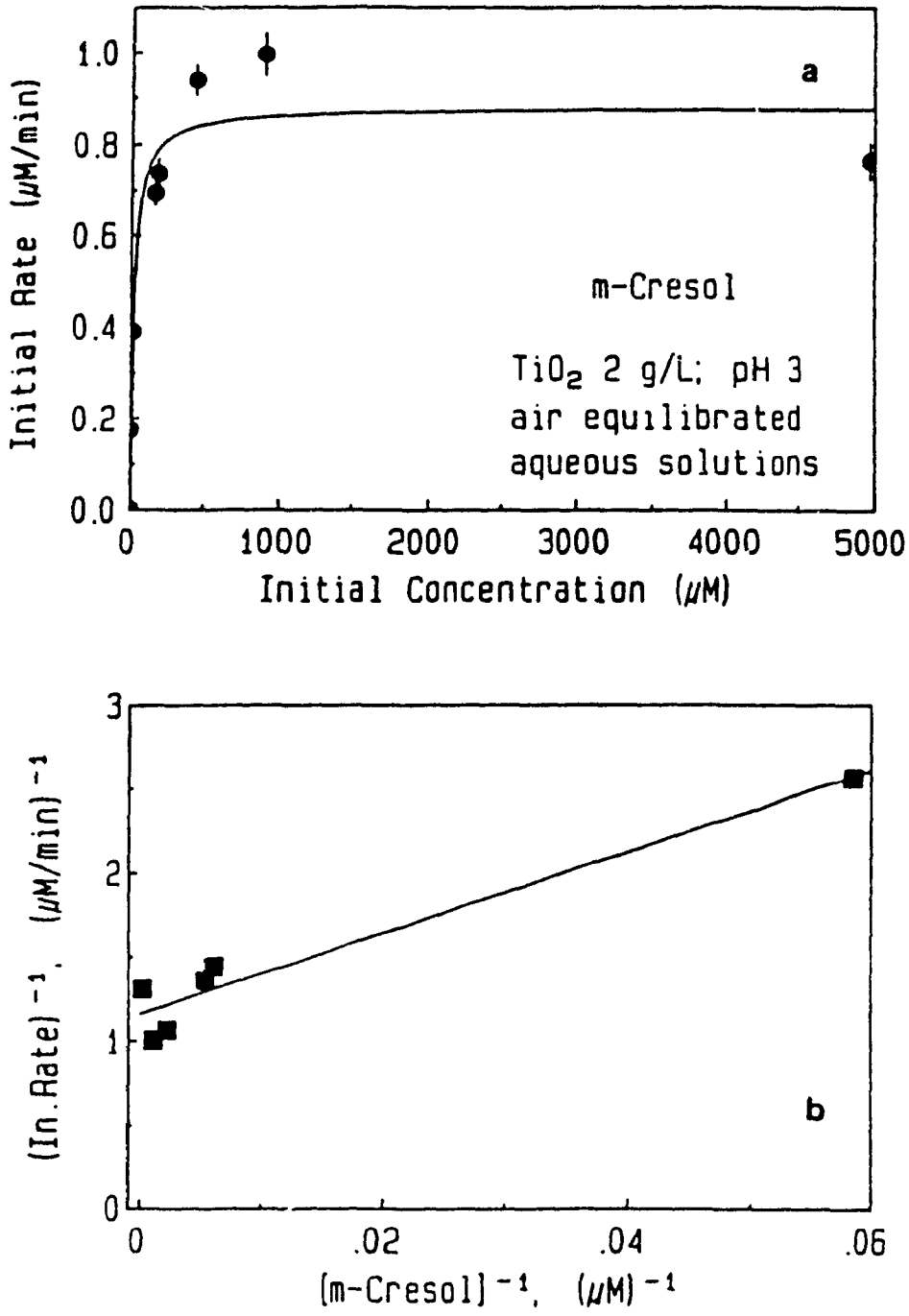


**Figure 4.11** (a) Plot showing the effect of the initial concentration on the initial rate of the photodegradation of *m*-cresol under air-equilibrated conditions; initial pH 3. (b) Linear transform of the Langmuir type isotherm (see text).

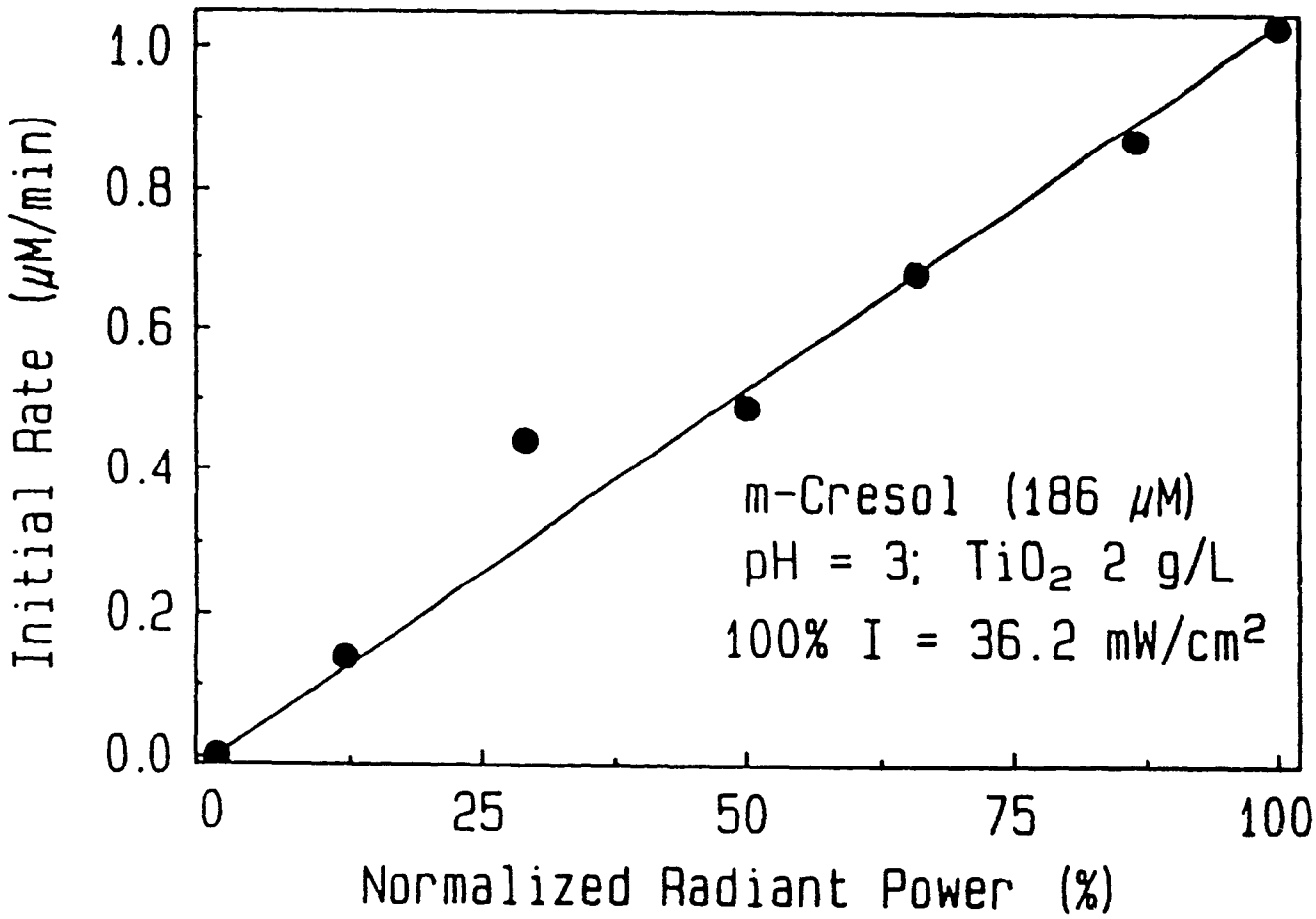


**Figure 4.12** Effect of the radiant power levels of the light source (see text) on the initial rate of the photomineralization of m-cresol (20 mg/L); initial pH 3; $TiO_2$, 2 g/L; 100% radiant power corresponds to 36.2 mW/cm$^2$.

## 4.2.10 Mechanism of the Photodegradation of Cresols

The photooxidations of the cresols in a heterogeneous medium occur by reaction between the oxidizing species (See Chapter 2) and the various cresols as a first step; this yields the intermediates (4-MCC, MHQ, and others). Subsequent reaction of these intermediate products with the oxidizing species ultimately yields $CO_2$ and $H_2O$ via a series of reactions which include ring cleavage and the formation of peroxides, aldehydes, and carboxylates as occurs in the photodegradation of surfactants.[20] With our present results, we summarize the photomineralization process by scheme 4.4.

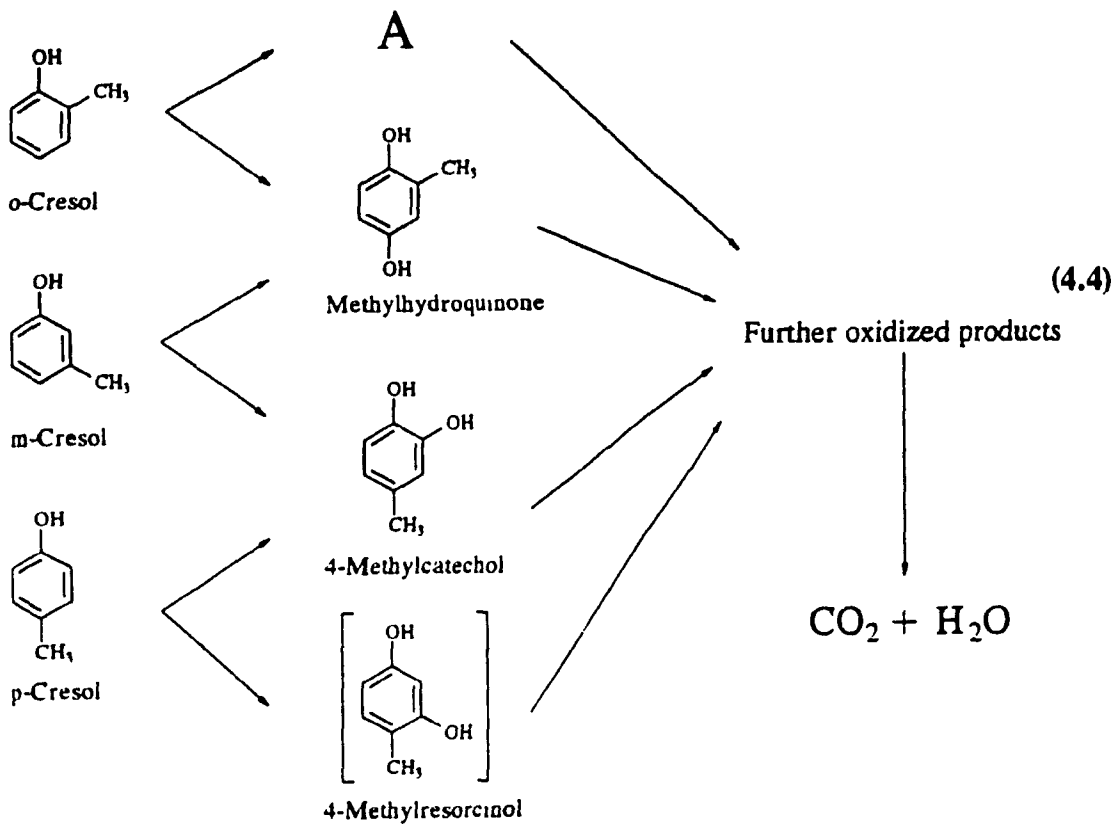


(4.4)

## 4.2.11 Kinetic Considerations

With the present results, the photomineralization of cresol can be summarized by reaction 4.5 (CR is a cresol):

$$\text{(site)} + \text{CR} \underset{k_{-5a}}{\overset{k_{5a}}{\rightleftharpoons}} (\text{CR})_{ads} \xrightarrow{k_{5b}} (\text{4-MCC})_{ads} \xrightarrow{k_{5c}} CO_2 + H_2O \qquad (4.5)$$

$$(\text{CR})_{ads} \rightarrow \text{MHQ} + \text{other intermediates}$$

The rate of formation of the final products $CO_2$ and $H_2O$ is then given by equation 4.6,

$$Rate = \frac{\frac{\phi I_a \beta A_p k_{trap} \tau_{\cdot OH}}{k_{rec}} k_{5b} K_{CR}[CR] N_s}{1 + 2K_{CR}[CR] + K_W[H_2O] + K_{MHQ}[MHQ] + \Sigma_i K_{Intm.}[Intm.]_i} \cdot \frac{K_{O_2}[O_2]}{(1 + K_{O_2}[O_2])} \qquad (4.6)$$

where $K_{CR}$ is the photoadsorption coefficient for the cresol, $k_{5b}$ is the rate constant for the conversion of $(CR)_{ads}$, and the other parameters have the same meaning as in equation 3.11, Chapter 3. Water, MHQ and other intermediates that form in the degradation process can, in principle, compete for the same adsorption sites as the cresols; they will act as inhibitors. It was also noted that molecular $O_2$ affects the rate of degradation and therefore the adsorption isotherm for $O_2$ has been included in equation 4.6. This equation has the same basic form as the Langmuir-Hinshelwood model (equation 2.25, Chapter 2) and is applicable for low light flux conditions.

## 4.3 CONCLUSIONS

The complete photomineralization of *ortho-*, *meta-* and *para*-cresol to $CO_2$ and water in air-equilibrated, irradiated $TiO_2$ suspensions takes place in ≈ 7-8 hours at pH 3. In excess molecular oxygen, degradation is faster (≤ 2.5 hr). The effect of such parameters as pH, initial cresol concentration, $TiO_2$ concentration and radiant power levels on the degradation of *m*-cresol was examined in detail; the effect these have on the overall rate is consistent with the model presented in Chapter 3.

Two major intermediates have been identified in the photodegradation of cresols: 4-methylcatechol and methylhydroquinone; other intermediates also form but were not identified under our experimental conditions. The present work adds another example of the classes of environmental organic contaminants that may be present in wastewaters and which can be degraded effectively by the photocatalytic method employed herein.

# REFERENCES


1. Callahan, M.A., Slimak, M., Gbel, N., May, I., Fowler, C., Freed, R., Jennings, P., Dupree, R., Whitemore, F., Maestri, B., Holt, B., and Gould, C., *"Water Related Environmental Fate of 129 Priority Pollutants"*, United States Environmental Protection Agency, Report No. EPA-44014-79-029a,b, NTIS, Washington, D.C., **1979**.

2. *Dangerous Prop. Ind. Mater. Rep.*, **1985**, *5*, 30, and references therein.

3. *Dangerous Prop. Ind. Mater. Rep.*, **1986**, *6*, 41, and references therein.

4. Ollis, D.F., Pelizzetti, E., Serpone, N., *Environ. Sci. Technol.*, **1991**, *25*, 1522, and references therein.

5. Matthews, R.W., in *"Photochemical Conversion and Storage of Solar Energy"*, Pelizzetti, E., Schiavello, M., Eds., Kluwer Academic Publishers, Dordrecht, The Netherlands, **1991**, p.427.

6. Al-Ekabi, H., and Serpone, N., *J. Phys. Chem.*, **1988**, *92*, 5726, [Part 1].

7. Al-Ekabi, H., Serpone, N., Pelizzetti, E., Minero, C., Fox, M.A., Draper, R.B., *Langmuir*, **1989**, *5*, 250, [Part 2].

8. Pelizzetti, E., Minero, C., Maurino, V., Sclafani, A., Hidaka, H., Serpone, N., *Environ. Sci. Technol.*, **1989**, *23*, 1385, [Part 3].

9. Borgarello, E., Serpone, N., Barbeni, M., Pelizzetti, E., *J. Photochem.*, **1986**, *33*, 35.

10. Pelizzetti, E., Pramauro, E., Minero, C., Serpone, N., Borgarello, E., in *"Photocatalysis and Environment"*, Schiavello, M., Ed., NATO ASI Series, Ser.C237, Kluwer Academic Publ., Dordrecht, The Netherlands, **1988**, pp. 469-497, and references therein.

11. Serpone, N., Borgarello, E., Pelizzetti, E., in *"Photocatalysis and Environment"*, Schiavello, M., Ed., NATO ASI Series, Ser.C237, Kluwer Academic Publ., Dordrecht. The Netherlands, **1988**, pp. 527-565, and references therein.

12. See for example: Grätzel, M., *"Heterogeneous Photochemical Electron Transfer"*, CRC Press, Inc., Boca Raton, Florida, **1989**, p. 125.

13. *"Handbook of Biochemistry and Molecular Biology"*, 3rd ed., Volume 1, "Physical and Chemical data", Fasman, G.D., ed., CRC Press, Cleveland, **1976.**

14. Barbeni, M., Pramauro, E., Pelizzetti, E., Borgarello, E., Grätzel, M., Serpone, N., *Nouv. J. Chim.*, **1984**, *8*, 550.

15. Barbeni, M., Pelizzetti, E., Borgarello, E., Serpone, N., *Chemosphere*, **1985**, *14*, 195.

16. Okamoto, K., Yamamoto, Y., Tanaka, H., Tanaka, M., Itaya, A., *Bull. Chem. Soc. Jpn.*, **1985**, *58*, 2015.

17. Okamoto, K., Yamamoto, Y., Tanaka, H., Itaya, A., *Bull. Chem. Soc. Jpn.*, **1985**, *58*, 2023.

18. See Chapter 5 of this work.

19. Laidler, K.J., *"Chemical Kinetics"*, 3rd. Edn., Harper & Row Publ., New York, **1987**, pp. 400-406.

20. Hidaka, H., Zhao, J., Suenaga, S., Pelizzetti, E., and Serpone, N., *J. Jpn. Oil Chem. Soc.*, **1990**, *39*, 45.

# CHAPTER 5

# THE PHOTOMINERALIZATION OF METHYLHYDROQUINONE AND 4-METHYLCATECHOL

## 5.1 INTRODUCTION

Both methylhydroquinone (MHQ) and 4-methylcatechol (4-MCC) were identified in Chapter 4 as the two major intermediate products from the complete photomineralization of cresols to $CO_2$ and $H_2O$. As part of these continuing studies into the photocatalyzed mineralization of organic substrates in the aqueous ecosystem, it was of interest to examine the temporal course of the degradation of these two species, catalyzed by irradiated $TiO_2$ slurries, to explore and understand the pathway(s) through which these and related species can be destroyed, particularly when they are present in low quantities (tens of mg/L levels) in wastewaters. 4-Methylcatechol was of particular interest as it was detected in an adsorbed state on the surface of $TiO_2$ particles in the photocatalyzed mineralization of *m*-cresol.[1] Moreover, they provide further examples of systematic studies carried out into the kinetics of processes occurring in irradiated heterogeneous media.[2-4]

## 5.2 PHOTOCATALYZED DEGRADATION OF MHQ AND 4-MCC

### 5.2.1 Photomineralization of Methylhydroquinone

In the absence of light, MHQ is only slightly adsorbed ($\leq$ 1.5%) onto the semiconductor particle surface. The disappearance of MHQ in aqueous $TiO_2$ dispersions

($[MHQ]_{ini}$ = 71.3 $\mu$M; $[TiO_2]$ = 2g/L; pH 3) irradiated by uv/visible light was monitored by High Performance Liquid Chromatography. The HPLC chromatograms in Figure 5.1 illustrate the decrease in concentration of MHQ as a function of irradiation time. The organic substrate degrades via reasonably good first-order kinetics ($k_{app} \approx 0.041 \pm 0.003$ $min^{-1}$; $t_{1/2}$ = 17 min) for about 3 half-lives (Figure 5.2 A). The total photo-degradation of MHQ is complete after ca. 1 hr of irradiation, as confirmed by the concomitant evolution of stoichiometric quantities (reaction 5.1) of $CO_2$ (Figure 5.2 B) which is also complete in $\approx$ 1 hr. In the absence of $TiO_2$ and within the time frame of our experiments, direct irradiation led to negligible, if any, decomposition of this substrate.

$$CH_3C_6H_3(OH)_2 + 8O_2 \xrightarrow[TiO_2]{h\nu} 7CO_2 + 4H_2O \qquad (5.1)$$

The process takes place via an intermediate, probably a trihydroxytoluene species (**I**),[2,5] the amount of which was estimated by a mass balance calculation. The intermediate **I** (or equivalents) forms and decays via first-order kinetics {$k_{app}$ are, respectively, $\approx$ 0.041 $min^{-1}$ and $\approx 0.14 \pm 0.05$ $min^{-1}$} as does the formation of $CO_2$ ($k_{app} \approx 0.041$ $min^{-1}$ and $\approx 0.14$ $min^{-1}$). The data presented in this section was fitted to equations of the form described in Chapter 3, Section 3.2 for consecutive first-order reactions.

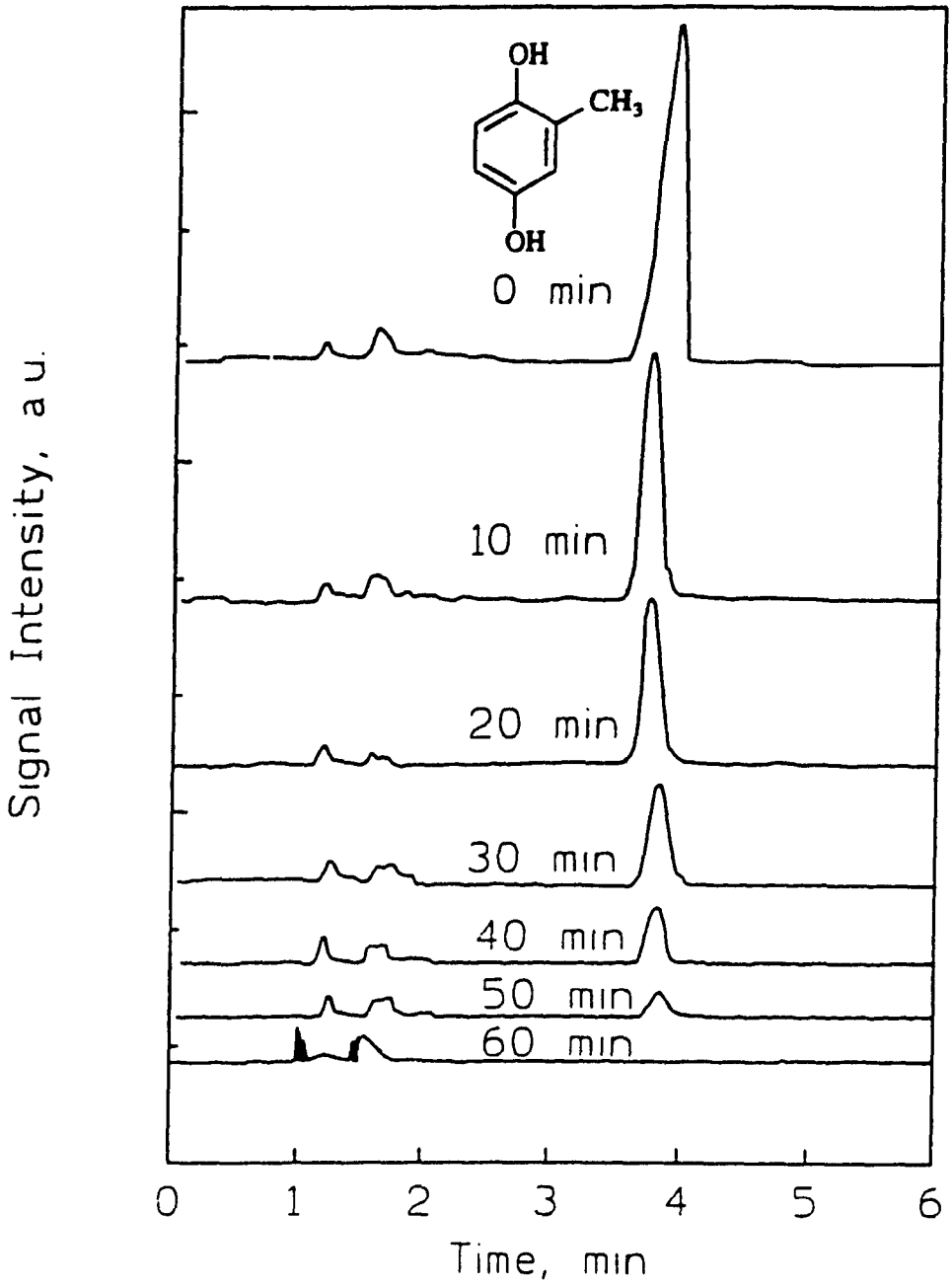


**Figure 5.1** HPLC chromatograms showing the decrease in concentration of MHQ as a function of irradiation time in irradiated aqueous $TiO_2$ dispersions; $[MHQ]_{ini} = 71.3\ \mu M$; $[TiO_2] = 2 g/L$; pH 3. The features between 1 and 2 min are attributed to the solvent and any other compounds not retained by the column.

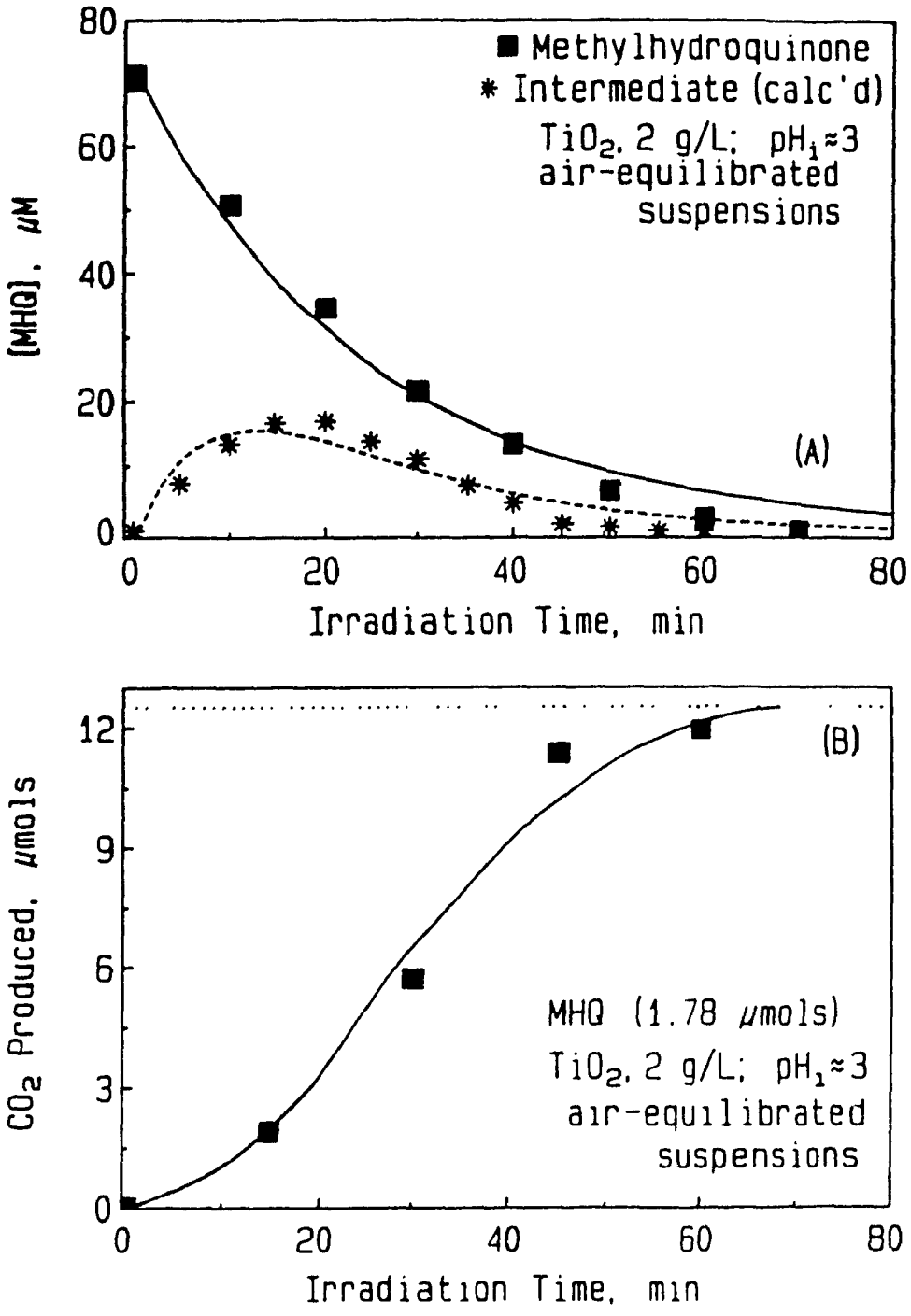


**Figure 5.2** (A) Photodegradation of MHQ (71.3 $\mu$M) in air-equilibrated aqueous suspensions of $TiO_2$ irradiated by light at wavelengths > 300 nm; pH 3; $TiO_2$, 2 g/L; 50 mL samples. The asterisked points are those of an unknown intermediate(s) the quantity of which was estimated by mass balance. **(B)** Stoichiometric evolution of $CO_2$ with irradiation time; same conditions as in (A) but volume of sample was 25 mL. Dashed line denotes the amount of $CO_2$ expected upon total mineralization of MHQ.

## 5.2.2 Photomineralization of 4-Methylcatechol

Under dark conditions, 4-MCC strongly adsorbs (≈ 53%; initial concentration, 63.6 $\mu$M; pH 3) to the surface of the $TiO_2$ particles. Irradiation of the air-equilibrated $TiO_2$/4-MCC aqueous suspension leads to degradation of the adsorbed organic substrate which disappears from solution in about 20 min with no detectable (under our conditions) intermediates, as illustrated by the HPLC chromatograms in Figure 5.3. Adsorption and complete disappearance of 4-methylcatechol in this time frame was confirmed by the diffuse reflectance spectra (illustrated in Figure 5.4) of the catalytic powder during the course of the mineralization.

Initially, a relatively intense spectral feature appears on the low energy side (≈ 450 nm) of the absorption edge (≈ 400 nm) of the $TiO_2$ semiconductor; we attribute this spectral feature to complexes formed by 4-MCC with surface $Ti^{IV}$ on $TiO_2$ particles, reminiscent of similar complexes formed between 8-hydroxyquinoline with $TiO_2$.[6] A similar feature was also observed in the $TiO_2$ catalyzed photomineralization of *m*-cresol[1]. After 10 min of irradiation, the intensity of this feature decreased significantly; by 20 min it had totally disappeared. The reflectance spectrum at 20 min is identical to that of pure $TiO_2$, thereby confirming the total decomposition of any 4-MCC adsorbed on the surface. However, the total evolution of stoichiometric amounts of $CO_2$, which occurs via apparent first-order kinetics ($k_{app} \approx 0.025 \pm 0.005$ min$^{-1}$), is observed only after ≈ 1 hr of irradiation (Figure 5.5 B). This suggests the intermediacy of one or more additional (probably *aliphatic* carboxylates which are not detectable under our experimental conditions) intermediates that retard $CO_2$ formation. As in the case of

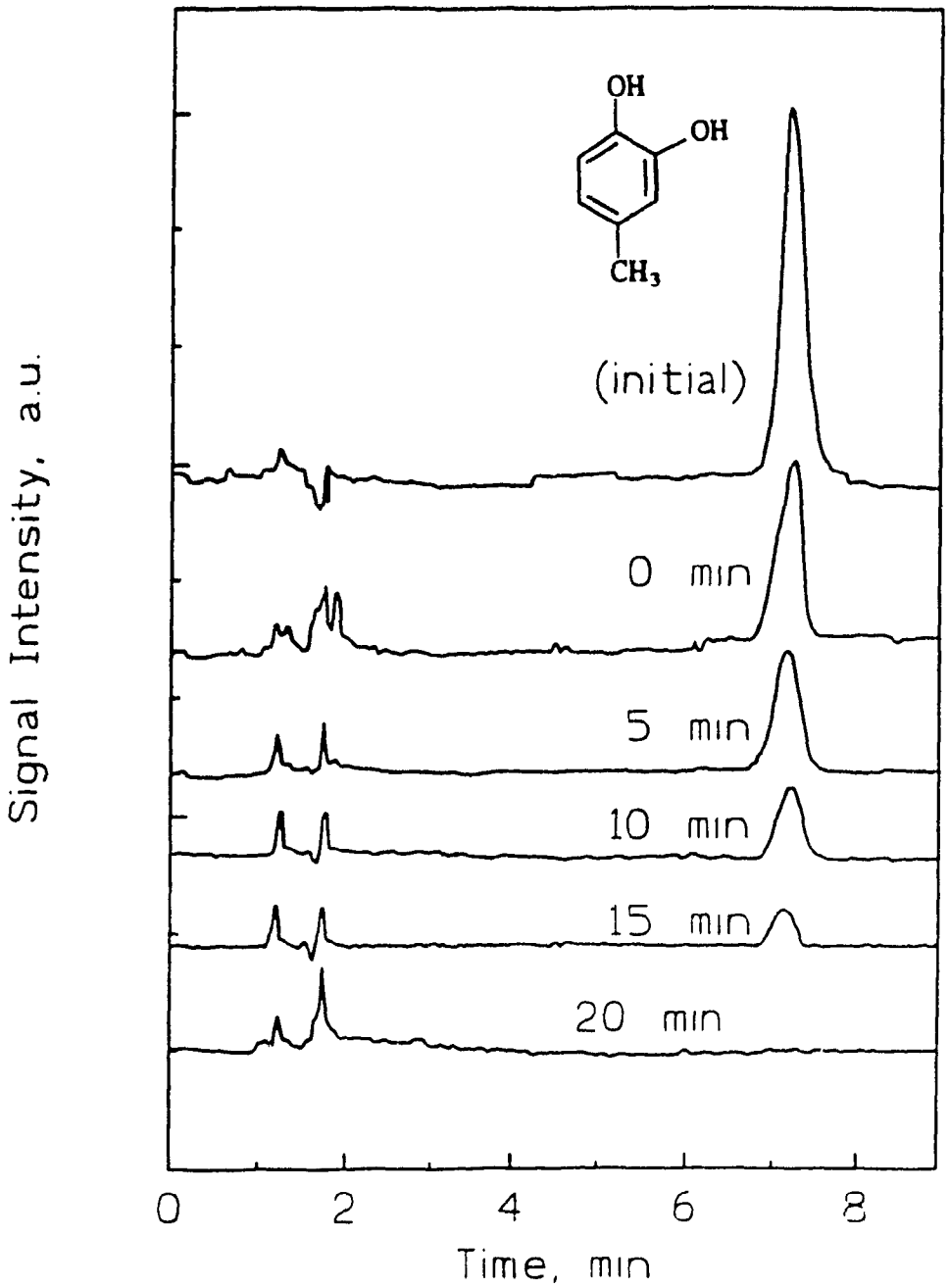


**Figure 5.3** HPLC chromatograms showing the decrease in concentration of 4-MCC as a function of irradiation time in irradiated aqueous $TiO_2$ dispersions; $[4\text{-MCC}]_{ini} = 63.6\ \mu M$; $[TiO_2] = 2 g/L$; pH 3. The features between 1 and 2 min are attributed to the solvent and any intermediates not retained by the column.

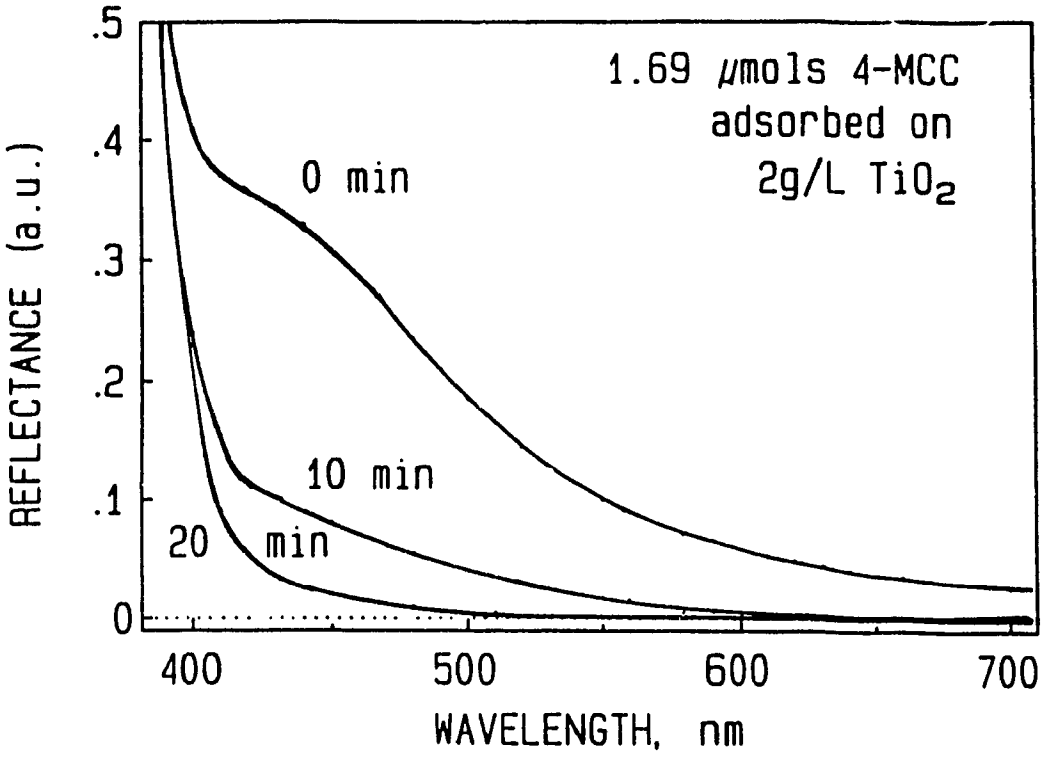


**Figure 5.4** Diffuse reflectance spectra of the catalyst powder after various irradiation periods for a suspension of $TiO_2$ and 4-MCC (see text).

MHQ, direct irradiation in the absence of $TiO_2$ also had a negligible effect on the overall degradation of 4-MCC within the time frame of these experiments.

## 5.2.3 Kinetic Considerations

### 5.2.3.1 Methylhydroquinone

It was noted earlier that the extent of MHQ adsorption in the dark is rather small ($\leq$ 1.5%); the extent of photoadsorption, however, is an unknown parameter. It is assumed that there exists a constant fraction, however small, of MHQ adsorbed or photoadsorbed on the catalyst's particle surface. The photomineralization of MHQ can

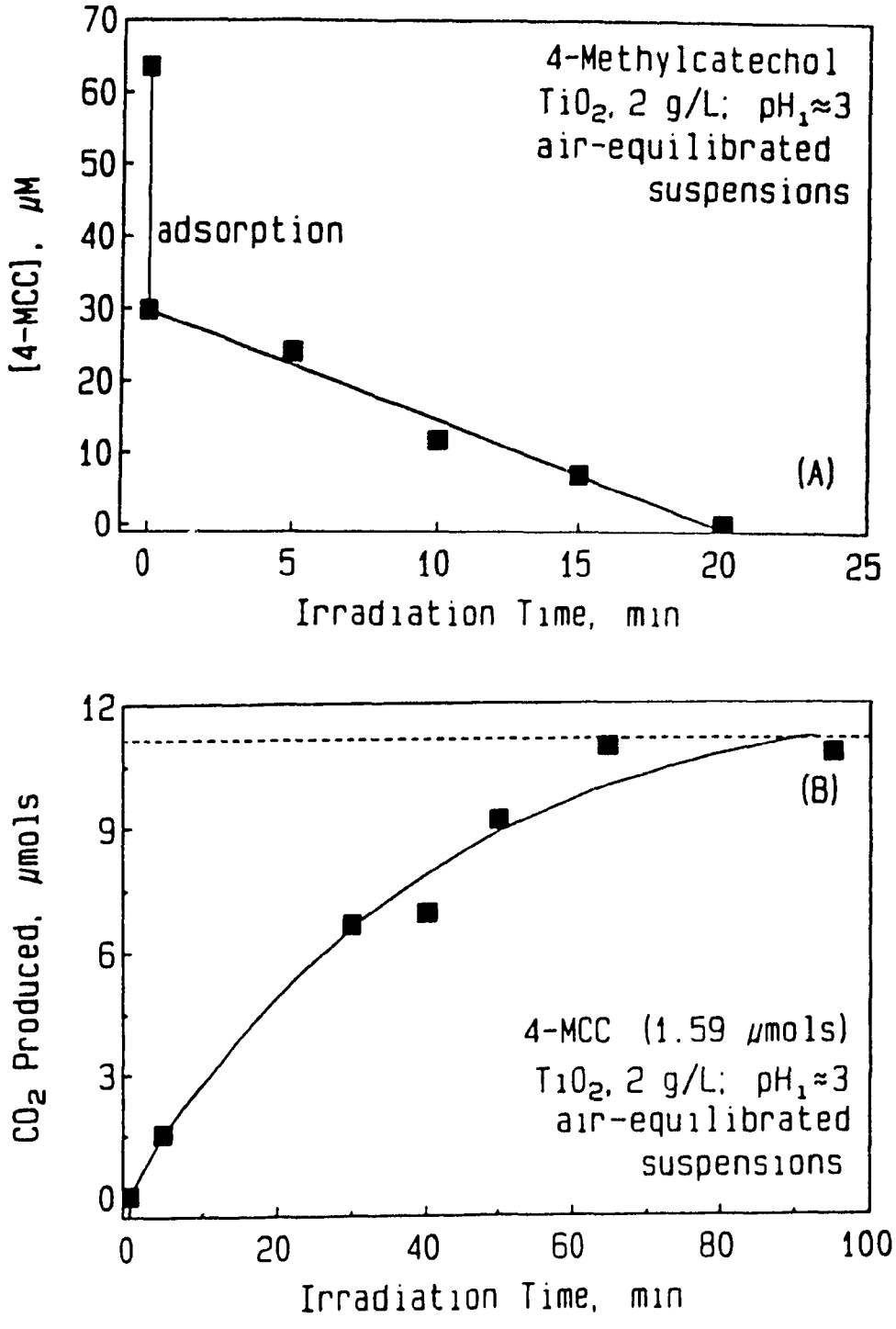


**Figure 5.5 (A)** Photodegradation of 4-methylcatechol (63.6 $\mu$M); same conditions as for Figure 5.2 A. **(B)** Stoichiometric formation of carbon dioxide as a function of irradiation time; same conditions as in (A) but volume of sample was 25 mL. Dashed line denotes the amount of $CO_2$ expected upon total mineralization of 4-MCC.

then be described by equation 5.2:

$$(site) + MHQ \underset{k_{-2a}}{\overset{k_{2a}}{\rightleftharpoons}} (MHQ)_{ads} \overset{k_{2b}}{\rightarrow} (I) \overset{k_{2c}}{\rightarrow} other\ intermediates \rightarrow CO_2 + H_2O \quad (5.2)$$

for which the rate of formation of the final products is:

$$Rate = \frac{\frac{\phi I_a \beta A_p k_{trap} \tau_{\cdot OH}}{k_{rec}} k_{2b} K_{MHQ}[MHQ] N_s}{1 + \alpha K_{MHQ}[MHQ] + K_W[H_2O] + \Sigma_i K_{Intm.}[Intm.]_i + K_{ions}[ions]} \cdot \frac{K_{O_2}[O_2]}{(1 + K_{O_2}[O_2])} \quad (5.3)$$

where $\alpha$ is $(k_{2b} + k_{2c})/k_{2c}$, $k_{2b}$ is the rate constant for the conversion of $(MHQ)_{ads}$, $K_{MHQ}$ is the photoadsorption coefficient for methylhydroquinone, and the other parameters have the same meaning as in equation 3.11, Chapter 3. It must be pointed out that any extraneous species present in the suspension, or intermediate formed in the process, can act as an inhibitor if it competes for the same adsorption sites where the oxidation process originates. Thus, water, anions (in the present case, $Cl^-$), and **I** can potentially inhibit the reaction. The binding isotherm expression for $O_2$ is also included, as it influences the overall process.[1,5,7,8] Equation 5.3 has the same form as the Langmuir-Hinshelwood expression (equation 2.25, Chapter 2) and is applicable for low light fluxes.

### 5.2.3.2 *4*-METHYLCATECHOL

In this particular case, we have noted above that this species is strongly adsorbed on the catalyst's surface and that its decomposition occurs in $\leq$ 20 min. as verified also from reflectance spectroscopy. Partitioning of this species between the heterogeneous

surface and the solution bulk complicates the process kinetics; they will have to await a more detailed modeling.

## 5.3 CONCLUSIONS

The total destruction of methylhydroquinone and 4-methylcatechol, to two innocuous products $CO_2$ and $H_2O$ occurs very effectively in short time in the presence of a light absorbing photocatalyst, $TiO_2$: within 1 hr for MHQ and in about 20 min for 4-MCC. Although the kinetic expressions do not permit unambiguously any inference as to the actual operational pathway (surface *versus* bulk solution reactions), it does appear that the compound adsorbed more strongly (4-MCC) degrades more rapidly. This would be consistent with the reaction occurring on the $TiO_2$ particle surface. Further work, which will necessitate the determination of some of the rate constants implicitly or explicitly indicated here, may yet provide additional clues as to the details of the photomineralization process.

# REFERENCES


1. See Chapter 4 in this thesis.

2. Al-Ekabi, H., and Serpone, N., *J. Phys. Chem.*, **1988**, *92*, 5726, [Part 1].

3. Al-Ekabi, H., Serpone, N., Pelizzetti, E., Minero, C., Fox, M.A., Draper, R.B., *Langmuir*, **1989**, *5*, 250, [Part 2].

4. Pelizzetti, E., Minero, C., Maurino, V., Sclafani, A., Hidaka, H., Serpone, N., *Environ. Sci. Technol.*, **1989**, *23*, 1385, [Part 3].

5. Okamoto, K., Yamamoto, Y., Tanaka, H., Tanaka, M., and Itaya, A., *Bull. Chem. Soc. Jpn.*, **1985**, *58*, 2015.

6. Houlding, V.H., Grätzel, M., *J. Am. Chem. Soc.*, **1983**, *105*, 5695.

7 Okamoto, K., Yamamoto, Y., Tanaka, H., Itaya, A., *Bull. Chem. Soc. Jpn.*, **1985**, *58*, 2023.

8. Meyer, G.J., Luebker, E.R.M., Lisensky, G.C., Ellis, A.B., in: *"Photochemistry on Solid Surfaces"*, Anpo, M., Matsuura, T., Eds., Elsevier, Amsterdam, **1989**, p. 388.

# CHAPTER 6

# THE PHOTOCATALYZED MINERALIZATION OF XYLENOLS IN AQUEOUS MEDIA WITH IRRADIATED TITANIA

## 6.1 INTRODUCTION

Phenols figure prominently in the list of priority pollutants put forth by the United States Environmental Protection Agency (See Table 1.1).[1] Phenolic substrates such as xylenols (dimethylphenols) are used as wood preservatives, most notably as components of creosote.[2] In fact, the six isomers of xylenol together comprise 35 wt % of the phenolic components of creosote (See Chapter 1, Figure 1.3).[2] Decontamination of creosote contaminated sites is a significant challenge to environmental chemists due to the persistent environmental problem presented.[2,3]

The photocatalyzed destruction (mineralization) of cresols (methylphenols) has been carried out using titanium dioxide (Degussa P-25) under ultraviolet/visible or simulated sunlight irradiation (see Chapter 4 of this thesis); total mineralization was demonstrated by following the temporal evolution of the products $CO_2$ (and $H_2O$) along with the concomitant disappearance of the original substrate. The work presented herein is part of systematic kinetic and mechanistic studies on $TiO_2$ mediated photo-oxidations of alkylated phenols. The effects of such parameters as pH, initial xylenol concentration, catalyst loading, radiant power levels of the light source, temperature, are also examined. Hydroxylated aromatic intermediates formed have been identified and rate data are

examined in the context of the kinetic principles described in Chapter 3. Photochemical efficiencies for the disappearance of the xylenols at 365 nm have also been determined.

## 6.2 PHOTOOXIDATIVE DEGRADATION OF XYLENOLS

### 6.2.1 Catalyst Loading

Photocatalyst loading in the light-induced splitting of $H_2S$,[4] in the photooxidation of organics,[5] or in the photoreduction of trace metals from dilute solutions[6] has often been 2 g/L of the semiconductor material ($TiO_2$, CdS, ZnO, and others). In this case, the initial rate of degradation of 3,4-xylenol (160 $\mu$M; ca. 20 mg/L) showed little change upon varying the concentration of $TiO_2$ between 0.6 and 2 g/L as illustrated in Figure 6.1a. A catalyst loading of 2 g/L is therefore equally appropriate under our conditions and was used throughout. The plot (Figure 6.1a) of initial rates ($R_{in}$) *versus* initial [3,4-xylenol] reveals similarities with Langmuir-Hinshelwood (LH) type behaviour $R_{in} = k'_{app}K[TiO_2]/(1 + K[TiO_2])$[7]. A computer fit of the Langmuir expression to the data points in Figure 6.1a yields a value of $k'_{app} = 12.5 \pm 1.8$ $\mu$M/min and the apparent adsorption coefficient $K = 4.2 \pm 2.1$ $\mu M^{-1}$. The linear transform of this expression (Figure 6.1b) yields a value of $k'_{app} = 10.1 \pm 1.4$ $\mu$M/min and the apparent adsorption coefficient $K = 1.18 \pm 0.17$ $\mu M^{-1}$. Both sets of values are in reasonable agreement.

### 6.2.2 Effect of pH

Another important parameter in reactions taking place on semiconductor particle surfaces in heterogeneous media is the pH of the suspensions, since it often dictates the

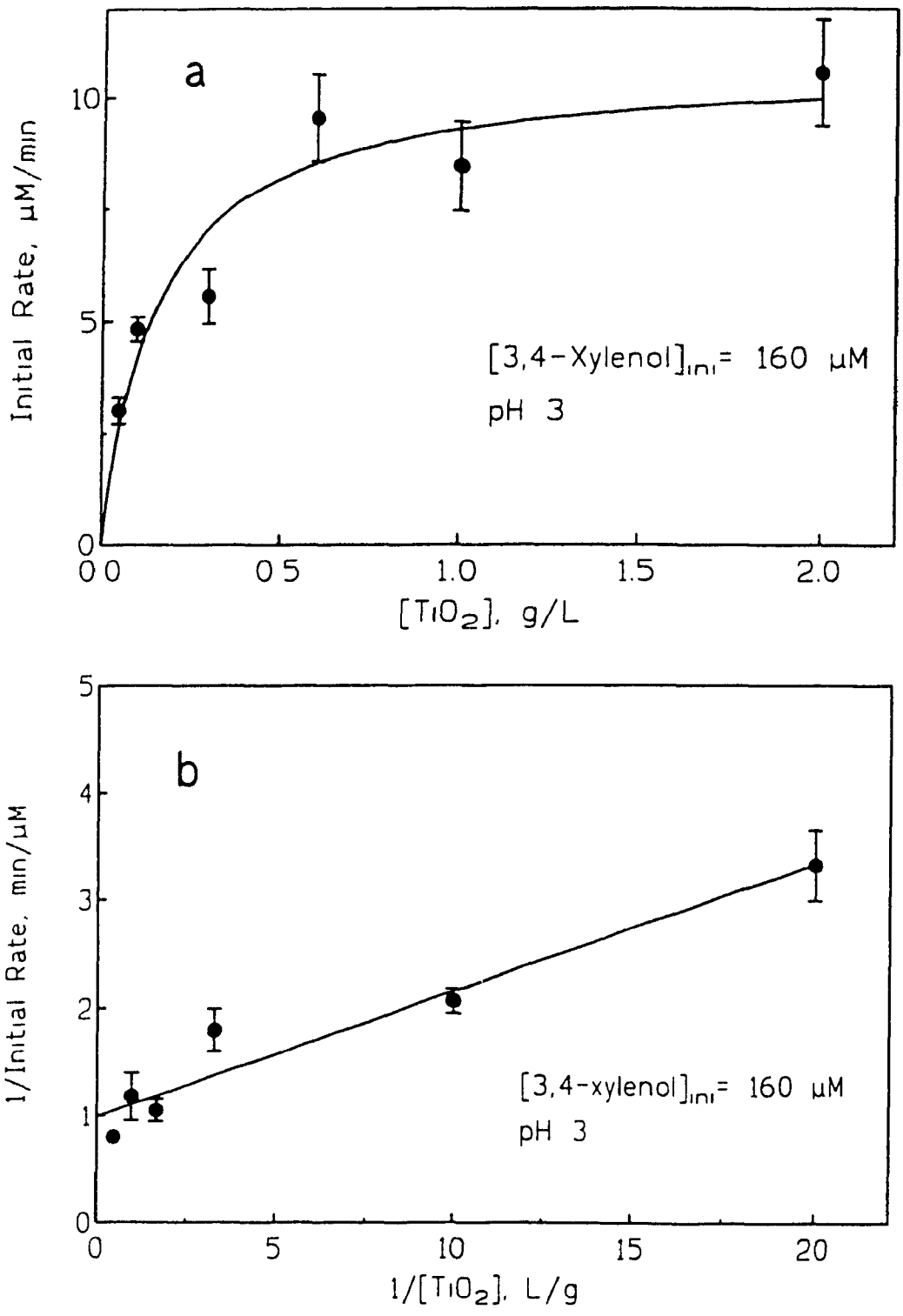


**Figure 6.1** (a) Plot showing the effect of the $TiO_2$ concentration on the initial rate of the photocatalyzed mineralization of 20 mg/L (160 $\mu$M) of 3,4-xylenol at pH 3. (b) Linear transform of the Langmuir type expression (see text).

surface characteristics of the photocatalyst. For the $TiO_2$ material used in this work, the point of zero charge (pzc) occurs at pH $\approx$ 5.6. Thus, at more acidic pH the semiconductor particle surface is positively charged, while at pH > 5.6 the surface is negatively charged (equations 6.1-6.2).

$$Ti^{IV}\text{-}OH + H^+ \rightleftharpoons Ti^{IV}\text{-}OH_2^+ \quad (6.1)$$

$$Ti^{IV}\text{-}OH + OH^- \rightleftharpoons Ti^{IV}\text{-}O^- + H_2O \quad (6.2)$$

This bears important consequences on the adsorption/desorption properties of the catalyst's particle surface, as well, no doubt, on the photoadsorption/photodesorption features of such surfaces. The influence, therefore, that pH changes will have on interfacial electron transfer kinetics (photoreductions and photooxidations) is evident.[8] Figure 6.2 illustrates the effect of pH on the rate of photodegradation of 3,4-xylenol (160 $\mu$M) at pH values ranging from 3 to 13. The plot in Figure 6.2 shows 3 distinct regions: The first region (pH 3 to 5) shows an increase in the apparent first-order rate constants ($k_{app}$) as a function of pH; the second region (pH 5 to 10) is relatively uninfluenced by the pH, whereas the third region pH 10-13 shows a sharp increase in $k_{app}$ as a function of pH. Clearly, degradation is most rapid in alkaline media where 3,4-xylenol is present as the phenoxide species ($pK_a$ of 3,4-xylenol = 10.4)[9] and slowest at pH 3. The slight increase in rate between pH 3 and 5 and its relative independence of pH at 5 < pH < 10 can best be explained by the charge on the $TiO_2$ particle surface. When the surface is positively charged and the phenol is neutral, adsorption would have

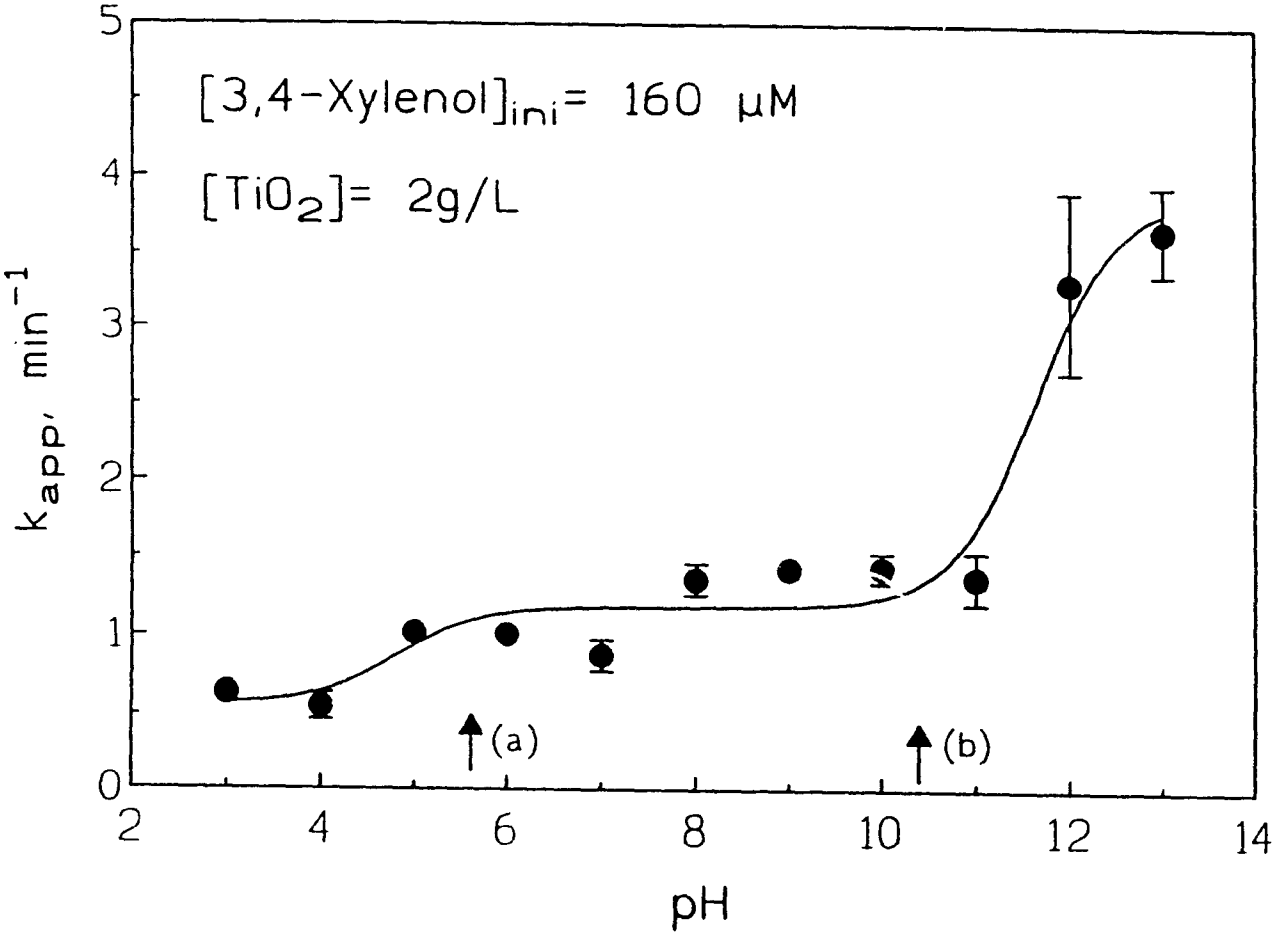


**Figure 6.2** Plots of the apparent first order rate constants for the photodegradation of 3,4-xylenol as a function of initial pH. (a) indicates the pzc ($\approx$ 5.6) value for the $TiO_2$ material used in this work, (b) indicates the $pK_a$ of 3,4-xylenol (10.4).

to originate from electrostatic attraction between the phenol dipole and the surface charge. By contrast, adsorption is diminished when the surface charge is negative as it would have to interact with the negative end of the phenolic dipole. The interaction between the negatively charged $TiO_2$ surface with 3,4-xylenol at pH's above its $pK_a$ is likely stronger because the phenoxide ion is a fairly good nucleophile.

While alkaline media might seem most suited to carry out the photomineralization of xylenols, a deliberate choice was made to investigate the process in acidic media (pH 3) to avoid the possible occurrence of direct photolysis, as witnessed in an earlier study on the photocatalyzed mineralization of 4-chlorophenol[10] and pentachlorophenol.[11]

### 6.2.3 Identification of Intermediates

At an initial pH of 3 and with the mobile phase used (50/50, methanol/water), the HPLC chromatograms showed several detectable intermediates formed for the six xylenols surveyed. Table 6.1 summarizes the retention times (r.t., min) of the xylenols and the intermediates **1-7**, as well as the detection wavelength for each intermediate.

The species that can form by reaction of •OH radicals with xylenols, (dihydroxydimethylbenzenes and dimethylbenzoquinones) as well as the corresponding retention time of each species, determined from originally pure substrates (when they were commercially available)[#] under identical experimental conditions, are shown in

---

# 2,3-Dimethylbenzoquinone was not commercially available but was synthesized by oxidizing 2,3-dimethylhydroquinone by bubbling air overnight through an aqueous solution. This allowed the determination of the retention time of 2,3-dimethylbenzoquinone. The compound was however not isolated; no quantitative work was attempted.

**Table 6.1** HPLC Retention Times of Intermediates Produced from the Photodegradation of Xylenols in Air-Equilibrated $TiO_2$ Aqueous Suspensions ([Xylenol] ≈ 20 mg/L; pH = 3).[a]

| Intermediate: Retention Time: $\lambda_{det}$: | **1** 2.1 min 214 nm | **2** 2.2 min 214 nm | **3** 4.3 min 254 nm | **4** 3.9 min 254 nm | **5** 2.4 min 214 nm | **6** 4.0 min 254 nm | **7** 2.8 min 214 nm | **8** 3.8 min 214 nm |
|---|---|---|---|---|---|---|---|---|
| 2,3-Xylenol (6.9 min) | ✓ | ✓ | ✓ | - | - | - | - | - |
| 2,4-Xylenol (7.6 min) | - | - | - | - | - | - | - | - |
| 2,5-Xylenol (7.4 min) | - | - | - | ✓ | - | - | - | - |
| 2,6-Xylenol (6.6 min) | - | - | - | - | ✓ | ✓ | - | - |
| 3,4-Xylenol (6.6 min) | ✓ | - | - | - | - | - | - | - |
| 3,5-Xylenol (7.3 min) | - | - | - | - | ✓ | ✓ | ✓ | ✓ |

a) Mobile phase: 50:50; methanol/water.

Table 6.2. Comparison of these r.t. aided considerably in identifying the intermediates formed. It was also observed that dihydroxybenzenes have a relatively large absorbance at $\lambda = 214$ nm ($\log \epsilon \approx 3.8$) and little absorbance at $\lambda = 254$ nm. The reverse is true for benzoquinones: they have high extinction coefficients at 254 nm ($\log \epsilon \approx 4.3$) and little absorbance at 214 nm. This fact also aided in the identification of intermediates.

The photooxidation of 2,3-xylenol yields three intermediates: one major intermediate (**3**) which was identified as 2,3-dimethylbenzoquinone, and trace amounts of two intermediates (**1**) and (**2**). Intermediate **2** was identified as 2,3-dimethylhydroquinone, while intermediate **1** which was also detected in the photooxidation of 3,4-xylenol is assigned as 3,4-dimethylcatechol. The photooxidation of 2,4-xylenol yields no detectable intermediates under our experimental conditions. 2,5-Xylenol yields one intermediate (**4**) which was identified as 2,5-dimethylbenzoquinone (2,5-DMBQ). Two intermediates were detected in the photodegradation of 2,6-xylenol (**5** and **6**). Intermediate **6** was identified as 2,6-dimethylbenzoquinone (2,6-DMBQ), while **5**, which was only detected in trace amounts, is most likely 2,6-dimethylhydroquinone (2,6-DMHQ) as it was also detected in the course of the mineralization of 3,5-xylenol. A single intermediate (**1**) was detected in the photodegradation of 3,4-xylenol; this was assigned as 3,4-dimethylcatechol (3,4-DMCC) as it was also seen in the photodegradation of 2,3-xylenol. Finally, four intermediates were detected in the photodegradation of 3,5-xylenol: three intermediates (**5**, **7**, and **8**) were detected in trace amounts. The major intermediate (**6**) was identified as 2,6-dimethylbenzoquinone (2,6-DMBQ). Intermediate **5**, also detected in the photodegradation of 2,6-xylenol, is likely 2,6-dimethylhydro-

**Table 6.2** Possible Intermediates in the Photomineralization of Xylenols in Air-Equilibrated $TiO_2$ Aqueous Suspensions (pH 3; [Xylenol] ≈ 20 mg/L)- Values in Parentheses Denote Retention Times.

| Xylenol | Possible Intermediates in the Photodegradation of Xylenols | | | |
|---|---|---|---|---|
| | Dimethyldihydroxybenzenes | | | Dimethylbenzoquinones |
| 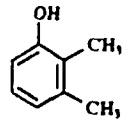 2,3-Xylenol (r.t. 6.9 min) | 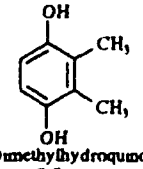 2,3-Dimethylhydroquinone (r.t. 2.2 min) | 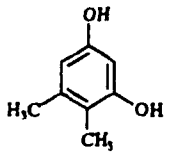 4,5-Dimethylresorcinol | 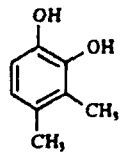 3,4-Dimethylcatechol | 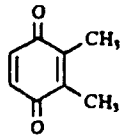 2,3-Dimethylbenzoquinone (r.t. 4.3 min) |
| 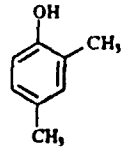 2,4-Xylenol (r.t. 7.6 min) | 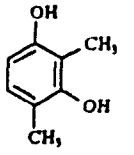 2,4-Dimethylresorcinol | 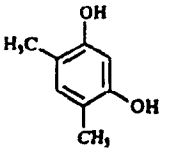 4,6-Dimethylresorcinol | 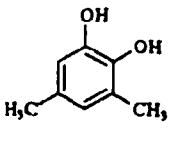 3,5-Dimethylcatechol | |
| 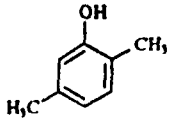 2,5-Xylenol (r.t. 7.4 min) | 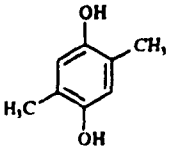 2,5-Dimethylhydroquinone | 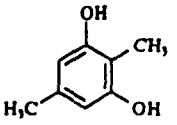 2,5-Dimethylresorcinol | 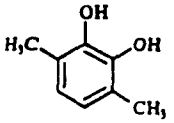 3,6-Dimethylcatechol | 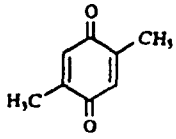 2,5-Dimethylbenzoquinone (r.t. 3.9 min) |
| 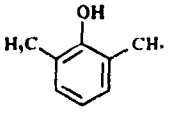 2,6-Xylenol (r.t. 6.6 min) | 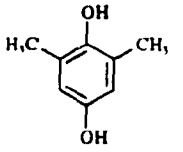 2,6-Dimethylhydroquinone | 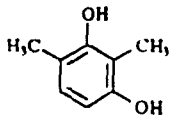 2,6-Dimethylresorcinol | | 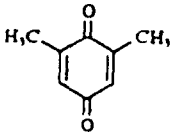 2,6-Dimethylbenzoquinone (r.t. 4.0 min) |
| 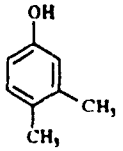 3,4-Xylenol (r.t. 6.6 min) | 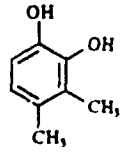 3,4-Dimethylcatechol | 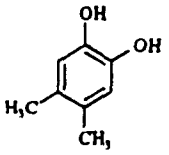 4,5-Dimethylcatechol | 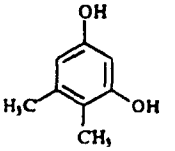 3,4-Dimethylresorcinol | |
| 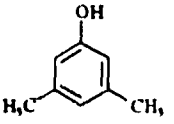 3,5-Xylenol (r.t. 7.3 min) | 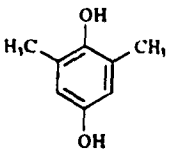 2,6-Dimethylhydroquinone | 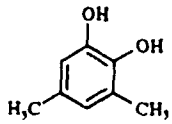 3,5-Dimethylcatechol | | 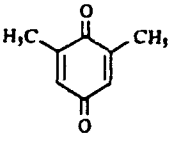 2,6-Dimethylbenzoquinone (r.t. 4.0 min) |

quinone (2,6-DMHQ). The identities of species **7** and **8** remain enigmatic; it is possible that one of them is 3,5-dimethylcatechol (3,5-DMCC) which was also expected, but not detected, in the photomineralization of 3,5-xylenol. It is likely that the quantities of this species were such that it was undetectable under our conditions. We have no evidence as to the identity of the second intermediate. We cannot rule out a possible trihydroxydimethylbenzene species for either **7** or **8**; trihydroxylated benzene intermediates have been reported in the photomineralization of phenol but in very small quantities (0.3% pyrogallol and 2.1% hydroxyhydroquinone).[12,13] Another possibility is the formation of hydrogen abstraction products; •OH radicals have been known to react with methylbenzenes (toluene and xylenes) in homogeneous solution via abstraction of a hydrogen atom from the methyl groups on the aromatic rings.[14] Possible products may be substituted benzyl alcohols or benzylic acids. The identification of intermediates **1-8** is summarized in Table 6.3.

## 6.2.4 Rate Data for the Degradation of Xylenols

None of the xylenols investigated in this work undergo detectable changes in the dark in the presence of $TiO_2$. Any degradation of these substrates is therefore attributed to light-induced processes. Direct irradiation of aqueous solutions of the xylenols with ultraviolet/visible light, in the absence of the semiconductor photocatalyst, leads to very small decreases in xylenol concentration, ($< 5\%$ after $\approx$ 1 hr of irradiation). For 20 mg/L of the xylenols, the apparent rate constants are $2.9 \pm 0.7 \times 10^{-4}$ min$^{-1}$ (2,3-xylenol), $1.1 \pm 0.1 \times 10^{-3}$ min$^{-1}$ (2,4-xylenol), $7.3 \pm 2.2 \times 10^{-4}$ min$^{-1}$ (2,5-xylenol),

**Table 6.3** Identification of Intermediates Detected in the Course of the Mineralization of Xylenols.

| Intermediate | Identification | Intermediate | Identification |
|---|---|---|---|
| 1 | 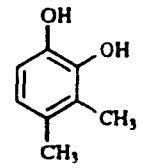 3,4-Dimethylcatechol | 5 | 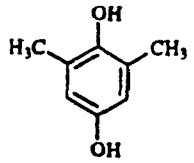 2,6-Dimethylhydroquinone |
| 2 | 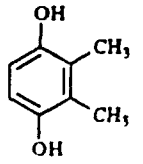 2,3-Dimethylhydroquinone | 6 | 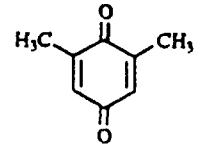 2,6-Dimethylbenzoquinone |
| 3 | 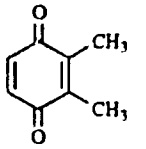 2,3-Dimethylbenzoquinone | 7 | See text |
| 4 | 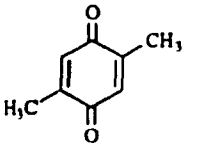 2,5-Dimethylbenzoquinone | 8 | See text |

7.5 ± 0.6 x $10^{-4}$ $min^{-1}$ (2,6-xylenol), 1.9 ± 0.1 x $10^{-3}$ $min^{-1}$ (3,4-xylenol) and 7.4 ± 0.5 x $10^{-4}$ $min^{-1}$ (3,5-xylenol). Thus, the apparent rate constants for direct photolysis are about 1 to 2 orders of magnitude smaller than those for catalyzed processes (5.4 x $10^{-2}$ to 12 x $10^{-2}$ $min^{-1}$; see below).

The photocatalyzed decomposition of the six xylenols in the presence of $TiO_2$ is presented in Figures 6.3 a-f. All six xylenols (20 mg/L) degrade via first-order kinetics

**Figure 6.3** Plots of normalized peak areas (or concentration) as a function of irradiation time showing the degradation of the six xylenols (ca. 20 mg/L) and formation and decomposition of major intermediates in the photomineralization process with irradiated $TiO_2$ present (2g/L at pH 3). (a) 2,3-xylenol, (b) 2,4-xylenol, (c) 2,5-xylenol, (d) 2,6-xylenol, (e) 3,4-xylenol and (f) 3,5-Xylenol. The curves are computer fits to equations noted in Chapter 3.

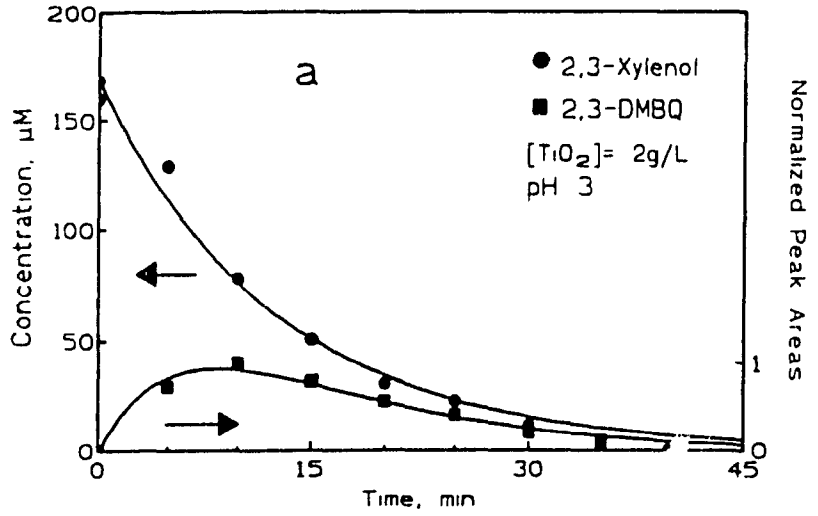
a
2,3-Xylenol
2,3-DMBQ
[TiO2]= 2g/L
pH 3
Concentration, µM
Normalized Peak Areas
Time, min

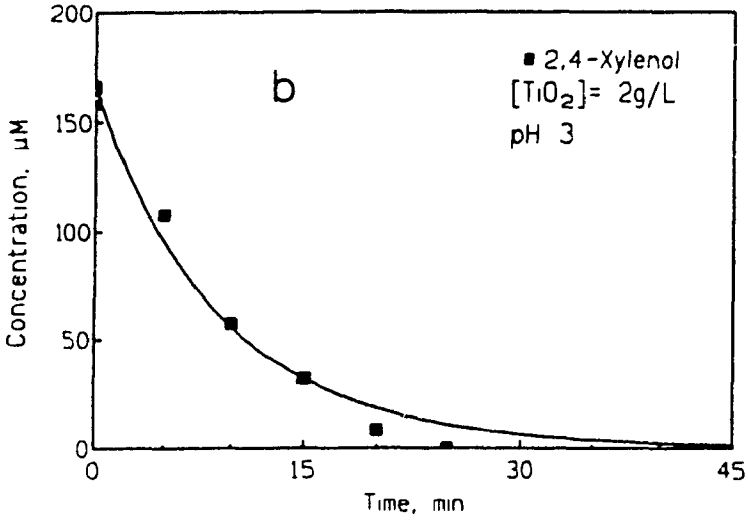
b
2,4-Xylenol
[TiO2]= 2g/L
pH 3
Concentration, µM
Time, min

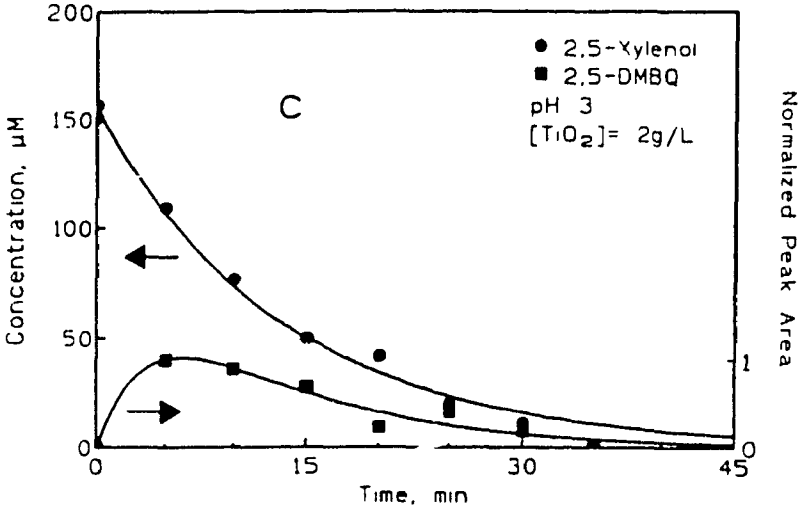
c
2,5-Xylenol
2,5-DMBQ
pH 3
[TiO2]= 2g/L
Concentration, µM
Normalized Peak Area
Time, min

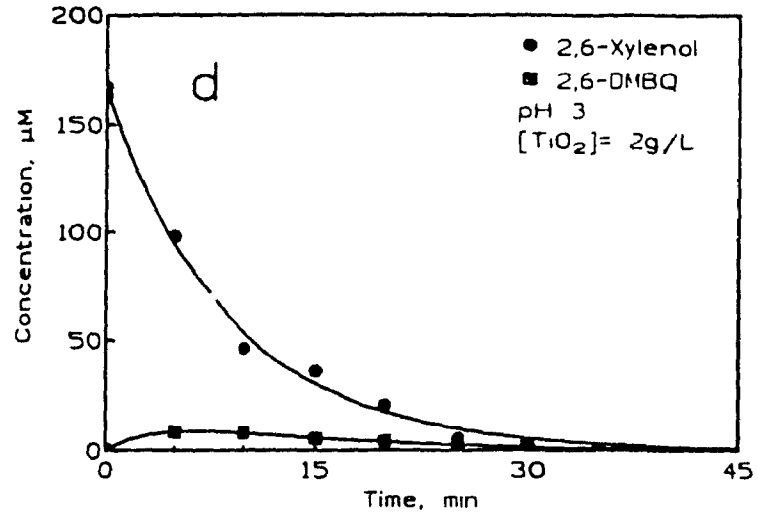
d
● 2,6-Xylenol
■ 2,6-DMBQ
pH 3
[TiO2]= 2g/L
Concentration, µM
Time, min
200
150
100
50
0
0
15
30
45

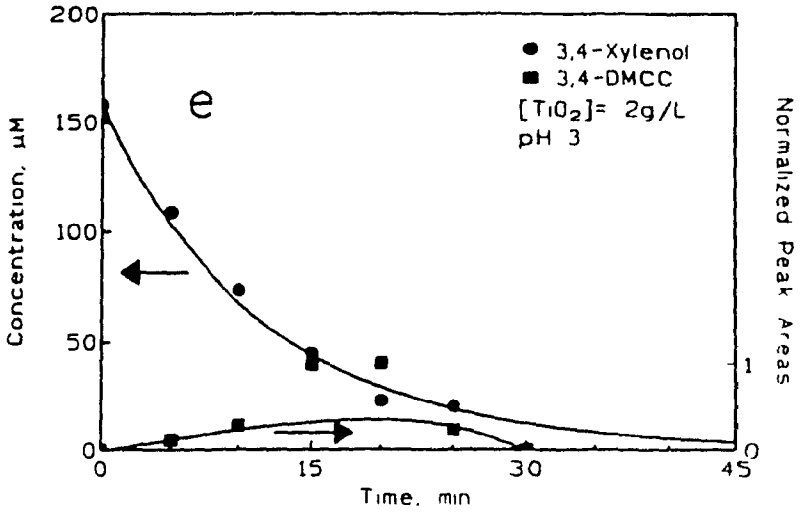
e
● 3,4-Xylenol
■ 3,4-DMCC
[TiO2]= 2g/L
pH 3
Concentration, µM
Normalized Peak Areas
Time, min
200
150
100
50
0
1
0
0
15
30
45

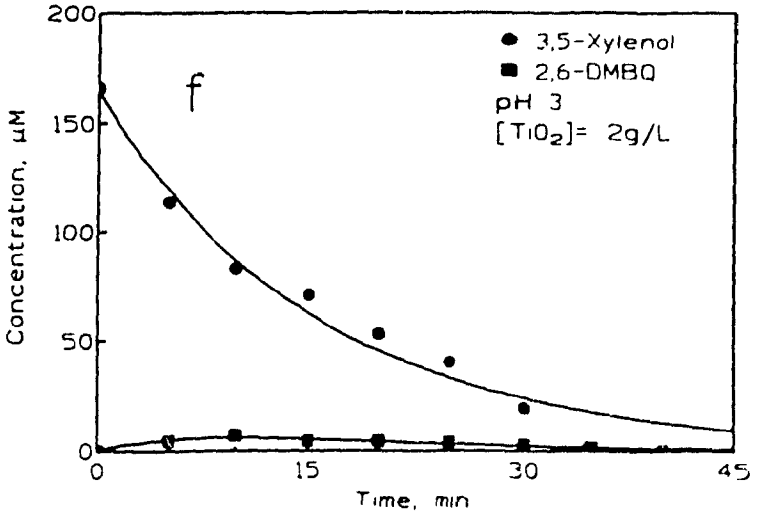
f
● 3,5-Xylenol
■ 2,6-DMBQ
pH 3
[TiO2]= 2g/L
Concentration, µM
Time, min
200
150
100
50
0
0
15
30
45

under identical experimental conditions of light source, initial pH, and $TiO_2$ concentration. The formation and subsequent degradation of the major intermediates detected in each case are also indicated. In every instance, total disappearance of the original xylenol and decomposition of the intermediate species occur in < 1 hr of irradiation. The corresponding apparent rate constants, initial rates, and half-lives for the degradation of the six xylenols as a function of initial concentration are summarized in Table 6.4. The apparent kinetic parameters for the formation and subsequent degradation of the major intermediates produced in the course of mineralization for the six xylenols were calculated as described in Chapter 3, section 3.2, and are presented in Table 6.5. All these intermediates formed and decayed via apparent first order kinetics, except for 3,4-DMCC which was observed in the course of the photodegradation of 3,4-xylenol; it formed via first order but disappeared via zero order kinetics.

The photocatalyzed mineralization process for the six xylenols follows the stoichiometric reaction 6.3, as evidenced by a quantitative product analysis in the case of 3,4-xylenol:

$$(CH_3)_2C_6H_3OH + 10\ O_2 \xrightarrow[TiO_2]{h\nu} 8\ CO_2 + 5\ H_2O \qquad (6.3)$$

The quantity of $CO_2$ evolved as a function of irradiation time is illustrated in Figure 6.4 for an oxygen-saturated aqueous solution of 3,4-xylenol. Approximately 33 $\mu$mols of $CO_2$ were expected from reaction 6.3 for $[3,4\text{-xylenol}]_{ini} = 165\ \mu M$. It is evident that after

**Table 6.4** Apparent Kinetics of the Mineralization of Xylenols Photocatalyzed by Irradiated $TiO_2$ in Air-Equilibrated Suspensions at pH 3.

| Xylenol | [Xylenol] ($\mu$M) | $k_{app}$ ($10^{-2}$ $min^{-1}$) | Initial Rate ($\mu$M/min) | $t_{1/2}$(app) (min) |
|---|---|---|---|---|
| 2,3-Xylenol | 168.3 | 7.9 ± 0.5 | 13.4 ± 0.9 | 8.7 |
| | 162.0 | 6.3 ± 0.9 | 10.1 ± 1.5 | 11.1 |
| 2,4-Xylenol | 165.5 | 10.9 ± 1.0 | 18.0 ± 1.7 | 6.3 |
| | 177.7 | 9.1 ± 0.7 | 16.1 ± 1.2 | 7.6 |
| 2,5-Xylenol | 156.7 | 7.6 ± 0.4 | 11.8 ± 0.7 | 9.2 |
| | 163.2 | 7.5 ± 0.4 | 12.2 ± 0.7 | 9.2 |
| 2,6-Xylenol | 163.3 | 11.3 ± 0.6 | 19 ± 1 | 6.1 |
| | 164.2 | 12.0 ± 0.8 | 20 ± 1 | 5.8 |
| 3,4-Xylenol | 16.3 | 28 ± 4 | 4.6 ± 0.7 | 2.5 |
| | 41.8 | 17.2 ± 1.1 | 7.2 ± 0.5 | 4.0 |
| | 85.8 | 10.0 ± 1.4 | 8.6 ± 1.0 | 6.9 |
| | 158.1 | 8.5 ± 0.6 | 13.5 ± 0.9 | 8.1 |
| | 158.4 | 7.9 ± 0.4 | 12.4 ± 0.7 | 8.8 |
| | 156.3 | 6.4 ± 0.4 | 10.0 ± 0.6 | 10.9 |
| | 164.2 | 7.0 ± 1.0 | 11.5 ± 1.7 | 9.9 |
| | 407.2 | 3.9 ± 0.3 | 15.8 ± 1.4 | 17.9 |
| 3,5-Xylenol | 166.3 | 6.4 ± 0.5 | 10.7 ± 0.8 | 10.8 |
| | 165.3 | 5.4 ± 0.3 | 8.9 ± 0.5 | 12.9 |

**Table 6.5** Apparent Kinetics of Formation of Intermediates Produced at pH 3 in Air-Equilibrated Irradiated $TiO_2$ Suspensions.

| Parameter | Source | | | | | |
|---|---|---|---|---|---|---|
| | 2,3-Xylenol | 2,4-Xylenol | 2,5-Xylenol | 2,6-Xylenol | 3,4-Xylenol | 3,5-Xylenol |
| [Xylenol], $\mu$M | 168.3 | 165.5 | 156.7 | 163.3 | 158.1 | 166.32 |
| $k_{app}$ (degradation), $min^{-1}$ | 0.079 | 0.11 | 0.076 | 0.11 | 0.085 | 0.064 |
| $k_{app}$ (formation), $min^{-1}$ | | | | | | |
| 2,3-Dimethylbenzoquinone | 0.12 | - | - | - | - | - |
| 2,5-Dimethylbenzoquinone | - | - | 0.10 | - | - | - |
| 2,6-Dimethylbenzoquinone | - | - | - | 0.093 | - | 0.090 |
| 3,4-Dimethylcatechol | - | - | - | - | 0.085 | - |
| $k_{app}$ (degradation), $min^{-1}$ | | | | | | |
| 2,3-Dimethylbenzoquinone | 0.12 | - | - | - | - | - |
| 2,5-Dimethylbenzoquinone | - | - | 0.24 | - | - | - |
| 2,6-Dimethylbenzoquinone | - | - | - | 0.24 | - | 0.12 |
| 3,4-Dimethylcatechol ($\mu$M/min) | - | - | - | - | 0.32 | - |

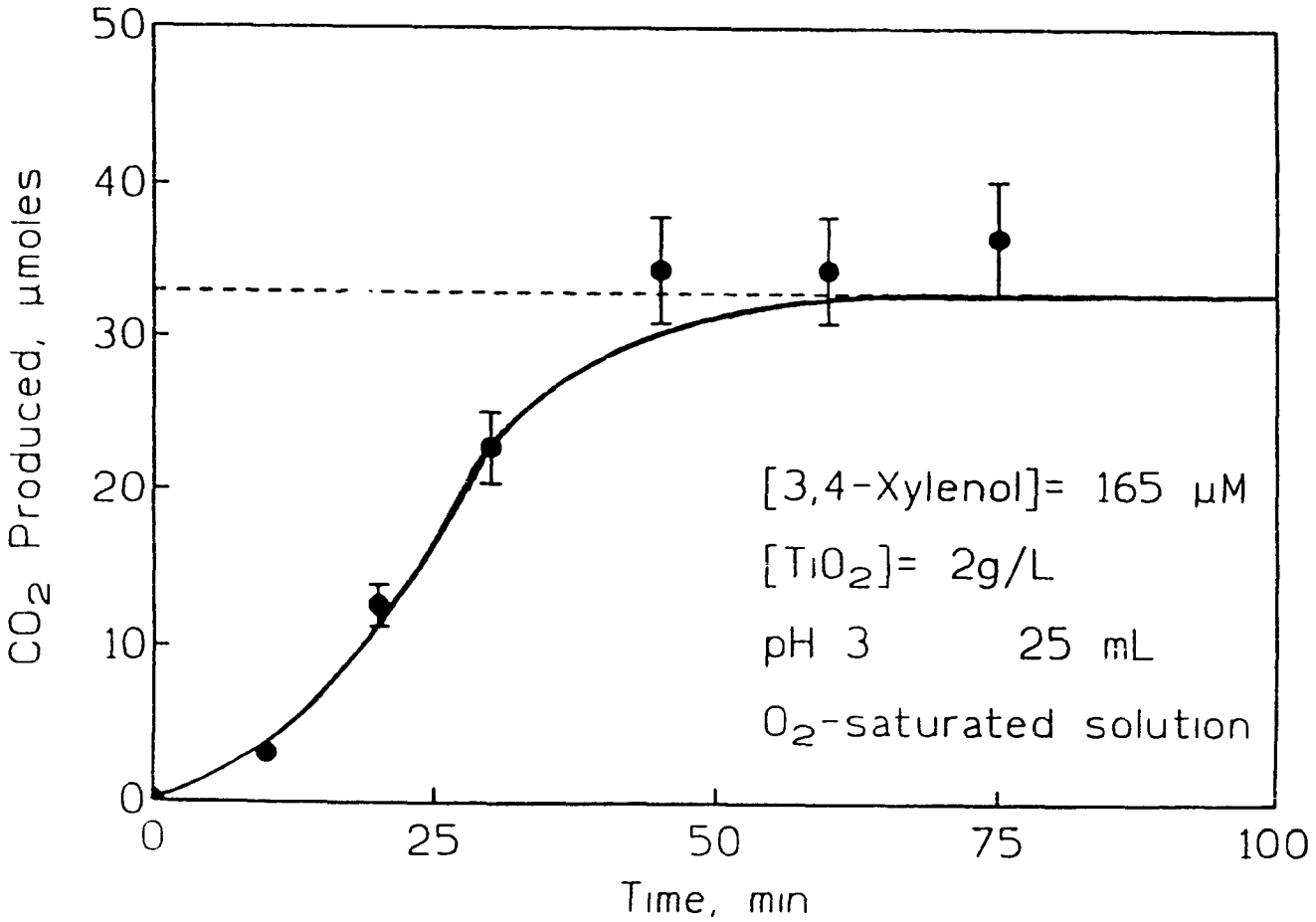


**Figure 6.4** Plot showing the temporal evolution of $CO_2$ from the photomineralization of 165 $\mu$M xylenol in the presence of 2 g/L $TiO_2$ at an initial pH of 3 in an oxygen-saturated suspension.

$\approx$ 1 hr of irradiation, when all the xylenol and the aromatic intermediate species have decomposed, the expected stoichiometric amount of $CO_2$ is produced.

## 6.2.5 Effect of Oxygen

The effect of the concentration of oxygen on the kinetics of decomposition of 3,4-xylenol was determined by carrying out the photoreaction under conditions where the suspension was saturated with $O_2$. The decomposition of this xylenol in both air-equilibrated and oxygen-saturated suspensions is compared in Figure 6.5. Good first-order kinetics are evident in both cases. The corresponding parameters are, air *versus* oxygen, respectively: $k_{app}$, 0.085 $min^{-1}$ and 0.16 $min^{-1}$; initial rates, 13.5 $\mu$M/min and 27.1 $\mu$M/min; $t_{1/2}$(app), 8.1 min and 4.3 min. Note that in the presence of excess oxygen, decomposition of 3,4-xylenol occurs in $<$ 0.5 hr.

## 6.2.7 Concentration Dependence

The photomineralization of 3,4-xylenol occurs via first order kinetics for all concentrations examined {16.3 $\mu$M ($\approx$2 mg/L) to 407.2 $\mu$M($\approx$50 mg/L)}, Figure 6.6 and Table 6.4. The initial rates vary from 4.6 $\mu$M/min to 15.8 $\mu$M/min. A plot of initial rates ($R_{in}$) *versus* initial [3,4-xylenol] reveals similarities with Langmuir-Hinshelwood (LH) type behaviour (Figure 6.7a): $R_{in} = k'_{app}K[3,4\text{-xylenol}]/(1 + K[3,4\text{-xylenol}])$.[7] A computer fit of the Langmuir expression to the data points of Figure 6.7a yields a value of $k'_{app} = 17.5 \pm 1.6$ $\mu$M/min and the apparent adsorption coefficient $K = 0.014 \pm 0.004$ $\mu M^{-1}$. The linear transform of this expression (Figure 6.7b) yields a value of $k'_{app}$

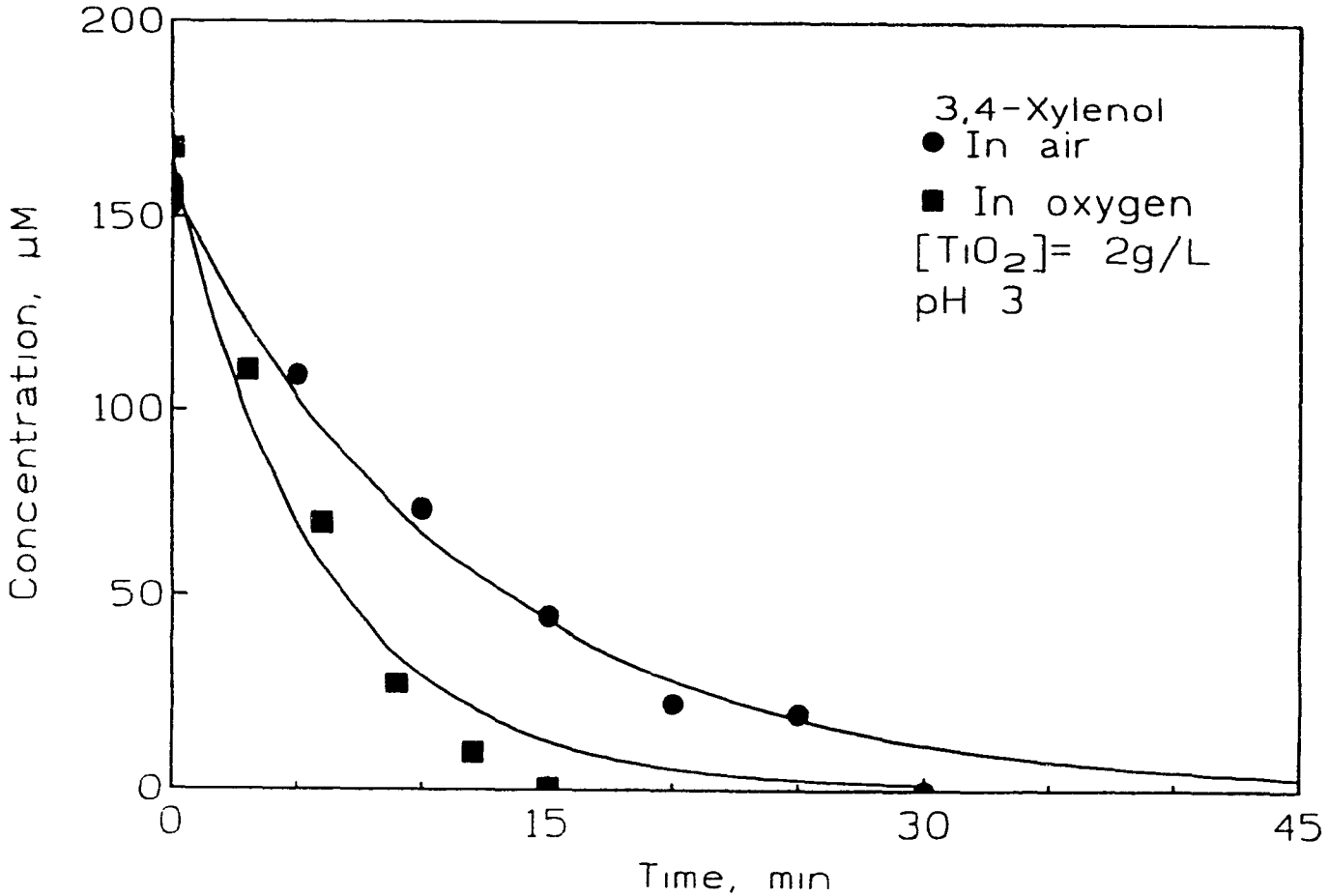


**Figure 6.5** Plot showing the photodegradation of ≈ 20 mg/L of 3,4-xylenol in the presence of 2 g/L $TiO_2$ in air-equilibrated suspensions and in oxygen-saturated suspensions; initial pH 3. The apparent rate constants were, air *versus* O2, respectively, kapp: 0.085 $min^{-1}$ and 0.16 $min^{-1}$

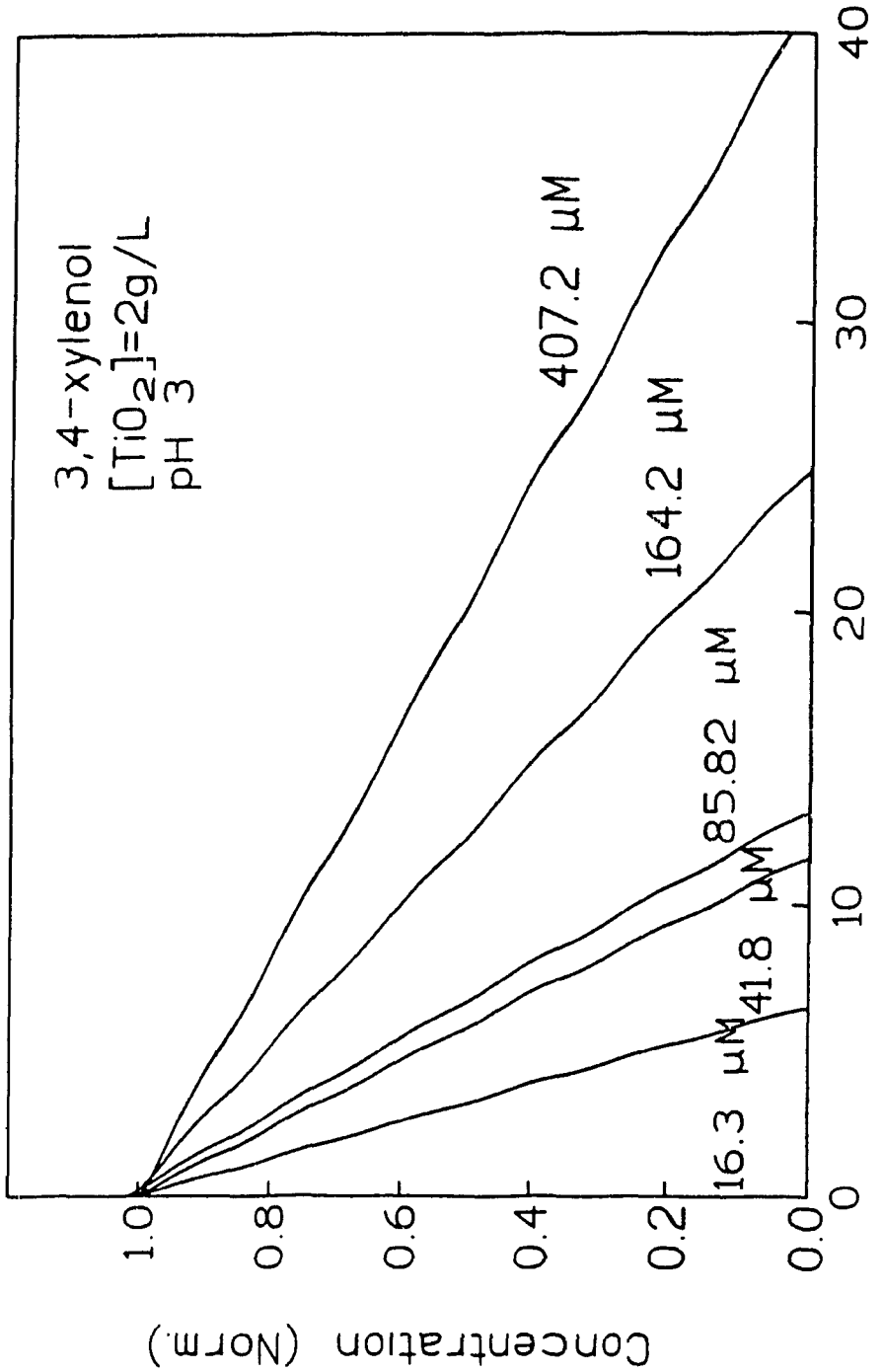


**Figure 6.6** Plot showing the initial rates of the photomineralization of 3,4-xylenol catalyzed by irradiated $TiO_2$ at various initial concentrations; initial pH 3.

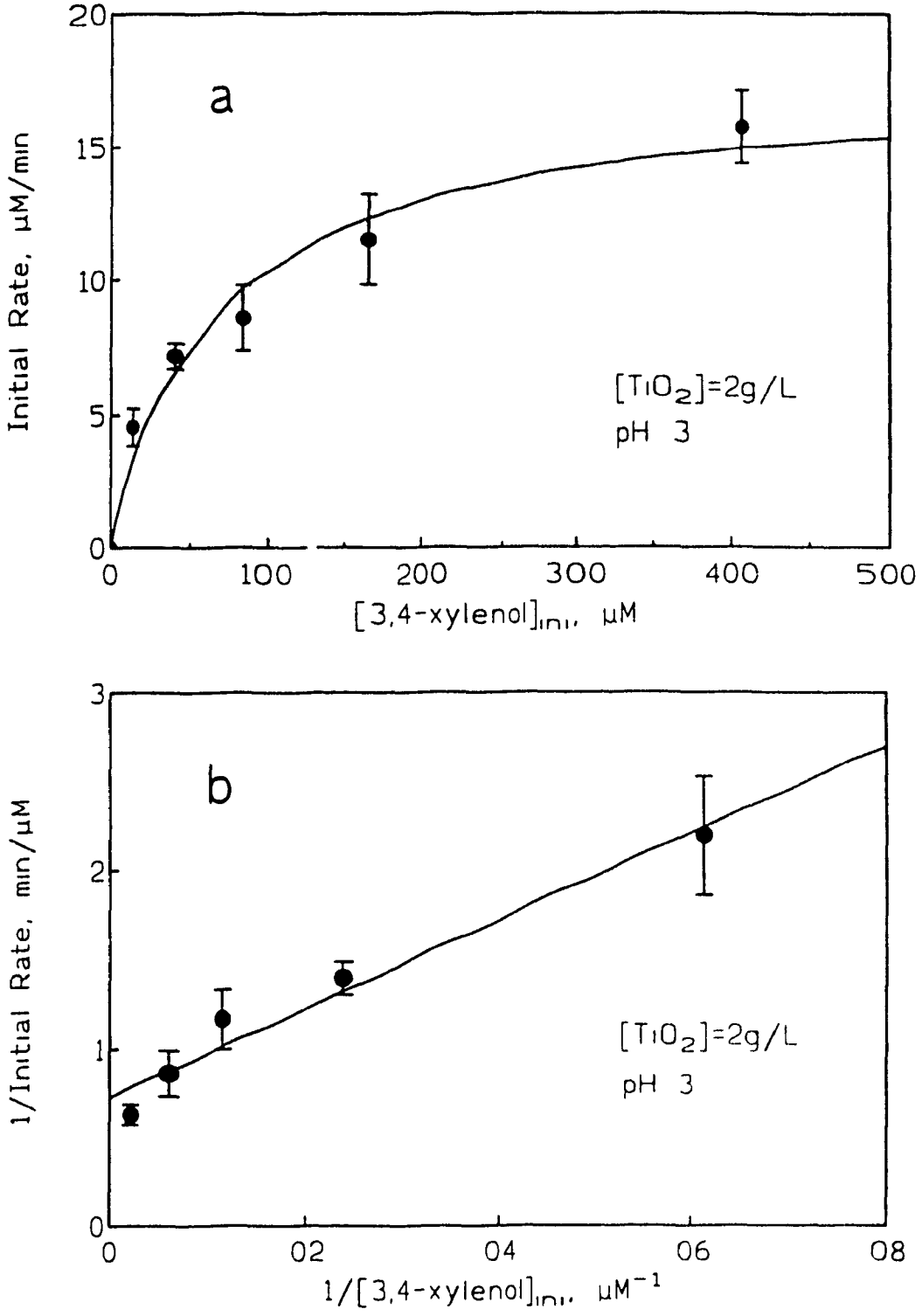


**Figure 6.7** (a) Plot showing the effect of the initial concentration on the initial rate of the photodegradation of 3,4-xylenol under air-equilibrated conditions; initial pH 3. (b) Linear transform of the Langmuir type expression (see text).

$= 13.7 \pm 1.6\ \mu M/min$ and the apparent adsorption coefficient $K = 0.030 \pm 0.004\ \mu M^{-1}$. Both sets of values are in reasonable agreement.

### 6.2.8 Radiant Power Level Dependence

Turchi and Ollis[15] have derived a detailed expression for expressing the effect of light intensity on the rates of photo-oxidation; a simpler version of this expression was derived earlier by Egerton and King.[16] In deriving the expression, several key assumptions were made;[15] these are: i) there is a steady state for reactive species, ii) the photocatalyst surface is rapidly and completely hydroxylated, iii) degradation proceeds via hydroxyl radicals, iv) the number of photogenerated electrons and holes are equal, v) recombination involves electron/hole pairs, and vi) there is rapid mass transfer of substrate onto the photocatalyst surface. The rate equation for the destruction of a pollutant S is given by:

$$r_S = k[\bullet OH][S] \tag{6.4}$$

where:

$$\frac{d[\bullet OH]}{dt} = k_{H_2O}[h^+][H_2O] - k_{OH}[\bullet OH] - k[\bullet OH][S] - \sum k_{Intm}[Intm][\bullet OH] \tag{6.5}$$

The first term in equation 6.5 refers to the formation of •OH via oxidation of water ($h^+ + H_2O \rightarrow \bullet OH + H^+$), the second term refers to the disappearance of •OH via the reverse reaction, and the last two terms refer to the reaction of •OH with the substrate S and any intermediates or other species which also react with •OH. At steady state,

$$k_{H_2O}[h^+][H_2O] - k_{OH}[\bullet OH] - k[\bullet OH][S] - \sum k_{Intm}[Intm][\bullet OH] = 0 \qquad (6.6)$$

giving the following expression for the rate:

$$r_S = k \frac{k_{H_2O}[h^+][H_2O]}{k_{OH} + k[P] + \sum k_{intm}[intm]} [P] \qquad (6.7)$$

but:

$$\frac{d[h^+]}{dt} = k_{exc}I - k_{rec}[h^+][e^-] - k_{H_2O}[h^+][H_2O] + k_{OH}[\bullet OH] \qquad (6.8)$$

where $k_{exc}$ is the rate constant for electron/hole formation, and $k_{rec}$ the rate constant for electron hole recombination. If $[h^+] \approx [e^-]$, then at steady state,

$$k_{exc}I - k_{rec}[h^+]^2 - k_{H_2O}[h^+][H_2O] + k_{OH}[\bullet OH] = 0 \qquad (6.9)$$

At high intensities (high $[h^+]$), electron/hole recombination predominates over hole trapping (reaction with $H_2O$) giving the expression:

$$[h^+] = \sqrt{\frac{k_{exc}I}{k_{rec}}}$$

at low light intensities, hole trapping effectively competes with electron/hole recombination giving:

$$[h^+] = \frac{k_{exc}I + k_{OH}[\bullet OH]}{k_{H_2O}[H_2O]} \qquad (6.11)$$

Based on the above derivation, it is therefore expected that the rate of photodegradation reactions will be proportional to $I^1$ at low intensities and $I^{1/2}$ at higher intensities. A similar conclusion was reached by Peterson *et al.*[17] Mass transfer limitations also come into play at high intensities (i.e. the behaviour of a system will depend on the relative rates of the photoinduced reactions *versus* the rates of fluid and mass transfer between the illuminated portion of the reactor and the dark core);[18] the expected rate limiting factor in this case will become mass transfer, i.e. the rate of photodegradation reactions will become independent of I (proportional to $I^0$) as shown in Figure 6.8.[18]

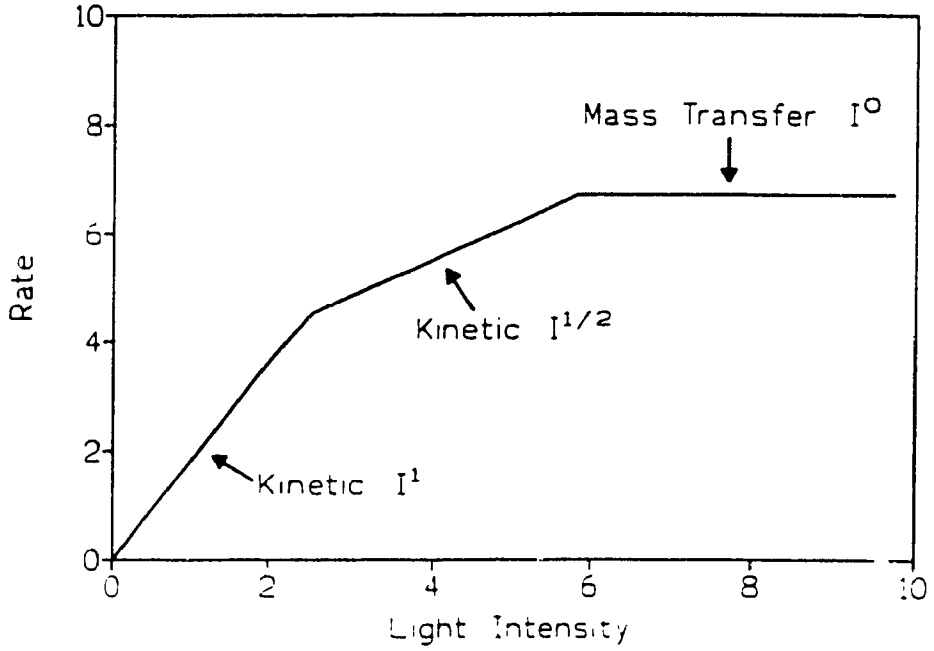


**Figure 6.8** Rate *versus* intensity plot showing the rate dependence on light intensity in the 3 operating regions (ref. 18).

The results reported below are well in agreement with theoretical predictions. It should be noted that based on these and other results, it is more advantageous to work in the low intensity region.

The dependence of the rate of photodegradation of 3,4-xylenol (165 $\mu$M) on the radiant power level of the light source is illustrated in Figure 6.9a. The plot can be divided into 3 distinct regions: regions A, B and C. In region A, (Figure 6.9b) the rate increases linearly with power level (low light fluxes). In region B, the rate increases as a function of the square root of the power level as illustrated in Figure 6.9c. Finally, in region C (Figure 6.9b), the rate is independent of the power level. The direct dependence of the rate on the radiant power at low intensities (% I $\leq$ 12 %) and on its square root (19.1 % $\leq$ % I $\leq$ 65.8 %) at higher intensities is similar to the behaviour noted by others for the photo-oxidation of isopropanol[16] phenol[13] and 3-chlorophenol[19] as illustrated in Figure 6.10.[13,16,19,20]

## 6.2.9 Photochemical Efficiencies

Owing to the bandgap of 3.2 eV of the semiconductor used ($TiO_2$), only light of wavelengths below 400 nm can drive the photocatalyzed process. The photochemical efficiencies for the decomposition of the xylenols were determined at 365 nm and *reflect the number of molecules of the xylenol that degraded per photon incident on the external reactor walls* (see Chapter 3, Experimental): 0.0060 (3,4-xylenol), 0.0067 (2,3-xylenol), 0.0067 (3,5-xylenol), 0.0074 (2,5-xylenol), 0.012 (2,4-xylenol), and 0.015 (2,6-xylenol). These results are comparable to those obtained for cresol under nealy identical

**Figure 6.9** (a) Effect of the radiant power levels of the light source (see text) on the initial rate of the photomineralization of 3,4-xylenol (165 $\mu$M); initial pH 3; $TiO_2$, 2 g/L; 100% radiant power corresponds to 176 mW/cm$^2$. (b) Regions where the dependence of the initial rate on the radiant power level is a function of $I^1$ at low light fluxes and $I^0$ at high light fluxes. (c) Region where the initial rate is a function of the square root of the radiant power at intermediate light fluxes.

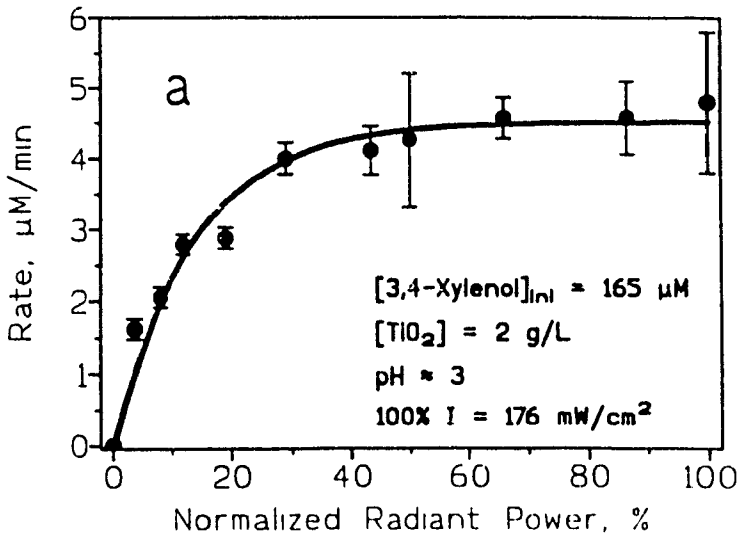
a
Rate, μM/min
Normalized Radiant Power, %
[3,4-Xylenol]ini = 165 μM
[TiO2] = 2 g/L
pH = 3
100% I = 176 mW/cm2

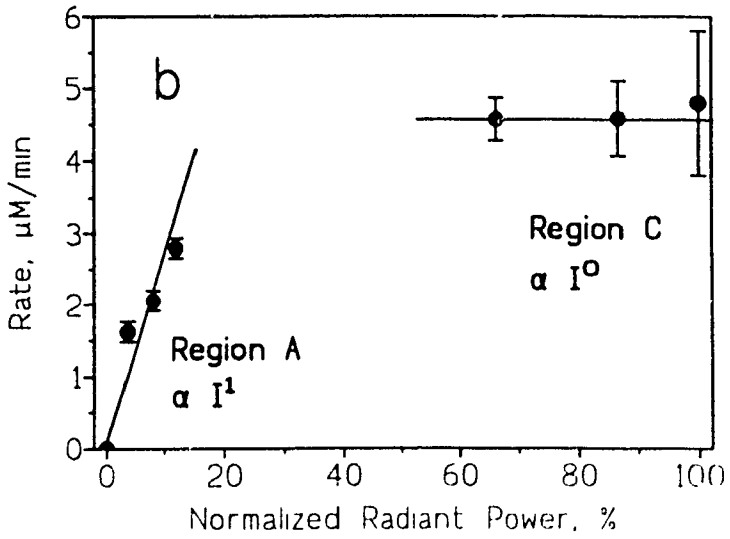
b
Rate, μM/min
Normalized Radiant Power, %
Region A
α I1
Region C
α I0

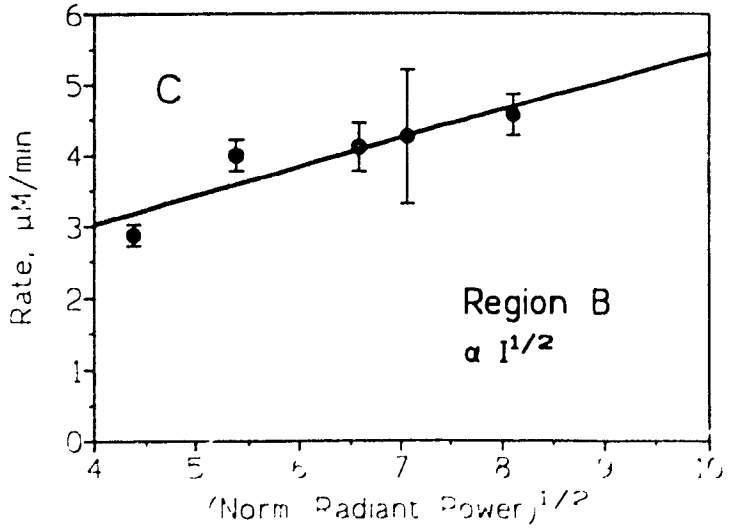
c
Rate, μM/min
(Norm Radiant Power)1/2
Region B
α I1/2

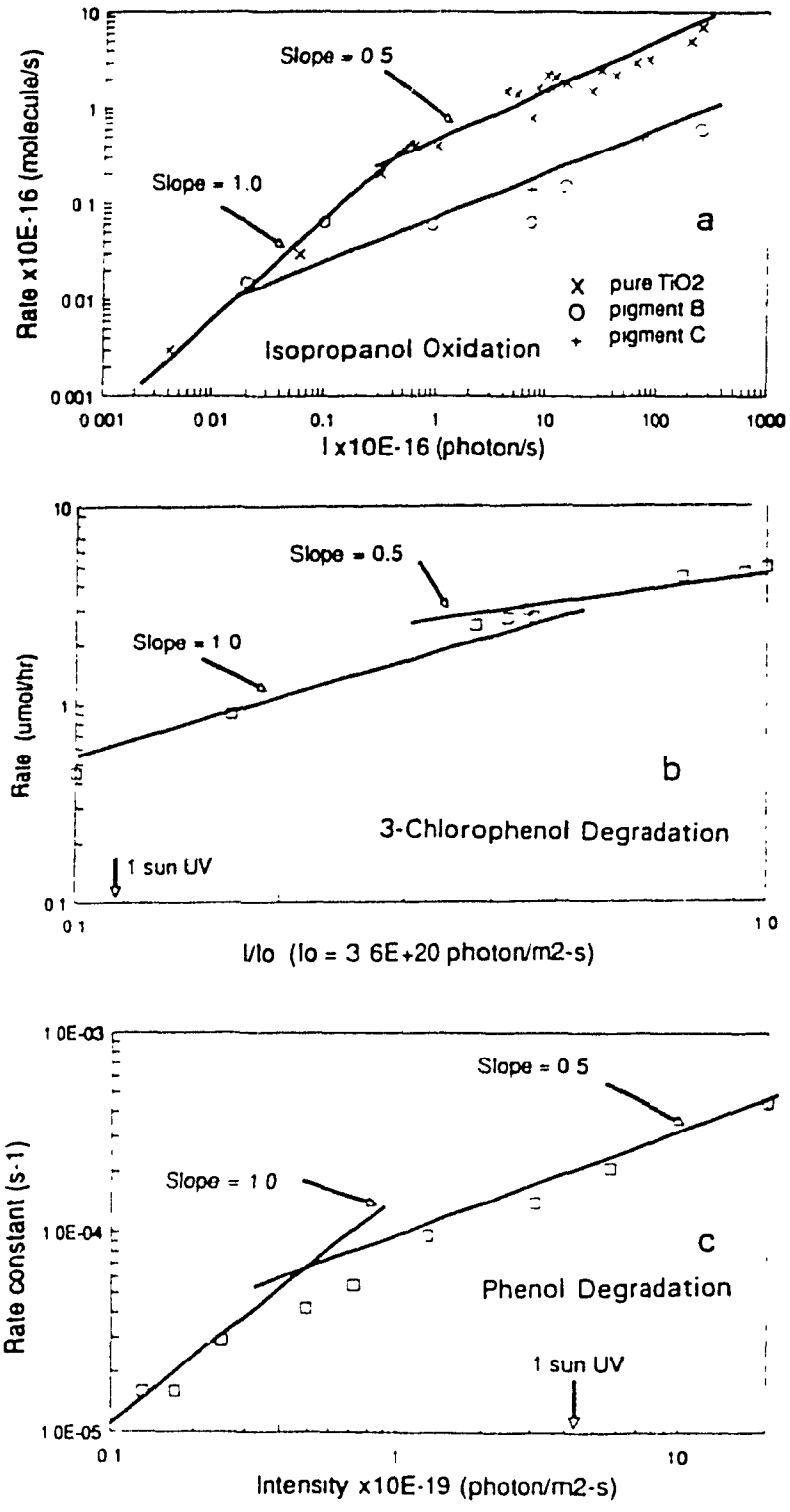


**Figure 6.10** Effect of the Intensity of the Photon Flux on the rates of Photo-oxidation in various systems as shown in reference 20: a) Phenol (ref. 13) b) Isopropanol (ref. 16) c) 3-Chlorophenol (ref. 19).

experimental conditions [0.0096 (*o*-cresol), 0.0076 (*m*-cresol), and 0.010 (*p*-cresol)].

## 6.2.10 Effect of Degussa P25 $TiO_2$ Batch Variation

The origin and/or method of preparation of the $TiO_2$ powder used in heterogeneous photocatalytic experiments greatly influences its photocatalytic properties.[21] For the $TiO_2$ material used in this work (Degussa P25), the outcome of varying the batch (Lot) of material was examined by looking at the degradation of 3,4-xylenol using three different batches of Degussa P25 $TiO_2$. The three batches used were Lot # RV1372, RV1177, and an unidentified batch. The results are shown in Figure 6.11 and the kinetic parameters are summarized in Table 6.6.

**Table 6.6** Kinetic Parameters for the disappearance of 3,4-xylenol obtained in the $TiO_2$ Batch Dependence Study. $[3,4\text{-Xylenol}]_{ini} = 160\ \mu M$, $[TiO_2]$ (Degussa P25) = 2g/L, pH 3.

| Lot # ($TiO_2$) | $k_{app}$ ($min^{-1}$) | $Rate_{ini}$ ($\mu M/min$) | $t_{1/2}$ (min) |
|---|---|---|---|
| RV1372 | 0.064 ± 0.004 | 10.6 ± 0.7 | 10.9 |
| Unknown | 0.094 ± 0.007 | 15.5 ± 1.0 | 7.3 |
| RV1177 | 0.078 ± 0.004 | 12.9 ± 0.7 | 8.8 |

Variations in the kinetic parameters from batch to batch of Degussa $TiO_2$ are similar to those seen for different runs using the same batch of $TiO_2$ (See Table 6.4). It is concluded that changing the batch of Degussa $TiO_2$ has no significant effect on the rate of photodegradation of 3,4-xylenol. The very slight variations from batch to batch and

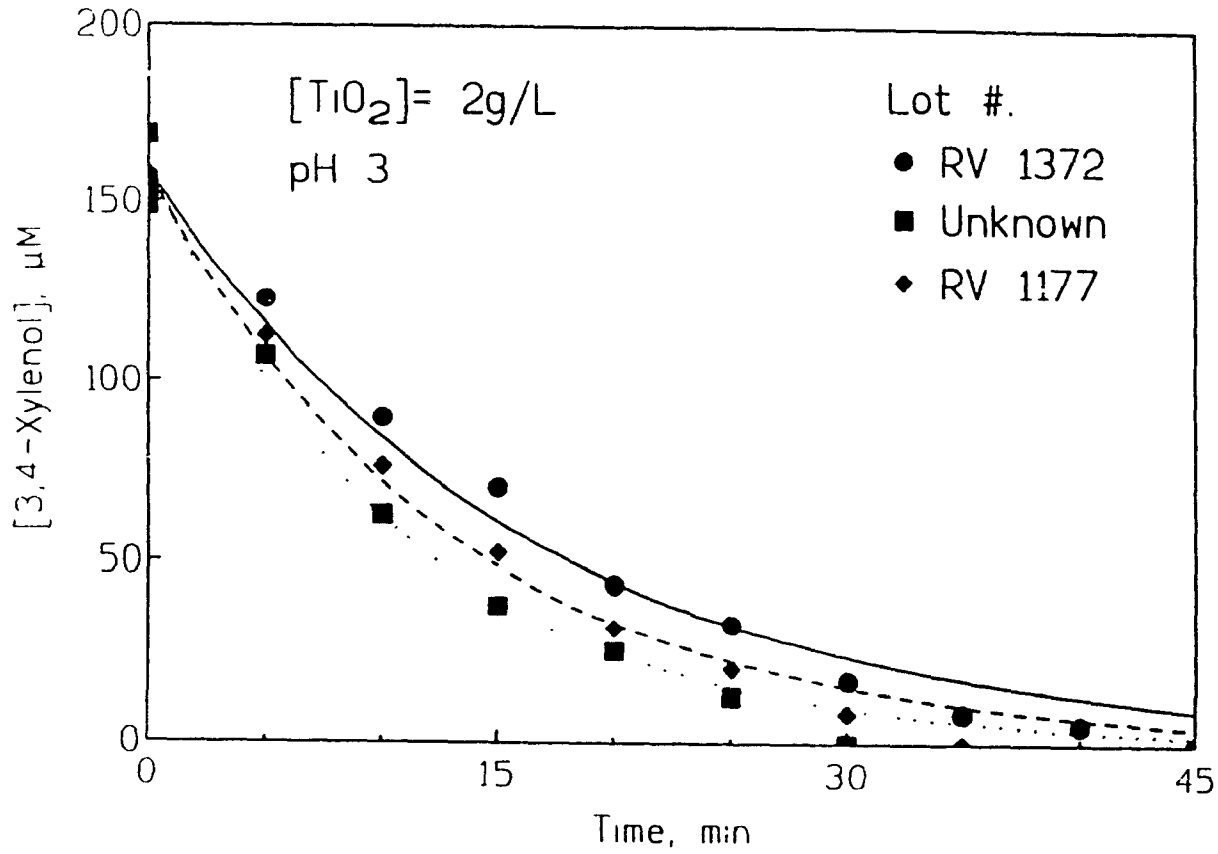


**Figure 6.11** Plot showing the effect of different lots of Degussa P25 $TiO_2$ on the rate of photodegradation of 3,4-xylenol. $[3,4\text{-xylenol}]_{in} = 160\ \mu M$, pH 3, $[TiO_2] = 2g/L$.

from run to run must be due to slight variations in the nature of the surface and its properties.

## 6.2.11 Mechanism of the Photodegradation of Xylenols

The photo-oxidations of the xylenols in a heterogeneous medium occur by reaction between the oxidizing species (See Chapter 2) and the various xylenols as a first step; this yields the intermediates detected (2,3-DMBQ, 2,5-DMBQ, 2,6-DMBQ, 3,4-DMCC and others). Subsequent reaction of these intermediate products with the oxidizing species ultimately yields $CO_2$ and $H_2O$ via a series of reactions which include ring cleavage and the formation of peroxides, aldehydes, and carboxylates as occurs in the photo-degradation of surfactants.[22] With our present results, we summarize the photomineralization process by scheme 6.12. The ring cleaved products have thus far eluded detection even with more sophisticated instruments (e.g. GC/MS/MS) besides HPLC.

## 6.2.12 Effect of Temperature

The effect of temperature on the rate of photodegradation of 3,4-xylenol was examined at 5 different temperatures (5, 20, 35, 50 and 60°C). The results are depicted in Figure 6.12 a. It can be seen that the initial rates increase (increase in slope) as a function of temperature. The activation energy for the reaction was obtained from the slope ($-E_a/R$) of an Arrhenius plot (ln k *versus* 1/T) shown in Figure 6.12 b. The rate measurement at 50°C was not used in the calculations (point with question mark). The

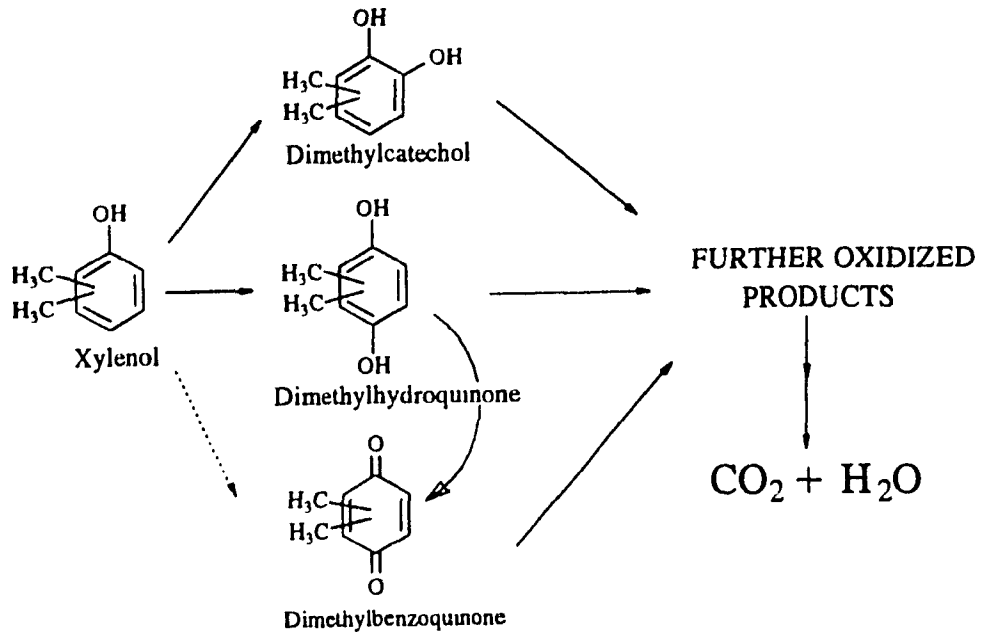


**(6.12)**

value obtained was $E_a = 2.1 \pm 0.2$ kcal/mol; this value is comparable to the values reported by Okamoto *et al*[13] for the photodegradation of phenol (2.4 kcal/mol), and by Al-Sayyed *et al*[23] for the degradation of 4-chlorophenol (1.3 kcal/mol). These values indicate that thermally activated steps are negligible, i.e. adsorption/desorption processes are almost temperature independent in this region.[23] The enthalpy and entropy of activation were obtained from an Eyring plot [ln (k/T) *versus* 1/T] shown in Figure 6.12c. The enthalpy of activation $\Delta H^{\#}$ was obtained from the slope ($-\Delta H^{\#}/R$) and found to be $1.4 \pm 0.2$ kcal/mol. The entropy of activation $\Delta S^{\#}$ was obtained from the y intercept [$(\Delta S^{\#}/R) + \ln (k/\hbar)$] and estimated to be $- 50 \pm 10$ cal/K mol.[##] The negative value obtained for $\Delta S^{\#}$ is consistent with adsorption or photoadsorption of the xylenol occuring during the photocatalytic process.

---

## R (gas constant) = 1.987 cal/K mol
*k* (Boltzmann constant) = $1.381 \times 10^{-16}$ erg/K mol
$\hbar$ (Planck constant) = $6.626 \times 10^{-27}$ erg/K mol

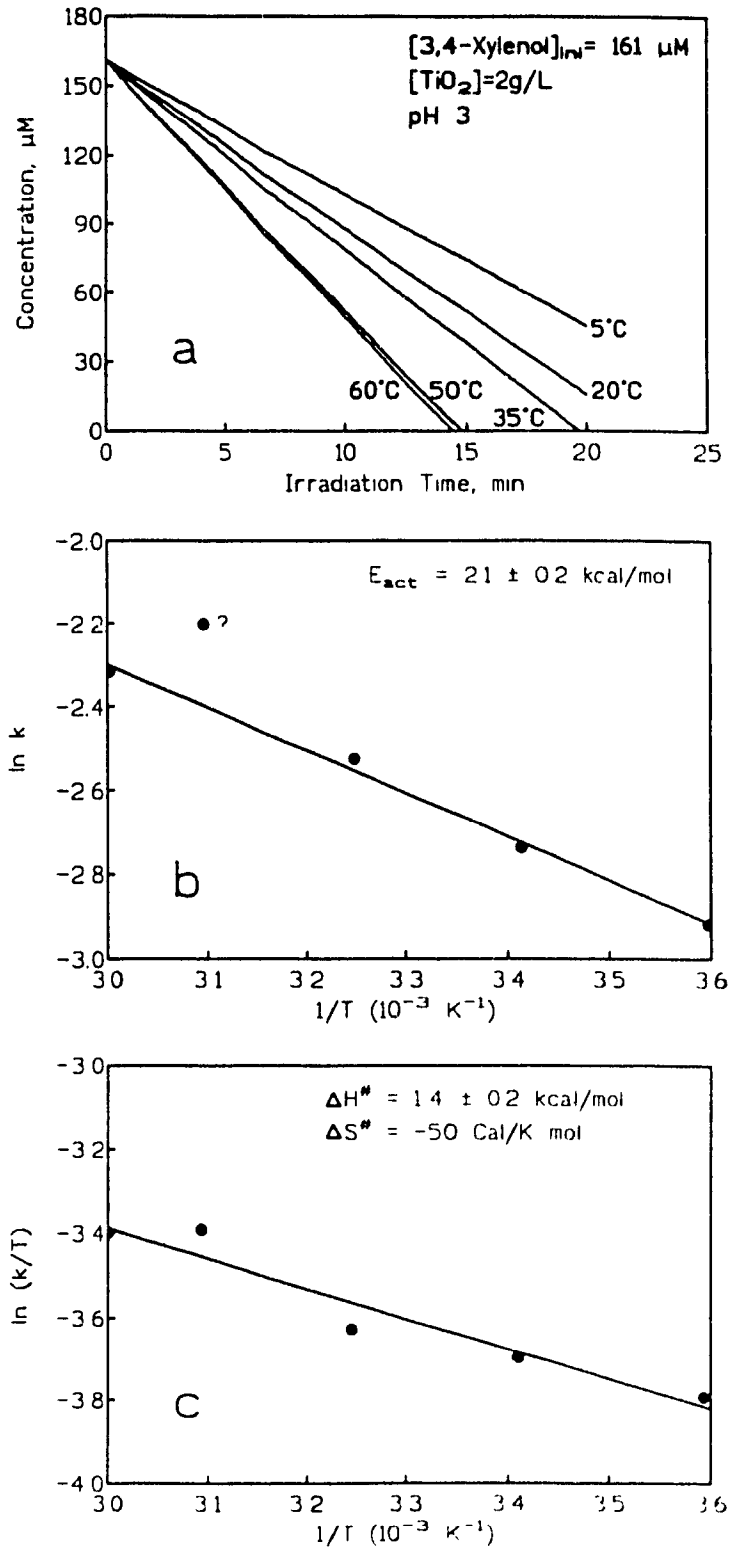


**Figure 6.12** **(a)** Temperature dependence of the initial rate of photodegradation of 3,4-Xylenol; **(b)** Arrhenius (ln k *versus* 1/T) plot for the photodegradation of 3,4-xylenol **(c)** Eyring (ln (k/T) *versus* 1/T) plot for the photodegradation of 3,4-xylenol.

## 6.2.13 Kinetic Considerations

With our present results, we can summarize the photomineralization of the xylenols by reaction 6.13 (X is a xylenol):

$$(site) + X \underset{k_{-13a}}{\overset{k_{13a}}{\rightleftarrows}} (X)_{ads} \overset{k_{13b}}{\rightleftarrows} (Intm.)_{ads} \overset{k_{13c}}{\longrightarrow} CO_2 + H_2O \qquad (6.13)$$

The rate of formation of the final products $CO_2$ and $H_2O$ is then given by equation 6.14, where $K_X$ is the photoadsorption coefficient for the xylenol, $k_{13b}$ is the rate constant for the conversion of $(X)_{ads}$, and the other parameters have the same meaning as in equation 3.11, Chapter 3.

$$Rate = \frac{\frac{\phi I_a^n \beta A_p k_{trap} \tau_{\bullet OH} k_{13b} K_X [X] S_s}{k_{rec}}}{1 + \frac{k_{13b}+k_{13c}}{k_{13c}} K_X[X] + K_W[H_2O] + \Sigma_i K_{Intm.}[Intm.]_i} \cdot \frac{K_{O_2}[O_2]}{(1 + K_{O_2}[O_2])} \qquad (6.14)$$

Water, dimethylbenzoquinones, dimethyldihydroxybenzenes and other intermediates that form in the degradation process can, in principle, compete for the same adsorption sites as the xylenols; they will act as inhibitors. It was also noted that molecular $O_2$ affects the rate of degradation and therefore the adsorption isotherm for $O_2$ has been included in equation 6.14. This equation has the same basic form as the expression from the Langmuir-Hinshelwood model (equation 2.25, Chapter 2) and is applicable for low (n=1), medium (n=1/2) and strong (n=0) light flux conditions.

## 6.3 CONCLUSIONS

The disappearance of 2,3-, 2,4-, 2,5-, 2,6-, 3,4- and 3,5-xylenol in air-equilibrated, irradiated $TiO_2$ suspensions takes place in $<$ 1 hr at pH 3. In excess molecular oxygen, the degradation of 3,4-xylenol is faster ($\leq$ 0.5 hr) and complete mineralization to $CO_2$ and $H_2O$ takes place in $\approx$ 1 hr.

Various experimental factors such as pH, temperature, photocatalyst concentration, substrate concentration, and light intensity can influence the overall rate of degradation; these were examined in some detail for 3,4-xylenol. The rate of the photocatalyzed reaction increased as a function of pH and temperature. Concentration dependence experiments (varying [$TiO_2$] or [3,4-xylenol]) indicate the reaction follows saturation-type kinetics. Finally, the reaction rate was found to be directly proportional to the light intensity (I) at low light fluxes, proportional to $I^{1/2}$ at higher fluxes, and independent of I at even higher fluxes. This result is consistent with both theoretical predictions and experimental observations by others.

The major intermediates have been identified in the photodegradation of xylenols: these are either dihydroxydimethylbenzenes or dimethylbenzoquinones; other intermediates also form but were not identified under our experimental conditions. The present work adds another example of the classes of environmental organic contaminants that may be present in wastewaters and which can be degraded effectively by the photocatalytic method employed herein.

# REFERENCES


1. Callahan, M.A., Slimak, M., Gbel, N., May, I., Fowler, C., Freed, R., Jennings, P., Dupree, R., Whitemore, F., Maestri, B., Holt, B., and Gould, C., *"Water Related Environmental Fate of 129 Priority Pollutants"*, United States Environmental Protection Agency, Report No. EPA-44014-79-029a,b, NTIS, Washington, D.C., **1979**.

2. *Mueller, J.G., Chapman, P.J., Pritchard, P.H., Environ. Sci. Technol.*, **1989**, *23*, 1197.

3. Goerlitz, D.F., Troutman, D.E., Godsy, E.M., and Franks, B.J., *Environ. Sci. Technol.*, **1985**, *19*, 955 and references therein

4. Borgarello, E., Serpone, N., Barbeni, M., Pelizzetti, E., *J. Photochem.*, **1986**, *33*, 35.

5. Pelizzetti, E., Pramauro, E., Minero, C., Serpone, N., Borgarello, E., in *"Photocatalysis and Environment"*, Schiavello, M., Ed., NATO ASI Series, Ser.C237, Kluwer Academic Publ., Dordrecht, The Netherlands, **1988**, pp. 469-497, and references therein.

6. Serpone, N., Borgarello, E., Pelizzetti, E., in *"Photocatalysis and Environment"*, Schiavello, M., Ed., NATO ASI Series, Ser.C237, Kluwer Academic Publ., Dordrecht, The Netherlands, **1988**, pp. 527-565, and references therein.

7. Laidler, K.J., *"Chemical Kinetics"*, 3rd. Edn., Harper & Row Publ., New York, **1987**, pp. 400-406.

8. See for example: Grätzel, M., *"Heterogeneous Photochemical Electron Transfer"*, CRC Press, Inc., Boca Raton, Florida, **1989**, p. 125.

9. Serjeant, E.P., Dempsey, B. *"Ionization Constants of Organic Acids in Aqueous Solution"* - IUPAC Chemical Data Series No. 23, Pergamon Press, Oxford, **1979**.

10. Barbeni, M., Pramauro, E., Pelizzetti, E., Borgarello, E., Grätzel, M., Serpone, N., *Nouv. J. Chim.*, **1984**, *8*, 550.

11. Barbeni, M., Pelizzetti, E., Borgarello, E., Serpone, N., *Chemosphere*, **1985**, *14*, 195.

12. Okamoto, K., Yamamoto, Y., Tanaka, H., Tanaka, M., Itaya, A., *Bull. Chem. Soc. Jpn.*, **1985**, *58*, 2015.

13. Okamoto, K., Yamamoto, Y., Tanaka, H., Itaya, A., *Bull. Chem. Soc. Jpn.*, **1985**, *58*, 2023.

14. Sehested, K., Corfitzen, H., Christensen, H.C., Hart, E.J., *J. Phys. Chem.* **1975**, *79*, 310.

15. Turchi, C.S., Ollis, D.F., *J. Catal.*, **1990**, *122*, 178.

16. Egerton, T.A., King, C.J., *J. Oil Col. Chem. Assoc.*, **1979**, *62*, 386.

17. Peterson, M.W., Turner, J.A., Nozik, A.J., *J. Phys. Chem.*, **1991**, *95*, 221.

18. Ollis, D.F., in *"Photochemical Conversion and Storage of Solar Energy"*, Pelizzetti, E., and Schiavello, M., Eds., Kluwer Academic Publishers, The Netherlands, **1991**, 593.

19. D'Oliveira, J.C., Al-Sayyed, G., Pichat, P., *Environ. Sci. Technol.*, **1990**, *24*, 990.

20. Turchi, C.S., in: *"Presentations to the National Academy of Sciences/National Research Council Committee on Potential Applications of Concentrated Solar Photons. Session 1: Water Treatment Advanced Photo-Oxidation Processes"*, SERI, **1990**.

21. Sclafani, A., Palmisano, L., Schiavello, M., *J. Phys. Chem.*, **1990**, *94*, 829.

22. Hidaka, H., Zhao, J., Suenaga, S., Pelizzetti, E., and Serpone, N., *J. Jpn. Oil Chem. Soc.*, **1990**, *39*, 45.

23. Al-Sayyed, G., D'Oliveira, J.-C., Pichat, P., *J. Photochem. Photobiol. A: Chem.*, **1991**, *58*, 99.

# CHAPTER 7

# THE PHOTOMINERALIZATION OF 2,3,5-TRIMETHYLPHENOL

## 7.1 INTRODUCTION

The photocatalyzed destruction using $TiO_2$ of most phenolic components of creosote has been carried out in this work (cresols, xylenols) and elsewhere (phenol,[1] pentachlorophenol[4]). In all cases, the process resulted in total mineralization of the phenolic compounds into $CO_2$ and $H_2O$ (or HCl for pentachlorophenol). The only phenolic component of creosote which has yet to be surveyed is 2,3,5-trimethylphenol (2,3,5-TMP). 2,3,5-TMP comprises 5 wt % of the phenolic components of creosote (See Chapter 1, Figure 1.3).[5] As part of these continuing studies into the photocatalyzed mineralization of methylated phenolic substrates in the aqueous ecosystem, it was of interest to examine the temporal course of the degradation of 2,3,5-TMP, catalyzed by irradiated $TiO_2$ slurries. The eventual aim of this work was to evaluate the practicality of using heterogeneous catalysis in the decontamination of a typical multicomponent waste sample, in this case coal tar creosote (Chapter 8). Hydroxylated aromatic intermediates formed in the photodegradation process have been identified and rate data are examined in the context of the kinetic principles described in Chapter 3.

## 7.2 PHOTOCATALYZED DEGRADATION OF 2,3,5-TMP

### 7.2.1 Identification of Intermediates

At an initial pH of 3 and with the mobile phase used (50/50, methanol/water), the HPLC chromatograms showed three detectable ($\lambda$ = 214, 254 nm) intermediates [**1** (trace amounts), **2**, and **3**] formed during the course of the degradation of 2,3,5-TMP. These have retention times of 2.6, 3.3 and 7.2 min, respectively. Three species can form by reaction of $^{\bullet}OH$ radicals with 2,3,5-TMP; these are 3,5,6-trimethylcatechol (3,5,6-TMCC), 2,3,5-trimethylhydroquinone (2,3,5-TMHQ), and 2,3,5-trimethyl-benzoquinone (2,3,5-TMBQ). The retention time of 2,3,5-TMHQ was determined from a commercially available sample and was identified as intermediate **2** on the basis of their having the same retention time under our experimental conditions. Intermediate **3** was identified as 2,3,5-TMBQ; it had little absorbance at 214 nm but significant absorbance at 254 nm, which is characteristic of benzoquinones. By default, Intermediate **1** is likely to be 3,5,6-trimethylcatechol. The identification of intermediates is summarized in Table 7.1.

### 7.2.2 Kinetics of the Photodegradation of 2,3,5-TMP

In the absence of light, 2,3,5-TMP is only slightly adsorbed ($\leq$ 10 %) onto the semiconductor particle surface. The disappearance of 2,3,5-TMP in aqueous $TiO_2$ dispersions ($[2,3,5\text{-TMP}]_{ini}$ = 159.3 $\mu$M; $[TiO_2]$ = 2g/L; pH 3) irradiated by uv/visible light was monitored by High Performance Liquid Chromatography. The organic substrate degrades via reasonably good first-order kinetics ($k_{app}$ = 0.14 $\pm$ 0.02 $min^{-1}$; $Rate_{ini}$ =

**Table 7.1** Identification of Intermediates in the Course of the Photomineralization of 2,3,5-TMP

| Substrate | Retention Time $\lambda_{det}$ (nm) | Intermediate |
|---|---|---|
| 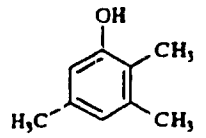 2,3,5-Trimethylphenol | 9.9 min (214 nm) | — |
| 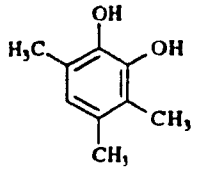 2,3,5-Trimethylcatechol | *2.6 min* * (214 nm) | 1 |
| 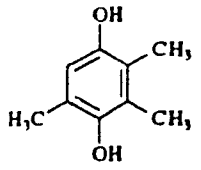 2,3,5-Trimethylhydroquinone | 3.3 min (214 nm) | 2 |
| 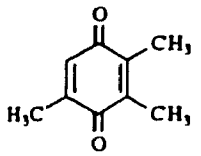 2,3,5-Trimethylbenzoquinone | *7.2 min* * (254 nm) | 3 |

* Retention times in italics denote "deduced" retention times based on the data presented.

$23 \pm 2$ $\mu$M/min; $t_{1/2} = 4.8$ min), Figure 7.1. The total photodegradation of 2,3,5-TMP is complete in $\leq 45$ min of irradiation. The formation and disappearance of the major intermediates were also monitored. 2,3,5-Trimethylhydroquinone formed via first-order kinetics ($k_{app} \approx 0.1$ min$^{-1}$) and degraded via zero order kinetics ($k_{app} \approx 7$ $\mu$M/min). The species 2,3,5-TMBQ also formed via first-order kinetics ($k_{app} \approx 0.003$ min$^{-1}$) and disappeared via zero order kinetics ($k_{app} \approx 2$ $\mu$M/min). In the absence of $TiO_2$, under otherwise identical conditions, direct irradiation led to negligible, if any, decomposition

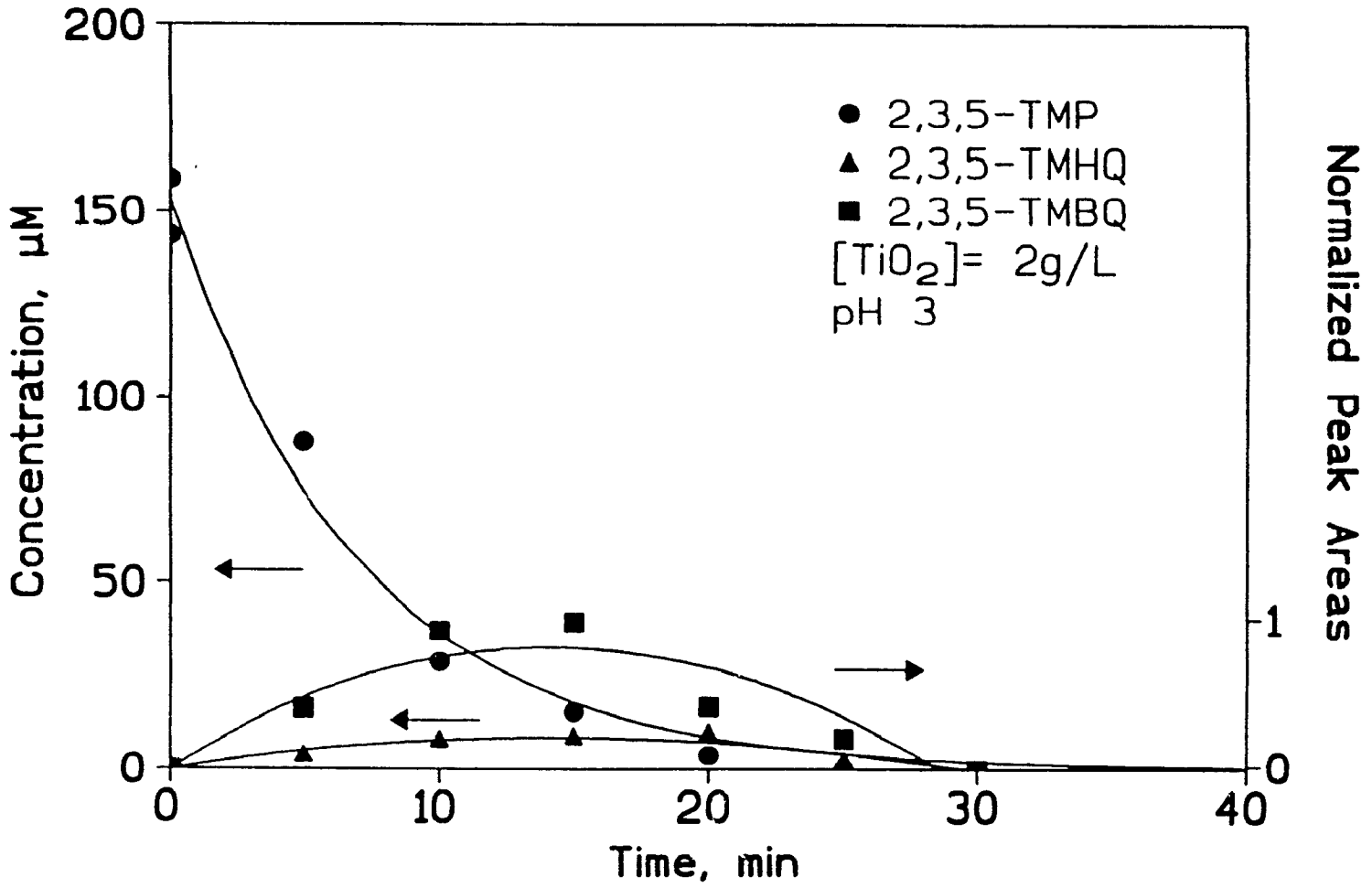


**Figure 7.1** Photodegradation of 2,3,5-TMP (159.3 $\mu$M) in air-equilibrated aqueous suspensions of $TiO_2$ irradiated by light of wavelengths > 300 nm; pH 3; $TiO_2$, 2 g/L; 50 mL samples.

of this substrate within the time frame of our experiments.

The photocatalyzed mineralization process for 2,3,5-TMP follows the stoichiometric reaction 7.1, as evidenced by a quantitative product analysis:

$$(CH_3)_3C_6H_2OH + \frac{23}{2}\ O_2 \xrightarrow[TiO_2]{h\nu} 9\ CO_2 + 6\ H_2O \qquad (7.1)$$

The quantity of $CO_2$ evolved as a function of irradiation time is illustrated in Figure 6.4 for an oxygen-saturated aqueous solution of 2,3,5-TMP. Approximately 32.8 $\mu$mols of $CO_2$ were expected from reaction 7.1 for $[2,3,5\text{-TMP}]_{in} = 146\ \mu M$. It is evident that after $\approx$ 1 hr of irradiation, when all the 2,3,5-TMP and intermediate species have decomposed, the expected stoichiometric amount of $CO_2$ is produced.

### 7.2.3 Effect of Oxygen

The effect of the concentration of oxygen on the kinetics of decomposition of 2,3,5-TMP was determined by carrying out the photoreaction under conditions where the suspension was saturated with $O_2$. The decomposition of this phenolic substrate in both air-equilibrated and oxygen-saturated suspensions is compared in Figure 7.3. Reasonably good first-order kinetics are evident in both cases. The corresponding parameters are, air *versus* oxygen, respectively: $k_{app}$, 0.14 $min^{-1}$ and 0.21 $min^{-1}$; initial rates, 23 $\mu$M/min and 34 $\mu$M/min; $t_{1/2}$(app), 4.8 min and 3.3 min. Note that in the presence of excess oxygen, decomposition of 2,3,5-TMP occurs in $< 25$ min.

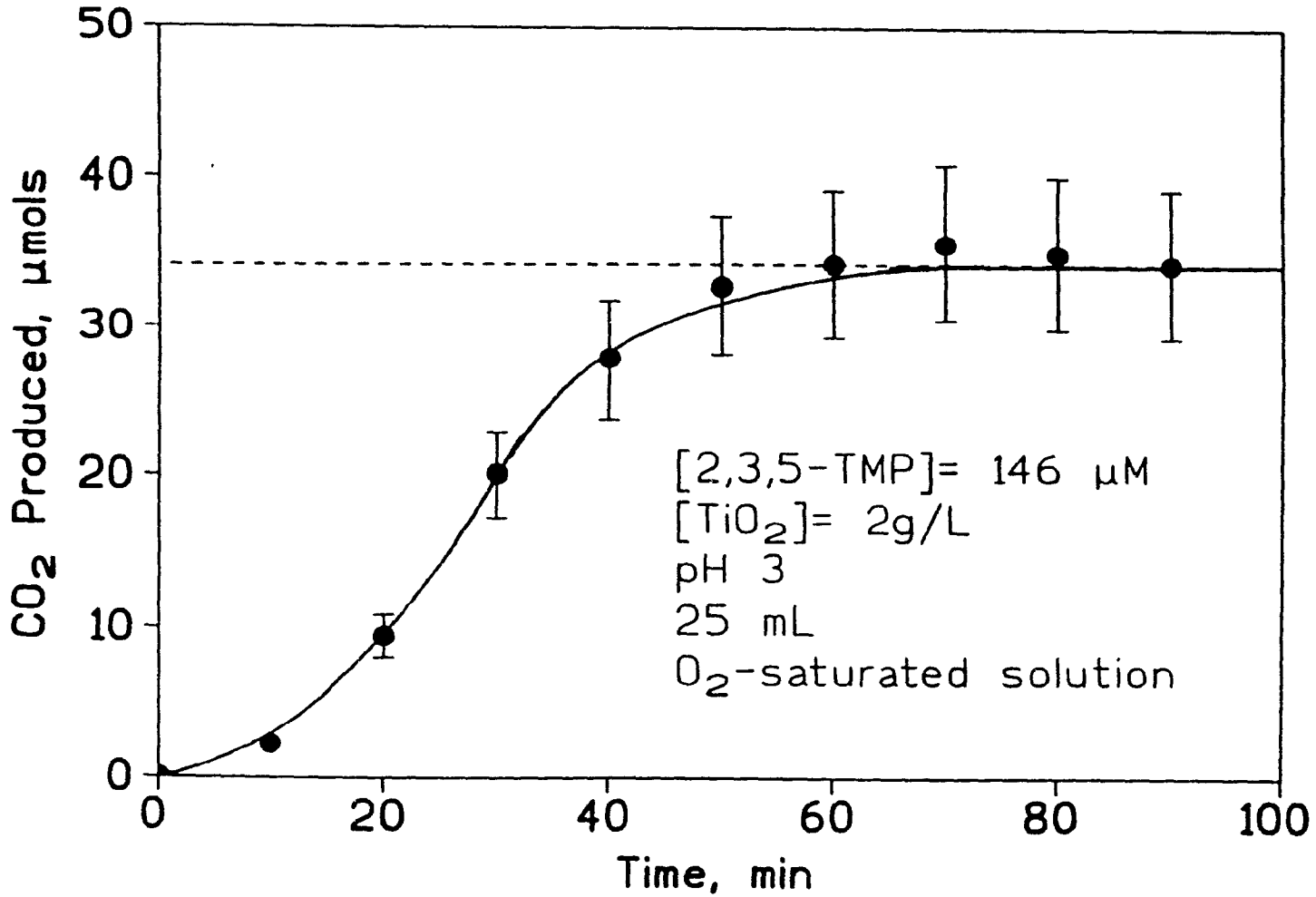


**Figure 7.2** Plot showing the temporal evolution of $CO_2$ from the photomineralization of 146 $\mu$M 2,3,5-TMP in the presence of 2 g/L $TiO_2$ at an initial pH of 3 in an oxygen-saturated suspension. The dotted line indicates the amount of $CO_2$ expected upon total mineralization.

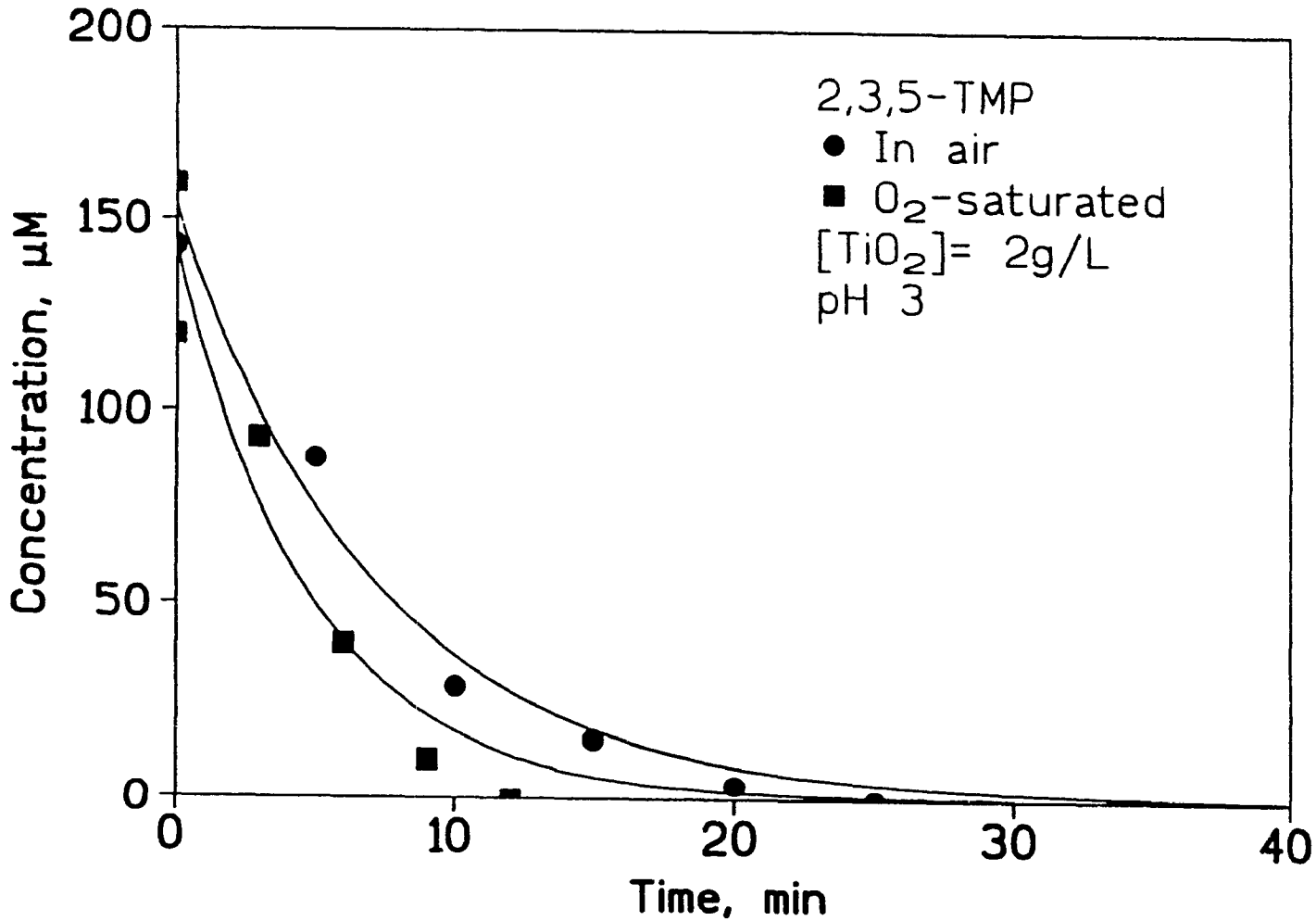


**Figure 7.3** Plot showing the photodegradation of ≈ 20 mg/L of 2,3,5-TMP in the presence of 2 g/L $TiO_2$ in air-equilibrated suspensions and in oxygen-saturated suspensions; initial pH 3. The apparent rate constants were, air *versus* O2, respectively: $k_{app}$, 0.143 $min^{-1}$ and 0.211 $min^{-1}$.

## 7.2.4 Mechanism of the Photodegradation of 2,3,5-TMP

The photooxidation of 2,3,5-TMP in irradiated $TiO_2$ suspensions occurs by reaction between the oxidizing species (taken here to be the surface-bound •OH-radicals) and 2,3,5-TMP as a first step; this yields the intermediates (2,3,5-TMHQ, 3,5,6-TMCC, 2,3,5-TMBQ, and others not identified). Subsequent reaction of these intermediate products with the oxidizing species ultimately yields $CO_2$ and $H_2O$ via a series of reactions which include ring cleavage and probably the formation of peroxides, aldehydes, and carboxylates as evidenced in the photodegradation of surfactants.[6] The present results suggest the photomineralization process occurs via scheme 7.2.

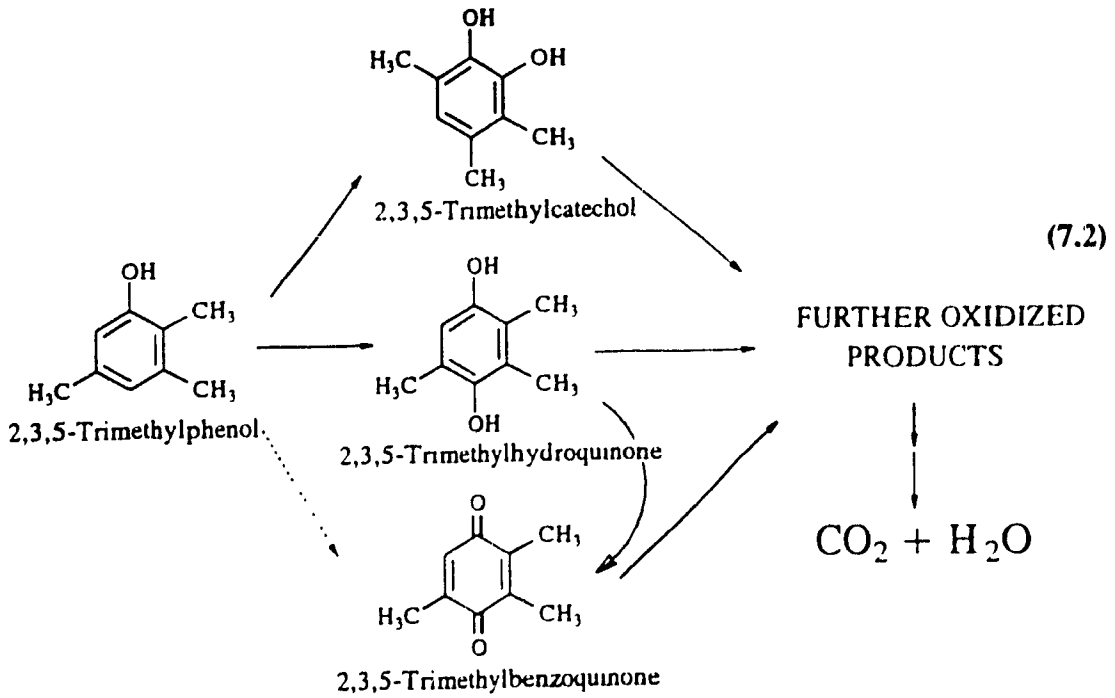


(7.2)

## 7.2.5 Kinetic Considerations

It was noted earlier that the extent of 2,3,5-TMP adsorption in the dark is small ($\leq$ 10 %); the extent of photoadsorption, however, is an unknown parameter. It is also assumed here that there exists a constant fraction, however small, of 2,3,5-TMP adsorbed or photoadsorbed on the catalyst's particle surface. The photomineralization of 2,3,5-TMP is then described by equation 7.3:

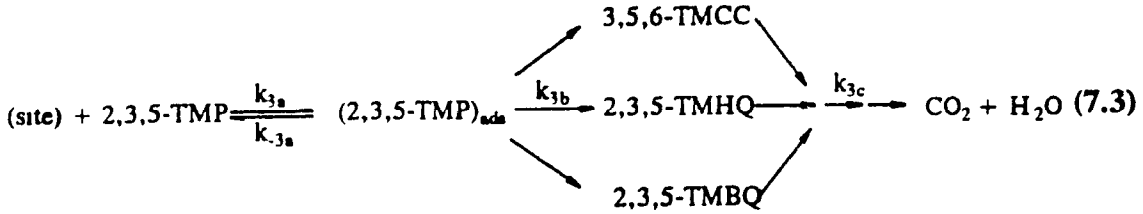


The rate of formation of the final products $CO_2$ and $H_2O$ is then given by equation 7.4,

$$Rate = \frac{\frac{\phi I_a \beta A_p k_{trap} \tau_{\cdot OH}}{k_{rec}} k_{3b} K_{TMP}[2,3,5\text{-}TMP] N_s}{1 + \alpha K_{TMP}[2,3,5\text{-}TMP] + K_W[H_2O] + \Sigma_i K_{intm.}[Intm.]_i + K_{ions}[ions]} \cdot \frac{K_{O_2}[O_2]}{(1 + K_{O_2}[O_2])} \qquad (7.4)$$

where $\alpha$ is $(k_{3b} + k_{3c})/k_{3c}$, $K_{TMP}$ is the photoadsorption coefficient for 2,3,5-TMP, $k_{3b}$ is the rate constant for the conversion of $(2,3,5\text{-TMP})_{ads}$, and the other parameters have the same meaning as in equation 3.11, Chapter 3. Water, 2,3,5-TMBQ, 2,3,5-TMHQ, 3,5,6-TMCC and other intermediates that form in the degradation process together with ions present in solution (in this case $Cl^-$) can, in principle, compete for the same adsorption sites as the 2,3,5-TMP; they will inhibit the reaction. Molecular $O_2$ affects the rate of degradation (Figure 7.3); the binding isotherm expression for molecular $O_2$

is also included in equation 7.4, as it influences the overall process.[1,2,7]

## 7.3 CONCLUSIONS

The disappearance of 2,3,5-trimethylphenol in air-equilibrated, irradiated $TiO_2$ suspensions takes place in $<$ 45 min at pH 3. In excess molecular oxygen, the degradation of 2,3,5-TMP is faster ($\leq$ 20 min) and complete mineralization to $CO_2$ and $H_2O$ takes place in $\approx$ 1 hr. The major aromatic intermediates formed during the photodegradation of 2,3,5-TMP were identified as 2,3,5-trimethylhydroquinone, 2,3,5-trimethylbenzoquinone, and 3,5,6-trimethylcatechol; other intermediates also form but were not identified under our experimental conditions. The present work completes the survey of the phenolic components of coal tar creosote.

# REFERENCES


1. K. Okamoto, Y. Yamamoto, H. Tanaka, M. Tanaka, and A. Itaya, *Bull. Chem. Soc. Jpn.*, **58** (1985) 2015.

2. K. Okamoto, Y. Yamamoto, H. Tanaka, and A. Itaya, *Bull. Chem. Soc. Jpn.*, **58** (1985) 2023.

3. Augugliaro, V., Palmisano, L., Sclafani, A., Minero, C., Pelizzetti, E., *Toxicol. Environ. Chem.*, **1988**, *16*, 89.

4. Barbeni, M., Pramauro, E., Pelizzetti, E., Borgarello, E., Serpone, N., *Chemosphere*, **1985**, *14*, 195.

5. Mueller, J.G., Chapman, P.J., Pritchard, P.H., *Environ. Sci. Technol.*, **1989**, *23*, 1197.

6. Hidaka, H., Zhao, J., Suenaga, S., Pelizzetti, E., and Serpone, N., *J. Jpn. Oil Chem. Soc.*, **1990**, *39*, 45.

7. Meyer, G.J., Luebker, E.R.M., Lisensky, G.C., Ellis, A.B., in: *"Photochemistry on Solid Surfaces"*, Anpo, M., Matsuura, T., Eds., Elsevier, Amsterdam, **1989**, p. 388.

# CHAPTER 8

# THE PHOTOCATALYZED MINERALIZATION OF *CREOSOTE* IN IRRADIATED $TiO_2$ MEDIA: *A PRACTICAL CASE STUDY*

## 8.1 INTRODUCTION

The wood-preserving industry is the largest industrial user of pesticides worldwide. The major chemicals used for wood-preserving purposes are creosote, pentachlorophenol, and CCA (copper, chrome, and arsenate).[1] The annual consumption of approximately 500 creosoting operations in the United States is about 454,000 metric tons; between 840 and 1,530 dry metric tons of hazardous waste sludge is generated by these wood treatment facilities.[1] Accidental spillage, misuse and improper disposal of creosote and pentachlorophenol have resulted in contaminated environments with potential health risks; one such problem is the contamination of groundwater in the vicinity of wood-preserving facilities. Examples include PCP- and creosote-contaminated sites at Pensacola, FL,[2] and at St. Louis Park, MN.[3]

Near-UV irradiation of creosote leachates in the presence of $TiO_2$ can rapidly and safely eliminate (mineralize) these hazardous substances in air-equilibrated aqueous media. The present remediation techniques use biotic and abiotic (volatilization, leaching, and direct photolysis) processes to restore contaminated sites with perhaps *in situ* biodegradation as the major method. However, the latter is not without its limitations:[1] (i) the pollutant(s) needs to be in a chemical state that is conducive to microbial utilization; (ii) excess organic carbon in the feed robs the microbial population of oxygen

and essential inorganic nutrients, thereby limiting its activity; and (iii) successful bioremediation necessitates the presence of acclimatized microbial population capable of degrading the pollutant(s). As a case in point, studies by Crawford and Mohn[4] indicate that bioremediation of a pentachlorophenol-contaminated site takes several months to bring the concentration of pentachlorophenol from 298 ppm down to 58 ppm, although acclimatization does accelerate the process. The specificity of a microbe to degrade a given organic pollutant is not a limitation in heterogeneous photocatalysis, since the •OH radical is indiscriminate in its attack of organics.

Creosote, a translucent brown-black oily liquid, is obtained from the distillation of coal tar and is a complex mixture of organic compounds: 85 wt % polycyclic aromatic hydrocarbons [PAHs] (Table 8.1), 10 wt % phenolic compounds (Table 8.2), and 5 wt % N-, S-, and O- heterocyclics (Table 8.3).[1] PAHs have much lower solubilities in water (e.g. naphthalene 31.7 mg/L) than phenols (e.g. o-cresol, 25920 mg/L). The phenols, therefore, constitute the bulk of the aqueous contaminants resulting from creosote spillage.[2a]

To date, the photodegradation of all major phenolic components of creosote has been carried out using irradiated aqueous suspensions of $TiO_2$, either in this work (cresols, xylenols, 2,3,5-trimethylphenol) or elsewhere (phenol,[5-7] pentachlorophenol[8]). In this work, the complete destruction of coal tar creosote using heterogeneous catalysis will be demonstrated with a special emphasis on the phenolic compounds. The photodegradation will be monitored by using high performance liquid chromatography, UV/Vis absorption and diffuse reflectance spectroscopies, and gas chromatography.

**Table 8.1** Predominant Polycyclic Aromatic Hydrocarbons in Coal Tar Creosote [Ref. 1]

| Compound | Relative wt % | Aqueous Solubility (ppm, 25°C) |
|---|---|---|
| Naphthalene | 13 | 31.7 |
| 2-Methylnaphthalene | 13 | 25.4 |
| Phenanthrene | 13 | 1.3 |
| Anthracene | 13 | 0.07 |
| 1-Methylnaphthalene | 8 | 28.5 |
| Biphenyl | 8 | 7.5 |
| Fluorene | 8 | 2.0 |
| 2,3-Dimethylnaphthalene | 4 | 3.0 |
| 2,6-Dimethylnaphthalene | 4 | 2.0 |
| Acenaphthene | 4 | 3.9 |
| Fluoranthene | 4 | 0.26 |
| Chrysene | 2 | 0.002 |
| Pyrene | 2 | 0.14 |
| Anthraquinone | 1 | - |
| 2-Methylanthracene | 1 | 0.04 |
| 2,3-Benzo[b]fluorene | 1 | 0.002 |
| Benzo[*a*]pyrene | 1 | 0.003 |

Quantitative $CO_2$ production will be demonstrated.

## 8.2 PHOTOMINERALIZATION OF CREOSOTE

Addition of 50 mL of creosote (360 ppm) to 100 mg of $TiO_2$ leads to an immediate adsorption of the water-insoluble creosote components (oily droplets, mostly PAH's) onto the $TiO_2$ particulates which turned from white to an intense dark beige color. The water-soluble phenolics likely remain largely in solution, as they typically adsorb only to a slight extent in the dark ($\leq$ 10 %); other water soluble components of

**Table 8.2** Predominant Heterocyclic Compounds in Coal Tar Creosote [Ref. 1]

| Compound | Relative wt % | Aqueous Solubility, ppm |
|---|---|---|
| N-Heterocyclics and *N*-containing aromatics: | | |
| Quinoline | 10 | 6178 (20 °C) |
| Isoquinoline | 10 | 4522 (20 °C) |
| Carbazole | 10 | 1 (20 °C) |
| 2,4-Dimethylpyridine | 10 | - |
| Acridine | 5 | 5 (20 °C) |
| Aniline | 5 | 3400 (25 °C) |
| 2-Methylquinoline | 5 | - |
| 4-Methylquinoline | 5 | - |
| Pyrrole | 5 | - |
| Pyrrolidine | 5 | - |
| *S*-Heterocyclics: | | |
| Benzo[*b*]thiophene | 10 | 130 (20 °C) |
| Dibenzothiophene | 10 | 2 (24 °C) |
| *O*-Heterocyclics: | | |
| Dibenzofuran | 10 | 10 (25 °C) |

**Table 8.3** Predominant Phenolic Compounds in Coal Tar Creosote [Ref. 1].

| Compound | Relative wt % | Aqueous Solubility, ppm |
|---|---|---|
| Phenol | 20 | 82000 (15 °C) |
| o-Cresol | 10 | 25920 (25 °C) |
| *m*-Cresol | 10 | 23500 (20 °C) |
| *p*-Cresol | 10 | 24400 (40 °C) |
| Pentachlorophenol | 10 | 14 (20 °C) |
| 2,5-Xylenol | 7.5 | 3544 (25 °C) |
| 3,5-Xylenol | 7.5 | 4888 (25 °C) |
| 2,3-Xylenol | 5 | 4570 (25 °C) |
| 2,4-Xylenol | 5 | 6232 (25 °C) |
| 2,6-Xylenol | 5 | 6049 (25 °C) |
| 3,4-Xylenol | 5 | 4766 (25 °C |
| 2,3,5-Trimethylphenol | 5 | - |

creosote which did not adsorb onto the catalyst surface may also be in solution. Following irradiation of the air equilibrated suspension, the temporal course of the degradation of these water soluble compounds was monitored via absorption spectroscopy (Figure 8.1). The spectra show that for the first 60 min of irradiation, there are no spectral changes at $\lambda < 240$ nm; however they do show greater absorptivity in the range 240-350 nm with increasing irradiation time. Maximum absorption is reached after ca. 1 hr, following which a dramatic decrease in absorption is evident throughout the wavelength range 200-400 nm from 150 min to 360 min. After 6 hrs of irradiation there are no more (water-soluble) aromatic species evident in solution.

The changes in the concentration of solution substrates were also followed by HPLC methods. Figure 8.2 illustrates the chromatograms as intensity *versus* retention time *versus* irradiation time plots. The changes observed here parallel those seen in Figure 8.1. After 6 hours, the chromatogram is identical to a water blank which contained $TiO_2$ but no creosote, thereby confirming the total disappearance of the water-soluble creosote aromatic components.

During irradiation, the catalyst particulates also showed significant color changes. Scanned color images of the solid particulates remaining upon filtration on the MSI nylon membrane filters are illustrated in Figure 8.3 as a function of irradiation time (minutes). As mentioned earlier, upon addition of the creosote solution to $TiO_2$, the $TiO_2$ particles turned a dark beige color (t=0). Upon irradiation, the beige color progressively becomes darker between t=0 and t=120 min. At 180 min, the color begins to progressively fade and the particles revert to their original white color after 900 min of irradiation. A

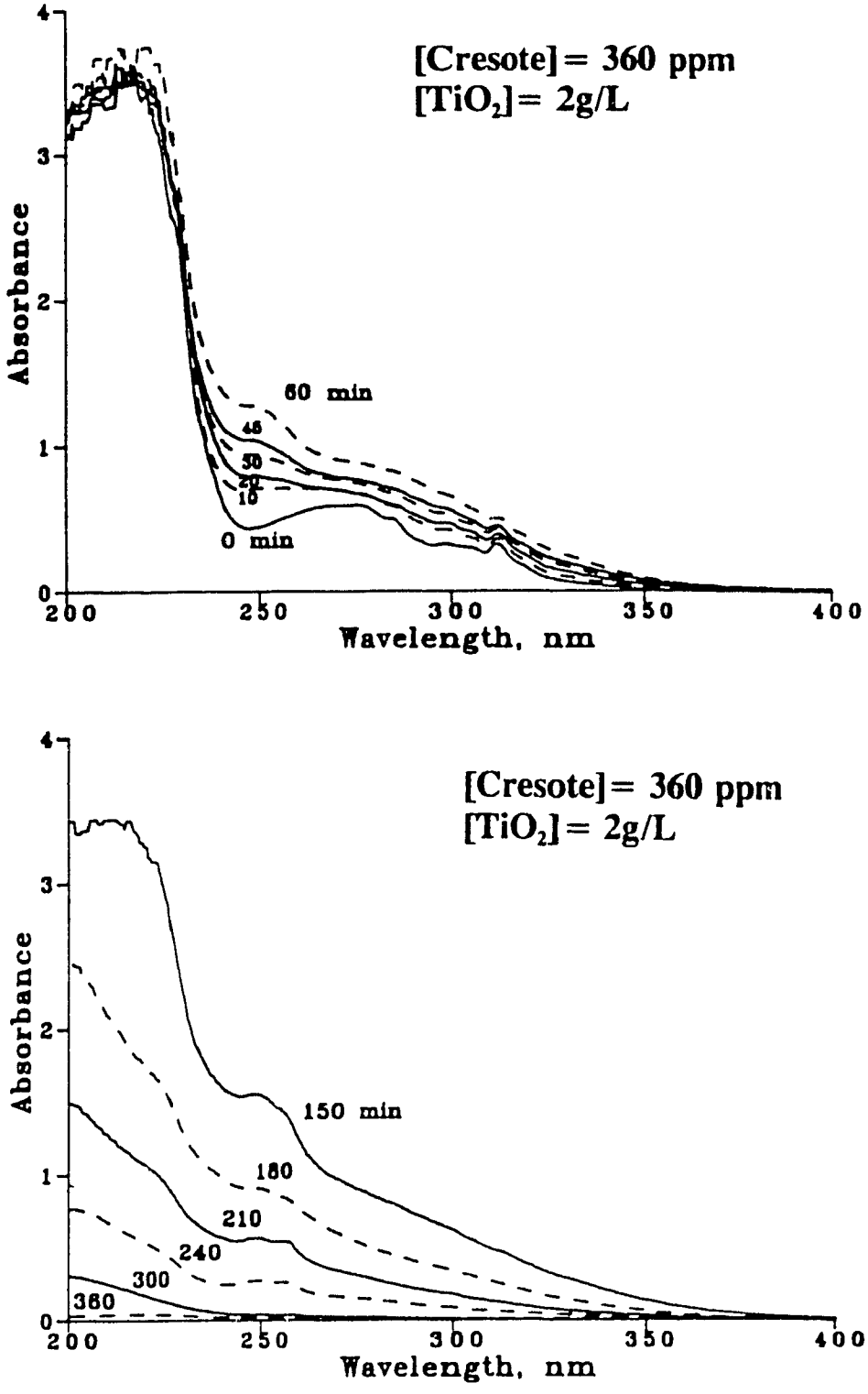


**Figure 8.1** Absorption spectra of the filtrates containing water-soluble components of creosote during the photocatalyzed degradation of 360 ppm of creosote under air-equilibrated conditions (see text).

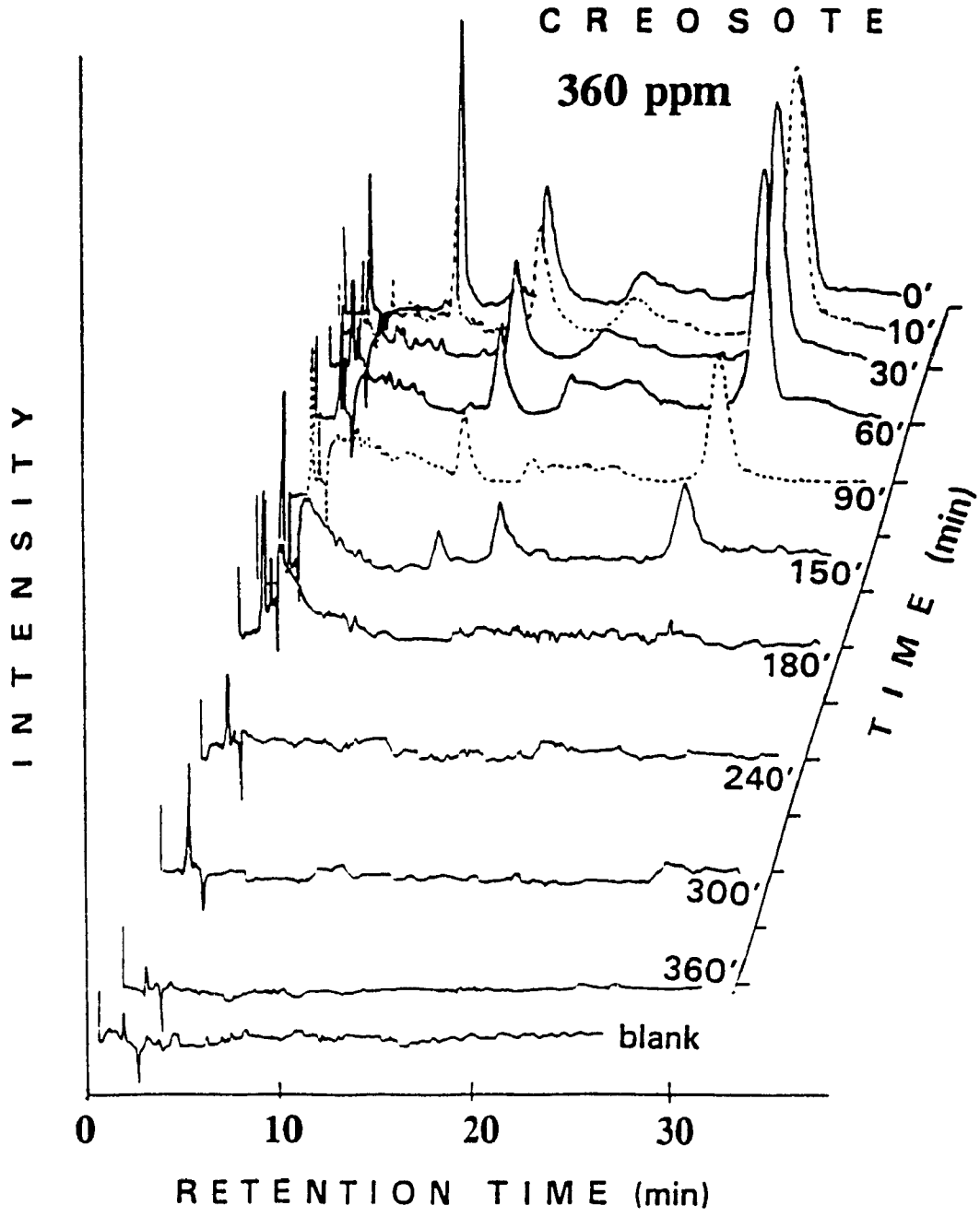


**Figure 8.2** HPLC chromatograms of the initial water-soluble substances in creosote and intermediates following light irradiation of an aqueous suspension containing the photocatalyst $TiO_2$ and creosote under air-equilibrated conditions. The samples used were those used to record the absorption spectra (see Figure 8.1). [mobile phase, 50/50 water/methanol]; the features at r.t. 1-3 min are attributed to the elution of the solvent and any other compounds not retained by the column.

**Figure 8.3** Scanned image of the $TiO_2$ particle filtrates (on MSI Nylon filters) as a function of irradiation time in minutes. A $TiO_2$ blank is included for comparison purposes.

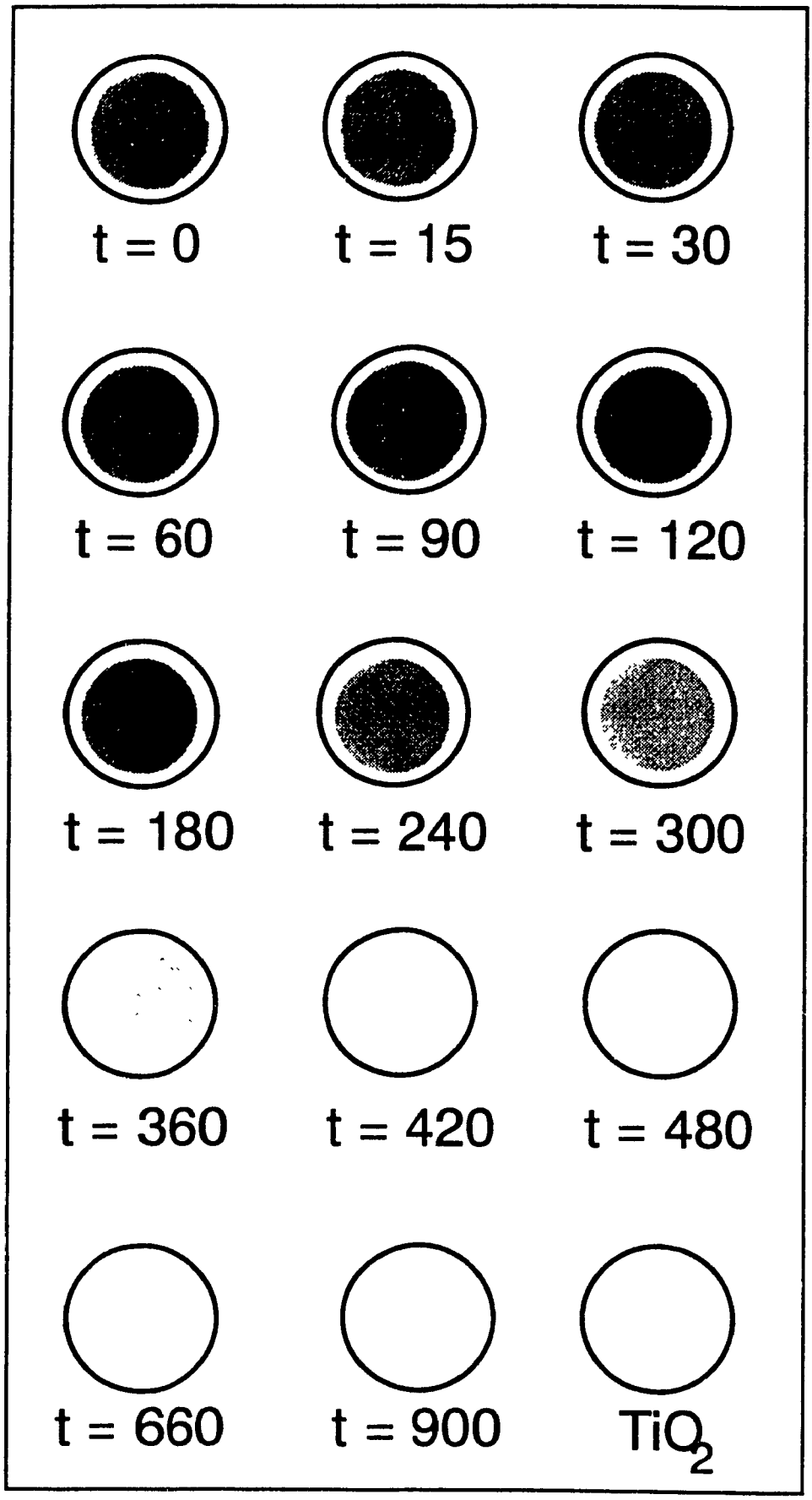
t = 0
t = 15
t = 30
t = 60
t = 90
t = 120
t = 180
t = 240
t = 300
t = 360
t = 420
t = 480
t = 660
t = 900
TiO2

sample of pure $TiO_2$ is also shown in Figure 8.3 for comparison purposes. This is indicative that although there were no compounds remaining in solution after 360 min of irradiation, the compounds adsorbed on the surface did not completely photodegrade until after about 900 min of irradiation.

The diffuse reflectance spectra of the filtrates illustrated above were also recorded, and a reflectance spectrum of pure $TiO_2$ particulates (blank) is also shown for comparison (Figure 8.4). The spectral features below 400 nm are due to $TiO_2$ particulates; the region above 400 nm shows increasing broad absorption to 850 nm up to 90 min of irradiation. These spectral features are reminiscent of surface complexes formed between $Ti^{IV}$ on the catalyst particle surface and various coordinating organic species.[9,10] Prolonged irradiation (time > 120 min) leads to absorption decrease until after 900 min of irradiation the appearance (white color) of the $TiO_2$ particulates has been restored.

Figure 8.5 summarizes the spectral changes as absorbance (at 215 nm in Figure 8.1) or reflectance (at 450 nm in Figure 8.4) *versus* irradiation time. Here also, there are relatively no changes at 215 nm until after ca. 3 hours of irradiation. At this point, all the water-soluble species *degrade collectively* via excellent first-order kinetics (solid line) after an "induction" period of ≈ 3 hrs: $k_{deg} = 0.0185 \pm 0.0004$ min$^{-1}$, $t_{1/2} = 36$ min; similar kinetics obtained at 250 nm ($0.0183 \pm 0.0009$ min$^{-1}$; $t_{1/2} = 38$ min.). The species that are adsorbed on the catalyst surface also *decay collectively* via good first-order kinetics (dashed line) at 450 nm after an "induction" period of ≈ 2 hrs: $k_{deg} = 0.0032 \pm 0.0002$ min$^{-1}$, $t_{1/2} = 216$ min. It is suspected that the slower degrading substances are

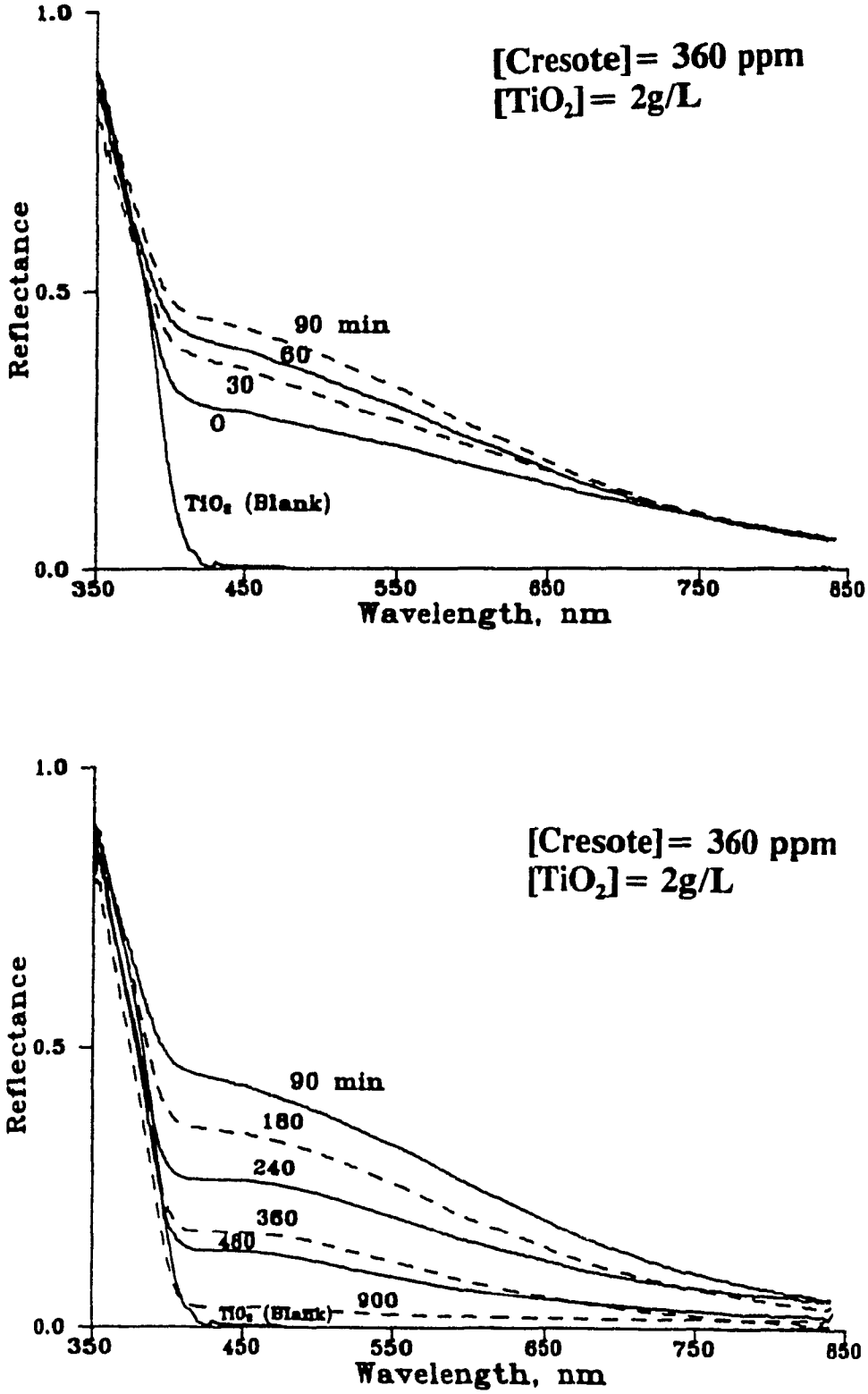


**Figure 8.4** Diffuse reflectance spectra of the $TiO_2$ particulates after filtration of the irradiated aliquots taken during the photocatalyzed degradation of creosote.

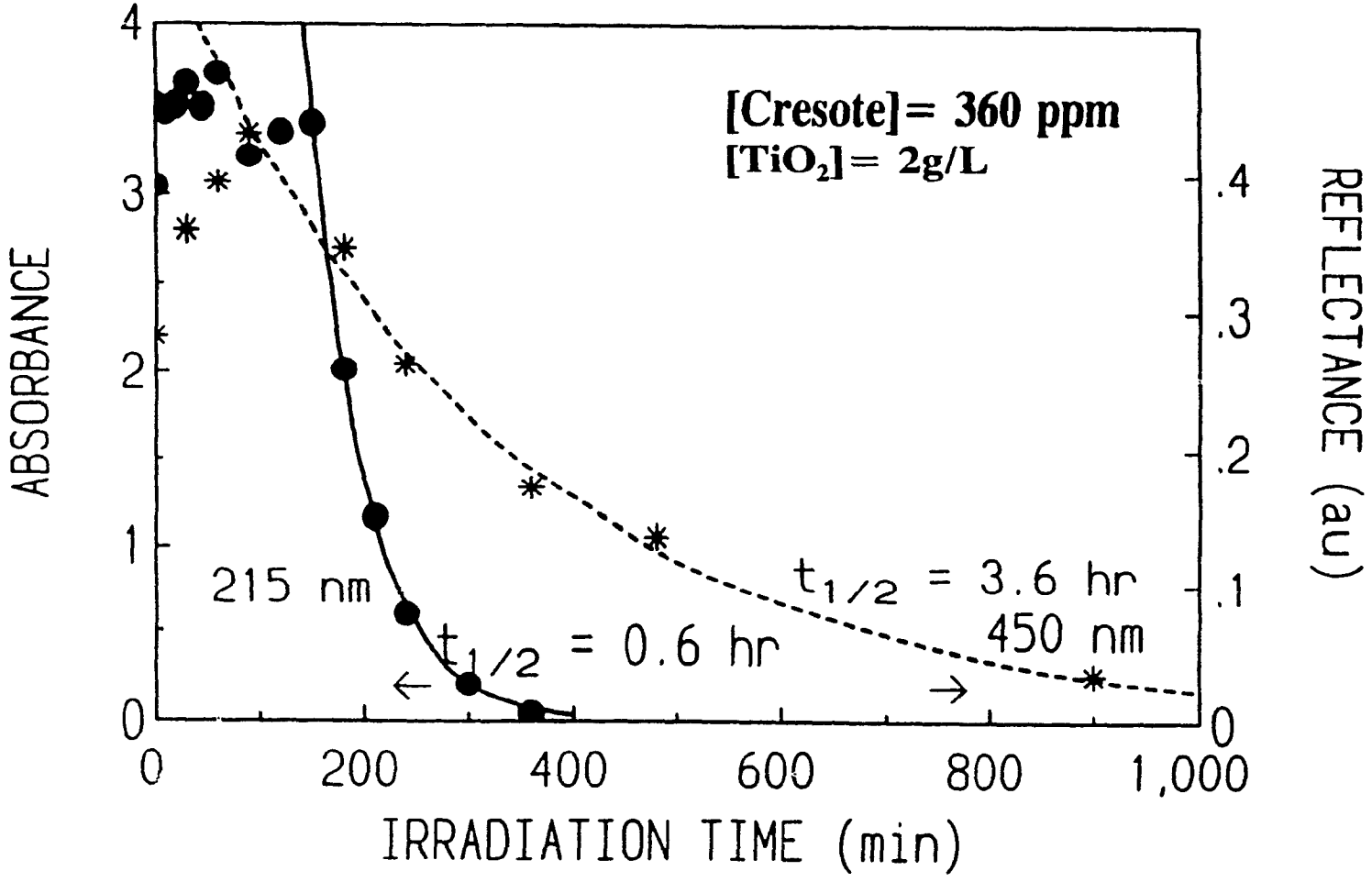


**Figure 8.5** Kinetic analyses of the changes in concentrations (as absorbance) from the data in Figures 8.1 and 8.4 at the wavelengths indicated.

the polycyclic aromatic hydrocarbons and other water-insoluble substrates. We estimate from these kinetics that after 24 hours of irradiation the concentrations of the observable species is reduced from 360 ppm to 6 ppb. Any attempt at describing the events occurring during the "induction period" would be too speculative at this time, owing to the complexity of the system examined. Such effort will have to await further studies with an analytical methodology that will identify the various intermediate products involved along the course of the mineralization.

Total mineralization necessitates demonstration of stoichiometric evolution of the ultimate oxidation product, $CO_2$. Experimental difficulties (air-equilibrated conditions in a sealed reactor, time of irradiation needed to mineralize 360 ppm, and not least the suspension running out of needed oxygen) suggested that total oxidation be demonstrated using an initial concentration of creosote of 100 ppm* and a saturated oxygen atmosphere in a septum-sealed pyrex glass reactor. The results are graphically illustrated in Figure 8.6 in terms of $\mu$mols of $CO_2$ evolved *versus* irradiation time. The data were fitted (solid line) to double exponential growth kinetics: $k_{CO2}^{(1)} = 0.042 \pm 0.008$ min$^{-1}$, $t_{1/2}^{(1)} = 17$ min and $k_{CO2}^{(2)} = 0.006 \pm 0.002$ min$^{-1}$, $t_{1/2}^{(2)} = 113$ min. The former values correspond to $CO_2$ formation from the *faster* degraded water-soluble components, while the latter kinetics correspond to $CO_2$ formation from the *slower* degraded substances (most likely the PAH's). The dashed line denotes the expected stoichiometric quantity of carbon dioxide, while the dotted curves represent the two growth kinetic components.

---

* The author thanks Mr R. Patterson of the SIRU Laboratory for kindly determining the percentage of carbon present in this sample of commercial coal-tar creosote.

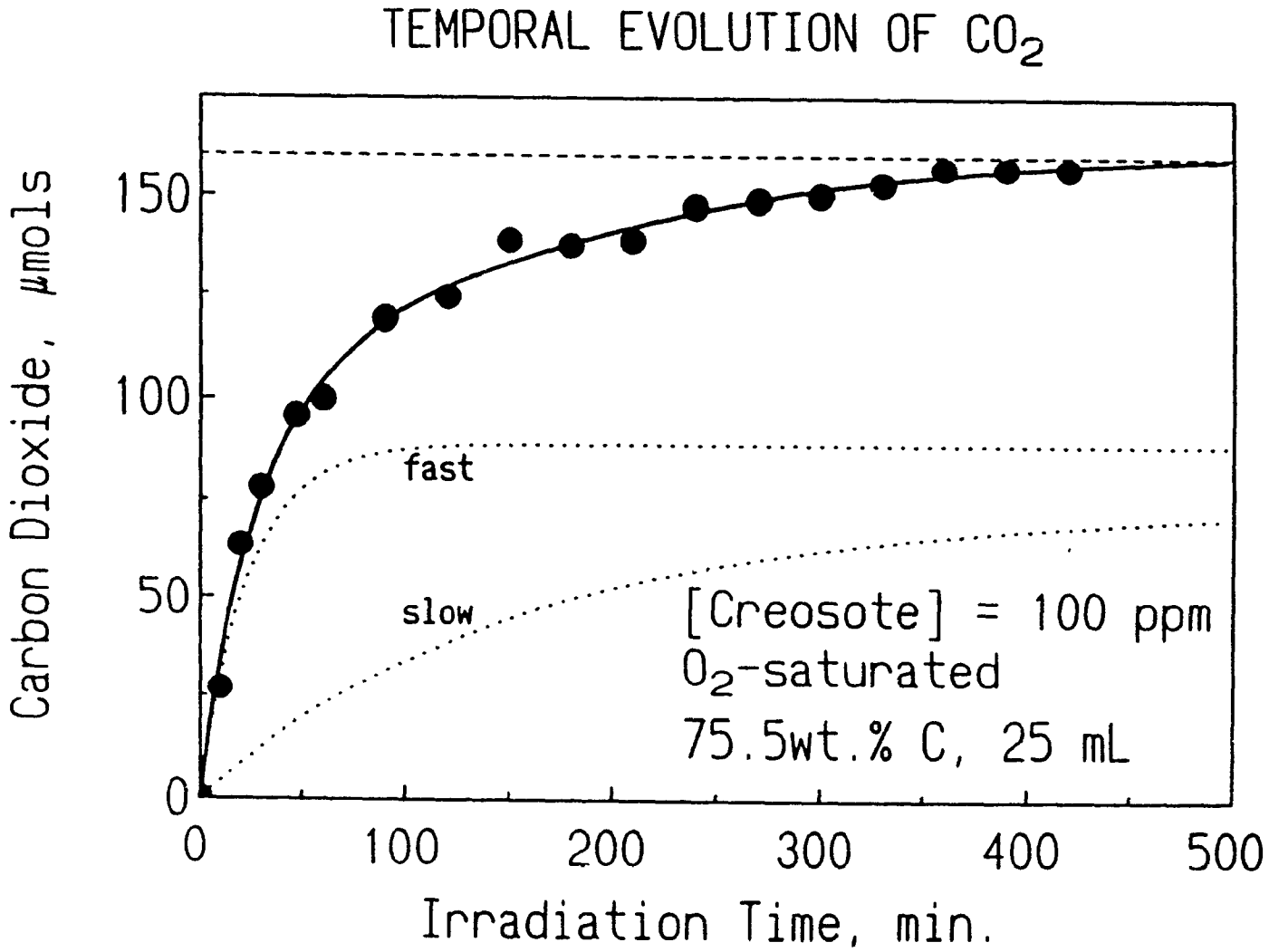


**Figure 8.6** Plots showing the double exponential evolution of stoichiometric quantities of carbon dioxide formed from the total photomineralization of 100 ppm of creosote under a saturated oxygen atmosphere. See text for additional details.

Under these conditions, total mineralization of 100 ppm creosote is achieved in ≈ 6-7 hours.

## 8.3 CONCLUSIONS

The photocatalyzed mineralization of creosote using heterogeneous photocatalysis was carried out in aqueous media. $TiO_2$ was used as the photocatalyst and total mineralization has been demonstrated by the quantitative analysis of $CO_2$, a final product. The photodegradation process was monitored both in solution (for water soluble compounds) and on the photocatalyst surface (for water insoluble compounds). This study illustrates the practicality of heterogeneous photocatalysis in the decontamination of typical multicomponent samples such as one is likely to encounter in polluted aquifers.

# REFERENCES


1. Mueller, J.G., Chapman, P.J., Pritchard, P.H., *Environ. Sci. Technol.*, **23**, 1197, **1989**.

2. a) Goerlitz, D.F., Troutman, D.E., Godsy, E.M., and Franks, B.J., *Environ. Sci. Technol.*, **19**, 955, **1985** and references therein.
b) Troutman, D.E., Godsy, E.M., Goerlitz, D.F., Ehrlich, G.G., Tallahassee, FL, U.S. Geological Survey Water Resources Investigations Report 84-4230, **1984**.

3. Ehrlich, G.G., Goerlitz, D.F., Godsy, E.M., Hult, M.F., *Ground Water*, **1982**, *20*, 703.

4. Crawford, R.L., Mohn, W.W., *Enzyme Microb. Technol.*, **1985**, *7*, 617.

5. Okamoto, K., Yamamoto, Y., Tanaka, H., Tanaka, M., *Bull. Chem. Soc. Jpn.*, **1985**, *58*, 2015.

6. Al-Ekabi, H., Serpone, N., *J. Phys. Chem.*, **1988**, *92*, 5726.

7. Augugliaro, V., Palmisano, L., Sclafani, A., Minero, C., Pelizzetti, E., *Toxicol. Environ. Chem.*, **1988**, *16*, 89.

8. Barbeni, M., Pramauro, E., Pelizzetti, E., Borgarello, E., Serpone, N., *Chemosphere*, **1985**, *14*, 195.

9. See Chapter 5 of this thesis.

10. Houlding, V.H., Grätzel, M., *J. Am. Chem. Soc.*, **1983**, *105*, 5695.

# CHAPTER 9

# PULSE RADIOLYTIC STUDIES OF THE REACTIONS OF PENTAHALOPHENOLS WITH •OH, $N_3^•$ AND $e^-_{(aq)}$:

## FORMATION OF PENTAHALOPHENOXYL, DIHYDROXYPENTAHALOCYCLOHEXADIENYL, AND SEMIQUINONE RADICALS

## 9.1 INTRODUCTION

The photocatalyzed oxidation of halogenated aromatics has been carried out successfully in aqueous dispersions of $TiO_2$.[1] Noteworthy examples include the mineralization of such environmental contaminants as 2,4,5-trichlorophenol,[2,3] pentachlorophenol,[4] 2-, 3-, and 4-fluorophenol,[5] 2,4-difluorophenol,[5] hexafluorobenzene[6] and pentafluorophenol.[6] Intermediates detected in the course of the degradation of pentafluorophenol included tetrafluorohydroquinone, tetrafluorocatechol, and 3,5,6-trifluoro-1,2,4-benzenetriol.[6] Although identification of intermediates was not carried out in the pentachlorophenol study[4] (its disappearance was monitored spectrophotometrically rather than by chromatographic methods as for pentafluorophenol), its photodegradation is presumed to proceed via similar intermediates (i.e., via dihydroxybenzenes, etc.). The hydroxyl radical has been implicated as a significant oxidant in the $TiO_2$-assisted photomineralization of these and many other organic compounds in aqueous environments,[2-6] since hydroxylated intermediates can be detected during the photodegradation of many of these species. One example is the detection of hydroquinone, catechol, 1,2,4-benzenetriol, *p*-benzoquinone, pyrogallol, and 2-hydroxy-1,4-benzoquinone as intermediates in the photooxidative mineralization of phenol.[7,8] However, since these same adducts could also be formed by hydration of a singly

oxidized cation radical, produced by direct interfacial electron transfer to an adsorbed organic substrate,[9] details concerning the primary process(es) initiated by photon activation of $TiO_2$ in aqueous media are still a matter of debate.[10] Hydroxyl radicals may originate from several possible routes[11-18] as described in Chapter 2. Irradiation of $TiO_2$ particles ($E_{bg} \approx 3.2$ eV) generates valence band holes ($h^+_{VB}$) and conduction band electrons ($e^-_{CB}$), equation 9.1, which are subsequently trapped on the particle surface where interfacial electron transfer to appropriate adsorbates can take place.

$$TiO_2 + h\nu \rightarrow h^+ + e^- \qquad (9.1)$$

Reaction of the holes with surface $OH^-$ groups or adsorbed water constitutes a major source of hydroxyl radicals,[11] with a minor contribution from the cleavage of $H_2O_2$ [7a,11,13-17,19] (formed via the superoxide radical anion [7b]) since $[H_2O_2]$ is small.[20] Both these mechanisms (i.e. •OH formation via $H_2O_2$ or via adsorbed $H_2O$ or $OH^-$) are consistent with the fact that no photodegradation of 4-chlorophenol occurs in the absence of either $O_2$ or $H_2O$ or both.[21]

The relative importance of direct oxidation of organic substrates by the photogenerated holes will depend on the magnitude of the pre-adsorption equilibria and may be insignificant for weakly adsorbed substrates.[22] A recent study[9] on 2,4,5-trichlorophenol by diffuse reflectance nanosecond flash photolysis suggests $h^+_{VB}$ oxidation of this and several other organic and inorganic substrates. Involvement of •OH radical as a redox precursor to these adsorbed oxidized species is not precluded by such observations. Hydration of surface-bound cation radicals may be slow. Formation of

hydroxylated products at intermediate stages of the oxidation is likely to occur significantly via direct •OH attack. The question of the role of $h^+_{VB}$ versus •OH in photooxidations by light-activated $TiO_2$ in aqueous media has recently been addressed.[10]

The role of electrons produced concurrently with the holes has not been established. The present view is that electrons are consumed via equation 9.2 to produce the superoxide radical anion, $O_2^{-}$•, since the degradation reaction requires oxygen,[21] and since $O_2^{-}$• radicals have been detected.[23]

$$(O_2)_{ads} + e^- \rightarrow (O_2^-\bullet)_{ads} \qquad (9.2)$$

It is not inconceivable, however, that electrons react via a parallel process with easily reduced organic substrates. Reductive dehalogenation of haloaromatics is known to occur rapidly in steady-state radiolysis.[24]

Radiolysis of water quantitatively produces either •OH or $e^-_{aq}$ in homogeneous solution and thereby affords a means of examining the reactivity of each with a specified organic substrate. Previous steady-state radiolysis studies[24, 25] have shown that •OH radicals and $e^-_{aq}$ induce the decomposition of 2-, 3-, and 4-chlorophenol: e.g., reactions of •OH and $e^-_{aq}$ with 2-chlorophenol occur with $k_{ADD} = 1.2 \times 10^{10}$ $M^{-1}s^{-1}$ and $k_r = 2.0 \times 10^8$ $M^{-1}s^{-1}$, respectively. Draper *et al*[26] found that •OH adds to 2,4,5-trichlorophenol ($k_{ADD} = 1.2 \times 10^{10}$ $M^{-1}s^{-1}$) to give the dihydroxytrichlorocyclohexadienyl species.

The main focus of the present pulse radiolysis study was to identify the products and assess the rates of reaction of •OH and the hydrated electron with a series of

pentahalophenols: pentabromophenol (PBP-OH), pentachlorophenol (PCP-OH), and pentafluorophenol (PFP-OH). The work was also aimed at establishing whether the nature of the halogen for an analogous series of haloaromatics might affect the reaction pathway, and whether addition of •OH to the aromatic ring, to give hydroxycyclohexadienyl species, is a principal reaction pathway as past evidence would suggest.[24-26] These studies were also needed to identify the primary oxidized species from surface-bound •OH radical attack on these pentahalophenols, whose photomineralization over $TiO_2$ aqueous dispersions was investigated earlier for PCP-OH[4] and recently for PFP-OH[6] to demonstrate the photooxidation process and to address the mechanistic details underlying it.

Herein, the nature, the spectroscopic properties, and the kinetics of formation and decay of radicals produced by the reaction of •OH, $N_3$•, and solvated $e^-$ with the three pentahalogenated substrates in a homogeneous phase, are reported.

## 9.2 REACTIONS OF PENTAHALOPHENOLS WITH VARIOUS RADICALS

The reactions of the pentahalophenols with a variety of radical species (•OH, $N_3$•, and $e_{(aq)}$) were monitored by observing changes in the optical density of the reaction medium. The desired radical species were generated radiolytically in solution by varying the composition of the solution and the gases used, as described earlier (see Chapter 3, Experimental).

## 9.2.1 Pentabromophenol

### 9.2.1.1 Pentabromophenoxyl Radical (PBP-O•)

The time-resolved absorption spectrum (Figure 9.1) of the product from the oxidation of PBP-O$^-$ anion by $N_3$• radicals (equation 9.3), pentabromophenoxyl radical (PBP-O•), is characterized by two bands, one at ≈ 330 nm [$\epsilon_{330}$ = (3.88 ± 0.45) x $10^3$ $M^{-1}cm^{-1}$] and the second at 470 nm [$\epsilon_{470}$ = (3.20 ± 0.35) x $10^3$ $M^{-1}cm^{-1}$], Table 9.1. The long wavelength feature is similar to the one reported for the 2,4,5-trichlorophenoxyl radical.[26]

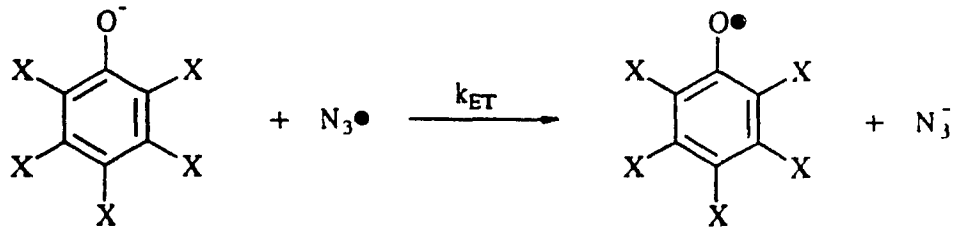


(9.3)

The oxidation (equation 9.3, X = Br) was monitored by observing the increase of the optical density at 470 nm as a function of [PBP-O$^-$] over the range from 5 x $10^{-5}$ to 2 x $10^{-4}$ M; the observed formation rate constant $k_{obs}$ ranging from 3.5 x $10^5$ to 1.3 x $10^6$ $s^{-1}$ (Appendix A and Table 9.2) gave a bimolecular rate constant $k_{ET}$ of 6.3 ± 0.9 x $10^9$ $M^{-1}s^{-1}$. The optical density at 370 nm (Figure 9.1, inset) decayed via second order kinetics: $k_d$ = 2.0 ± 0.4 x $10^9$ $M^{-1}s^{-1}$. Monitoring the increase in the optical density at 350 nm over the same [PBP-O$^-$] gave $k_{obs}$ = 3.1 x $10^5$ to 1.2 x $10^6$ $s^{-1}$, and $k_{ET}$ = 6.0 ±

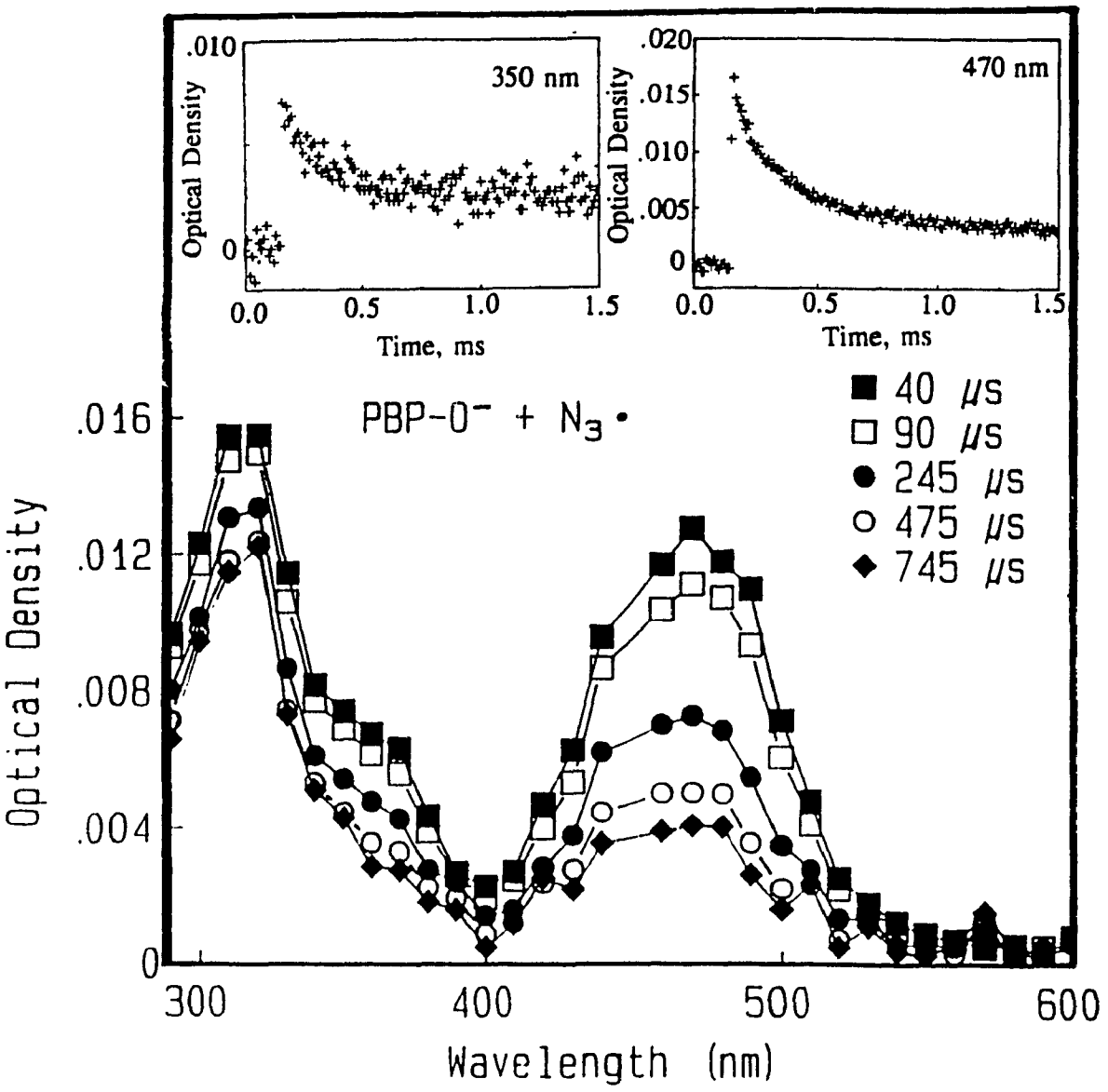


**Figure 9.1** Transient absorption spectra of PBP-O• at 40, 90, 245, 475, and 745 $\mu$s after irradiation of 2 x $10^{-4}$ M pentabromophenoxide at pH 8 (buffered) in a 0.01 M $NaN_3$ aqueous solution; the solution was $N_2O$-saturated. [•OH]= 1.97 x $10^{-6}$ M. Insets show the decays of the optical density at 350 nm and 470 nm.

**Table 9.1** Comparison of the Optical and Kinetic Properties of PXP-O• with Values Published for Similar Radicals

| Radical | $\lambda_{max}$ | $\epsilon_{max}$, $M^{-1}cm^{-1}$ | $k_f$, $M^{-1}s^{-1}$ | $k_d$, $M^{-1}s^{-1}$ | Ref |
|---|---|---|---|---|---|
| 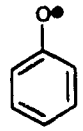 | 400 nm | $2.20 \times 10^3$ | $4.3 \times 10^9$ | - | 27<br>28 |
| 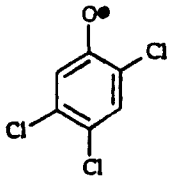 | 430 nm | $3.60 \times 10^3$ | $4.3 \times 10^9$ | $7.7 \times 10^8$ | 26 |
| 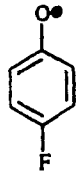 | 390 nm | $2.92 \times 10^3$ | $4.6 \times 10^9$ | - | 27 |
| 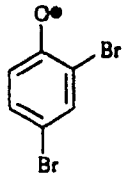 | 420 nm | $3.70 \times 10^3$ | - | $1 \times 10^8$ | 32 |
| 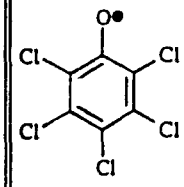 | 440 nm | $2.39 \times 10^3$ | $3.7 \times 10^9$ | $9.1 \times 10^8$ | This Work |
| 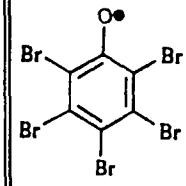 | 330 nm<br>470 nm | $3.88 \times 10^3$<br>$3.20 \times 10^3$ | $5.9 \times 10^9$ | $2.8 \times 10^9$ | This work |

**Table 9.2** Observed Kinetics of Formation and Decay of Transients in Various PBP-O$^-$ Reaction Systems.[a]

| Reaction System | Formation | | Decay | |
|---|---|---|---|---|
| | λ, nm | $k_{obs}$, $s^{-1}$ | λ, nm | $2k/\epsilon$, $s^{-1}$ |
| PBP-O$^-$ + $N_3^-$ + OH• | 470 | (3.5-12.7) x $10^5$ [b] | 470[c]<br>460[c]<br>350[c] | (1.3 ± 0.3) x $10^6$<br>(1.2 ± 0.2) x $10^6$<br>(3.7 ± 0.7) x $10^6$ |
| PBP-O$^-$ + N3• + ascorbate[d] | 390[e] | (1.0 ± 0.2) x $10^5$ | 470[f] | (1.1 ± 0.2) x $10^5$ |
| PBP-O$^-$ + OH• [g] | 460 | 1.6 x $10^6$ | 460<br>330 | (1.3 ± 0.2) x $10^6$<br>(1.4 ± 0.3) x $10^6$ |
| PBP-O$^-$ + OH• + ascorbate[h] | 380 | (6.9 ± 2.0) x $10^4$ | 460 | (5.5 ± 1.0) x $10^4$ |
| PBP-O$^-$ + $e^-_{aq}$ [i] | <br>480<br>330 | <br>4.3 x $10^5$<br>8 x $10^5$ | 715<br>460[j]<br>330[j] | 5.1 x $10^6$<br>8.6 x $10^5$<br>5.4 x $10^5$ |
| PBP-O$^-$ + $e_{aq}$ + ascorbate[k] | | | 480<br>380 | 5.5 x $10^4$<br>9 x $10^4$ |

a) General conditions: $N_2O$-saturated solutions (25 mM); pH 8 buffered with $10^{-3}$ M phosphate; [$NaN_3$] = 0.01 M; [t-BuOH]= 0.2 M. b) [PBP-O$^-$]= (5 to 20) x $10^{-5}$ M; [•OH]= 1.97 x $10^{-6}$ M. c) [PBP-O$^-$]= 2.0 x $10^{-4}$ M; [•OH]= 1.88 x $10^{-6}$ M. d) [PBP-O$^-$]= 2.0 x $10^{-4}$ M; [ascorbate]= 5 x $10^{-5}$ M. e) [•OH]= 2.85 x $10^{-6}$ M. f) [•OH]= 7.37 x $10^{-6}$ M. g) [PBP-O$^-$]= 2.0 x $10^{-4}$ M; [•OH]= 4 x $10^{-6}$ M. h) [PBP-O$^-$]= 2.0 x $10^{-4}$ M; [•OH]= 3.38 x $10^{-6}$ M; [ascorbate]= 2.65 x $10^{-5}$ M. i) [PBP-O$^-$]= 2.0 x $10^{-4}$ M; [$e^-_{aq}$]= 2.2 x $10^{-6}$ M. j) [$e^-_{aq}$]= 1.15 x $10^{-6}$ M. k) [PBP-O$^-$]= 2.0 x $10^{-4}$ M; [$e^-_{aq}$]= 2.5 x $10^{-6}$ M; [ascorbate]= 5 x $10^{-5}$ M.

0.9 x $10^9$ $M^{-1}s^{-1}$. The transient absorbing at 350 nm* also decayed via second order kinetics (Figure 9.1, inset): $k_d$ = 3.6 ± 1.0 x $10^9$ $M^{-1}s^{-1}$. The similarity of $k_d$ at 350 nm and at 470 nm confirms that both bands originate from one species. Also the bimolecular rate constants for equation 9.3 at 350 and at 470 nm are virtually identical. The kinetics of formation and decay of the PBP-O• radical correlate well with those of similar compounds (Table 9.1).[26-28] Further confirmation of the nature of the radical was obtained by generating the same species in the presence of ascorbate.

Most phenoxyl radicals rapidly oxidize the ascorbate anion with rate constants typically in the range 4 x $10^8$ to 20 x $10^8$ $M^{-1}s^{-1}$ [29] as shown in equation 9.4.

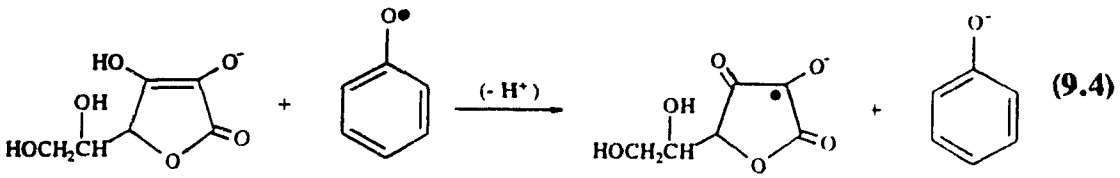


ascorbate ascorbate trioxo radical anion

(9.4)

The oxidized ascorbate trioxo radical anion ($pK_a$ = -0.4) has a characteristic absorption at $\lambda_{max}$ = 360 nm ($\epsilon_{360}$ = 3.30 x $10^3$ $M^{-1}cm^{-1}$),[29] which can be used to identify phenoxyl radicals and to selectively remove the phenoxyl radical absorption from complex spectra of product(s) mixtures (see below).**

The spectrum illustrated in Figure 9.2 was obtained under otherwise identical

---

* This wavelength (350 nm) was chosen because of minimal interference from ground state absorption of PBP-O⁻.

** Attempts to find another suitable reducing agent to react with PBP-O• in the same manner as ascorbate but which was transparent in the 360 nm region were unsuccessful: triphenylamine is not water soluble and the water soluble triethyl amine proved ineffective.

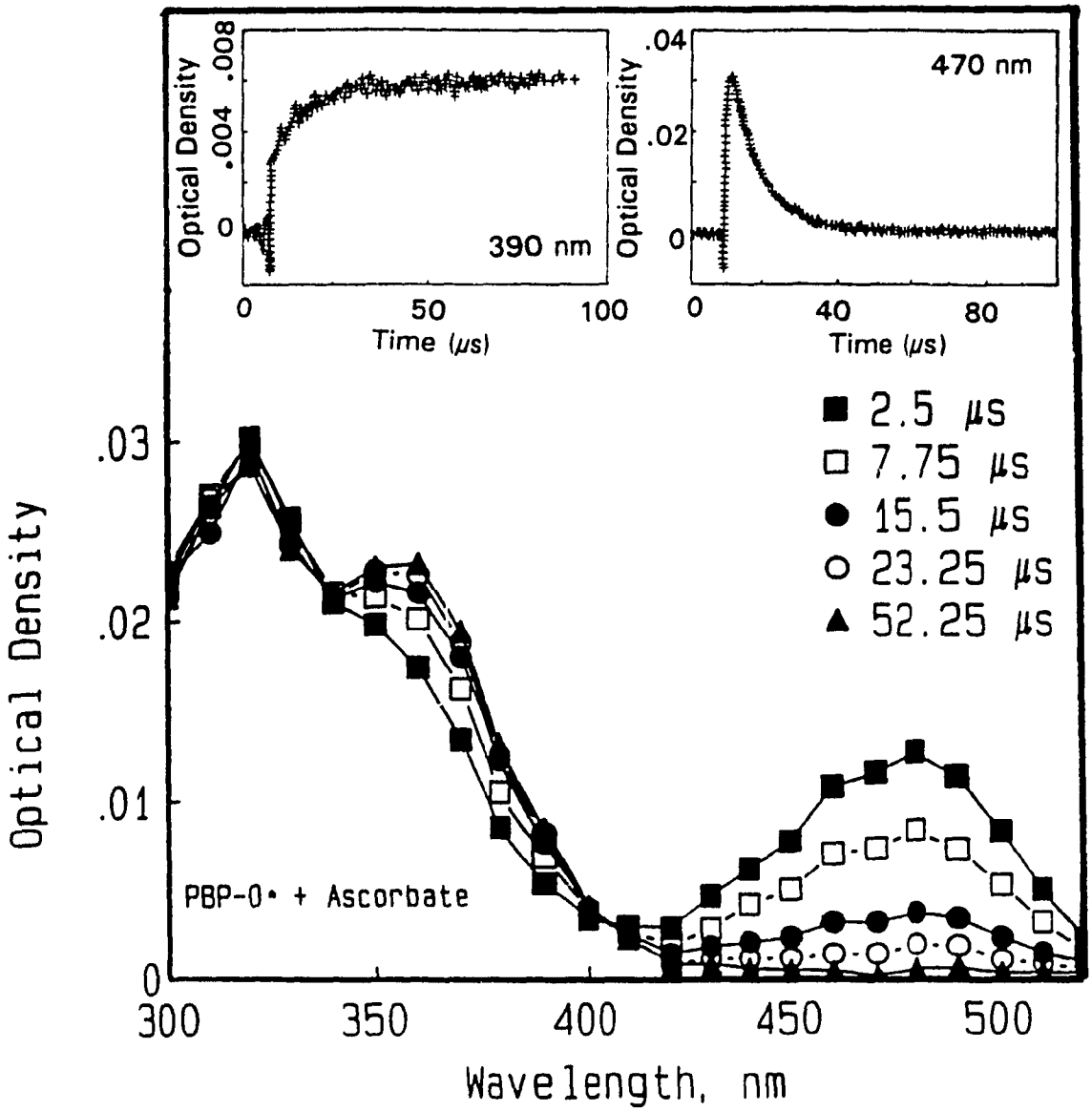


**Figure 9.2** Changes in the optical spectrum of PBP-O• in the presence of ascorbate. The spectra were recorded at 2.5, 7.75, 15.5, 23.25 and 52.25 $\mu$s following irradiation of 2 x $10^{-4}$ M pentabromophenoxide in an $N_2O$-saturated aqueous solution at pH 8 containing 0.01 M $NaN_3$ and 5 x $10^{-5}$ M ascorbate. [•OH]= 3.17 x $10^{-6}$ M. The right inset shows the decay of the 470-nm absorbance; [•OH]= 7.37 x $10^{-6}$ M. The left inset shows the growth observed at 390 nm; [•OH]= 2.85 x $10^{-6}$ M.

conditions to those used for Figure 9.1. In the presence of 5 x $10^{-5}$ M ascorbate, the absorption of PBP-O• at 470 nm decayed rapidly with a concomitant growth of a transient at 360 nm, which is attributed to the ascorbate trioxo radical anion. Isosbestic points are seen at ≈ 410 nm and at about 340 nm.

The PBP-O• absorption at 470 nm decayed via first order kinetics [$k_{obs}$ = 1.1 ± 0.2 x $10^5$ $s^{-1}$] in the presence of ascorbate, while the transient feature at 390 nm (no interference from the 330 nm band) grew in with $k_{obs}$ = 1.0 ± 0.2 x $10^5$ $s^{-1}$ (Figure 9.2 inset). The similarity of the two k values confirms the oxidation of PBP-O$^-$ by azide radicals to produce the pentabromophenoxyl radical.

### 9.2.1.2 Pentabromophenol •OH Radical Adduct

Hydroxyl radicals typically add to halogenated phenols (e.g., 2,4,5-trichlorophenol[26] and 2-chlorophenol[24]) to form dihydroxycyclohexadienyl radicals, in competition with H atom abstraction and electron transfer.[27] The absorption spectrum of the product of the reaction of •OH with PBP-O$^-$, illustrated in Figure 9.3, is characterized by a sharp band at 330 nm, a broad band at ≈ 460 nm, and a poorly resolved feature at 430 nm. The transients absorbing at 330 nm and 460 nm decayed via second order kinetics (Table 9.2): $2k/\epsilon$ = 1.4 ± 0.2 x $10^6$ and 1.3 ± 0.2 x $10^6$ $s^{-1}$, respectively, (Figure 9.3 insets). The similarity of the value of the decay constant at 460 nm to that of the second order decay constant of the PBP-O• radical [460 nm of Figure 9.1; $2k/\epsilon$ = 1.2 ± 0.2 x $10^6$ $s^{-1}$] indicates that PBP-O• is formed in the reaction of PBP-O$^-$ with •OH (equation 9.5a).

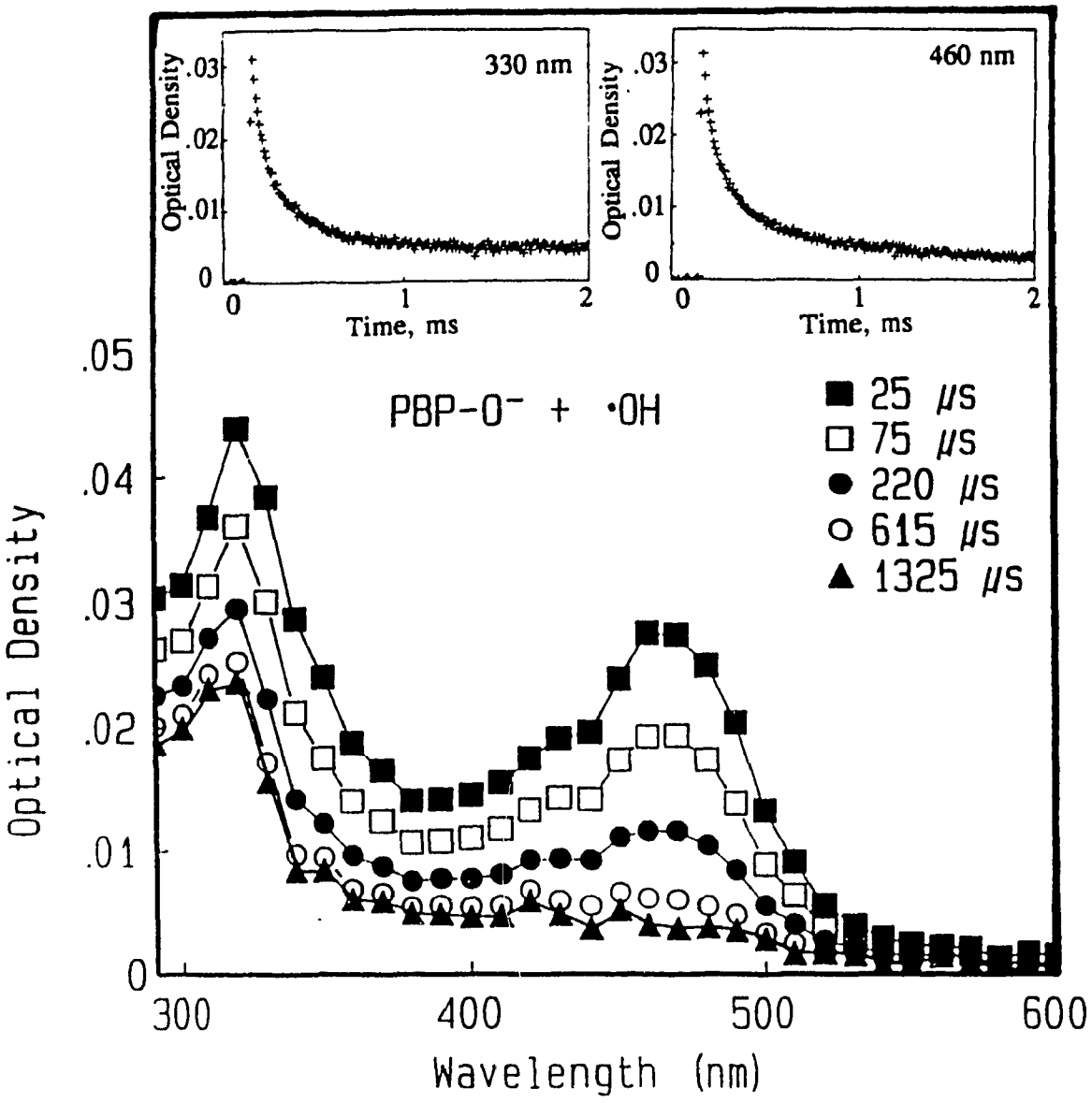


**Figure 9.3** Transient absorption spectra of the product(s) of the reaction between PBP-O$^-$ and •OH at 25, 75, 220, 615 and 1325 $\mu$s following irradiation of a $N_2O$-saturated aqueous solution of 2 x $10^{-4}$ M PBP-O$^-$ at pH 8 (buffered); [•OH] = 4 x $10^{-6}$ M. The inset shows the decay of optical density due to products of the (PBP-O$^-$ + •OH) reaction at 330 nm and at 460 nm.

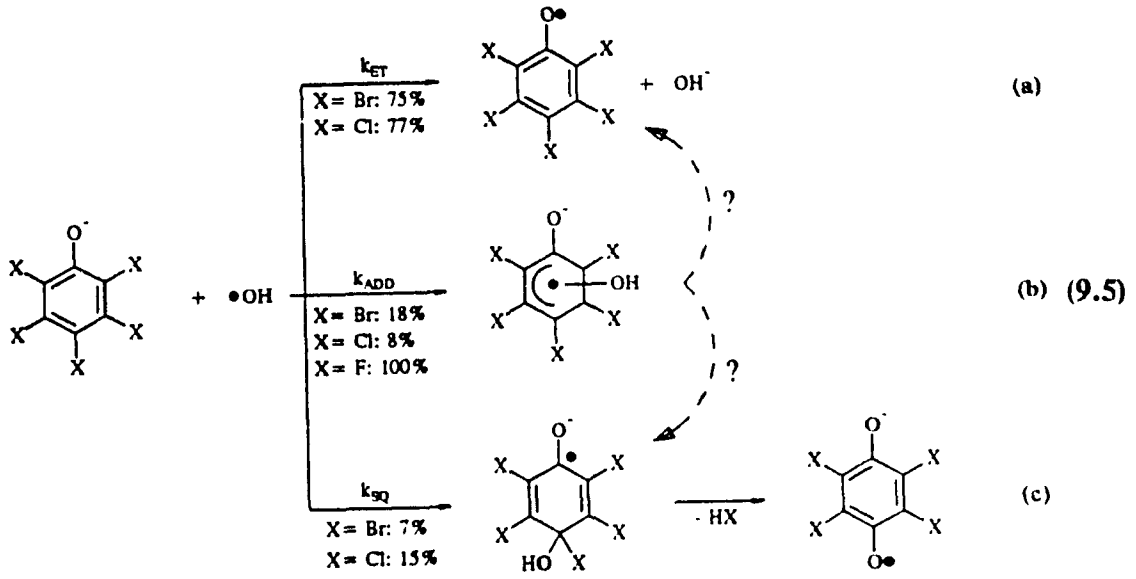


In the presence of 5 x $10^{-5}$ M ascorbate, the transient at 460 nm decayed rapidly as a new band grew in at ≈ 370 nm (Figure 9.4) via first order kinetics, $k_{obs}$ = 6.9 ± 2.0 x $10^{4}$ $s^{-1}$. This also confirms the existence of PBP-O•.

Subtraction of the contribution of the PBP-O• absorption from the (PBP-O + •OH) spectrum gives the spectrum shown in Figure 9.5. We attribute the major portion of the absorption in the difference spectrum to the •OH radical adduct of PBP-O (equation 9.5b), the dihydroxypentabromocyclohexadienyl radical anion, after noting the similarity of this spectrum with that of the •OH adduct of PFP-O (see below).# The

---

# Attempts to oxidize the •OH radical adduct to remove its spectral contribution were unsuccessful: the alkaline conditions used precluded $Fe(CN)_6^{4-}$ as a potential oxidant; $IrCl_6^{2-}$, which oxidizes the 2,4,5-trichlorophenol •OH adduct in acidic media proved ineffective. Persulfate had no noticeable effect on the absorbance decay (as noted for PBP-O• in the presence of ascorbate). This is not surprising as the oxidation of the OH adduct to yield a quinone implicates the elimination of a bromine atom and would therefore not be expected to proceed at a rapid rate.

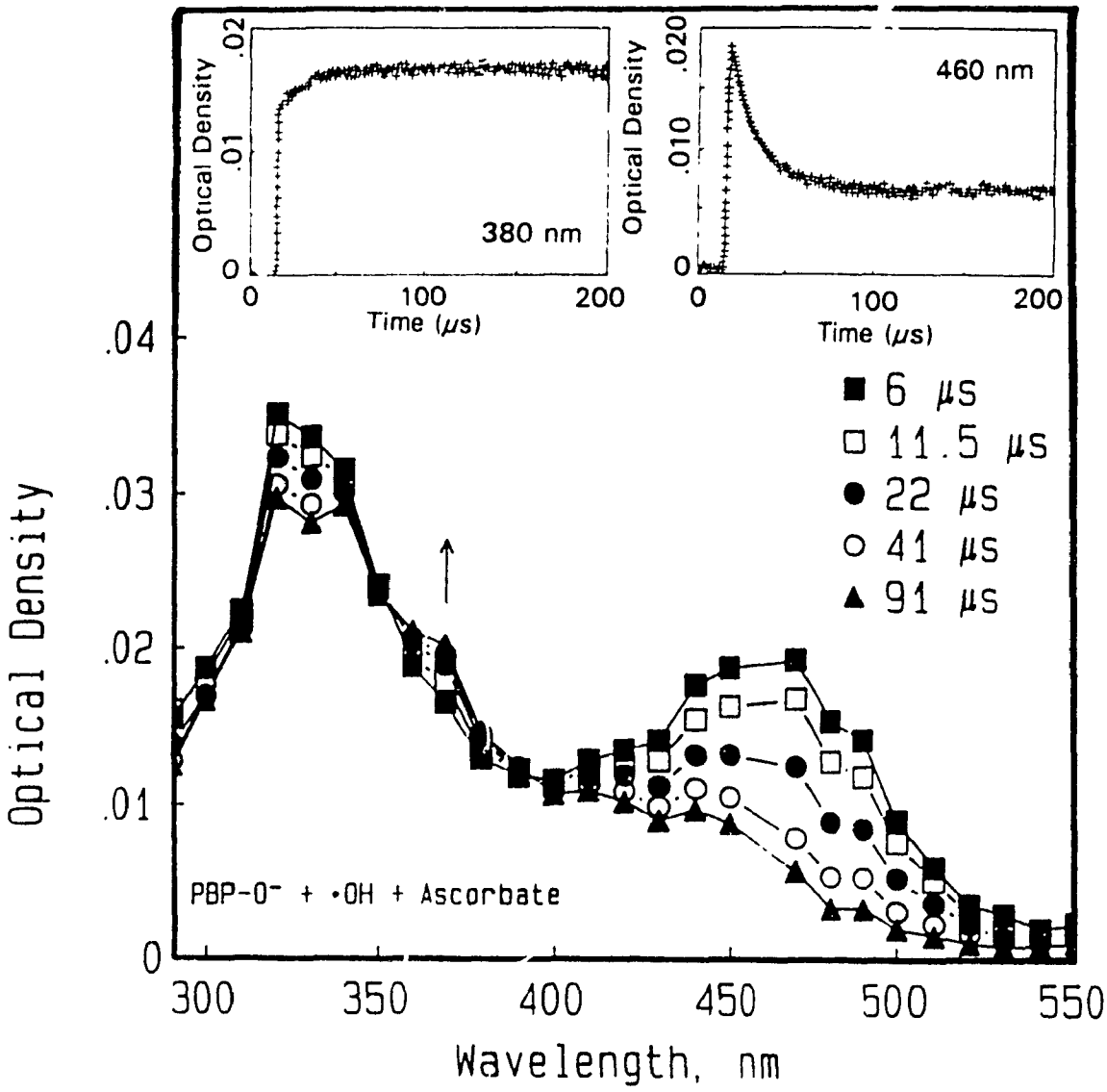


**Figure 9.4** Changes in the optical spectrum of the products of the (PBP-O$^{\cdot}$ + •OH) reaction in the presence of ascorbate. The spectra were recorded at 6, 11.5, 22, 41, and 91 $\mu$s following irradiation of a $N_2O$-saturated aqueous solution containing 2 x $10^{-4}$ M pentabromophenoxide and 5 x $10^{-5}$ M ascorbate at pH 8; [•OH]= 2.78 x $10^{-6}$ M. The left inset shows the growth observed at 380 nm; [•OH] = 3.38 x $10^{-6}$ M. The right inset shows the decay observed at 460 nm: [•OH] = 3.38 x $10^{-6}$ M.

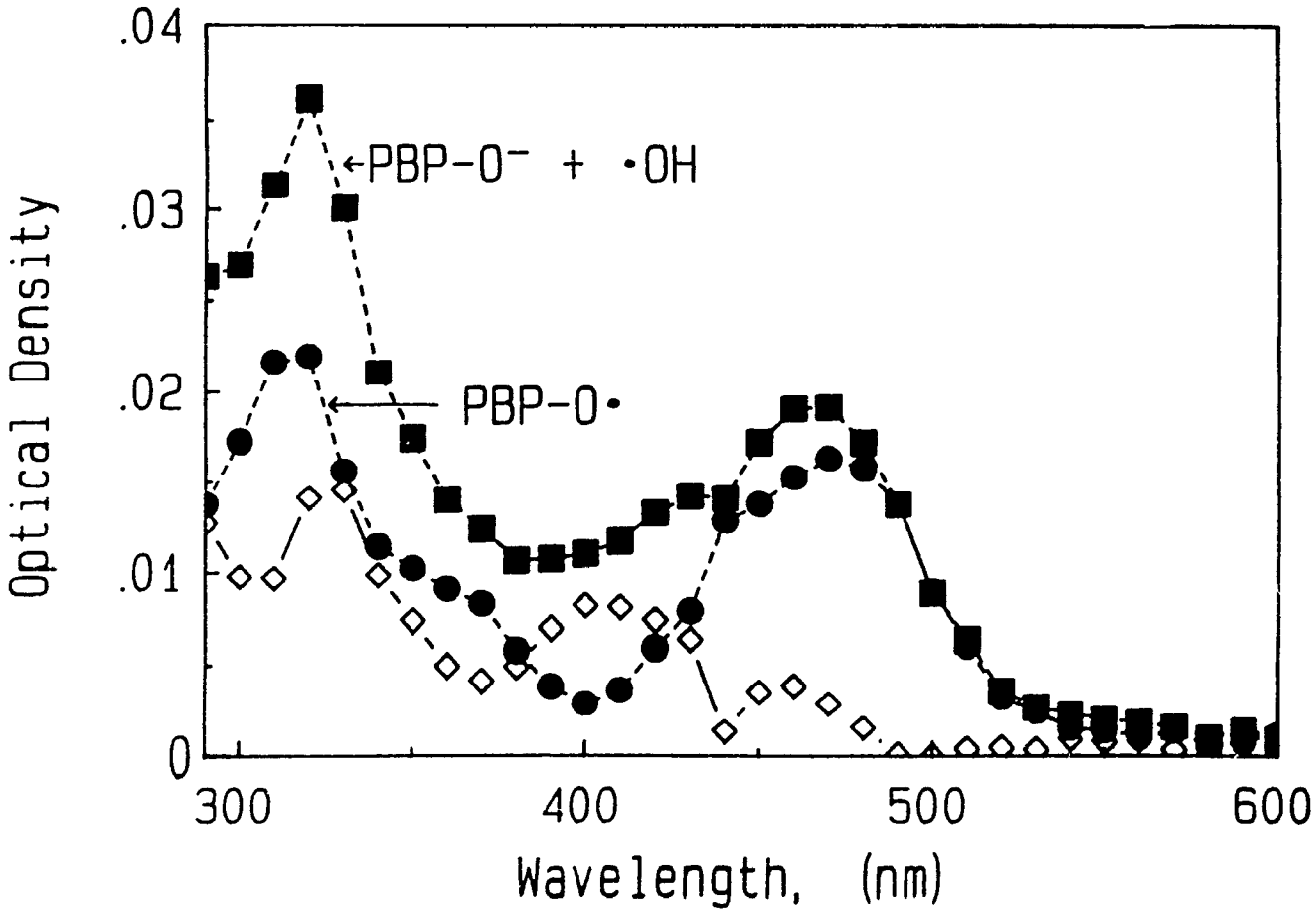


**Figure 9.5** Transient difference absorption spectrum of the dihydroxypentabromocyclohexadienyl radical HO•-PBP-O⁻ (+ other species) (◇) as calculated from the transient absorption spectrum of the products of the reaction between PBP-O⁻ solution and •OH (■) at 75 $\mu$s following irradiation of an aqueous solution 2 x $10^{-4}$ M PBP-O⁻, buffered at pH 8. The solution was $N_2O$-saturated. [•OH] = 4 x $10^{-6}$ M. (●) represents the contribution to the product spectrum of the pentabromophenoxyl radical.

overlap of the HO•-PBP-O⁻ absorption bands with those of PBP-O•, together with the possible interference from the semiquinone radical anion (another likely product, equation 9.5c), precluded an estimate of the rate of decay of the •OH adduct. However, assuming the band at 320-330 nm is due solely to the HO•-PBP-O⁻ radical, the extinction coefficient ($\epsilon_{330}$) of the OH-adduct is estimated to be $\approx 7.6 \times 10^3$ $M^{-1}cm^{-1}$ (Table 9.3). Although the error in this value may be quite large, it is of the same order of magnitude as $\epsilon_{320}$ (=5300 $M^{-1}$ $cm^{-1}$) for the dihydroxytrichlorocyclohexadienyl radical.[24,26,30]

The ratio of the absorbance of PBP-O• at 490 nm (extrapolated to time zero) to that at 470 nm, under the conditions of Figure 9.1 [$\epsilon_{470} = (3.20 \pm 0.35) \times 10^3$ $M^{-1}cm^{-1}$], gave $\epsilon_{490} = (2.86 \pm 0.60) \times 10^3$ $M^{-1}cm^{-1}$ and a [PBP-O•] of $3.0 \pm 0.7 \times 10^{-6}$ M, i.e., 75% of the total products. This parallels the findings of Schuler *et al*[31] for the reaction of p-bromophenol with •OH. Thus, 25% or the remaining ($1 \times 10^{-6}$ M) •OH radicals react with PBP-O⁻ to produce HO•-PBP-O⁻ and/or other radical species.

An •OH radical addition at the *para* position of PBP-O⁻ would yield the tetrabromo-*p*-semiquinone anion radical (bromanil radical anion) which, by comparison with the chloranil analogue (see below and equation 9.5c, X = Br), absorbs around 450 nm. Semiquinone radicals and semiquinone anion radicals typically have high extinction coefficients: for example, for the p-benzosemiquinone anion radical, $\epsilon_{425} = 7.30 \times 10^3$ $M^{-1}cm^{-1}$; for the chloranil radical, $\epsilon_{448} = 6.00 \times 10^3$ $M^{-1}cm^{-1}$.[32] Semiquinone radicals have pK values in the range 3-6;[32] therefore the anion radical should form under our reaction conditions (pH 8 buffer). If we take the extinction coefficient at 450 nm to be $\epsilon_{450} \approx 6.00 \times 10^3$ $M^{-1}cm^{-1}$ (as in the protonated form of chloranil[32]), the amount of

**Table 9.3** Comparison of the Optical and Kinetic Properties of HO•-PXP-O⁻ with Values Published for Similar Radicals

| Radical | $\lambda_{max}$, nm | $\epsilon_{max}$, $M^{-1}cm^{-1}$ | $k_f$, $M^{-1}s^{-1}$ | $k_d$, $M^{-1}s^{-1}$ | Ref. |
|---|---|---|---|---|---|
| 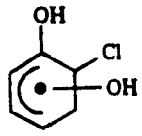 | 300 | - | $1.2 \times 10^{10}$ | - | 24 |
| 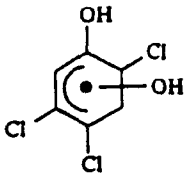 | 320 | $5.30 \times 10^3$ | $1.2 \times 10^{10}$ | $5.6 \times 10^8$ | 26 |
| 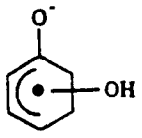 | - | - | $9.6 \times 10^9$ | - | 30 |
| 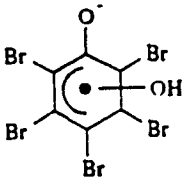 | 330 | $7.61 \times 10^3$ | $1.4 \times 10^9$ | - | This Work |
| 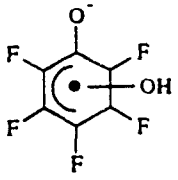 | 300<br>430 | $3.56 \times 10^3$<br>$1.69 \times 10^3$ | $4.6 \times 10^9$ | $5.4 \times 10^4$ | This Work |
| 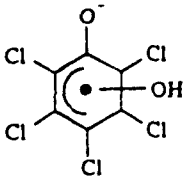 | $\leq$ 320 | $(2.45 \times 10^4)$? | $3.8 \times 10^8$ | - | This work |

semiquinone formed is estimated at $\approx$ 3.0 x $10^{-7}$ M, or $\approx$ 7% of the total quantity of radicals formed. The second major product ($\approx$ 18%) of the reaction of PBP-O$^-$ with •OH radicals is attributed to the adduct, dihydroxypentabromocyclohexadienyl (HO•-PBP-O$^-$) radical.

The values of $k_{ET}$, $k_{Add}$, and $k_{SQ}$(bromanil) of equations 9.5 (X = Br) were determined from $k_{obs}$ = 1.6 x $10^6$ $s^{-1}$ and from the product ratio: $k_{ET}$ = 5.9 x $10^9$ $M^{-1}s^{-1}$, $k_{Add}$ = 1.4 x $10^9$ $M^{-1}s^{-1}$, and $k_{SQ}$(bromanil) = 5.8 x $10^8$ $M^{-1}s^{-1}$.

Phenoxyl radicals are probably formed via elimination of $H_2O$ (or $OH^-$ for the PXP-O species) following •OH addition, rather than by direct (outer sphere) electron transfer owing to a possible unfavourable reorganization energy for the •OH/$OH^-$ transformation. These results are silent on the details, but interestingly the amount of PBP-O• expected via $OH^-$ loss is about 40% contrary to the observed 75% of the product mixture. Additional electron transfer via an inner sphere transition state, different from the OH-adduct, cannot be precluded. It is therefore inferred that •OH radicals react with PBP-O as shown in equations 9.5 (X = Br).

### 9.2.1.3 Dehalogenation to Phenyl Radical via Electron Attachment

The transient absorption spectrum of the product(s) arising from the reaction between PBP-O and $e_{aq}$, illustrated in Figure 9.6, shows two bands one at $\approx$ 330 nm and one at $\approx$ 470 nm. These transient absorptions decayed concurrently via second order kinetics: $2k/\epsilon$ = 5.4 x $10^5$ $s^{-1}$ (330 nm) and 8.6 x $10^5$ $s^{-1}$ (460 nm), Figure 9.6 inset. Phenoxide ions react with electrons to give the corresponding electron adduct which loses

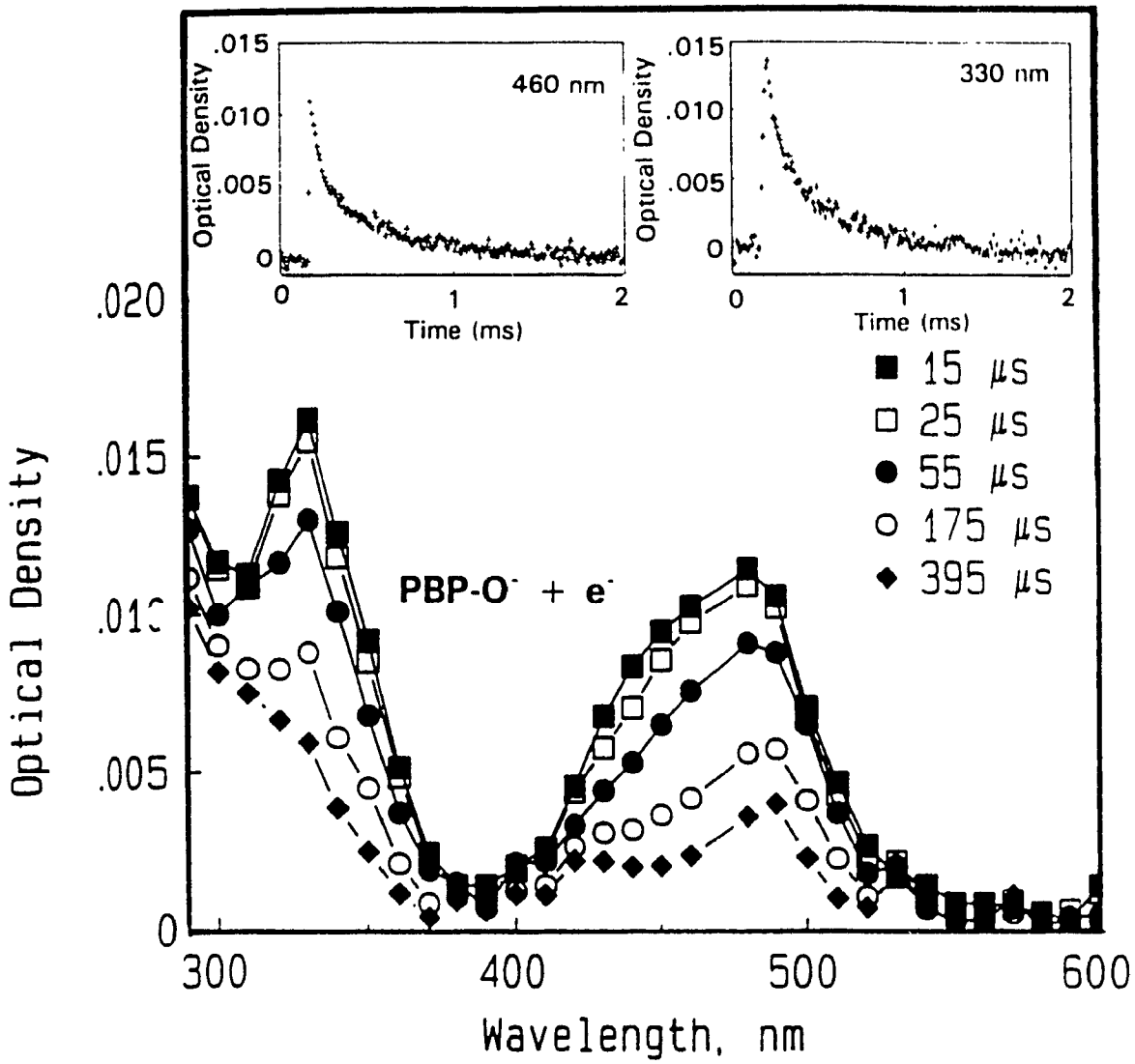


**Figure 9.6** Transient absorption spectra of tetrabromophenoxyl radical(s) resulting from the reaction of PBP-OH with $e^-$ at 15, 25, 55, 175 and 395 $\mu$s following irradiation of a 2 x $10^{-4}$ M PBP-OH and 0.2 M t-BuOH aqueous $N_2$-saturated solution at pH 8; [e] = 1.15 x $10^{-6}$ M. The left inset shows the decay at 330 nm and the right inset shows the decay at 460 nm.

halogen to produce isomeric hydroxyphenyl radicals (equation 9.6).[24,31,33] Their bimolecular rate of formation ($k_e$ = 2.6 x $10^{10}$ $M^{-1}s^{-1}$) was monitored by observing the decay of the transient absorption of the hydrated electron ($e^-_{aq}$) at 715 nm. The rate constant, $k_e$ was one to two orders of magnitude greater than the values noted for the reactions of the 2-bromophenoxide and 4-chlorophenoxide anions with the hydrated electron (Table 9.4).[31,33]

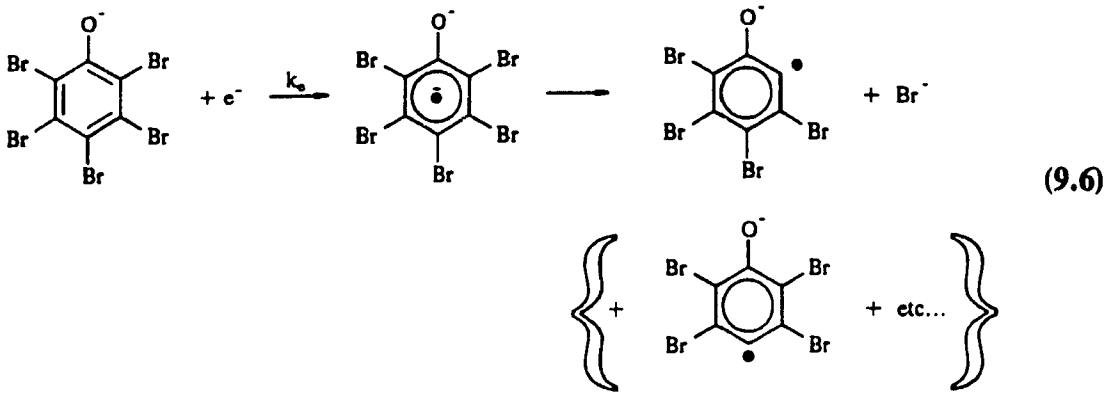


**(9.6)**

The growth rates of the transients at 330 nm and 480 nm, monitored at a fixed dose, $[e^-_{aq}]$ = 2.2 x $10^{-6}$ M (other conditions as in Figure 9.6), were slower than the decay rate at 715 nm: $k_{obs}$ = 8 x $10^5$ $s^{-1}$ (330 nm), 4.3 x $10^5$ $s^{-1}$ (480 nm), and 5.1 x $10^6$ $s^{-1}$ (715 nm). This order of magnitude difference in rate constants indicates that the spectrum of Figure 9.6 is that of secondary products resulting from the electron adduct (equation 9.6). No spectral evidence of the direct $e^-$-adduct was seen even at time delays (4 $\mu$s) shorter than those noted in Figure 9.6, possibly due to rapid protonation to produce isomeric tetrabromophenoxyl radicals (equation 9.7). This finds a parallel with the mechanism of the reaction between p-bromophenol and the electron.[31]

**Table 9.4** Comparison of the Rate of Reaction of PBP-O$^{\cdot}$ with $e^-_{aq}$ with Published Values for Similar Compounds

| Compound | k, $M^{-1}s^{-1}$ | Ref. |
|---|---|---|
| 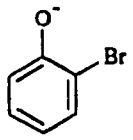 | $2.3 \times 10^9$ | 31 |
| 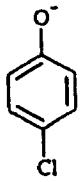 | $6.4 \times 10^8$ | 33 |
| 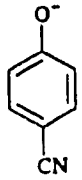 | $2 \times 10^9$ | 33 |
| 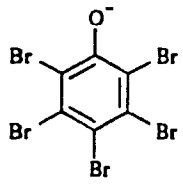 | $2.6 \times 10^{10}$ | This work |

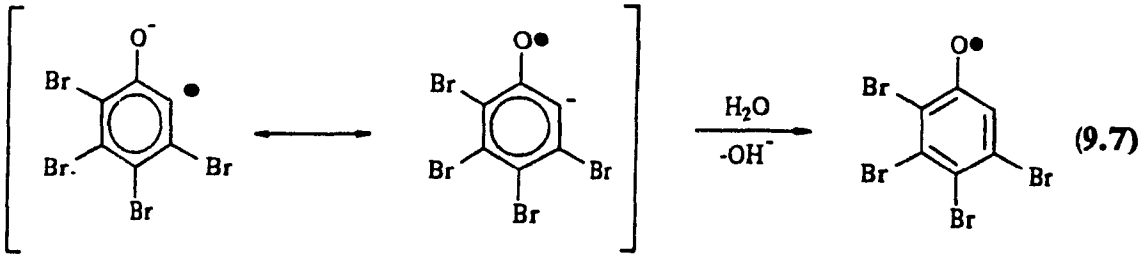


(9.7)

The formation of phenoxyl radicals was confirmed by carrying out the same reaction in the presence of ascorbate. The absorption band at ≈ 460 nm decayed rapidly and was accompanied by the transient growth at 360 nm (which was attributed to the ascorbate trioxo radical anion), with two isosbestic points at ≈ 400 nm and at ≈ 350 nm (Figure 9.7). The transient monitored at 480 nm decayed via first order kinetics, $k_{obs}$ = 5.5 x $10^4$ $s^{-1}$, while the transient at 380 nm grew in (minimal interference from the 330 nm band) with $k_{obs}$ = 9 x $10^4$ $s^{-1}$ (Figure 9.7 insets).

## 9.2.2 Pentachlorophenol

### 9.2.2.1 Pentachlorophenoxyl Radicals (PCP-O•)

The oxidation of the PCP-O⁻ anion by $N_3$• yields the pentachlorophenoxyl radical (PCP-O•; equation 9.3 for X = Cl) which is characterized by an absorption spectrum with a band at 440 nm and a weaker feature at wavelengths ≤ 320 nm (Figure 9.8). A band at ≈ 440 nm was also observed for the 2,4,5-trichlorophenoxyl radical produced from the reaction of 2,4,5-trichlorophenol with $N_3$•.[26] The rate of growth of the transient at 440 nm was $k_{f'}$ = (3.4 ± 0.6) x $10^9$ $M^{-1}s^{-1}$. The transient decayed via second order kinetics with $k_d$ = (9.1 ± 1.8) x $10^8$ $M^{-1}s^{-1}$. These constants correlate with literature values (Table 9.1) for other similar species.

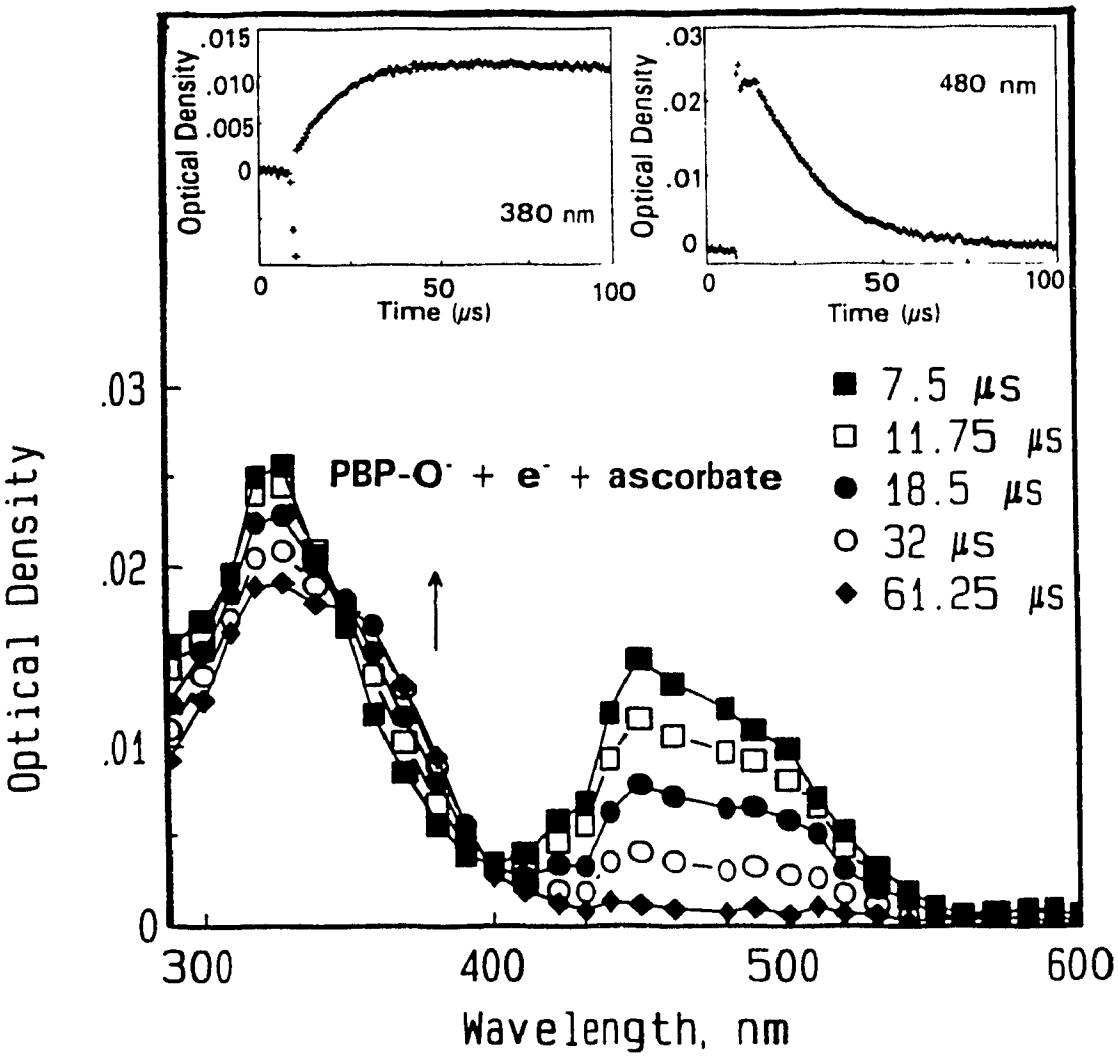


**Figure 9.7** Changes in the optical spectrum of tetrabromophenoxyl radical(s) resulting from the reaction of PBP-OH with $e^-$ following the addition of ascorbate. The spectra were recorded at 7.5, 11.75, 18.5, 32 and 61.25 $\mu$s after the pulse following irradiation of a 2 x $10^{-4}$ M PBP-OH, 0.2 M t-BuOH, and 2.5 x $10^{-5}$ M ascorbate aqueous $N_2$-saturated solution at pH 8; $[e^-]$ = 2 x $10^{-6}$ M. The left inset shows the growth at 380 nm, $[e^-]$ = 2.6 x $10^{-6}$ M; the right inset shows the decay at 480 nm, [e] = 2.5 x $10^{-6}$ M.

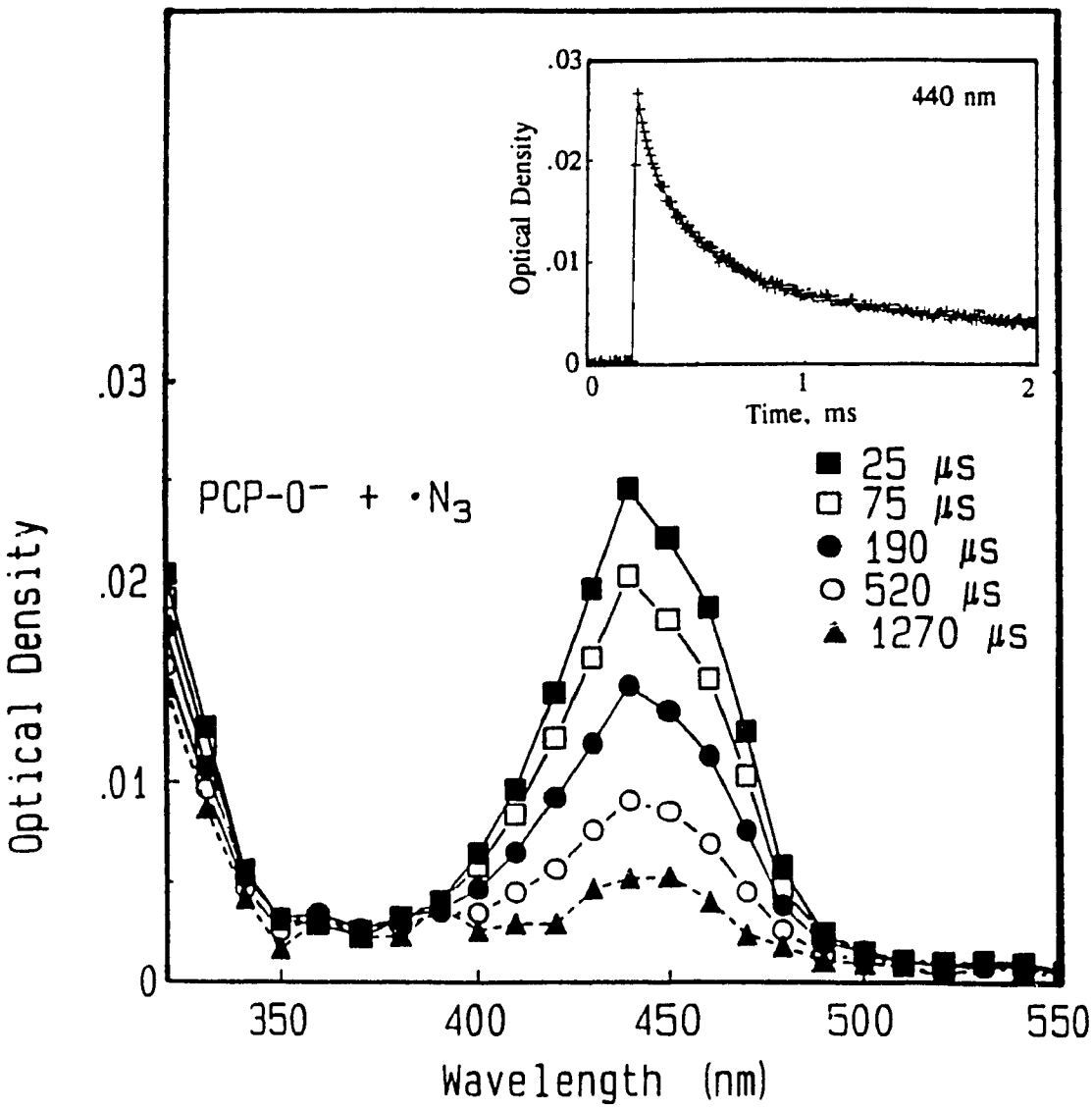


**Figure 9.8** Transient absorption spectra of PCP-O• at 25, 75, 190, 520, and 1270 μs after irradiation of 2.5 x $10^{-4}$ M pentachlorophenoxide at pH 8 (buffered) in a 0.01 M $NaN_3$ aqueous solution; the solution was $N_2O$-saturated. [•OH] = 2.95 x $10^{-6}$ M. Inset shows the decays of the optical density at 440 nm.

In the presence of ascorbate (Figure 9.9), the first order decay of the 440 nm transient was accompanied by a concomitant first order absorption growth of the ascorbate trioxo radical anion at ≈ 360 nm (isosbestic point at ≈ 400 nm): $k_{obs}$ = (7.4 ± 1.6) x $10^4$ $s^{-1}$ (440 nm), (7.4 ± 1.5) x $10^4$ $s^{-1}$ (360 nm). The relevant kinetic data are summarized in Table 9.5.

### 9.2.2.2 PENTACHLOROPHENOL •OH RADICAL ADDUCT

The absorption spectrum of the product(s) of the reaction between •OH and the pentachlorophenoxide anion is depicted in Figure 9.10. It is characterized by a band at ≈ 320 nm and broad, ill-defined bands at ≈ 380-450 nm. The transient, monitored at 340 and 450 nm (Figure 9.10 insets), decayed via second order kinetics in both cases (see Table 9.5). In the presence of 2.5 x $10^{-5}$ M ascorbate (Figure 9.11), an isosbestic point was seen at ≈ 390 nm with a rapid first order decay of the 450 nm band, $k_{obs}$ = (2.1 ± 0.6) x $10^4$ $s^{-1}$, being accompanied by a coincident absorption growth of the ascorbate trioxo radical anion at 360 nm, $k_{obs}$ = (3.0 ± 0.9) x $10^4$ $s^{-1}$. This suggests the formation of the pentachlorophenoxyl radical, PCP-O• (equation 9.5b for X = Cl). Unlike the case of PBP-O•, the band at 450 nm is not due to the PCP-O• radical alone. The ≈ 450 nm absorbance was only partially influenced by ascorbate, such that PCP-O• decayed rapidly in the presence of ascorbate while the other radicals appeared unaffected by its presence, even at higher ascorbate concentration (5 x $10^{-5}$ M). If the 450 nm band were entirely due to PCP-O•, an estimate of the quantity of this radical, on the basis of the product(s) absorbance, would give the unlikely possibility that [PCP-O•] > [•OH].

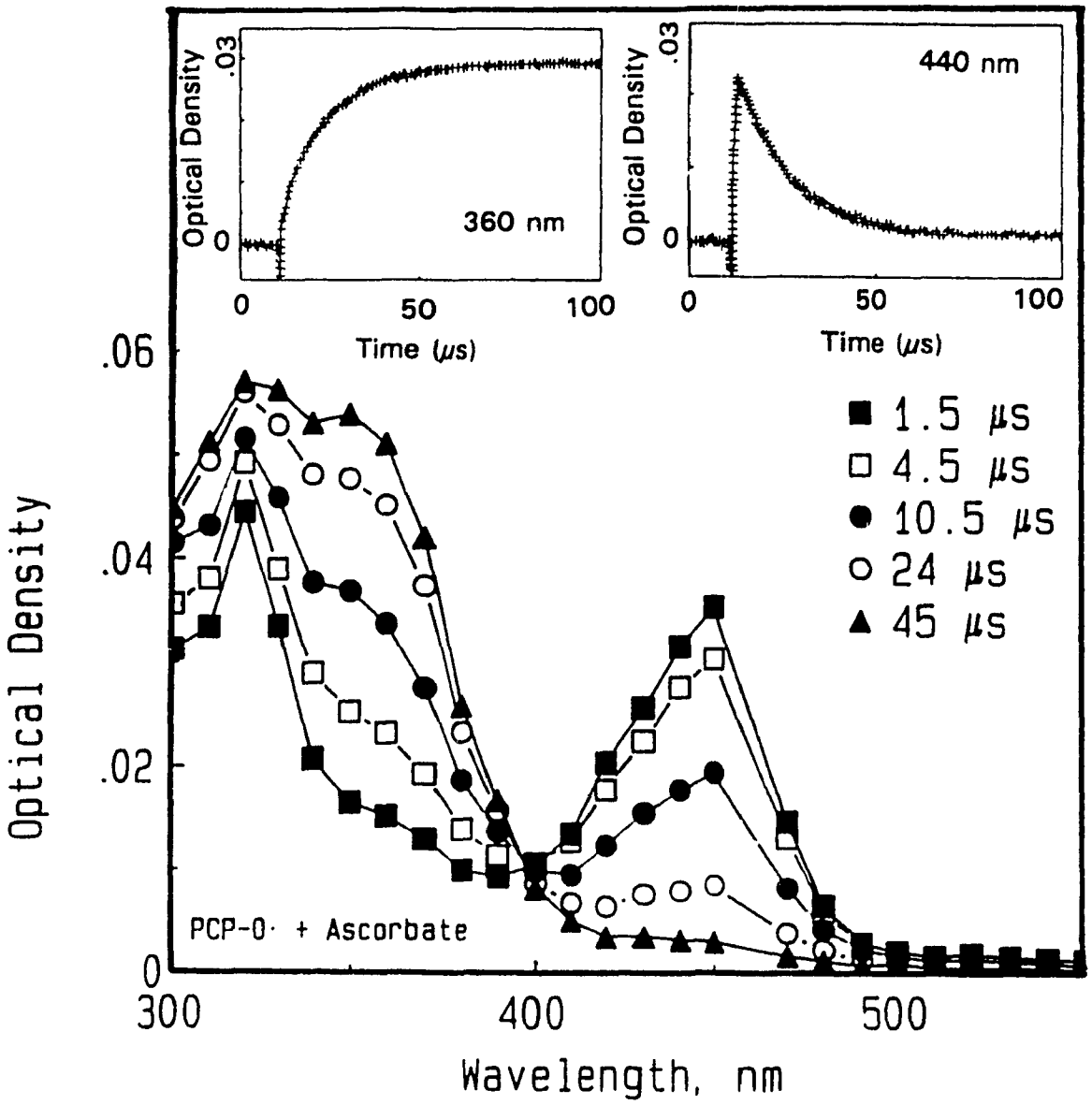


**Figure 9.9** Changes in the optical spectrum of PCP-O• in the presence of ascorbate. The spectra were recorded at 1.5, 4.5, 10.5, 25, and 45 $\mu$s following irradiation of 2.5 x $10^{-4}$ M pentachlorophenoxide in a $N_2O$-saturated aqueous solution at pH 8 containing 0.01 M $NaN_3$ and 5 x $10^{-5}$ M ascorbate. [•OH]= 5.76 x $10^{-6}$ M. The right inset shows the decay of the 440 nm absorbance of PCP-O• in the presence of ascorbate, [•OH]= 3.41 x $10^{-6}$ M. The left inset shows the growth of the 360 nm absorbance, [•OH]= 3.21 x $10^{-6}$ M.

**Table 9.5** Observed Kinetics of Formation and Decay of Transients in Various PCP-O$^-$ Reaction Systems.[a]

| Reaction System | Formation | | Decay | |
|---|---|---|---|---|
| | λ, nm | $k_{obs}$, $s^{-1}$ | λ, nm | $2k/\epsilon$, $s^{-1}$ |
| PCP-O$^-$ + $N_3^-$ + OH• [b] | 440[c] | (6.1-83) x $10^4$ | 440 | (7.6 ± 1.6) x $10^5$ |
| PCP-O$^-$ + $N_3$• + ascorbate[d] | 360 | (7.4 ± 1.5) x $10^4$ | 440[e] | (7.4 ± 1.6) x $10^4$ |
| PCP-O$^-$ + OH• [f] | | | 450<br>340 | (6.5 ± 1.0) x $10^5$<br>(3.0 ± 0.6) x $10^5$ |
| PCP-O$^-$ + OH• + ascorbate[g] | 360 | (3.0 ± 0.9) x $10^4$ | 450 | (2.1 ± 0.6) x $10^4$ |

a) General conditions: $N_2O$-saturated solutions (25 mM); pH 8 buffered with $10^{-3}$ M phosphate; [$NaN_3$]= 0.01 M; [t-BuOH]= 0.2 M.
b) [PCP-O$^-$]= 2.5 x $10^{-4}$ M; [•OH]= 2.95 x $10^{-6}$ M.
c) [PCP-O$^-$]= (1.3 to 25) x $10^{-4}$ M; [•OH]= 1.14 x $10^{-6}$ M.
d) [PCP-O$^-$]= 2.5 x $10^{-4}$ M; [•OH]= 3.21 x $10^{-6}$ M; [ascorbate]= 5 x $10^{-5}$ M.
e) [•OH]= 3.41 x $10^{-6}$ M.
f) [PCP-O$^-$]= 2.5 x $10^{-4}$ M; [•OH]= 5.1 x $10^{-6}$ M.
g) [PCP-O$^-$]= 2.5 x $10^{-4}$ M; [•OH]= 2.91 x $10^{-6}$ M; [ascorbate]= 2.5 x $10^{-5}$ M.

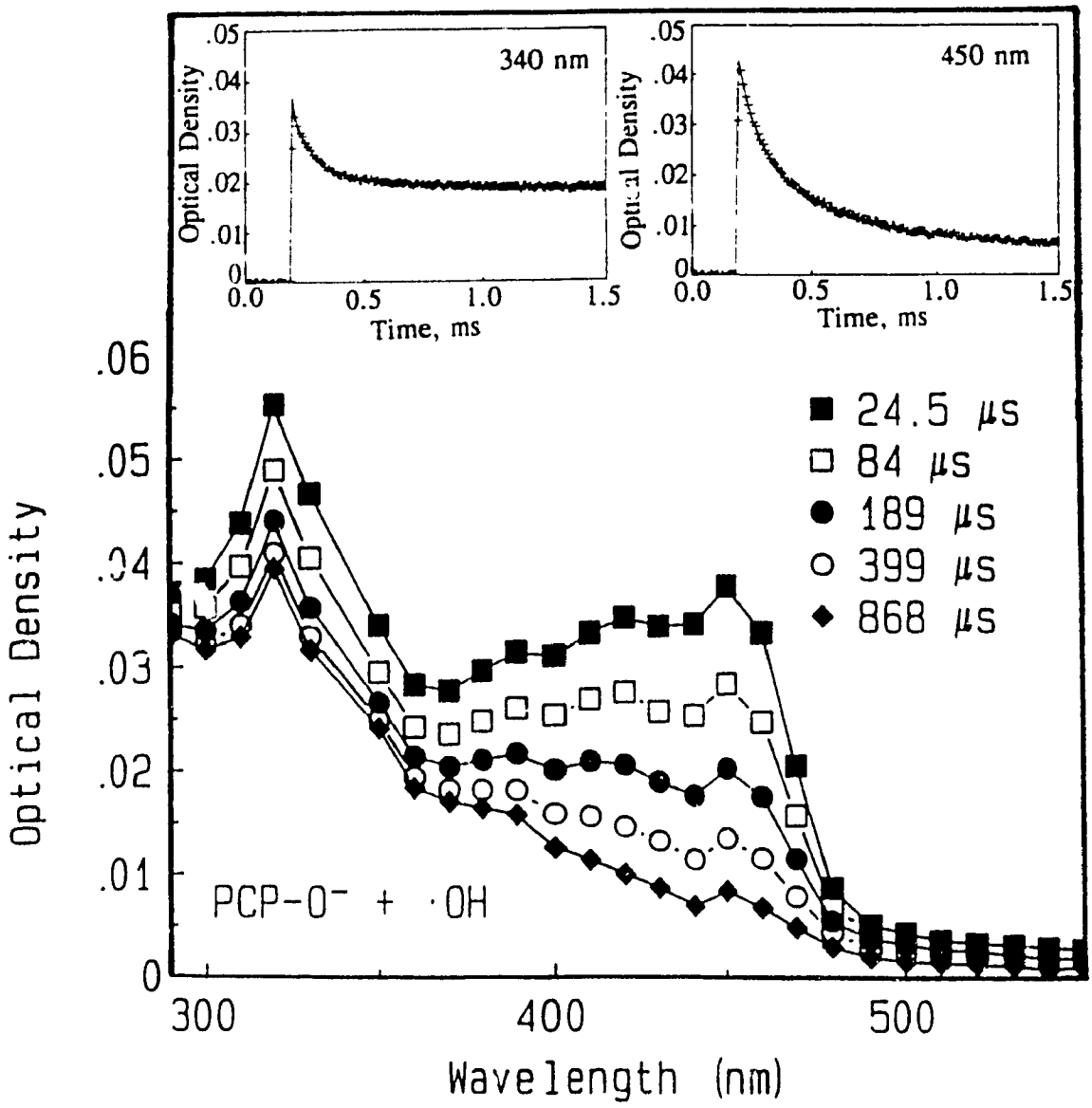


**Figure 9.10** Transie: .bsorption spectra of the product(s) of the reaction between PCP-O and •OH at 24.5, 84, 189, 399 and 868 μs following irradiation of an aqueous 2.5 x $10^{-4}$ M PCP-O. $N_2O$-saturated aqueous solution buffered at pH 8; [•OH]= 5.1 x $10^{-6}$ M. The insets show the decays of the optical density at 340 nm and 450 nm.

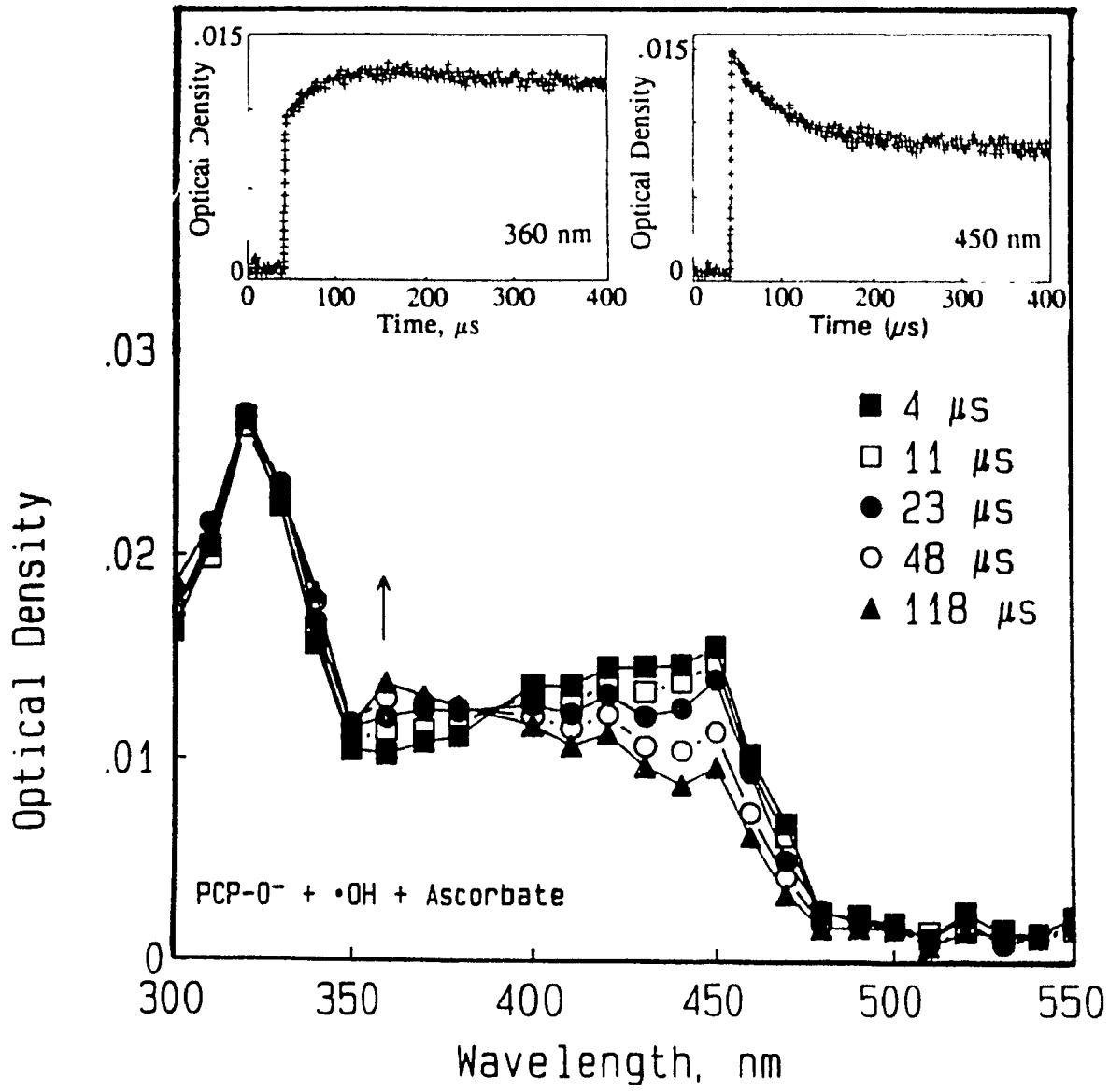


**Figure 9.11** Changes in the optical spectrum of the products of the (PCP-O + •OH) reaction in the presence of ascorbate. The spectra were recorded at 4, 11, 23, 48, and 118 $\mu$s following irradiation of a $N_2O$-saturated aqueous solution containing 2.5 x $10^{-4}$ M pentachlorophenoxide and 2.5 x $10^{-5}$ M ascorbate at pH 8; [•OH]= 4.78 x $10^{-6}$ M. The left inset shows the growth observed at 360 nm; [•OH] = 4.38 x $10^{-6}$ M. The right inset shows the decay observed at 450 nm; [•OH] = 3.38 x $10^{-6}$ M.

Thus, the reaction between PCP-O$^-$ and •OH likely yields PCP-O• as the major product, and some of the adduct HO•-PCP-O$^-$, in keeping with the results from PBP-O$^-$.

Figure 9.12 shows the (PCP-O$^-$ + •OH) total product(s) absorption spectrum, the spectrum of PCP-O•, and the difference spectrum which we assign to the •OH adduct and/or the semiquinone radical. When [•OH] is 5.2 x $10^{-6}$ M, [PCP-O•] is 3.98 x $10^{-6}$ M, or $\approx$ 77% of the products.## Comparison of the spectrum of the adduct HO•-PFP-O$^-$ (Figure 9.13) with the difference spectrum of Figure 9.12 suggests that an additional radical must be present, probably the tetrachloro-*p*-semiquinone radical anion (chloranil radical anion), equation 9.5c for X = Cl. The protonated form of the chloranil radical has an absorption band at $\lambda$ = 448 nm and $\epsilon_{448}$ = 6.00 x $10^3$ $M^{-1}cm^{-1}$;[32] the deprotonated form should absorb at longer wavelengths. Consequently, we assign the band (in the difference spectrum) at 450-460 nm to this species.[32] If we take this $\epsilon$ under the conditions of Figure 9.10, we estimate the quantity of the chloranil radical anion produced to be $\approx$ 8.1 x $10^{-7}$ M, or $\approx$ 15% of the product mixture, while [HO•-PCP-O$^-$] $\approx$ 4.1 x $10^{-7}$ M, or $\approx$ 8% of the total products (equation 9.5). In keeping with the remarks on HO•-PBP-O species, the band at $\approx$ 320 nm of the difference spectrum (Figure 9.12) is tentatively ascribed to the •OH adduct of PCP-O$^-$.

The above considerations permit an estimation of the constants $k_{ET}$, $k_{Add}$, and $k_{SQ}$ (equation 9.5) from $k_{obs}$ = 1.2 x $10^6$ $s^{-1}$ for the reaction between PCP-O$^-$ and •OH radical, and from the products ratio. Thus, $k_{ET}$ = 3.7 x $10^9$ $M^{-1}s^{-1}$, $k_{Add}$ = 3.8 x $10^8$ $M^{-1}s^{-1}$, and $k_{SQ}$ = 7.1 x $10^8$ $M^{-1}s^{-1}$.

---

## The calculations were based on the assumption that the absorbance at 500 nm was entirely due to PCP-O•.

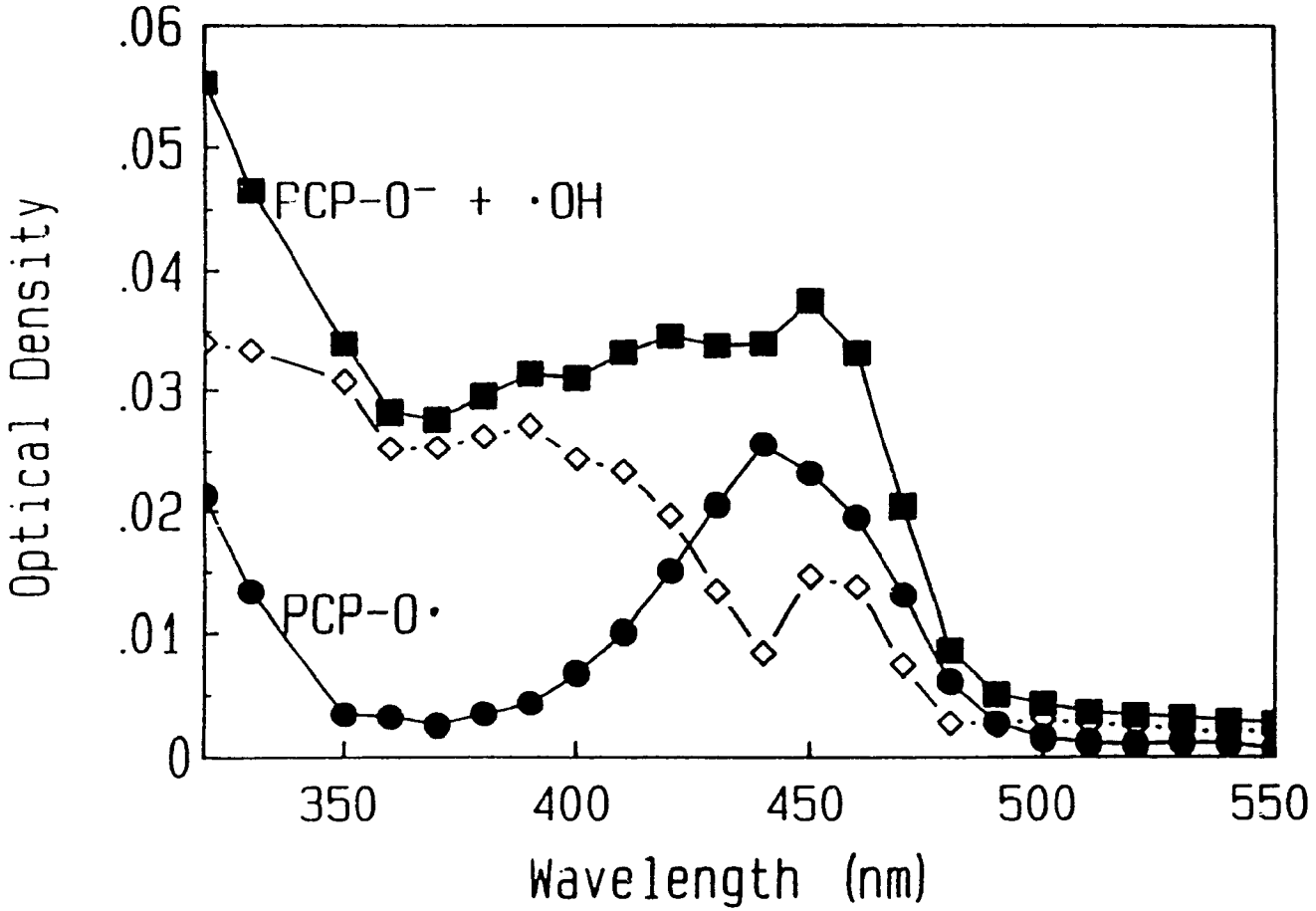


**Figure 9.12** Transient absorption spectrum of the products of the ($PCP\text{-}O^{\cdot}$ + •OH) reaction corrected (◇) for the absorbance due to PCP-O• based on the transient absorption spectrum of the total products of the reaction between $PCP\text{-}O^{\cdot}$ and •OH (■) at 24.5 $\mu$s following irradiation of an aqueous solution $2.5 \times 10^{-4}$ M $PCP\text{-}O^{\cdot}$ buffered at pH 8. The solution was saturated with $N_2O$. [•OH]= $5.2 \times 10^{-6}$ M. (●) represents the contribution of the pentachlorophenoxyl radical to the product spectrum.

## 9.2.3 Pentafluorophenol

### 9.2.3.1 Pentafluorophenol OH Adduct (HO•-PFP-O⁻)

Radiolysis of an aqueous solution of the pentafluorophenoxide anion, PFP-O⁻, yields the dihydroxypentafluorocyclohexadienyl radical (HO•-PFP-O⁻); equation 9.5b for X = F) whose absorption spectrum (Figure 9.13) shows bands at 300 and 430 nm. The bimolecular rate of •OH addition to PFP-O⁻ measured at 300 nm is $k_{ADD}$ = (4.4 ± 0.8) x $10^9$ $M^{-1}s^{-1}$, while at 430 nm $k_{ADD}$ = (4.8 ± 0.9) x $10^9$ $M^{-1}s^{-1}$. Absorption decay at both wavelengths occurred via second order kinetics (Figure 9.13 insets, and Table 9.6) with decay constants for HO•-PFP-O⁻ of 5.0 ± 1.0 x $10^8$ $M^{-1}s^{-1}$ (300 nm) and 5.9 ± 1.2 x $10^8$ $M^{-1}s^{-1}$ (430 nm). The similarity of these two values confirms that both bands originate from one species.

The values of the rate constants for both formation and decay of the species assigned as HO•-PFP-O⁻ are fairly typical of •OH adducts of halogenated phenols (e.g., for 2,4,5-trichlorophenol, $k_{ADD}$ = 1.2 x $10^{10}$ $M^{-1}s^{-1}$ and $k_d$ = 5.6 x $10^8$ $M^{-1}s^{-1}$;[26] for 2-chlorophenol, $k_{ADD}$ = 1.2 x $10^{10}$ $M^{-1}s^{-1}$ [24]; Table 9.3).

To verify that HO•-PFP-O⁻ was the only reaction product and that no pentafluorophenoxyl radicals (PFP-O•) formed, as was the case for PBP-O⁻ and PCP-O⁻, the reaction was carried out in the presence of 6.3 x $10^{-5}$ M ascorbate for 6 x $10^{-4}$ M PFP-O⁻. Ascorbate had no effect on the absorption decay indicating the absence of PFP-O•.

Oxidation of PFP-O⁻ with $N_3$• radical gave no PFP-O• species. A transient growth did form slowly at 320 nm ($k_{obs}$ = 1.9 x $10^4$ $s^{-1}$) followed by a very slow decay

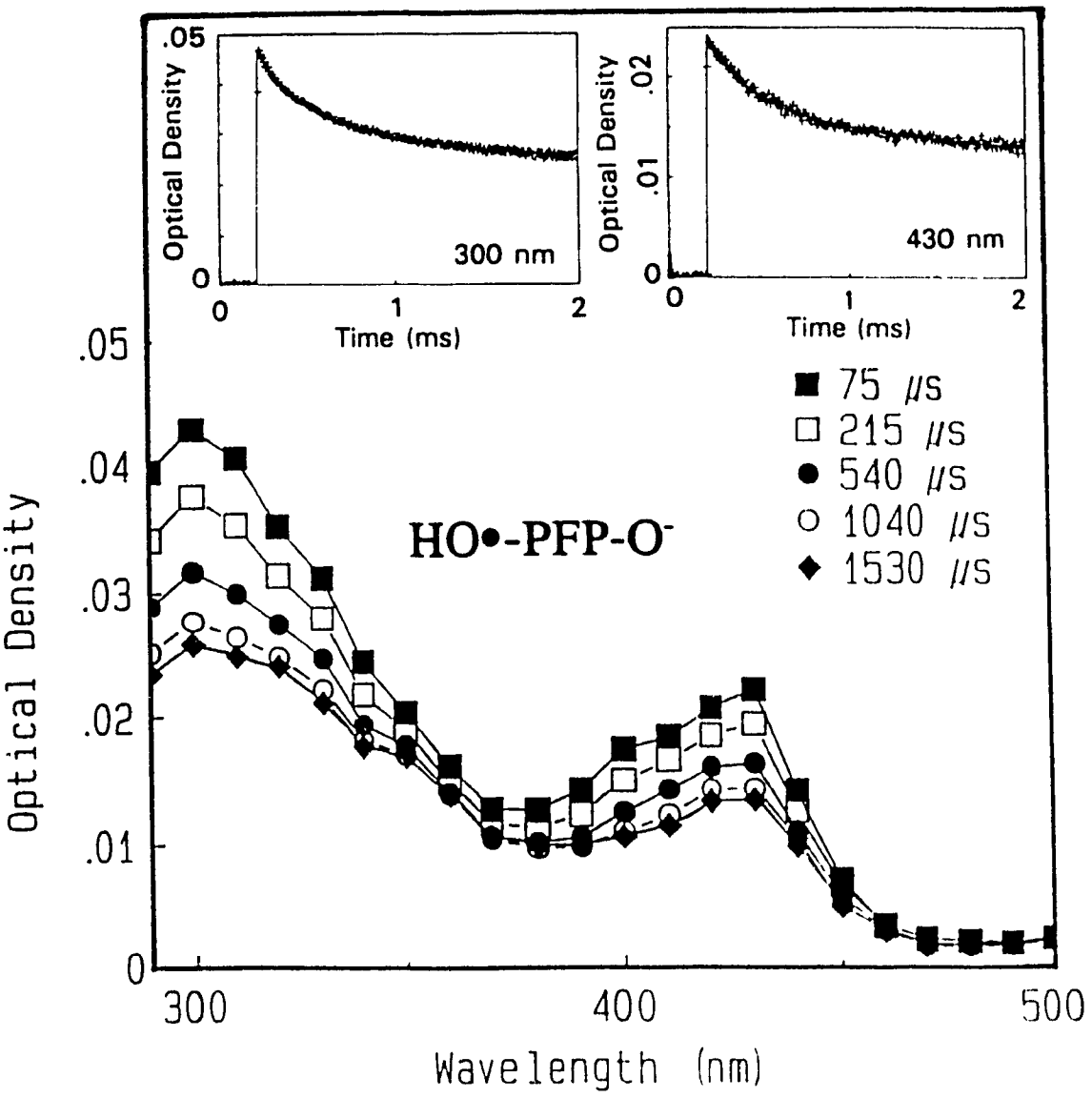


**Figure 9.13** Transient absorption spectra of the HO•-PFP-O radical monitored at 75, 215, 540, 1040, and 1530 $\mu$s following irradiation of a 5 x $10^{-4}$ M aqueous PFP-O solution buffered at pH 8. The solution was $N_2O$-saturated; [•OH] = 3.92 x $10^{-6}$ M. The insets show the decay of the optical density at 300 nm and 430 nm.

**Table 9.6** Observed Kinetics of Formation and Decay of Transients in Various PFP-O$^-$ Reaction Systems.[a]

| Reaction System | Formation | | Decay | |
|---|---|---|---|---|
| | λ, nm | $k_{obs}$, $s^{-1}$ | λ, nm | $2k/\epsilon$, $s^{-1}$ |
| PFP-O$^-$ + OH• [b] | 430[c]<br>300[d] | (3.0-24) x $10^5$<br>(3.1-21) x $10^5$ | 430<br>300 | (7.0 ± 1.4) x $10^5$<br>(2.8 ± 0.3) x $10^5$ |
| PFP-O$^-$ + $N_3^-$ + OH• [e] | 320 | 1.9 x $10^4$ | | |

a) General conditions: $N_2O$-saturated solutions (25 mM); pH 8 buffered with $10^{-3}$ M phosphate; [$NaN_3$]= 0.01 M; [t-BuOH]= 0.2 M.
b) [PFP-O$^-$]= 5.0 x $10^{-4}$ M; [•OH]= 3.92 x $10^{-6}$ M.
c) [PFP-O$^-$]= (5 to 50) x $10^{-4}$ M; [•OH]= 1.83 x $10^{-6}$ M.
d) [PFP-O$^-$]= (5 to 50) x $10^{-4}$ M; [•OH]= 1.52 x $10^{-6}$ M
e) [PFP-O$^-$]= 5.0 x $10^{-4}$ M; [•OH]= 3.43 x $10^{-6}$ M.

on a timescale of 2 ms. The transient species displayed none of the spectral or kinetic characteristics of phenoxyl radicals. We do not exclude addition of $N_3$• to the ring.

## 9.3 CONCLUSIONS

Reaction of •OH radical with the anion of pentafluorophenol yields exclusively the •OH adduct, HO•-PFP-O⁻, while those of pentabromo- and pentachlorophenol react with •OH to form mainly the respective phenoxyl radicals, i.e., electron transfer products (≈ 75% PBP-O• and ≈ 77% PCP-O•). Thus, the nature of the halogen substituents bears directly on the reaction mechanism of pentahalophenols, from simple •OH addition (PFP-O⁻) to mainly electron transfer (PBP-O⁻ and PCP-O). Clearly, addition of •OH radicals to aromatic rings is not the sole reaction pathway for pentahalophenols in homogeneous phase, and the nature and extent of the products formed vary with the nature of the halogen.

In heterogeneous media ($TiO_2$ dispersions), photooxidations may well proceed via analogous pathways even though analysis of products at intermediate stages of oxidation would suggest •OH additions to aromatic rings.[6-8] Recent work[9,10] has begun to address the details of these pathways. It would seem that direct oxidation by valence band holes and oxidation via •OH radicals cannot be distinguished in aqueous media.[10] The nature of the halogen also bears on the spectral red shifts in the absorption spectra of the radicals produced as X varies from F to Br. More important, the nature of X influences the rates of formation of the various radical products: for •OH adducts, $k_{ADD}$ varies in the order F (10) > Br (3) > Cl (1), while for phenoxyl radicals, $k_{-1}$ changes as Br >

Cl; the reverse is true for the production of semiquinone radicals (Cl > Br).

Electrons react reductively with halo-aromatics (as noted for PBP-$O^{\cdot}$; $k_e$ = 2.6 x $10^{10}$ $M^{-1}s^{-1}$) to yield isomeric tetrahalophenoxyl radicals. To the extent that phenoxyl radicals can hydrolyze to give hydroxylated intermediates (see Figure 12.2), photomineralization of these pentahalophenols can also occur via a reductive pathway. This calls attention to the complexity of the process. The possible role of conduction band electrons in the $TiO_2$-catalyzed photodegradations, therefore, cannot be dismissed.

# REFERENCES


1. Matthews, R.W., in *"Proceedings of the I.P.S.8 Conference"*, Pelizzetti, E. and Schiavello, M., Eds., Kluwer Publications, Dordrecht, The Netherlands, **1991**.

2. Barbeni M., Morello, M., Pramauro, E., Pelizzetti, E., Vincenti, M., Borgarello, E., Serpone, N. *Chemosphere* **1987**, *16*, 1165.

3. Al-Ekabi, H., Serpone, N. *J. Phys. Chem.* **1988**, *92*, 5727.

4. Barbeni, M., Pramauro, E., Pelizzetti, E., Borgarello, E., Serpone, N. *Chemosphere* **1985**, *14*, 195.

5. Minero, C., Aliberti, C., Pelizzetti, E., Terzian, R., Serpone, N. *Langmuir* **1991**, *7*, 928.

6. Minero, C., Pelizzetti, E., Terzian, R., Serpone, N., *submitted*, **1992**.

7. (a) Okamoto, K., Yamamoto, Y., Tanaka, H., Tanaka, M., Itaya, A. *Bull. Chem. Soc. Jpn.* **1985**, *58*, 1985.
   (b) Okamoto, K., Yamamoto, Y., Tanaka, H., Itaya, A. *Bull. Chem. Soc. Jpn.* **1985**, *58*, 2023.

8. Augugliaro, V. Palmisano, L., Sclafani, A., Minero, C., Pelizzetti, E., *Toxicol. Environ. Chem.* **1988**, *16*, 89.

9. Draper, R.B., and Fox, M.A. *Langmuir* **1990**, *6*, 1396.

10. Lawless, D., Serpone, N., Meisel, D. *J. Phys. Chem.* **1991**, *95*, 5166.

11. Matthews, R.W. *J. Chem. Soc. Faraday Trans. 1* **1984**, *80*, 457.

12. Izumi, I., Dunn, W.W., Wilbourn, K.O., Fan, F.F., Bard, A.J. *J. Phys. Chem.* **1980**, *84*, 3207.

13. Fujihira, M., Satoh, Y., Osa, T. *Bull. Chem. Soc. Jpn.* **1982**, *55*, 666.

14. Izumi, I., Fan, F.F., Bard, A.J. *J. Phys. Chem.* **1981**, *85*, 218.

15. Cundall, R.B., Rudham, R., Salim, M.S. *J. Chem. Soc. Faraday Trans. 1* **1976**, *72*, 1642.

16. Harvey, P.R., Rudham, R., Ward, S. *J. Chem. Soc. Faraday Trans. 1* **1983**, *79*, 1381.

17. Herrmann, J.-M., Pichat, P. *J. Chem. Soc. Faraday Trans. 1* **1980**, *76*, 1138.

18. Kormann, C., Bahnemann, D.W., Hoffman, M.R. *Environ. Sci. Technol.* **1988**, *22*, 798.

19. (a) Matthews, R.W. *Water Res.* **1986**, *20*, 569.
(b) Matthews, R.W. *J. Catal.* **1986**, *97*, 565.
(c) Matthews, R.W. *J. Phys. Chem.* **1987**, *91*, 3328.
(d) Matthews, R.W. *Sol. Energy* **1987**, *38*, 405.
(e) Matthews, R.W. *Aust. J. Chem.* **1987**, *40*, 667.

20. Serpone, N., Borgarello, E., Barbeni, M., Pelizzetti, E., Pichat, P., Herrmann, J.-M., Fox, M.A. *J. Photochem.* **1987**, *36*, 373.

21. Barbeni, M., Pramauro, E., Pelizzetti, E., Borgarello, E., Grätzel, M., Serpone, N. *Nouv. J. Chim.* **1984**, *8*, 547.

22. Turchi, C.S., Ollis, D.F. *J. Catal.* **1990**, *122*, 178.

23. Anpo, M., Kubokawa, Y. *Rev. Chem. Intermed.* **1987**, *8*, 105; and references therein.

24. Getoff, N., Solar, S. *Radiat. Phys. Chem. (Int. J. Radiat. Appl. Instrum. Part C)* **1986**, *28*, 443.

25. Getoff, N., Solar, S. *Radiat. Phys. Chem. (Int. J. Radiat. Appl. Instrum. Part C)* **1988**, *31*, 121.

26. Draper, R.B., Fox, M.A., Pelizzetti, E., Serpone, N. *J. Phys. Chem.* **1989**, *93*, 1938.

27. Alfassi, Z.B., Schuler, R.H. *J. Phys. Chem.* **1985**, *89*, 3359.

28. Land, E.J., Ebert, M. *Trans. Faraday Soc.* **1967**, *63*, 1181.

29. Schuler, R.H. *Radiat. Res.* **1977**, *69*, 417.

30. Matthews, R.W., Sangster, D.F. *J. Phys. Chem.* **1965**, *69*, 1938.

31. Schuler, R.H., Neta, P., Zemel, H., Fessenden, R.W. *J. Am. Chem. Soc.* **1976**, *98*, 3825.

32. Khudanov, I.V., Kuz'min, V.A. *Russ. Chem. Rev.* **1975**, *44*, 801; and references therein.

33. Anbar, M., Hart, E.J. *J. Am. Chem. Soc.* **1964**, *86*, 5633.

# CHAPTER 10

# PULSE RADIOLYTIC STUDIES OF THE REACTION OF XYLENOLS WITH •OH, $N_3$•, AND H• RADICALS:

## FORMATION OF DIMETHYLPHENOXYL, DIHYDROXYDIMETHYLCYCLOHEXADIENYL, AND HYDROXYDIMETHYLCYCLOHEXADIENYL RADICALS

## 10.1 INTRODUCTION

The photocatalyzed oxidation of methylated phenols was carried out successfully in aqueous dispersions of $TiO_2$ (see Chapters 4, 6 and 7). The compounds surveyed include o-, m-, and p-cresol, the six isomers of dimethylphenol (the so called xylenols), and 2,3,5-trimethylphenol. As noted earlier, the hydroxyl radical has been implicated as a significant oxidant in the $TiO_2$-assisted photomineralization of these and many other organic compounds in aqueous environments,[1-6] since hydroxylated intermediates can be detected during the photodegradation of many of these species. These hydroxylated species can be formed either by addition of •OH or by hydration of a singly oxidized cation radical, produced by direct interfacial electron transfer from a surface-bound •OH radical (a surface trapped hole) to an adsorbed organic substrate.[7] There are a number of studies in the literature that report on the rates and mechanisms of •OH and other radical reactions with cresols,[8-11] there are however no such studies reported for xylenols.

The main focus of the present study was to identify the products and assess the rates of reaction of oxidizing radicals such as •OH and $N_3$• and reducing radicals such as H• with a series of isomeric xylenols: 2,3-, 2,4-, 2,5-, 2,6-, 3,4- and 3,5-xylenol. The work was also aimed at establishing whether addition of •OH to the aromatic ring,

to give hydroxycyclohexadienyl species, is a principal reaction pathway as present evidence would suggest.[12-14] These studies were also needed to identify the primary oxidized species from surface-bound •OH radical attack on these xylenols, whose photomineralization over $TiO_2$ aqueous dispersions has been described earlier (see Chapter 6).

Herein, the nature, the spectroscopic properties, and the kinetics of formation and decay of radicals produced by the reaction of •OH, $N_3$•, and H• with xylenols in homogeneous phase, are reported.

## 10.2 REACTIONS OF XYLENOLS WITH VARIOUS RADICAL SPECIES

The reactions of xylenols with a variety of radical species (•OH, $N_3$•, and H•) were monitored by observing changes in the optical density of the reaction medium. The desired radical species were generated radiolytically in solution by varying the composition of the solution and the gases used, as was described in the experimental section of this work (Chapter 3).

### 10.2.1 Reaction with $N_3$•:

Following the work on the pentahalophenols, it was instructive to determine the spectral properties of the phenoxyl radicals produced by interaction of the xylenols with the azide radical. Two xylenols were arbitrarily chosen: 2,6- and 3,4-xylenol.

### 10.2.1.1 2,6-DIMETHYLPHENOXYL RADICAL

The absorption spectrum (Figure 10.1) of the product from the oxidation of 2,6-xylenol with $N_3$• radicals, the 2,6-dimethylphenoxyl radical, shows two absorption maxima, one at 390 nm [$\epsilon_{390}$ = (3160 ± 150) $M^{-1}cm^{-1}$] and the second at 375 nm [$\epsilon_{375}$ = (2925 ± 300) $M^{-1}cm^{-1}$], Table 10.1. The spectrum is similar to those reported for cresols and 3,5-xylenol in aqueous phase.[15]

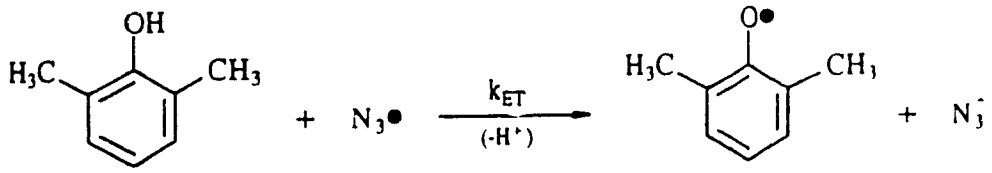


**(10.1)**

The oxidation of 2,6-xylenol by $N_3$• (equation 10.1) was monitored by observing the increase of the optical density at 375 nm as a function of the concentration of 2,6-xylenol over the range from 1 x $10^{-4}$ to 3 x $10^{-4}$ M; the observed formation rate constant $k_{obs}$ ranging from 2.68 x $10^5$ to 8.08 x $10^5$ $s^{-1}$ (Table 10.2 and Appendix B) gave a bimolecular rate constant $k_{ET}$ of (2.8 ± 0.6) x $10^9$ $M^{-1}s^{-1}$ for the oxidation. The optical density at both 375 and 390 nm (Figure 10.1, inset) decayed via second order kinetics: $k_d$ = (4.2 ± 0.9) x $10^9$ $M^{-1}s^{-1}$. The kinetics of formation and decay of the 2,6-dimethylphenoxyl radical as well as its spectral properties correlate well with those of similar compounds (Table 10.1).[4,9,15]

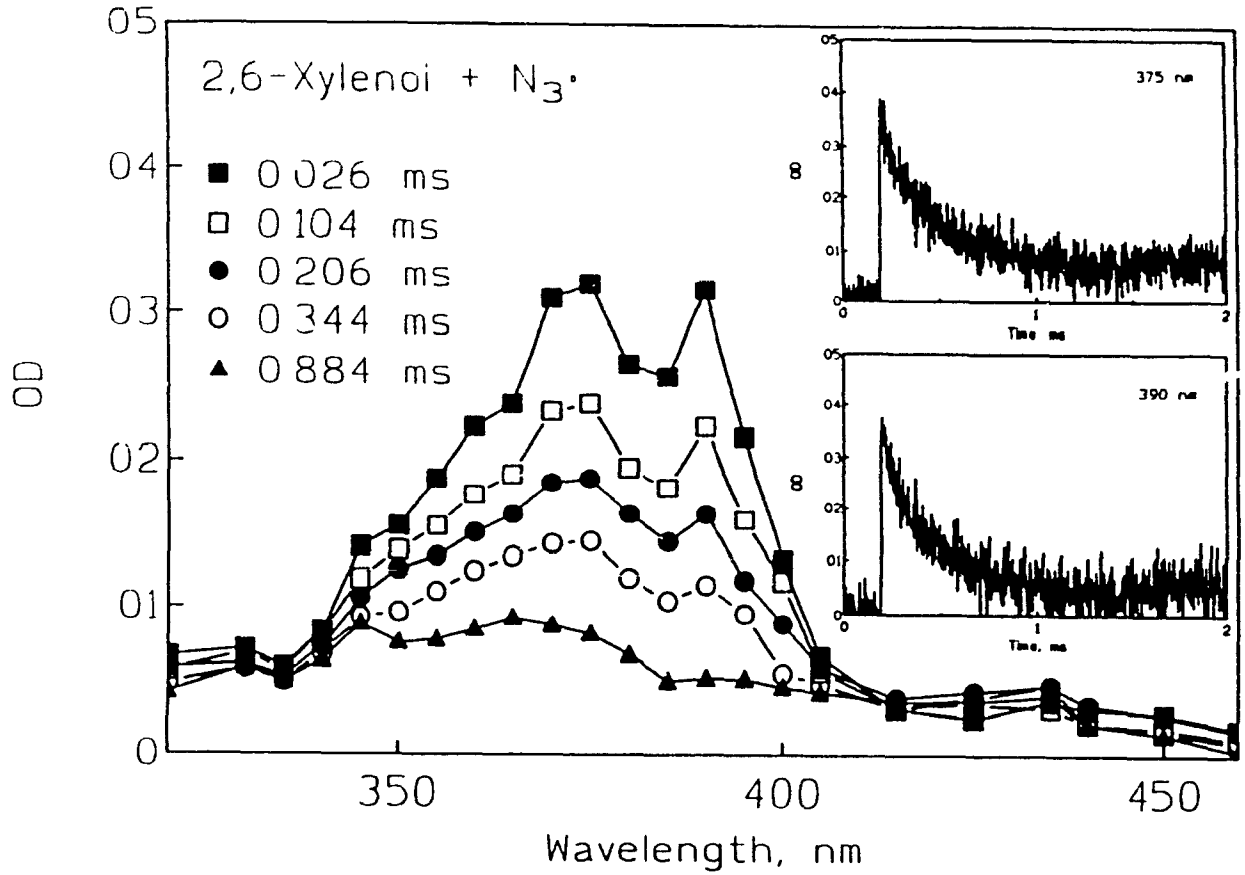


**Figure 10.1** Transient absorption spectra of 2,6-dimethylphenoxyl radical at 0.026, 0.104, 0.206, 0.344 and 0.884 ms following irradiation of 3 x $10^{-4}$ M 2,6-Xylenol at pH 5.8 in a 0.01 M $NaN_3$ aqueous solution; the solution was $N_2O$-saturated; [•OH]= 5.20 x $10^{-6}$ M. Insets show the decays of the optical density at 375 and 390 nm.

**Table 10.1** Comparison of the Optical and Kinetic Properties of Dimethylphenoxyl radicals with Values Published for Similar Radicals

| Radical | $\lambda_{max}$ (nm) | $\epsilon_{max}$ ($M^{-1}cm^{-1}$) | $k_r$ ($M^{-1}s^{-1}$) | $k_d$ ($M^{-1}s^{-1}$) | Ref |
|---|---|---|---|---|---|
| 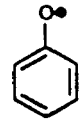 | 400 | 2200 | $4.3 \times 10^9$ | - | 8,9 |
| 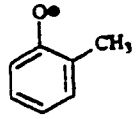 | 395<br>380<br>363 | - | $4.4 \times 10^8$ | - | 8,15 |
| 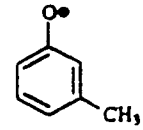 | 412<br>381<br>372 | - | $1.8 \times 10^8$ | - | 8,15 |
| 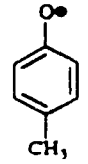 | 405<br>385<br>368 | 2400<br>-<br>- | $1.5 \times 10^9$ | - | 8,9,15 |
| 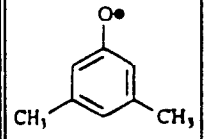 | 427<br>404 | - | - | - | 15 |
| 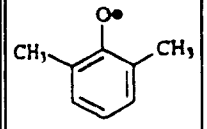 | 390<br>375 | 3160<br>2925 | $2.8 \times 10^9$ | $4.2 \times 10^9$ | This work |
| 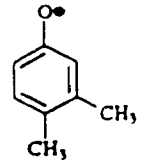 | 415<br>400 | 3260<br>2890 | $4.1 \times 10^9$ | $1.5 \times 10^9$ | This work |

**Table 10.2** Observed Kinetics of Formation and Decay of Phenoxyl Radicals in Various Reaction Systems.[a]

| Reaction System | Formation | | Decay | |
|---|---|---|---|---|
| | λ, nm | $k_{obs}$, $s^{-1}$ | λ, nm | $k_{obs}(k/\epsilon l)$, $s^{-1}$ |
| 2,6-Xylenol + $N_3^-$ + OH• | 375[b] | (2.68-8.08) x $10^5$ | 375[c]<br>390[c] | (5.11 ± 0.3) x $10^5$<br>(5.21 ± 0.3) x $10^5$ |
| 3,4-Xylenol + $N_3^-$ + OH• | 415[d] | (2.31-11.9) x $10^5$ | 400[c]<br>415[c] | (2.22 ± 0.3) x $10^5$<br>(1.87 ± 0.2) x $10^5$ |

a) General conditions: $N_2O$-saturated solutions (25 mM); pH 5.8; [$NaN_3$] = 0.01 M
b) [2,6-xylenol]= (1 - 3) x $10^{-4}$ M; [•OH]= 3.34 x $10^{-6}$ M.
c) [2,6-xylenol]= 3.0 x $10^{-4}$ M; [•OH]= (3 - 10) x $10^{-6}$ M.
d) [3,4-Xylenol]= (0.5 - 3) x $10^{-4}$ M; [•OH]= 1.68 x $10^{-6}$ M.
e) [3,4-Xylenol]= 3 x $10^{-4}$ M; [•OH]= (1 - 7) x $10^{-6}$ M.

### 10.2.1.2 *3,4*-DIMETHYLPHENOXYL RADICAL:

The reaction of 3,4-xylenol with $N_3$• was also carried out under similar conditions as those used for the 2,6-xylenol. The results showed the formation of the corresponding phenoxyl radical (Figure 10.2). The spectrum of the 3,4-dimethylphenoxyl radical is also characterized by two bands, one at 400 nm [$\epsilon_{400}$ = (2890 ± 300) $M^{-1}cm^{-1}$] and the second at 415 nm [$\epsilon_{415}$ = (3260 ± 500) $M^{-1}cm^{-1}$], Table 10.1. The spectrum was again similar to those reported for cresols and the 3,5-xylenol.[15]

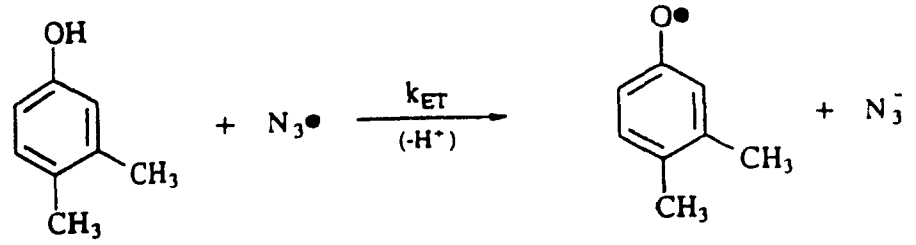


(10.2)

The oxidation of 3,4-xylenol (equation 10.2) was monitored by observing the increase of the optical density at 415 nm as a function of [3,4-xylenol] over the range from 5 x $10^{-5}$ to 3 x $10^{-4}$ M; the observed formation rate constant $k_{obs}$ ranging from 2.31 x $10^5$ to 1.19 x $10^6$ $s^{-1}$ (Appendix B and Table 10.2) gave a bimolecular rate constant $k_{ET}$ of (4.1 ± 0.6) x $10^9$ $M^{-1}s^{-1}$ for the oxidation. The optical density at both 400 and 415 nm (Figure 10.2, inset) decayed via second order kinetics: $k_d$ = (1.5 ± 0.3) x $10^9$ $M^{-1}s^{-1}$. The kinetics of formation and decay of the 3,4-dimethylphenoxyl radical as well as its spectral properties correlate well with those of similar compounds (Table 10.1).[8,9,15]

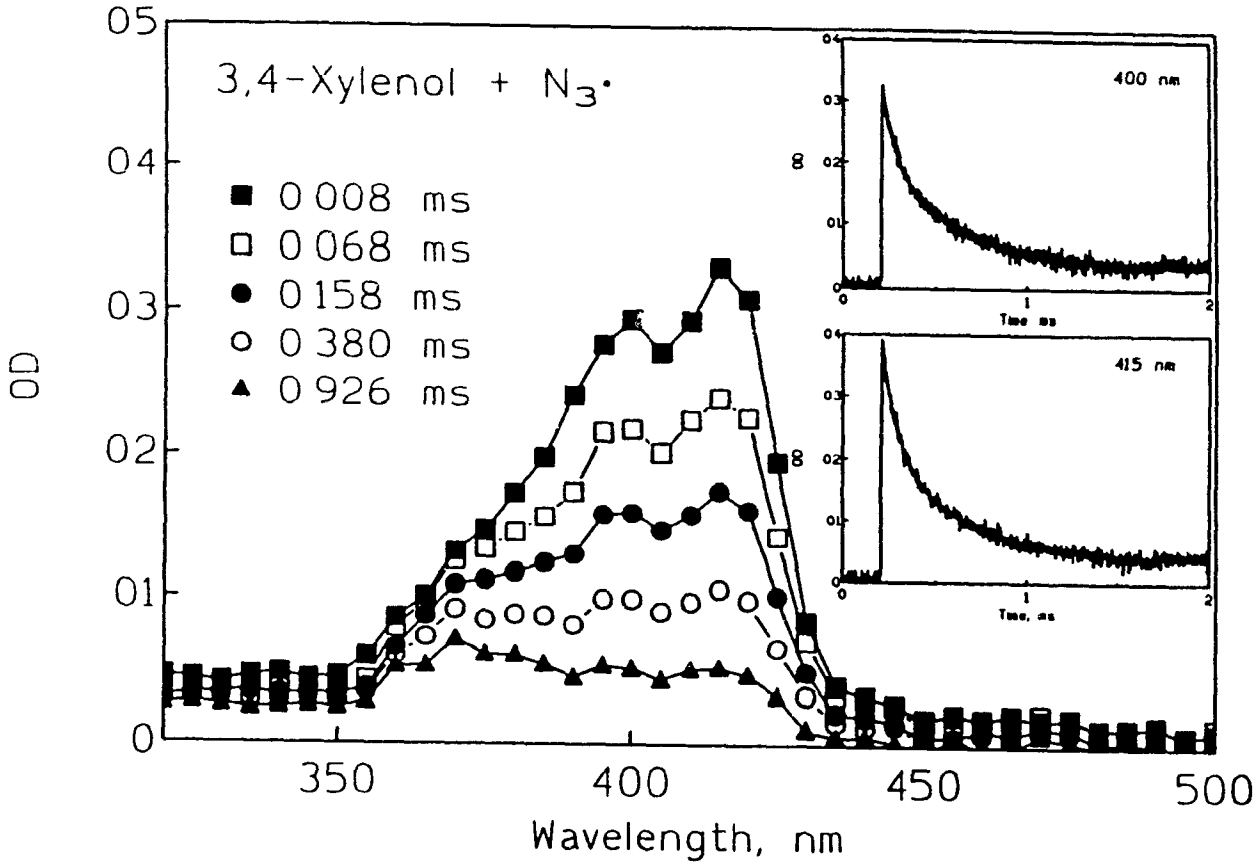


**Figure 10.2** Transient absorption spectra of 3,4-dimethylphenoxyl radical at 0.008, 0.068, 0.158, 0.380 and 0.926 ms following irradiation of 3 x $10^{-4}$ M 3,4-Xylenol at pH 5.8 in a 0.01 M $NaN_3$ aqueous solution; the solution was $N_2O$-saturated; [•OH]= 4.78 x $10^{-6}$ M. Insets show the decays of the optical density at 400 and 415 nm.

## 10.2.2 Reaction of the Xylenols with •OH Radicals:

### 10.2.2.1 Dihydroxydimethylcyclohexadienyl Radicals:

Hydroxyl radicals typically add to phenols (e.g., phenol,[9] cresol,[9] 2,4,5-trichlorophenol[14]) to form dihydroxycyclohexadienyl radicals (•OH-adducts), in competition with H atom abstraction and electron transfer.[8] Phenoxyl radicals can also be formed via either electron transfer or via unimolecular elimination of $H_2O$ from the •OH-adduct.[9] The reaction of •OH with all the isomers of xylenol was examined in this work.

The absorption spectrum of the product of the reaction between •OH and 2,6-xylenol is shown in Figure 10.3. It shows an absorption maximum at 320 nm. The optical density at 320 nm decayed via second order kinetics [$k/\epsilon\ell = (6.1 \pm 1.2) \times 10^5$ $s^{-1}$]. The extinction coefficient at 320 nm is $\epsilon_{320} = 2670 \pm 350$ $M^{-1}$ $cm^{-1}$ giving a value of $k_d = (4.1 \pm 0.9) \times 10^9$ $M^{-1}$ $s^{-1}$ for the second order decay rate constant.

The rate constant for •OH addition to 2,6-xylenol was measured at different concentrations of 2,6-xylenol between $1 \times 10^{-4}$ and $2.5 \times 10^{-4}$ M: $k_{obs}$ varies between $1.49 \times 10^5$ and $3.2 \times 10^6$ $s^{-1}$ (Appendix B and Table 10.3) giving a rate constant $k_{add} = (1.2 \pm 0.2) \times 10^{10}$ $M^{-1}$ $s^{-1}$ for reaction 10.3. The kinetics of formation and decay of the radical formed as well as its spectral properties correlate well with those of hydroxycyclohexadienyl radicals reported in the literature, and confirm its identity as the dihydroxy-2,6-dimethylcyclohexadienyl radical (Table 10.4).

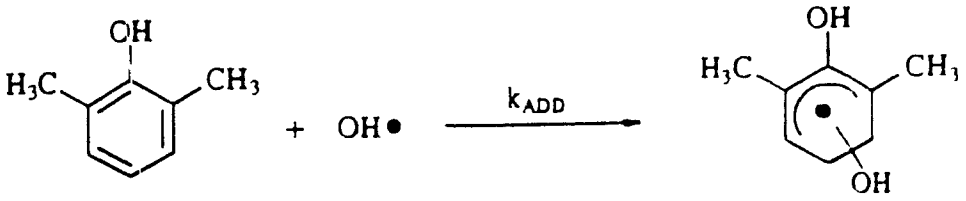


(10.3)

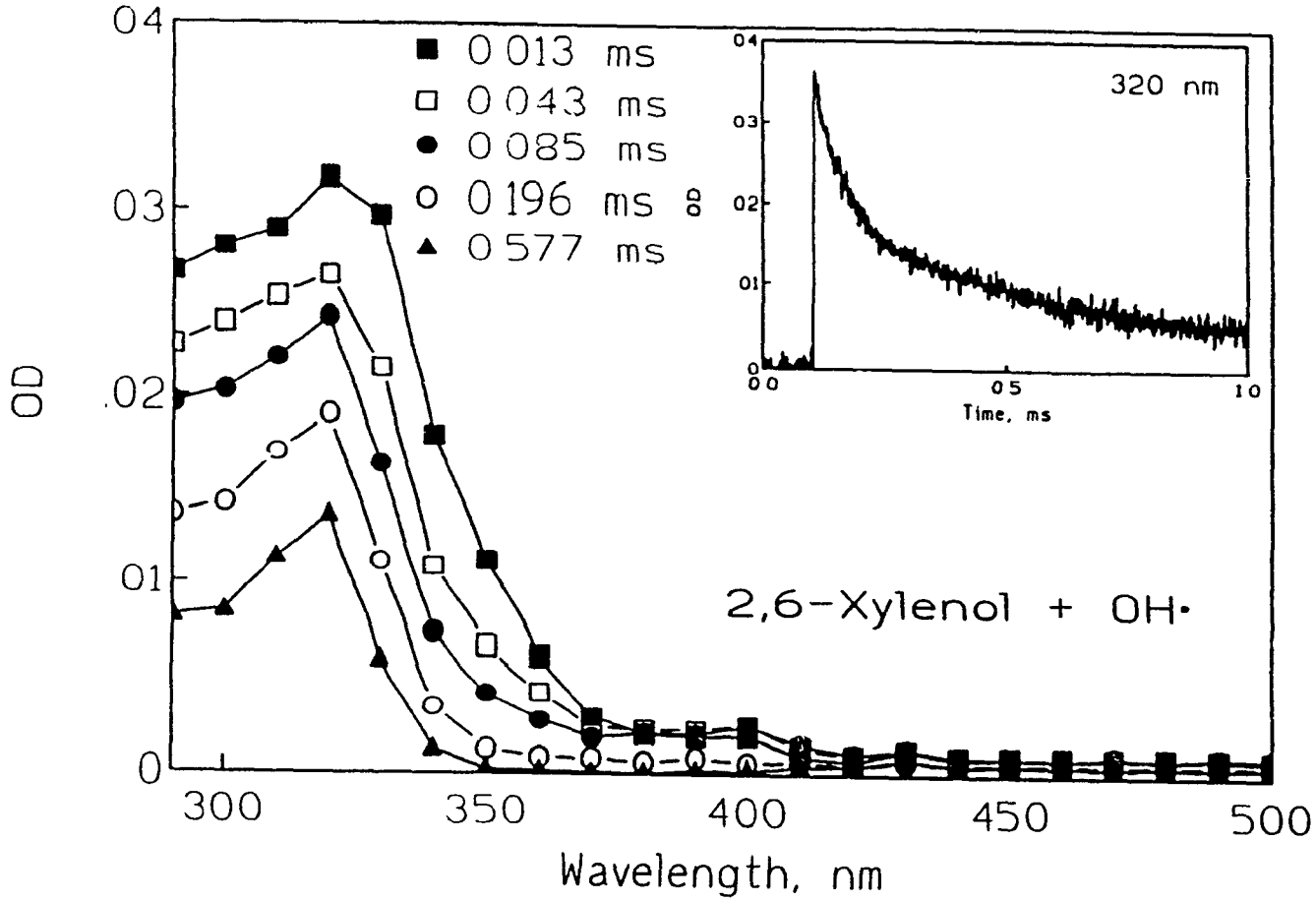


**Figure 10.3** Transient absorption spectra of the dihydroxy-2,6-dimethylcyclohexadienyl radical monitored at 0.013, 0.043, 0.085, 0.196 and 0.577 ms following irradiation of a 2.5 x $10^{-4}$ M aqueous 2,6-Xylenol solution buffered at pH 4. The solution was $N_2O$-saturated; [•OH]= 5.02 x $10^{-6}$ M. The inset shows the decay of the optical density at 320 nm.

**Table 10.3** Observed Kinetics of Formation and Decay of OH-adducts of xylenols in Various Reaction Systems.[a]

| Reaction System | Formation | | Decay | |
|---|---|---|---|---|
| | λ, nm | $k_{obs}$, $s^{-1}$ | λ, nm | $k_{obs}(k/\epsilon l)$, $s^{-1}$ |
| 2,3-xylenol + OH• | 300[b] | (9.82 - 27.3) x $10^5$ | 300[c] | (7 ± 2) x $10^4$ |
| 2,4-xylenol + OH• | 300[d] | (8.42 - 24.2) x $10^5$ | 300[e] | (1.4 ± 0.2) x $10^5$ |
| 2,5-xylenol + OH• | 330[f] | (1.01 - 3.30) x $10^6$ | 330[g] | (3.9 ± 0.8) x $10^5$ |
| 2,6-xylenol + OH• | 320[h] | (1.49 - 3.2) x $10^6$ | 320[i] | (6.1 ± 1.2) x $10^5$ |
| 3,5-xylenol + OH• | 310[j] | (1.06 - 2.93) x $10^6$ | 310[k] | (3.4 ± 0.7) x $10^5$ |

a) General conditions: $N_2O$-saturated solutions (25 mM); pH 4 ($10^{-3}$ M phosphate buffer).
b) [2,3-xylenol]= (1 - 2.5) x $10^{-4}$ M; [•OH]= 2.5 x $10^{-6}$ M.
c) [2,3-xylenol]= 2.5 x $10^{-4}$ M; [•OH]= (2.3 - 9) x $10^{-6}$ M.
d) [2,4-Xylenol]= (1 - 2.5) x $10^{-4}$ M; [•OH]= 2.69 x $10^{-6}$ M.
e) [2,4-Xylenol]= 2.5 x $10^{-4}$ M; [•OH]= (3 - 10) x $10^{-6}$ M.
f) [2,5-Xylenol]= (1 - 3) x $10^{-4}$ M; [•OH]= 3 x $10^{-6}$ M.
g) [2,5-Xylenol]= 3 x $10^{-4}$ M; [•OH]= (2.8 - 10) x $10^{-6}$ M.
h) [2,6-Xylenol]= (1 - 2.5) x $10^{-4}$ M; [•OH]= 4.22 x $10^{-6}$ M.
i) [2,6-Xylenol]= 2.5 x $10^{-4}$ M; [•OH]= (3 - 10) x $10^{-6}$ M.
j) [3,5-Xylenol]= (1 - 3) x $10^{-4}$ M; [•OH]= 2.8 x $10^{-6}$ M.
k) [3,5-Xylenol]= 3 x $10^{-4}$ M; [•OH]= (2 - 9) x $10^{-6}$ M.

**Table 10.4** Comparison of the Optical and Kinetic Properties of dihydroxydimethylcyclohexadienyl radicals with Values Published for Similar Radicals.

| Radical | $\lambda_{max}$, nm | $\epsilon_{max}$, $M^{-1}$ $cm^{-1}$ | $k_f$, $M^{-1}$ $s^{-1}$ | $k_d$, $M^{-1}$ $s^{-1}$ | Ref |
|---|---|---|---|---|---|
| | 330 | 4400 | $1.4 \times 10^{10}$ | $3.6 \times 10^{9}$ | 9 |
| | 320 | 4300 | $6.8 \times 10^{9}$ | $1.6 \times 10^{9}$ | 17 |
| 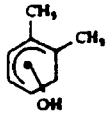 | 326 | 4700 | $6.7 \times 10^{9}$ | $1.4 \times 10^{9}$ | 17 |
| 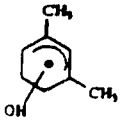 | 328 | 6000 | $7.5 \times 10^{9}$ | $1.3 \times 10^{9}$ | 17 |
| 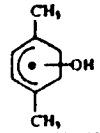 | 312 | 4300 | $7.0 \times 10^{9}$ | $1.2 \times 10^{9}$ | 17 |
| 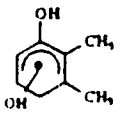 | 300 | 2880 ± 460 | $(1.2 \pm 0.2) \times 10^{10}$ | $(5 \pm 1) \times 10^{8}$ | a |
| 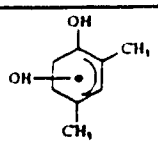 | 300 | 3300 ± 520 | $(1.0 \pm 0.2) \times 10^{10}$ | $(1.2 \pm 0.3) \times 10^{9}$ | a |
| 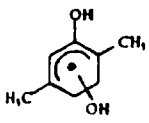 | 330 | 3040 ± 300 | $(1.0 \pm 0.2) \times 10^{10}$ | $(2.9 \pm 0.5) \times 10^{9}$ | a |
| 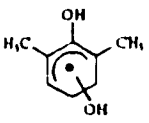 | 320 | 2670 ± 350 | $(1.2 \pm 0.2) \times 10^{10}$ | $(4.1 \pm 0.9) \times 10^{9}$ | a |
| 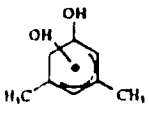 | 310 | 2830 ± 140 | $(9.6 \pm 0.2) \times 10^{9}$ | $(2.4 \pm 0.5) \times 10^{9}$ | a |

a) This work

The reactions of 2,3-, 2,4-, 2,5-, 3,4-, and 3,5- xylenol with •OH were also examined. The 2,3-, 2,4-, 2,5-, and 3,5-xylenols showed behavior similar to 2,6-xylenol producing the corresponding •OH-adducts (equation 10.3). The experimental conditions and observations are summarized in Table 10.3, while the spectral and kinetic properties of the radicals produced are summarized in Table 10.4 where comparisons are made to values reported in the literature for analogous substances. The time resolved absorption spectra for the corresponding •OH radical adducts are included in Appendix B. The reaction between •OH and 3,4-xylenol produced a different product composition and will be discussed in the next section.

The rate constants for •OH addition to xylenols have been determined[16] in the gas phase. These values are compared to the values obtained in aqueous solution in this work in Table 10.5. It can be seen that both sets of values are within the same order of magnitude, though the rate constants in the gas phase are larger by a factor of about 4 to 6. This is not surprising as diffusion rates of the molecules involved are bound to be faster in the gas phase.

The formation of benzyl type radicals has been reported in alkaline solutions by reaction of $O^{-}$• (deprotonated form of •OH) with methylated benzenes via abstraction of a H• atom from a methyl group.[17] These benzyl radicals are also formed in acidic solutions via water elimination from •OH radical adducts.[17] Benzyl radicals formed from methylated benzenes are characterized by 3 bands: one in the 260-270 nm region with $\epsilon \approx 15000\ M^{-1}cm^{-1}$ and two bands in the 300-330 nm region with $\epsilon \approx 3000\text{-}5000\ M^{-1}cm^{-1}$. Methylated benzyl radicals typically decay via second order kinetics with $k \approx 2 \times 10^{9}$

**Table 10.5** Comparison of Rates of •OH Addition to Xylenols in Aqueous Solution and in the Gas Phase.

| Xylenol | $k_{add}$, $M^{-1}s^{-1}$ (Gas Phase)[a] | $k_{add}$, $M^{-1}s^{-1}$ (Aqueous Solution)[b] |
|---|---|---|
| 2,3-Xylenol | $(4.83 \pm 1.22) \times 10^{10}$ | $(1.2 \pm 0.2) \times 10^{10}$ |
| 2,4-Xylenol | $(4.31 \pm 1.11) \times 10^{10}$ | $(1.0 \pm 0.2) \times 10^{10}$ |
| 2,5-Xylenol | $(4.82 \pm 1.38) \times 10^{10}$ | $(1.0 \pm 0.2) \times 10^{10}$ |
| 2,6-Xylenol | $(3.97 \pm 1.04) \times 10^{10}$ | $(1.2 \pm 0.2) \times 10^{9}$ |
| 3,4-Xylenol | $(4.90 \pm 1.28) \times 10^{10}$ | $(9 \pm 1) \times 10^{9}$ [See Text] |
| 3,5-Xylenol | $(6.81 \pm 1.81) \times 10^{10}$ | $(9.6 \pm 0.2) \times 10^{9}$ |

a) From ref. 16. These values were obtained at 296 K.
b) This work. These values were obtained at 293 K.

$M^{-1}s^{-1}$; they are, however, formed at slower rates than the •OH-adducts (e.g. for toluene: the rate constant for H• atom abstraction is $k_{abs} = 4.0 \times 10^{8}$ $M^{-1}s^{-1}$, and the rate constant for •OH-adduct formation is $k_{add} = 6.8 \times 10^{9}$ $M^{-1}s^{-1}$).[17] The percentages of H• atom abstraction products from mono and dimethyl benzenes by reaction with •OH range between 6 and 12 % in alkaline solution with •OH addition products making up the remaining fraction.[17] Based on the data presented in this work, the possibility that some H• atom abstraction products may have been formed cannot be excluded entirely. However, kinetic and spectral data, as well as the experimental conditions used (acidic pH) seem to favour the notion that the major (initial) product is the •OH adduct. Another reaction pathway that is open to •OH-adducts of xylenols is the elimination of $H_2O$ to form phenoxyl radicals, as opposed to benzyl radicals, owing to the presence of an OH group on the ring in addition to the methyl groups. Phenoxyl radicals are detectable

under our experimental conditions.

### 10.2.2.2 Reaction of 3,4-Xylenol with •OH Radicals

The absorption spectrum of the product(s) of the reaction between •OH radicals and 3,4-xylenol is depicted in Figure 10.4; this spectrum was recorded under similar conditions to those used for the other five isomers of xylenol (see Figure 10.3 and Appendix B). It shows one band with an absorption maximum at 300 nm as well as a weaker feature between 400 and 420 nm. The optical density at 300 nm decayed via second order kinetics with $k/\epsilon\ell = (1.9 \pm 0.3) \times 10^5\ s^{-1}$. The optical density for the weaker feature built up at a visibly slower rate ($k_{obs} \approx 10^4\ s^{-1}$) (see Figure 10.4, insets) and also decayed via second order kinetics with $k/\epsilon\ell \approx 2 \times 10^5\ s^{-1}$ at 415 nm. This suggests that the two bands may well originate from different species; the similarity of the value of the decay constant at 415 nm to that of the second order decay constant of the 3,4-dimethylphenoxyl radical [415 nm of Figure 10.2; $k/\epsilon\ell = 1.9 \pm 0.2 \times 10^5\ s^{-1}$] indicates that the 3,4-dimethylphenoxyl radical is formed in the reaction of 3,4-xylenol with •OH radicals.

Subtraction of the contribution of the 3,4-dimethylphenoxyl radical absorption (open squares) from the (3,4-Xylenol + •OH) spectrum (filled squares) gives the spectrum shown in Figure 10.5 (filled circles). We attribute the absorption in the difference spectrum to the •OH radical adduct of 3,4-Xylenol, i.e. to the dihydroxy 3,4-dimethylcyclohexadienyl radical, after noting the similarity of this spectrum with those of the •OH adducts of the other 5 xylenols (see Figure 10.3, Table 10.4, and

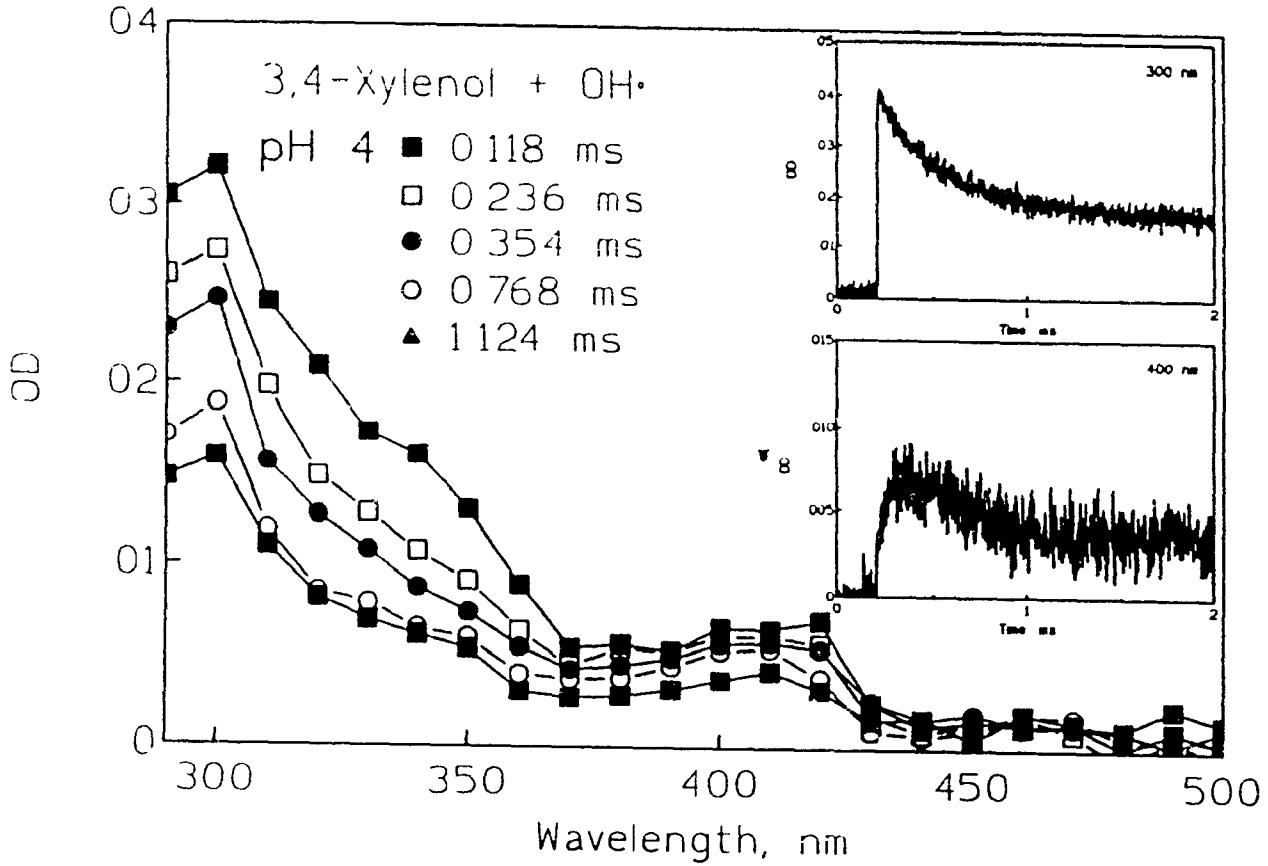


**Figure 10.4** Transient absorption spectra of the reaction product between 3,4-Xylenol and •OH monitored at 0.118, 0.236, 0.354, 0.768 and 1.124 ms following irradiation of a 3 x $10^{-4}$ M aqueous 3,4-Xylenol solution buffered at pH 4. The solution was $N_2O$-saturated; [•OH]= 6.01 x $10^{-6}$ M. Insets show the decay of the optical density at 300 and 400 nm.

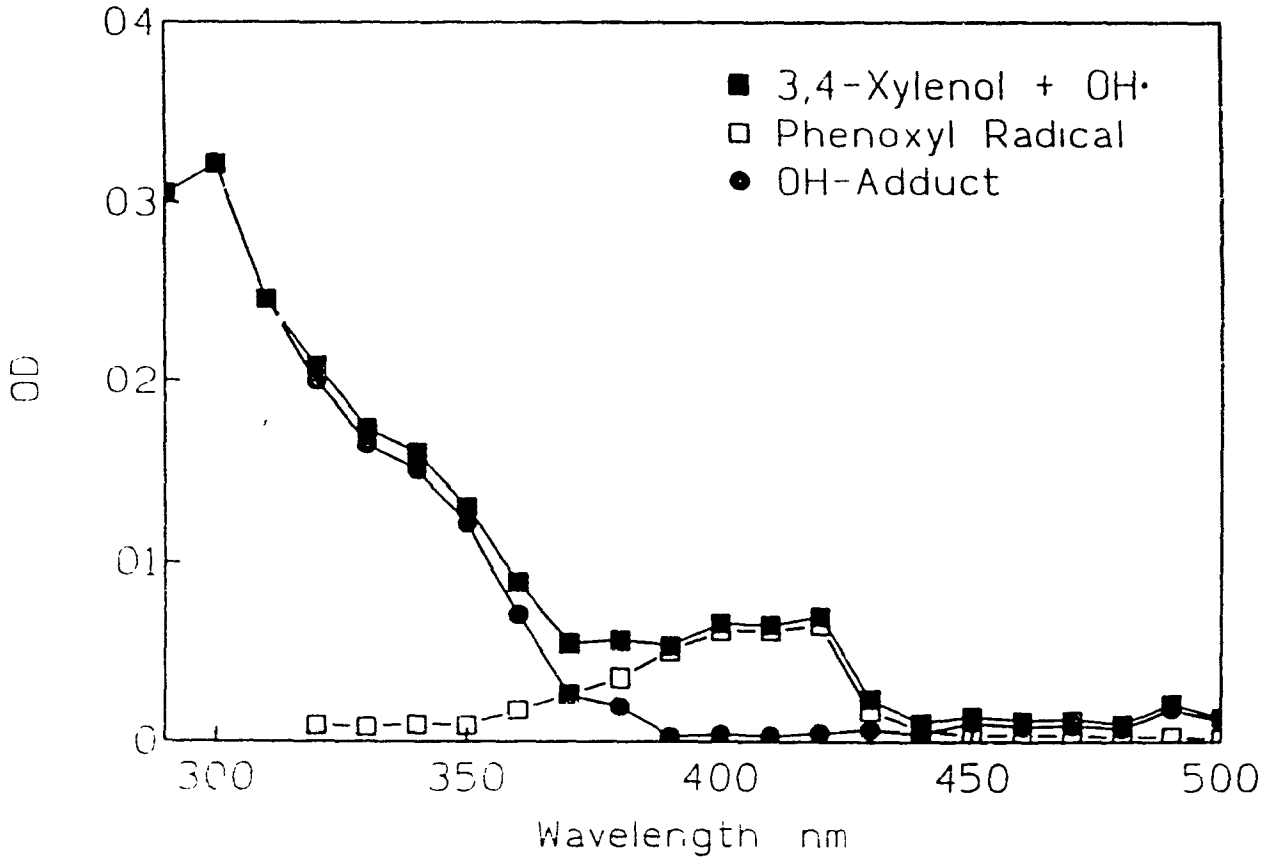


**Figure 10.5** Transient difference absorption spectrum of the dihydroxy-3,4-dimethylcyclohexadienyl radical (●) as calculated from the transient absorption spectrum of the products of the reaction between 3,4-Xylenol and •OH (■) at 118 $\mu$s following irradiation of a $2 \times 10^{-4}$ M aqueous solution of 3,4-Xylenol, buffered at pH 4. The solution was $N_2O$ saturated. [•OH]= $6.01 \times 10^{-6}$ M. The open squares (□) represent the contribution to the product spectrum of the 3,4-dimethylphenoxyl radical.

Appendix B).

The kinetic data were unclear as to whether the 3,4-dimethylphenoxyl radical was formed via unimolecular elimination of $H_2O$ from the •OH-adduct {$k/\epsilon\ell = (1.9 \pm 0.3)$ x $10^5$ $M^{-1}s^{-1}$ for the disappearance of the •OH-adduct; $k_{obs} \approx 10^4$ $s^{-1}$ for the formation of the phenoxyl radical}. In order to establish the source of the phenoxyl radical, the absorption spectrum for the products of the reaction between •OH and 3,4-xylenol was recorded on a shorter timescale (0-200 $\mu$s). The spectrum (Figure 10.6) shows the decrease in optical density of the 300 nm band and the concomitant growth of the 400 nm band; a clean isosbestic point is clearly seen at $\approx$ 370 nm. The shape of the band at 300 nm as well as the product distribution ($\approx$24 % •OH-adduct converted to phenoxyl) seem to indicate that only one isomer of the •OH-adduct (most probably one with the •OH adding in one of the two available *ortho* positions) undergoes $H_2O$ elimination to form the corresponding phenoxyl radical. The major portion of the •OH-adduct likely undergoes a bimolecular reaction; this is consistent with the observed kinetics (second order) for the decay of the optical density at 300 nm.

The rate of formation of the phenoxyl radical was independent of the initial concentration of 3,4-xylenol in acid media (pH 4); this observation is consistent with phenoxyl radicals being formed via $H_2O$ elimination. The mechanism shown in scheme 10.4 is proposed for the reaction of •OH radicals with 3,4-xylenol at pH 4 to form the dihydroxy-3,4-dimethylcyclohexadienyl radical and subsequently the 3,4-dimethyl phenoxyl radical. The behaviour of 3,4-xylenol in its reaction with •OH is identical to the behaviour reported by Land and Ebert[9] for both phenol and p-cresol. In both cases,

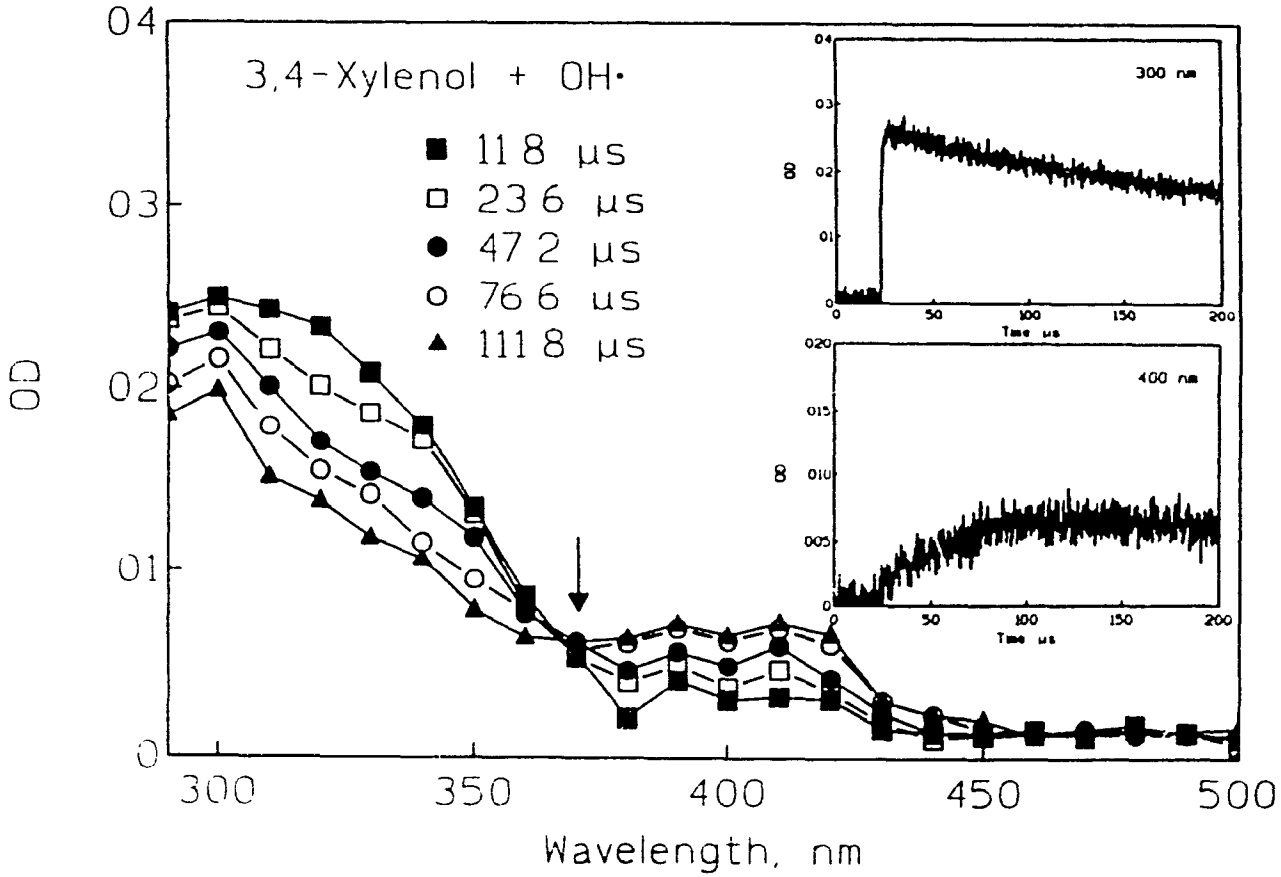


**Figure 10.6** Transient absorption spectra of the reaction product(s) between 3,4-Xylenol and •OH monitored at 11.8, 23.6, 47.2, 76.6 and 111.8 µs following irradiation of a 3 x $10^{-4}$ M aqueous 3,4-Xylenol solution buffered at pH 4. The solution was $N_2O$-saturated; [•OH]= 2.99 x $10^{-6}$ M. Insets show the decay of the optical density at 300 nm and the increase in optical density at 400 nm.

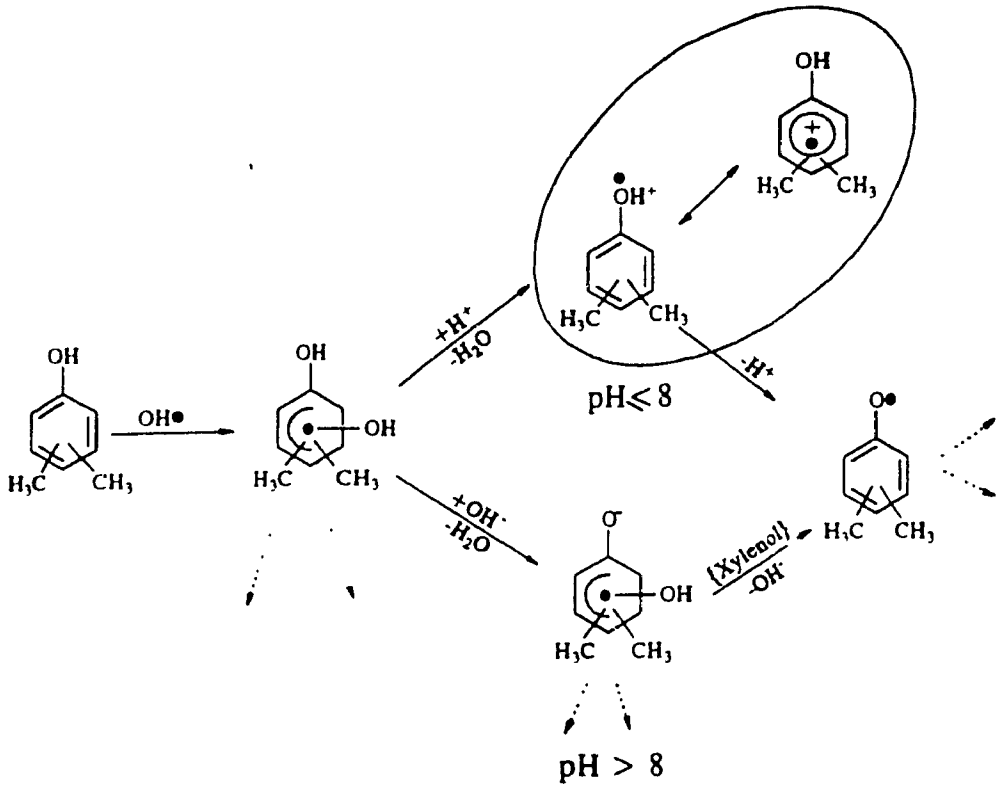


(10.4)

the initial product is a dihydroxycyclohexadienyl radical which then undergoes unimolecular $H_2O$ elimination to form the corresponding phenoxyl radical. Land and Ebert[9] also noted that the $H_2O$ elimination step was catalyzed by both acids and bases with the uncatalyzed rate of elimination being $\leq 10^3\ s^{-1}$. Although no evidence for the formation of phenoxyl radicals from the other five isomers of xylenol was seen in this work, their formation is not precluded as the amounts formed may have been too small to detect. [Taking $\epsilon_{max} \approx 3000\ M^{-1}cm^{-1}$, $1.33 \times 10^{-6}$ M of the phenoxyl radicals would have to form to give an absorbance change of 0.01]. The mechanism depicted above (scheme 10.4) is presumed to apply to all the xylenols examined.

The extinction coefficient at 300 nm of the dihydroxy-3,4-dimethylcyclohexadienyl

radical was obtained from the $OD_0$ at 300 nm (prior to phenoxyl formation): $\epsilon_{300}$= 3030 $\pm$ 200 $M^{-1}$ $cm^{-1}$ giving a value of $k_d \approx$ 1.5 x $10^9$ $M^{-1}$ $s^{-1}$ for the observed second order decay rate constant. The first order component that forms the phenoxyl radical must be small as the observed decay of the •OH-adduct followed good second order kinetics.

The rate constant for •OH addition to 3,4-xylenol was measured as a function of the concentration of 3,4-xylenol which was varied between 1 x $10^{-4}$ and 4 x $10^{-4}$ M: $k_{obs}$ varied between 1.04 x $10^6$ and 3.84 x $10^6$ $s^{-1}$ ($\lambda$=300 nm) giving a rate constant of (9 $\pm$ 1) x $10^9$ $M^{-1}s^{-1}$ for the addition step in scheme 10.4. The kinetics of formation and decay of this •OH-adduct as well as its spectral properties correlate well with those of other •OH-adducts of xylenols reported earlier (see Table 10.4).

### 10.2.2.3 pH Dependence of the Reaction of 3,4-Xylenol with •OH Radicals

The reaction of 3,4-xylenol with the •OH radical was also examined as a function of pH. The pH range was limited to between pH 4 and 10 in order to minimize interference from H• radicals (pH $\leq$ 3) and O• radicals (pH $\geq$ 10) [$pK_a$ (•OH) = 11.9].[18] The data obtained are summarized in Table 10.6. They are divided into two basic groups based on one important observation: in the first pH range (4 < pH < 8), the rate of formation of the phenoxyl radical was independent of the initial concentration of 3,4-xylenol whereas at pH $\geq$ 9 the rate was found to depend on the concentration of 3,4-xylenol (see Figure 10.7). In addition, the formation of the phenoxyl radical from the •OH-adduct could be monitored spectrophotometrically (as per Figure 10.6 for pH 4) for the first group; this was not the case at pH 9 and 10. The spectra at pH 10 are included

**Table 10.6** Data Obtained from the pH Dependence Study of the Reaction of 3,4-Xylenol with •OH.

| 3,4-Xylenol + •OH (300 nm) | | | Phenoxyl Formation(415 nm) | | |
|---|---|---|---|---|---|
| **pH** | **$k_f$ $M^{-1}s^{-1}$ [a]** | | **$k_{obs}$ $s^{-1}$ (fixed dose) [b]** | | **% Conversion to Phenoxyl** |
| 4[c] | $9 \pm 1 \times 10^9$ | | $4.4 \pm 0.2 \times 10^4$ | | 24 %[d] |
| 5 | - | | - | | 19 %[e] |
| 6[f] | $1.1 \pm 0.2 \times 10^{10}$ | | $3.3 \pm 0.4 \times 10^4$ | | 26 %[g] |
| 7 | - | | - | | 39 %[h] |
| 8[i] | $5.1 \pm 0.6 \times 10^9$ | | $4.8 \pm 0.7 \times 10^4$ | | 33 %[j] |
| **pH** | **$k_{obs}$ $M^{-1}s^{-1}$ [k]** | **$k_{ADD}$ $M^{-1}s^{-1}$ [l]** | **$k_{obs}$ $M^{-1}s^{-1}$ [k]** | **$k_{ET}$, $M^{-1}s^{-1}$ [m]** | **% Phenoxyl in Product** |
| 9[n] | $5.6 \pm 0.5 \times 10^9$ | $3.2 \times 10^9$ | $5.4 \pm 0.6 \times 10^9$ | $2.3 \times 10^9$ | 42 %[o] |
| 10[p] | $5.1 \pm 0.6 \times 10^9$ | $3.2 \times 10^9$ | $5.3 \pm 0.5 \times 10^9$ | $2.0 \times 10^9$ | 38 %[q] |

a) Rate constant for the addition of •OH to 3,4-xylenol as determined from a concentration dependence study. b) Observed rate constant at fixed [•OH]. c) [3,4-xylenol] = (1 - 4) x $10^{-4}$ M; $k_{obs}$ = (1.04 - 3.84) x $10^6$ $s^{-1}$; [•OH] = 2.72 x $10^{-6}$ M. d) [3,4-xylenol] = 3 x $10^{-4}$ M; [•OH] = 6 01 x $10^{-6}$ M. e) [3,4-xylenol] = 3 x $10^{-4}$ M; [•OH] = 4.47 x $10^{-6}$ M. f) [3,4-xylenol] = (1 - 3) x $10^{-4}$ M; $k_{obs}$ = (0.915 - 4.15) x $10^6$ $s^{-1}$; [•OH] = 1.83 x $10^{-6}$ M. g) [3,4-xylenol] = 3 x $10^{-4}$ M; [•OH] = 4.34 x $10^{-6}$ M. h) [3,4-xylenol] = 3 x $10^{-4}$ M, [•OH] = 4.26 x $10^{-6}$ M. i) [3,4-xylenol] = (0.5 - 2.5) x $10^{-4}$ M; $k_{obs}$ = (0.831 - 1.51) x $10^6$ $s^{-1}$; [•OH] = 1.62 x $10^{-6}$ M. j) [3,4-xylenol] = 3 x $10^{-4}$ M; [•OH] = 4.29 x $10^{-6}$ M. k) Observed rate constant for the reaction of 3,4-Xylenol + •OH as determined from a concentration dependence study at 300 and 415 nm. l) Rate constant for •OH addition. m) Rate constant for direct electron transfer. n) [3,4-xylenol] = (0.5 - 2.5) x $10^{-4}$ M; $k_{obs}$ = (8.42 - 15.9) x $10^5$ $s^{-1}$; [•OH] = 1.68 x $10^{-6}$ M. o) [3,4-xylenol] = 3 x $10^{-4}$ M; [•OH] = 4.21 x $10^{-6}$ M. p) [3,4-xylenol] = (0.5 - 3) x $10^{-4}$ M; $k_{obs}$ = (7.7 - 22.5) x $10^5$ $s^{-1}$; [•OH] = 1.42 x $10^{-6}$ M. q) [3,4-xylenol] = 3 x $10^{-4}$ M; [•OH] = 4.35 x $10^{-6}$ M. **General Conditions:** All solutions were buffered with $10^{-3}$ M Phosphate buffer and $N_2O$-saturated.

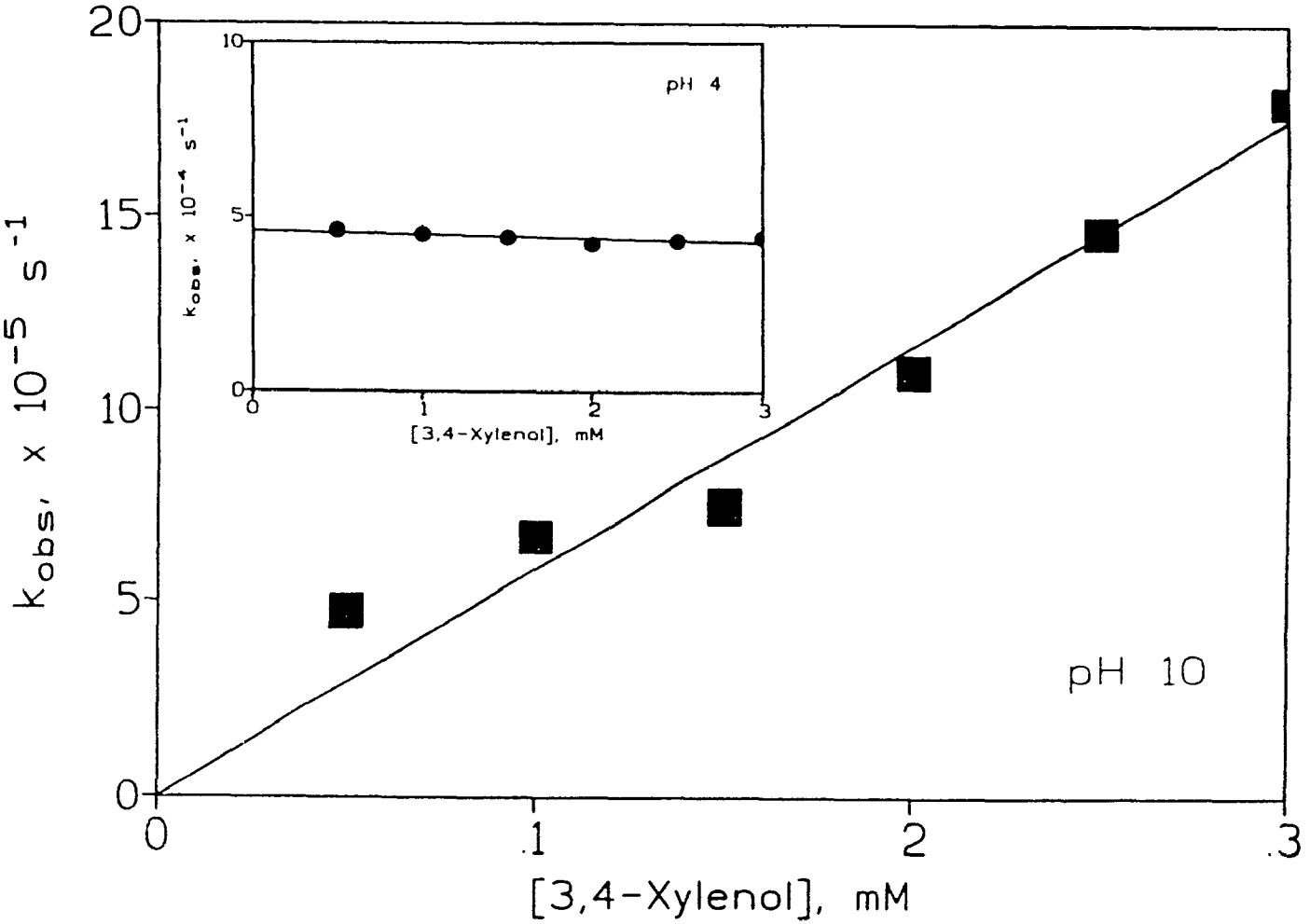


**Figure 10.7** [3,4-Xylenol] dependence of the observed rate constants (415 nm) for the formation of the 3,4-dimethylphenoxyl radical at pH 4 (inset) and pH 10, at constant [•OH]. The solutions were $N_2O$-saturated; [•OH]= 2.72 x $10^{-6}$ M at pH 4; [•OH]= 1.42 x $10^{-6}$ M at pH 10.

in Figures 10.8 and 10.9 to illustrate this point. It can be seen that the long timescale (2 ms) spectrum of the reaction products (3,4-xylenol + •OH) is similar to the one at pH 4 shown earlier (see Figure 10.4) except that the relative quantity of the phenoxyl radical (band at ≈ 410 nm) is greater. By contrast with the observations at pH 4 (Figure 10.6), even at timescales as short as 20 μs (Figure 10.9), there are no indications that the phenoxyl radical originates from the •OH-adduct, as the spectra showed no isosbestic point. Interestingly, the cut-off seems to occur somewhere between pH 8 and 9, i.e. at less than 2 pH units from the $pK_a$ of 3,4-xylenol ($pK_a$ = 10.4).[19]

The following should be noted at this point: the $pK_a$ of the dihydroxy-3,4-dimethylcyclohexadienyl radical is probably ≈ 8, by inference from the work of Draper *et al*[14] who found that the value of the $pK_a$ of the dihydroxy-2,4,5-trichlorocyclohexadienyl radical (4.8) was approximately 2 $pK_a$ units lower in value than the $pK_a$ (= 7.4) of 2,4,5-trichlorophenol. Deprotonation of the •OH-adduct should therefore occur readily at pH > 8. The spectrum of the anion radical could interfere and could have veiled an isosbestic point.

It is therefore proposed that at pH ≤ 8, the reaction of 3,4-xylenol with •OH proceeds via the mechanism described by the lower portion of scheme 10.4. At pH > 8, the reaction could conceivably proceed via either (i) the mechanism of scheme 10.4 with the $H_2O$ elimination step occurring at much faster rates than at pH ≤ 8, or (ii) alternatively the reaction could proceed via ***inner sphere*** electron transfer from the 3,4-dimethylphenoxide anion to the •OH radical, as shown in equation 10.5.

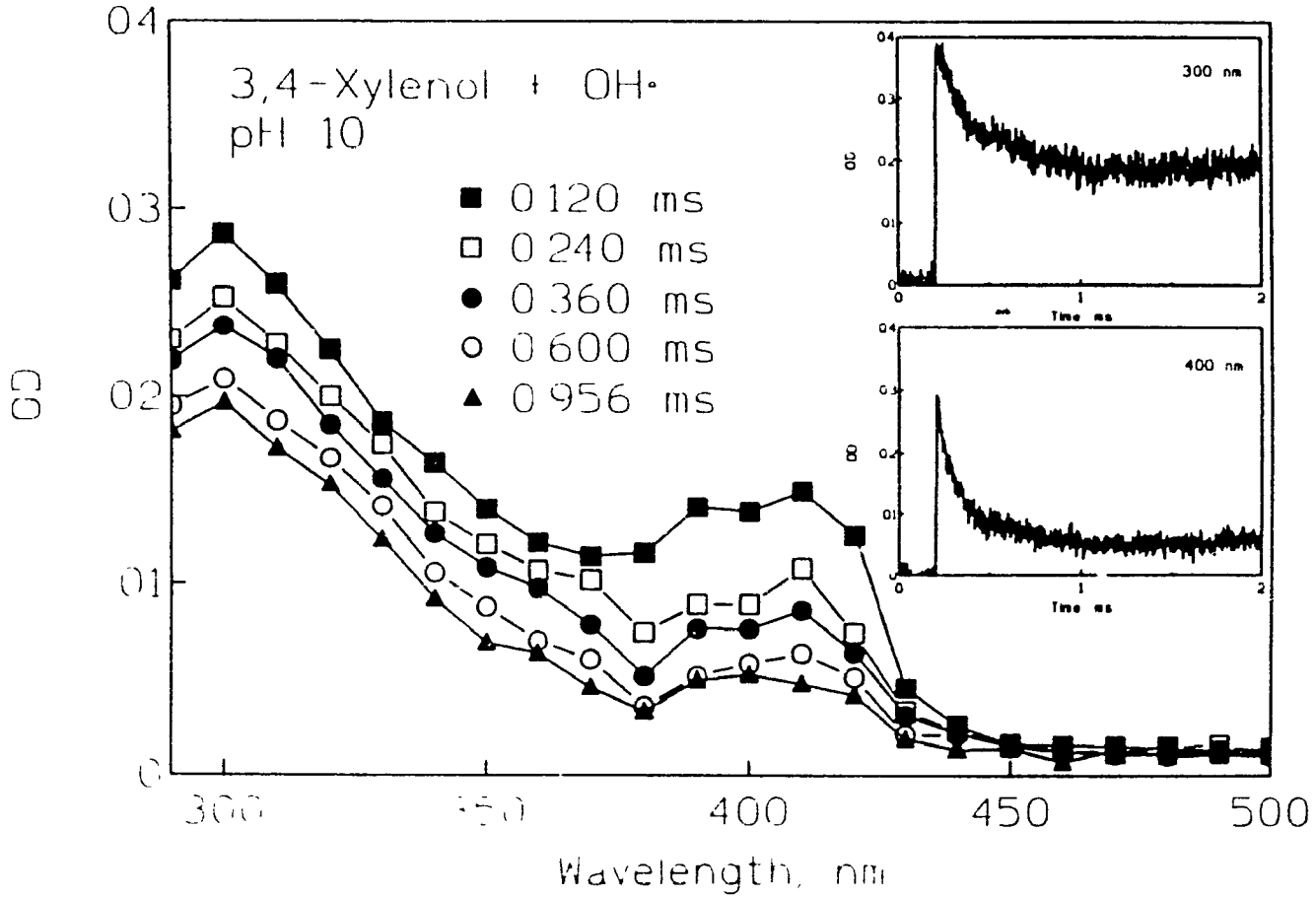


**Figure 10.8** Transient absorption spectra of the reaction product(s) between 3,4-Xylenol and •OH monitored at 0.120, 0.240, 0.360, 0.600 and 0.956 ms following irradiation of a 3 x $10^{-4}$ M aqueous 3,4-Xylenol solution buffered at pH 10. The solution was $N_2O$-saturated; [•OH]= 6.10 x $10^{-6}$ M. Insets show the decay of the optical density at 300 and 400 nm.

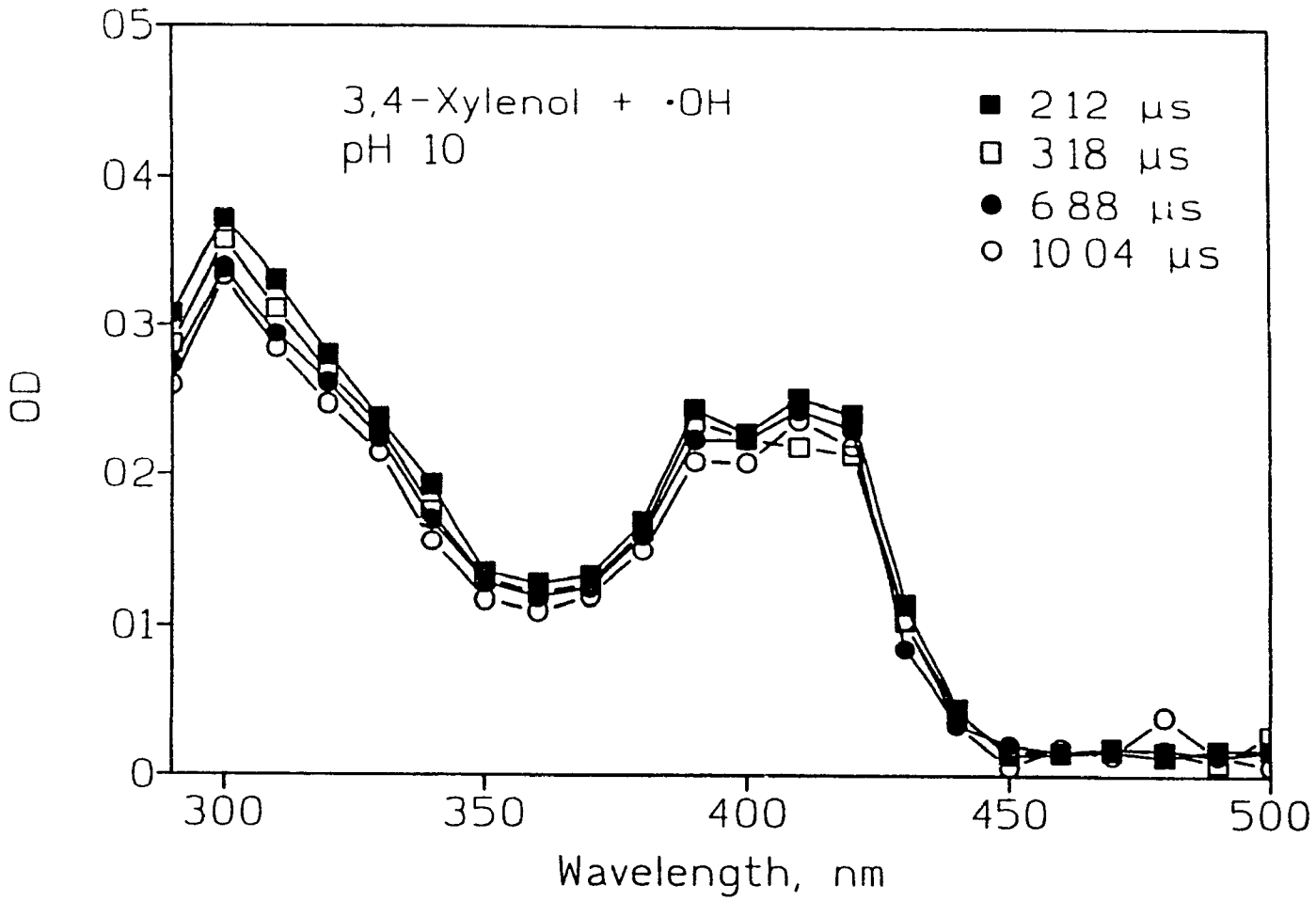


**Figure 10.9** Transient absorption spectra of the reaction product(s) between 3,4-Xylenol and •OH monitored at 2.12, 3.18, 6.88, and 10.04 $\mu$s following irradiation of a 3 x $10^{-4}$ M aqueous 3,4-Xylenol solution buffered at pH 10. The solution was $N_2O$-saturated; [•OH]= 5.97 x $10^{-6}$ M.

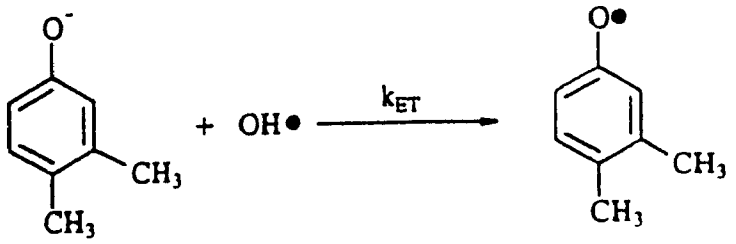


(10.5)

The above mechanism is consistent with the observation that the observed rate of phenoxyl formation was dependent on the initial concentration of 3,4-xylenol. Values of $k_{ET}$ at pH 9 and 10 were calculated and are reported in Table 10.6.

Formation of phenoxyl radicals by direct ***outer sphere*** electron transfer is precluded, owing to a possible unfavourable reorganization energy for the •OH/OH transformation as is known to be the case in homogeneous phase.[20] However, it is not known whether the same rationale applies for surface bound •OH/OH transformation in heterogeneous phase. Electron transfer via an inner sphere transition state, similar to or different from the •OH-adduct, cannot be precluded in homogeneous phase.

## 10.2.3 Reaction with H• Radicals:

### 10.2.3.1 Hydroxy-2,6-dimethylcyclohexadienyl Radical

The time resolved absorption spectra of the H•-adduct of 2,6-xylenol, the product of the reaction of 2,6-xylenol with H• radicals, are shown in Figure 10.10. The spectra are characterized by one absorption maximum at 320 nm. The disappearance of the H•-adduct (320 nm) occurred via second order kinetics, $k/\epsilon\ell = (5.6 \pm 1.0) \times 10^5\ s^{-1}$. The extinction coefficient at 320 nm is $\epsilon_{320} = 2460 \pm 270\ M^{-1}cm^{-1}$, giving a value of (3.5

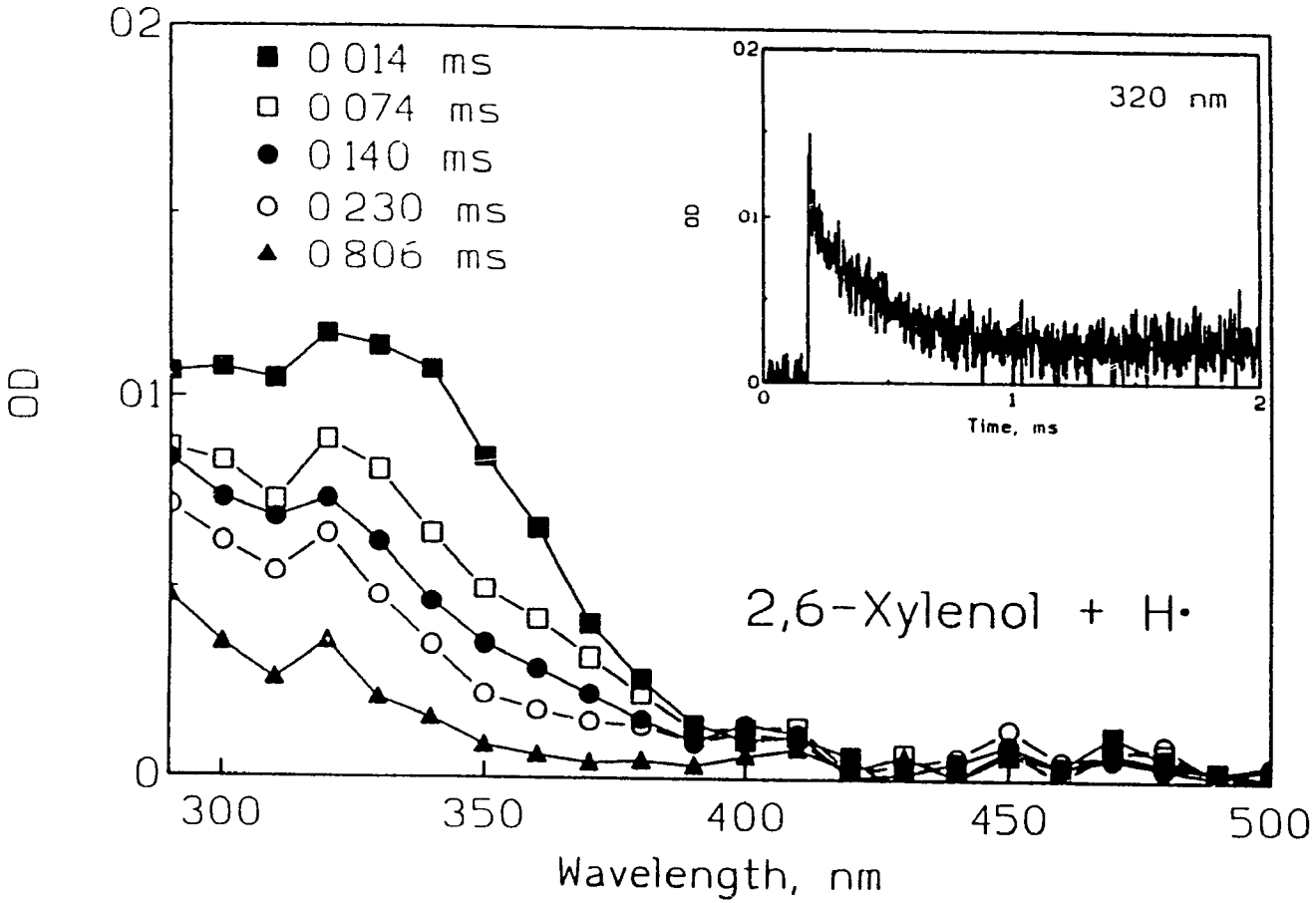


**Figure 10** Transient absorption spectra of Hydroxy-2,6-dimethylcyclohexadienyl radical at 0.014. 0.074, 0.140, 0.230 and 0.806 ms following irradiation of 4 x $10^{-4}$ M 2,6-Xylenol at pH 1 (buffered) in a 0.2 M *tert*-butyl alcohol aqueous solution. The solution was $N_2$-saturated; [H•]= 2.49 x $10^{-6}$ M. The inset shows the decay of the optical density at 320 nm.

$\pm$ 0.7) x $10^9$ $M^{-1}s^{-1}$ for the second order decay rate constant.

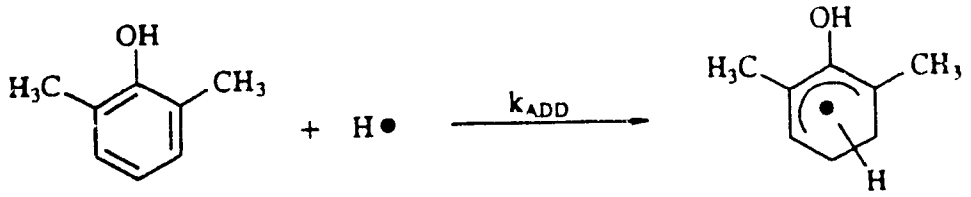


(10.6)

The rate of addition of H• to 2,6-xylenol (equation 10.6) was monitored by observing the increase of the optical density at 320 nm at constant [H•] (2.19 x $10^{-6}$ M), as a function of [2,6-xylenol] over the range from 1 x $10^{-4}$ M to 4 x $10^{-4}$ M; the observed formation rate constant $k_{obs}$ ranging from 3.95 x $10^5$ to 7.4 x $10^5$ $s^{-1}$, gave a bimolecular rate constant for equation 10.6: $k_{add}$ = (1.1 $\pm$ 0.3) x $10^9$ $M^{-1}s^{-1}$. The kinetics of formation and decay of the hydroxy-2,6-dimethylcyclohexadienyl radical as well as its spectral properties correlate well with those of similar compounds (see Table 10.7) and confirm its identity.

## 10.3 CONCLUSIONS

2,6- and 3,4-xylenol react with $N_3$• radicals to form the corresponding dimethyl-phenoxyl radicals (Table 10.1). H• reacts with 2,6-xylenol to form the hydroxy-2,6-dimethylcyclohexadienyl radical (H•-adduct).

Reaction of •OH radicals with 2,3-, 2,4-, 2,5-, 2,6- and 3,5-xylenol yields exclusively the •OH-adducts (dihydroxydimethylcyclohexadienyl radicals) as the initial products (Table 10.4); subsequent $H_2O$ elimination from the •OH-adducts to yield

**Table 10.7** Comparison of the Optical and Kinetic Properties of the hydroxy-2,6-dimethylcyclohexadienyl radical with values published for similar radicals.

| Radical | $\lambda_{max}$, nm | $\epsilon_{max}$, $M^{-1}cm^{-1}$ | $k_f$, $M^{-1}s^{-1}$ | $k_d$, $M^{-1}s^{-1}$ | Ref |
|---|---|---|---|---|---|
| 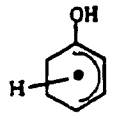 | 330 | 3800 | $1.8 \times 10^9$ | - | 9 |
| 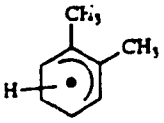 | 328 | 4500 | $2.0 \times 10^9$ | $4.1 \times 10^9$ | 17 |
| 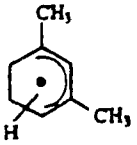 | 326 | 5900 | $2.6 \times 10^9$ | $3.9 \times 10^9$ | 17 |
| | 338 | 4300 | $2.2 \times 10^9$ | $3.6 \times 10^9$ | 17 |
| 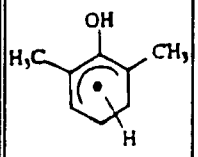 | 320 | 2245 | $1.1 \times 10^9$ | $3.5 \times 10^9$ | a |

a) This work.

phenoxyl or benzyl type radicals has not been ruled out. 3,4-Xylenol reacts with •OH to form both an •OH-adduct and a phenoxyl radical. At pH $\leq$ 8, the 3,4-phenoxyl radical is formed via $H_2O$ elimination from the •OH-adduct; by contrast, at pH $\geq$ 9, both radicals appear to form concurrently. The mechanism of the reaction of 3,4-xylenol with •OH is more consistent with the behaviour of phenol and cresol[9] than with the behaviour of methylated benzenes[17], unlike the other isomers. Thus, the position of the methyl substituents in xylenols bears directly on the reaction mechanism and the nature of the products.

In heterogeneous media ($TiO_2$ dispersions), photo-oxidations may well proceed via analogous pathways even though analysis of intermediate products along the various stages of oxidation would suggest •OH additions to aromatic rings.[1-6] Recent work[7,20] has begun to address the details of these pathways. Direct oxidation by valence band holes and oxidation via •OH radicals may be a moot point as the two pathways cannot be distinguished experimentally in aqueous media.[21]

# REFERENCES


1. Barbeni M., Morello, M., Pramauro, E., Pelizzetti, E., Vincenti, M., Borgarello, E., Serpone, N. *Chemosphere* **1987**, *16*, 1165.

2. Al-Ekabi, H., Serpone, N. *J. Phys. Chem.* **1988**, *92*, 5727.

3. Al-Ekabi, H., Serpone, N., Pelizzetti, E., Minero, C., Fox, M.A., Draper, R.B. *Langmuir* **1989**, *5*, 250.

4. Barbeni, M., Pramauro, E., Pelizzetti, E., Borgarello, E., Serpone, N. *Chemosphere* **1985**, *14*, 195.

5. Minero, C., Aliberti, C., Pelizzetti, E., Terzian, R., Serpone, N. *Langmuir* **1991**, *7*, 928.

6. (a) Okamoto, K., Yamamoto, Y., Tanaka, H., Tanaka, M., Itaya, A. *Bull. Chem. Soc. Jpn.* **1985**, *58*, 1985.
(b) Okamoto, K., Yamamoto, Y., Tanaka, H., Itaya, A. *Bull. Chem. Soc. Jpn.* **1985**, *58*, 2023.

7. Draper, R.B., and Fox, M.A. *Langmuir* **1990**, *6*, 1396.

8. Alfassi, Z.B., Schuler, R.H. *J. Phys. Chem.* **1985**, *89*, 3359.

9. Land, E.J., Ebert, M. *Trans. Faraday Soc.* **1967**, *63*. 1181.

10. Savel'eva, O.S., Shevchuk, L.G., Vysotskaya, N.A., *J. Org. Chem. USSR*, **1972**, *8*, 283-286.

11. Feitelson, J., Hayon, E., *J. Phys. Chem.*, **1973**, *77*, 10.

12. Getoff, N., Solar, S. *Radiat. Phys. Chem. (Int. J. Radiat. Appl. Instrum. Part C)* **1986**, *28*, 443.

13. Getoff, N., Solar, S. *Radiat. Phys. Chem. (Int. J. Radiat. Appl. Instrum. Part C)* **1988**, *31*, 121.

14. Draper, R.B., Fox, M.A., Pelizzetti, E., Serpone, N. *J. Phys. Chem.* **1989**, *93*, 1938.

15. Land, E.J., Porter, G. *Trans. Faraday Soc.* **1963**, *59*, 2016.

16. Atkinson, R., Aschman, S.M., *Int. J. Chem. Kin.*, **1990**, *22*, 59.

17. Sehested, K., Corfitzen, H., Christensen, H.C., Hart, E.J., *J. Phys. Chem.* **1975**, *79*, 310.

18. Buxton, G.V., Greenstock, C.L., Helman, W.P., Ross, A.B., *J. Phys. Chem. Ref. Data*, **1988**, *17*, 513.

19. Serjeant, E.P., Dempsey, B. *"Ionization Constants of Organic Acids in Aqueous Solution"* - IUPAC Chemical Data Series No. 23, Pergamon Press, Oxford, **1979**.

20. Meisel, D., personal communication to Serpone, N., **1992**.

21. Lawless, D., Serpone, N., Meisel, D., *J. Phys. Chem.*, **1991**, *95*, 5166.

# CHAPTER 11

# SONOCHEMICAL OXIDATION OF PHENOL, HYDROQUINONE, CATECHOL, AND BENZOQUINONE IN AQUEOUS MEDIA: KINETIC AND MECHANISTIC ASPECTS

## 11.1 INTRODUCTION

Several photochemical methods have been developed in recent years for the decontamination of polluted waters[1] including the photocatalyzed mineralization of organics discussed in this thesis. Although these methods present good alternatives to more traditional methods for destroying or removing organic pollutants from aquatic ecosystems, such as extraction, ultrafiltration, phase transfer and incineration, they can only be used when the polluted waters are optically clear, enough to allow the passage of light. One alternative to these methods is the use of ultrasounds which can also lead to the decomposition of such undesirable organics in aqueous solutions as phenol,[2,3] *p*-nitrophenol,[4] and others.[5]

Ultrasonic waves in liquids induce certain chemical reactions and accelerate certain reaction rates, not otherwise possible by other means.[5] The reactions are believed to result, directly or indirectly, from acoustic cavitation (formation, growth and implosive collapse of bubbles). Hydrodynamic models suggest a temperature of ca. 5000 K and a pressure of $\approx$ 1000 atm are created during transient cavitation.[5-8] Under such conditions, a molecule from a volatile solvent, or solute at high concentrations, that finds itself within the bubble will undergo pyrolysis. The two principal products resulting from the sonication of water are $H_2O_2$ and $H_2$[5,9] with •OH radicals and H• atoms as the

intermediates; the latter were demonstrated through spin trapping EPR experiments by Riesz and co-workers (equation 11.1).[10]

$$H_2O + ))))) \rightarrow \bullet OH + H\bullet \rightarrow H_2O_2 + H_2 \qquad (11.1)$$

The wide range of oxidation and reduction reactions observed in aqueous sonochemistry are often the result of secondary reactions of the radical intermediates.[5]

The heterogeneously photocatalyzed degradation of phenol in the presence of irradiated aqueous $TiO_2$ suspensions has been studied extensively.[11-15] From the nature of the intermediates detected in these studies, it was inferred that •OH radicals play an important role in the degradation processes. Because •OH radicals play a role in photodegradation reactions, and the fact that the •OH radical can also be generated sonochemically, the sonochemical oxidation of phenol, first reported by Zechmeister *et al*,[16] Lur'e,[2] and subsequently, by Chen and co-workers,[3] has been re-examined under conditions different from those reported earlier.

The aim of the present study was to probe the sonodegradation of phenol towards a more quantitative and mechanistic understanding of the sono-induced oxidative transformation process. In this regard, each of the aromatic intermediate products formed, notably hydroquinone, catechol, and *p*-benzoquinone, detected during the course of the reaction were also examined. In most cases, the reactions proceed via zero-order kinetics. A simple description of the events leading to the observed intermediate products is given. The results are consistent with the notion that the •OH radicals oxidize the organic substrates.

## 11.2 SONOCHEMICAL OXIDATION OF PHENOL

Ultrasonic irradiation (50 Watts/cm$^2$) of a 100 mL air-equilibrated aqueous solution of phenol (pH 3; 68 $\mu$M) resulted in a zero-order decrease (k = 0.10 $\mu$M/min) of the concentration of phenol and the first-order appearance and subsequent zero-order decomposition of hydroquinone (HQ), catechol (CC) and *p*-benzoquinone (BQ) (Figure 11.1a). The quantity of HQ and CC evolved simultaneously: $\approx$ 14 $\mu$M after about 8 hr of sonication. The maximum concentration of BQ, ca. 17 $\mu$M, was reached after $\approx$ 5 hr. When the sonolysis was carried out at pH 5.7, phenol (51 $\mu$M) also decomposed via zero-order kinetics (k = 0.081 $\mu$M/min) and only HQ and CC were detected but at lower concentrations (Figure 11.1b): ca. 10.5 $\mu$M after $\approx$ 8 hr and $\approx$ 6.5 $\mu$M after ca. 6 hr, respectively. All intermediates observed in the course of the sonochemical oxidation of phenol at pH 3 and 5.7 formed via first-order and decayed via zero-order kinetics. Tables 11.1 and 11.2 summarize some of the kinetic data under various conditions. The zero-order sonodegradation of phenol was also carried out at pH 12. The degradation was slower at this pH than at pH 3 and 5.7 (Figure 11.2); in addition, neither HQ, CC, nor BQ were detected under these conditions.

## 11.3 SONOCHEMICAL OXIDATION OF INTERMEDIATES

The sonochemical fate of HQ, BQ and CC at pH 12 could not be determined as the compounds are unstable at this pH. (They rapidly react to yield intensely colored solutions). This may explain why none of these compounds were detectable during the sono-induced oxidative decomposition of phenol at pH 12. The sonochemical oxidation

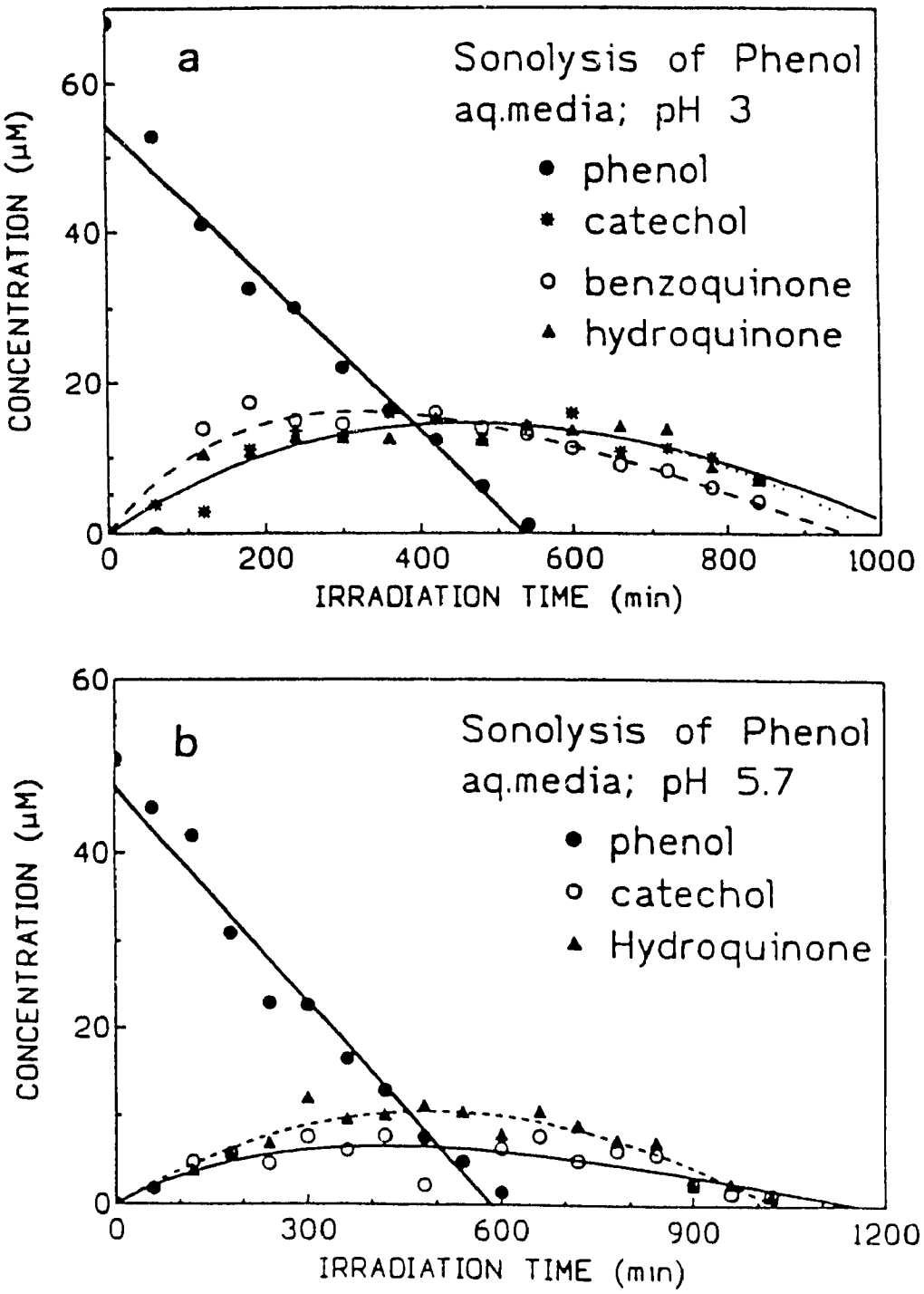


**Figure 11.1** a) Plot of concentrations as a function of sonoirradiation time showing the degradation of phenol, $[phenol]_{ini}$ = 68.1 $\mu$M, and the formation and degradation of the three intermediates observed: hydroquinone, catechol and *p*-benzoquinone. Other conditions: air-equilibrated aqueous media, pH 3, 20 kHz, and 50 Watts power.
(b) Similar observations but at pH 5.7; [phenol] = 50.8 $\mu$M. Note that BQ was not observed under these conditions.

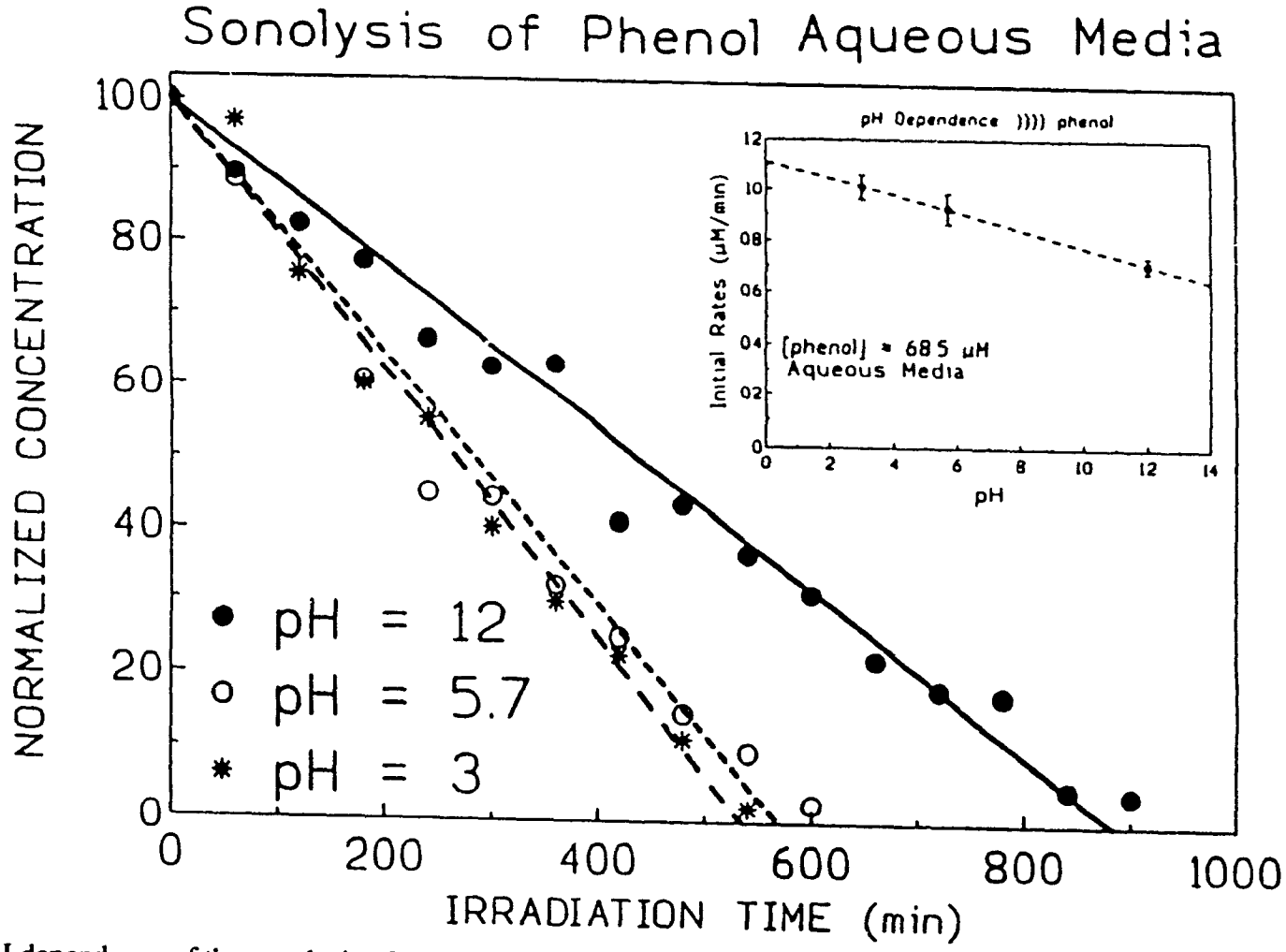


**Figure 11.2** pH dependence of the sonolysis of phenol. The inset illustrates the linear dependence of the initial rates of disappearance of phenol on pH. Other conditions as in Figure 11.1; [phenol] = 68.5 $\mu$M.

**Table 11.1** Summary of Sonolysis Rate Data in Aqueous Media at pH 3 (power, 50 Watts)

| Compound, ($[]_{in}$, $\mu$M) | $k_d$ ($\mu$M/min)[a] | Intermediates | $k_f$ ($min^{-1}$)[b] | $k_d$ ($\mu$M/min)[a] |
|---|---|---|---|---|
| Phenol (68.1) | 0.10 ± 0.005 | Catechol<br>Hydroquinone<br>*p*-Benzoquinone | ≈ 0.001<br>≈ 0.001<br>≈ 0.005 | ≈ 0.1<br>≈ 0.08<br>≈ 0.04 |
| Catechol (53.8) | 0.054 ± 0.002 | - | - | - |
| Hydroquinone (43.7) | 0.050 ± 0.003 | *p*-Benzoquinone<br>Intermediate 5.1 | ≈ 0.05<br>≈ 0.01 | ≈ 0.04<br>(≈ 0.01 $min^{-1}$) |
| *p*-Benzoquinone (42.7) | 0.23 ± 0.07 | Hydroquinone<br>Intermediate 5.1 | ≈ 0.009<br>(Trace quantities) | ≈ 0.07<br>- |

a) Zero-order decay kinetics.
b) First-order kinetics of formation.

**Table 11.2** Summary of Sonolysis Rate Data in Aqueous Media at other pH's (power, 50 Watts)

| Compound, ($[]_{ini}$, $\mu$M) | pH | $k_d$ ($\mu$M/min)[a] | Intermediates | $k_f$ ($min^{-1}$)[b] | $k_d$ ($\mu$M/min)[a] |
|---|---|---|---|---|---|
| Phenol (50.8) | 5.7 | 0.081 $\pm$ 0.005[c] | Catechol<br>Hydroquinone | $\approx$ 0.002<br>$\approx$ 0.0005 | $\approx$ 0.02<br>$\approx$ 0.15 |
| Phenol (68.7) | 12 | 0.071 $\pm$ 0.003 | None detected | - | - |
| Catechol (47.3) | 5.4 | (0.0034 $\pm$ 0.0001 $min^{-1}$) | Intermediate 5.1 | $\approx$ 0.015 | ? |
| Hydroquinone (37.1) | 5.4 | 0.076 $\pm$ 0.005 | Intermediate 5.1 | $\approx$ 0.006 | ($\approx$ 0.006 $min^{-1}$) |
| *p*-Benzoquinone (47.9) | 5.6 | (0.018 $\pm$ 0.003 $min^{-1}$) | Hydroquinone<br>Intermediate 5.1 | $\approx$ 0.03<br>(Trace quantities) | $\approx$ 0.05<br>- |

a) Zero-order decay kinetics.
b) First-order kinetics of formation.
c) Corrected $k_d$ for 68.5 $\mu$M is 0.093 $\pm$ 0.006 $\mu$M/min

of HQ, BQ and CC was carried out at other pH's and the results obtained are presented below.

The sonolysis of hydroquinone (44 $\mu$M; pH 3) takes place via zero-order kinetics (Figure 11.3a): k = 0.050 $\mu$M/min; two intermediate species were detected: *p*-benzoquinone and a species whose retention time was 5.1 min under the HPLC conditions used; this species is believed to be hydroxy-*p*-benzoquinone. The first-order formation of BQ was faster than the formation of the latter intermediate (0.05 *versus* 0.01 $min^{-1}$, Table 11.1). While BQ degraded via a zero-order path, the intermediate 5.1 transformed via first-order kinetics.

Benzoquinone (43 $\mu$M, pH 3) also sonochemically transformed in aqueous media via a zero-order path in a relatively short time: ca. 3 hr and k $\approx$ 0.23 $\mu$M/min. The major aromatic intermediate detected was hydroquinone (ca. 25 $\mu$M after $\approx$ 3 hr); small traces of the intermediate 5.1 were also observed (Figure 11.3b). The formation of *p*-benzoquinone from the sonolysis of hydroquinone, and the appearance of HQ from the corresponding sonolysis of *p*-benzoquinone find relevance in the primary radicals formed by the sonolysis of water (equation 11.1; see below). Note the presence of the intermediate 5.1 in both cases (Figures 11.3a and 11.3b).

The sonolysis of catechol in air-equilibrated acidic aqueous media occurred via zero-order kinetics (pH 3, 54 $\mu$M; k $\approx$ 0.054 $\mu$M/min) and produced no intermediates detectable by the HPLC techniques. By contrast, when the sonolysis was done at pH 5.4, the catechol disappeared via excellent first-order kinetics (Figure 11.4a; k = 3.4 $\pm$ 0.1 x $10^{-3}$ $min^{-1}$) and traces of the intermediate 5.1 were also seen. Under otherwise identical

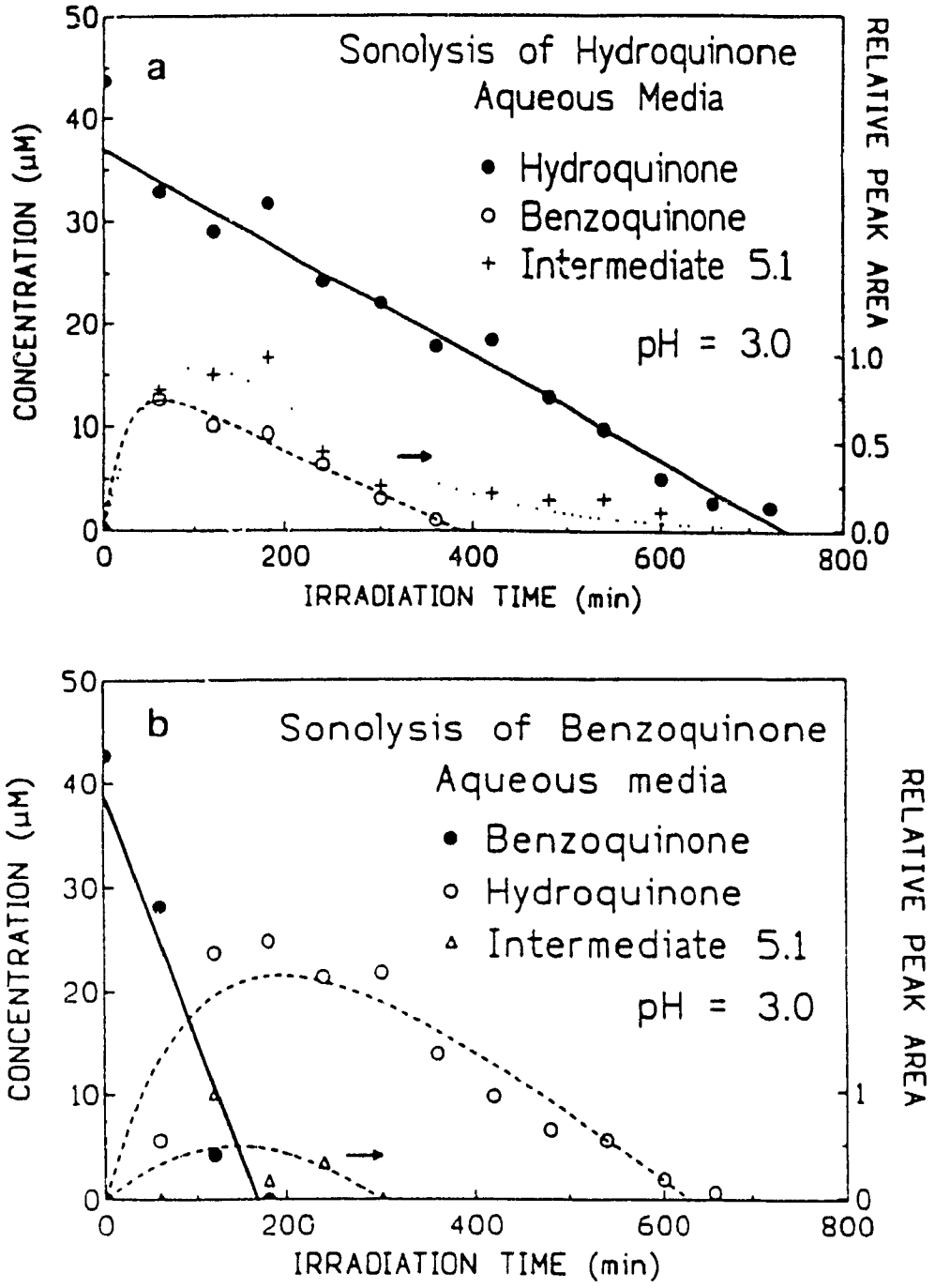


**Figure 11.3** (**a**) Sonolysis of hydroquinone in air-equilibrated aqueous media at pH 3 and 50 Watts power; [HQ] = 43.7 $\mu$M. Plot also shows the formation and disappearance of BQ and the intermediate whose retention time was 5.1 min. under the HPLC conditions used. Other conditions as in Figure 11.1. (**b**) Sonolysis of *p*-benzoquinone (42.7 $\mu$M) as a function of irradiation time (50 Watts power). Other conditions as in Figure 11.1.

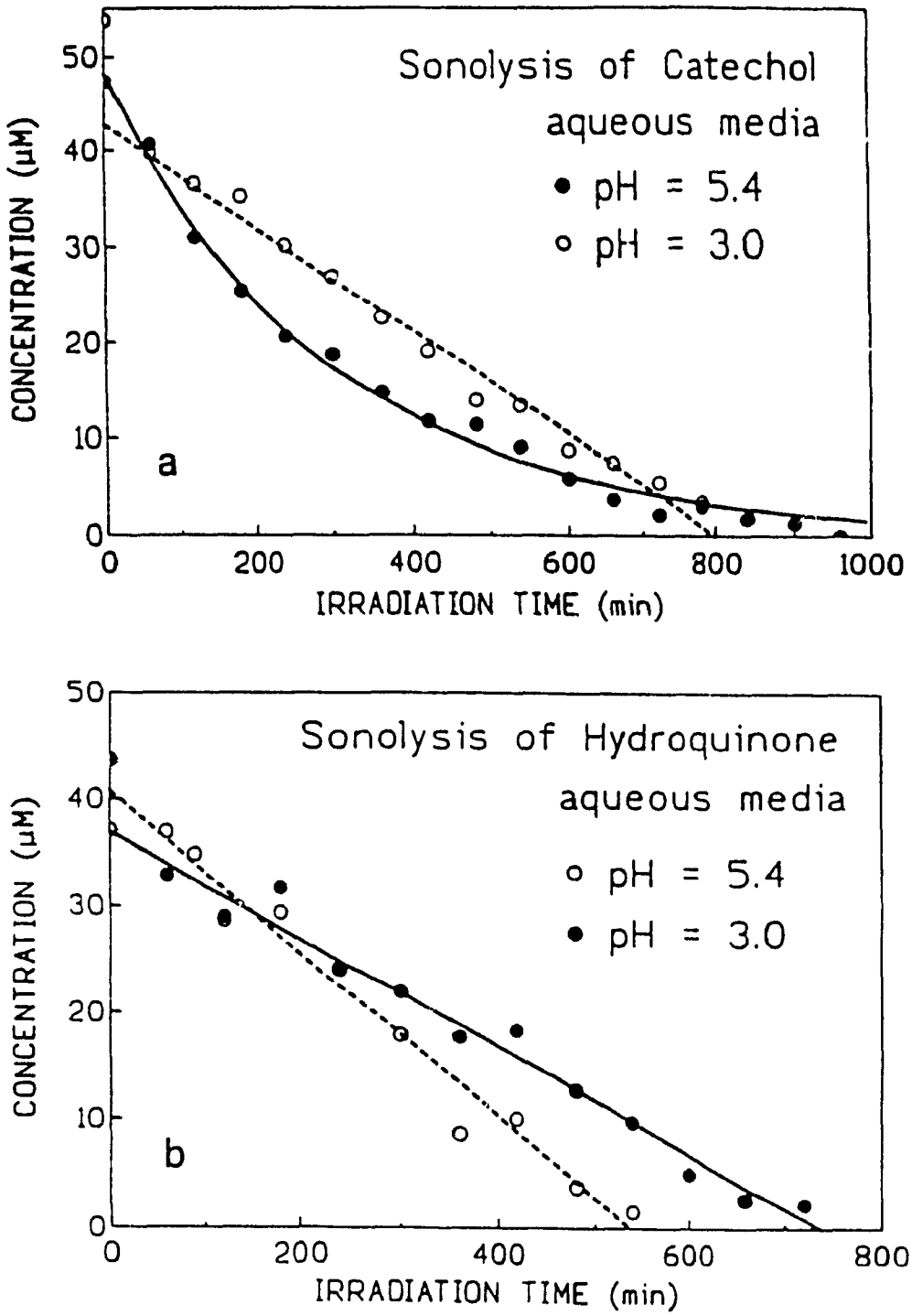


**Figure 11.4** (**a**) pH dependence of the sonolysis of catechol. Other conditions as in Figure 11.1 and in Tables 11.1 and 11.2. (**b**) pH dependence of the sonolysis of hydroquinone. Other conditions as in Figure 11.1 and in Tables 11.1 and 11.2.

conditions, hydroquinone (37 $\mu$M) sonochemically transformed via zero-order kinetics in air-equilibrated aqueous media at pH 5.4 (Figure 11.4b; k $\approx$ 0.076 $\mu$M/min); only the intermediate 5.1 was observed. At pH 5.6, the sonolysis of BQ (k = 0.018 $\pm$ 0.003 $min^{-1}$) gave hydroquinone as the major intermediate product, together with trace quantities of the intermediate 5.1.

## 11.4 TOTAL ORGANIC CARBON DETERMINATION

To examine whether sonodegradation of phenol led to its mineralization to carbon dioxide, as demonstrated by heterogeneous photocatalysis methods in titania suspensions,[9-13] the quantity of total organic carbon remaining in a solution of phenol was determined initially ($[Phenol]_{ini}$= 75 $\mu$M; pH 12) and at various stages to ca. 12 hours of insonation. During this period, the TOC analyses showed little, if any, variation with time indicating no loss of total organic carbon, even though phenol and the intermediate products had degraded.

## 11.5 POWER DEPENDENCE

Figure 11.5a illustrates the power dependence of the sonolysis of phenol (100 $\mu$M) in air-equilibrated aqueous media at pH 3 for 25, 50, and 75 Watts/cm. It is noteworthy that while the decrease of [phenol] follows zero-order kinetics at 25 and 50 Watts, the sonolysis occurs via first-order kinetics at 75 Watts power. This notwithstanding, the sonolysis of phenol is linearly dependent on the power, increasing with increasing power (Figure 11.5b).

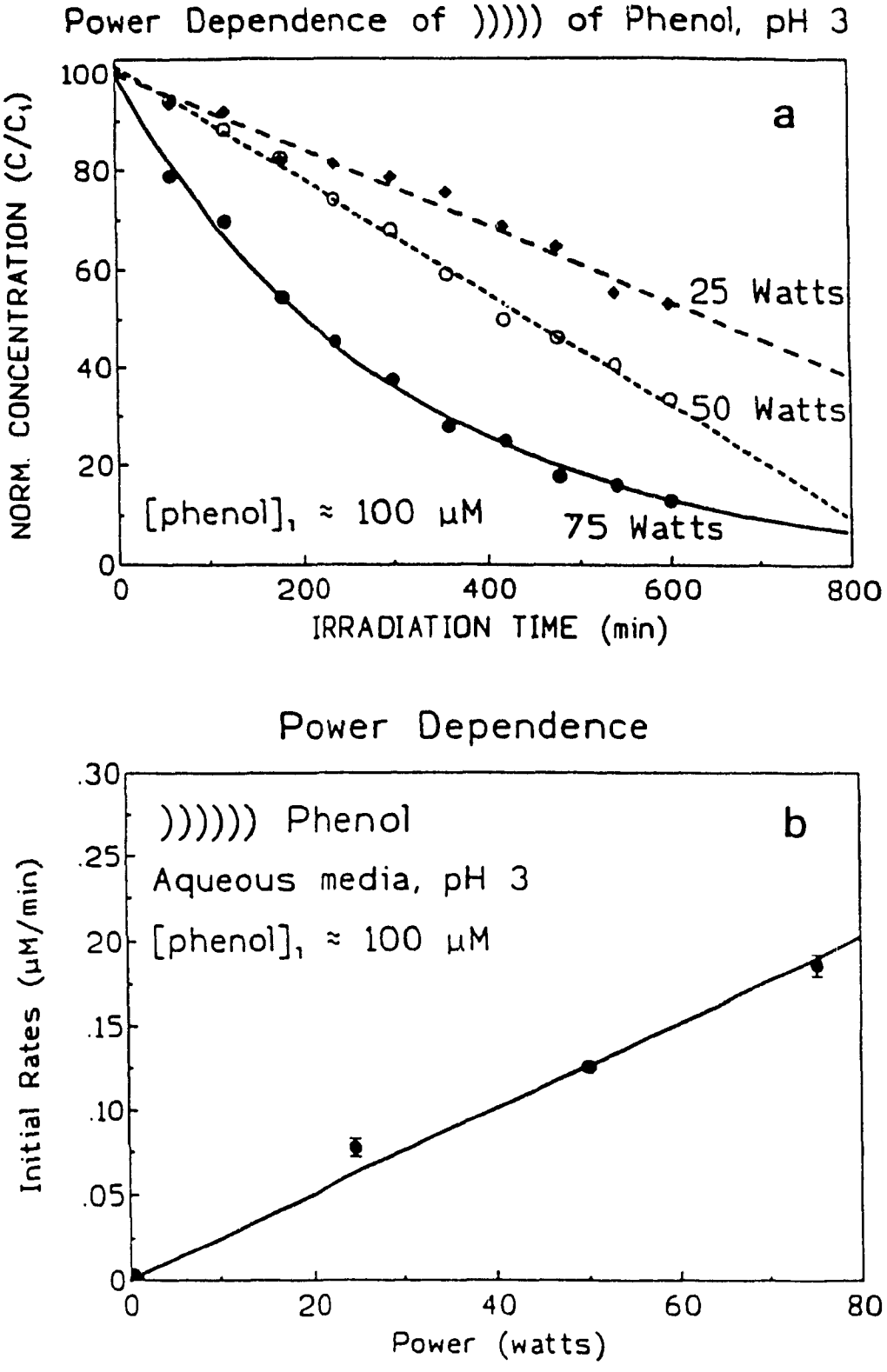


**Figure 11.5** (a) Power dependence in the sonolysis of phenol, 100 $\mu$M, as a function of time in air-equilibrated aqueous media at pH 3. (b) Initial rates *versus* power in the sonodegradation of phenol. Other conditions as in Figure 11.5a.

## 11.5 SONO-OXIDATIVE DECOMPOSITION OF PHENOL - INTERPRETATION OF RESULTS

Ultrasounds accelerate many otherwise known reactions and initiate formation of novel compounds.[17] When used less discriminately, ultrasounds can be used to degrade environmental contaminants in wastewaters and drinking waters, ideally to $CO_2$ and water, or at least to compounds far less toxic than the original substrates. The destruction of pollutants using ultrasounds alone or in combination[18] with another technique (e.g., photochemistry) might be potentially useful in the detoxification of contaminated effluents. The relative number of studies in the environmental area has been rather small.[19]

The early work of Zechmeister and coworkers[16] showed that mixtures of halobenzene, halothiophene, and halofuran in a silver nitrate solution and irradiated with ultrasounds yield silver acetylide as the major intermediate. Other aromatic and heterocyclic rings can be cleaved with ultrasounds, with decompositions occurring even in the absence of silver ions.[16] Insonation of phenol in an alkaline medium under an argon atmosphere yields only trace amounts of acetylene.[20]

By contrast to water, substrates in an aqueous system are not directly affected by the cavitational collapse, but rather react with the decomposition products of water (equation 11.1). Although solutes present in relatively high concentration may undergo pyrolysis within the gas bubble, dilute inorganic or organic solutes, typically used in sonochemical reactions, possess much lower vapour pressures than water; they are therefore unable to diffuse into the cavitation bubble and are thereby unaffected by the

intense high temperatures and pressures generated by the cavitational collapse. Instead, these solutes may be pyrolysed at the cooler ( $\approx$ 2000° K) interface and/or may react with the species emanating from the pyrolysis of the solvent (here, water), such as •OH and/or H• radicals formed at the interface, depending on the prevailing gaseous atmosphere.[19] It is these secondary reactions, therefore, that will dominate in aqueous media. Some of the radicals may also escape into the bulk solution and react with the solutes.[21]

Insonation of an air-equilibrated aqueous solution of phenol at pH 3 and at 50 Watts/cm$^2$ leads to the quantitative oxidative conversion of phenol (Figure 11.1) in about 9 hr into three major intermediate species: catechol, hydroquinone, and *p*-benzoquinone. Other products are also possible (pyrogallol, resorcinol), but undetected in the present work, together with 2-cyclohexen-1-ol and/or cyclohexanone produced from the reductive process mediated by the H• radical.[22] Formation and detection of these necessitated relatively high concentrations of phenol, $\approx$ 53 to 160 mM and insonation for ca. 16 to 20 hours.[22] Sonication under otherwise identical conditions of the three major intermediate species, as well as at other pH's, yield hydroxy-p-benzoquinone (believed to be *the intermediate 5.1*) in trace quantities. More remarkable, insonation of hydroquinone yields p-benzoquinone, while irradiation of the latter yields the reduced product hydroquinone. Both oxidative and reductive processes operate during insonation in aqueous media. This calls attention to and confirms the presence of oxidizing (•OH) and reducing (H•) radicals. At pH 12, neither HQ, CC, or BQ were detected from the insonation of phenol under the conditions used. The intermediates were not examined at

pH 12 as the solutions rapidly became intensely colored.

The cause for the slower sono-oxidation of phenol in alkaline media is worth considering (see Figure 11.2 and compare the data from Tables 11.1 and 11.2). At pH 12, phenol exists as the negatively charged phenoxide ion ($pK_a \approx 10$). To the extent that the gas bubble/liquid interface is hydrophobic,[23] charged species are poised away from the interfacial region relative to their neutral counterparts; the concentration of solvent radicals is highest at the interface. Thus, phenol is more easily oxidized at acidic pH's. Similarly, the sono-oxidation of pyridine[20] is facilitated in alkaline media, since in acidic solutions pyridine exists as the pyridinium cation.

With the experimental set-up used, the possible formation of carbon dioxide could not be detected. The temporal variation of total organic carbon was examined for the insonation of an alkaline phenolic solution at pH 12. Within experimental error, no loss of TOC was observed for 12 hours of ultrasonic irradiation, even though both the phenol and the aromatic intermediates had been transformed (ring cleaved), presumably to species of higher oxygen-to-carbon ratios. The present findings confirm the earlier observations by Chen and Smith[22] who also noted less than 2-3% loss of TOC and find precedence in the work of Currell and coworkers.[20] Thus, although most of the phenol in solution is converted into compounds of higher oxidation states, only a small fraction must be converted to carbon dioxide. Oxidation reactions are almost completely suppressed by the strong reducing ability of the H• radical,[23] unless a scavenger (e.g., air oxygen) is present to attenuate the reductive process(es). The analysis of these high oxygen-to-carbon ratio compounds was not pursued further, but no doubt they are

complex aliphatic species. Formation of the ultimate oxidation product, carbon dioxide, would have necessitated a pure oxygen atmosphere.[20] The atmosphere under which phenol is insonated determines whether the end product will be acetylene (argon, nitrogen, air, helium) or carbon dioxide (oxygen, ozone).[19] In this regard, it is noteworthy that acetylene is rapidly converted by ultrasounds to a variety of end-products under an argon atmosphere: $H_2$, CO, $CH_4$, a variety of non-aromatic hydrocarbons containing 2 to 8 carbons {$C_5H_4$, $C_5H_6$, $C_6H_2$, $C_6H_4$, $C_6H_5$, $C_6H_6$, and $C_7H_8$}, formic and acetic acids, formaldehyde, acetaldehyde, benzene, phenyl-acetylene, styrene, naphthalene, and water-insoluble soot.[24]

## 11.6 KINETIC ASPECTS

To describe the kinetic events during the ultrasonic irradiation, it is relevant to develop a rate expression from a simple scheme which assumes that the oxidative decomposition of phenol (and those of the intermediates HQ, CC, and BQ) results principally by its interaction with the •OH radicals produced during the cavitational collapse. A simple description of the events is summarized by equations 11.2-11.5. Following the formation of •OH and H• radicals, these can recombine or may lead to the products $H_2O_2$ and $H_2$, respectively, together with their being scavenged by organic solutes (phenol, HQ, CC, BQ) present at or near the interface.

$$H_2O + ))))) \underset{k_{-1}}{\overset{k_1}{\rightleftarrows}} \bullet OH + H\bullet \qquad (11.2)$$

$$\bullet OH + \bullet OH \xrightarrow{k_2} H_2O_2 \qquad (11.3)$$

$$\bullet H + \bullet H \xrightarrow{k_3} H_2 \qquad (11.4)$$

$$\bullet OH + Phenol \xrightarrow{k_4} Products \qquad (11.5)$$

The rate of conversion of phenol (or other substrates) is given by:

$$Rate = -\frac{d[Phenol]}{dt} = k_4[\bullet OH][Phenol] \qquad (11.6)$$

Using the steady-state condition for production of •OH and H• radicals under continuous insonation, we have

$$[\bullet OH] = \frac{k_1[H_2O]P}{k_{-1}[H\bullet] + k_2[\bullet OH] + k_4[Phenol]} \qquad (11.7)$$

and since [•OH] = [•H] from reaction 11.2

$$[\bullet OH] = \frac{k_1[H_2O]P}{(k_{-1} + k_2)[\bullet OH] + k_4[Phenol]} \qquad (11.8)$$

where P denotes the power of the insonation source { ))))) in equation 11.2}. Since both $H_2O_2$ and $H_2$ have been observed to form under similar conditions in the sonolysis of water, it is likely that $k_2 > k_1$, that is the reverse of equation 11.2 is slower than 11.3.

Thus the rate of loss of phenol as a function of insonation time (equation 11.9) is:

$$Rate = \frac{k_1 k_4 [Phenol] P}{k_2 [\bullet OH] + k_4 [Phenol]} \qquad (11.9)$$

At low concentrations of phenol, i.e., $k_2[\bullet OH] > k_4[\text{phenol}]$, and at constant power P, the rate of loss of phenol should follow first-order kinetics with respect to phenol concentration, while at high [phenol], where $k_2[\bullet OH] < k_4[\text{phenol}]$, the rate should follow zero-order kinetics at constant power P. Both these expectations are verified in the present study (see Figures 11.2-11.4). In most cases, zero-order kinetics are observed, except for catechol which is sonochemically oxidized via first-order kinetics at pH 5.4. Moreover, equation 11.9 shows that for constant concentration of phenol, the rate should increase linearly with increase in the insonation power P (see Figure 11.5b).

Contrary to the zero-order kinetic behaviour at 25 and 50 Watts/cm$^2$ (Figure 11.5a), the sono-oxidation of phenol occurs via excellent first-order kinetics at 75 Watts/cm$^2$. No doubt the higher power must alter the interface and consequently the relative concentration of the solute at the interface, in a manner such that $k_2[\bullet OH] > k_4[\text{phenol}]$; alternatively, the higher power increases [•OH] and increases $k_2$ of equation 11.3 faster than $k_4$. The interface is sensitive to variations in both the solution medium (changes in pH) and in the insonation power.

Where $k_2[\bullet OH] < k_4[\text{phenol}]$, equation 11.9 simplifies to Rate = $k_1$P. Hence for constant power P, the values $k_d$ in Table 11.1 (second column) for the conversion of phenol, CC, HQ, and BQ reflect the formation of the free radicals of equation 11.2. The corresponding pseudo first-order constants are 0.0015 min$^{-1}$ (phenol), 0.0010 min$^{-1}$ (HQ),

0.0011 $min^{-1}$ (CC), and 0.0054 $min^{-1}$ (BQ); note the consistency of these values with the first-order rate constants $k_f$ of Table 11.1 (fourth column). The variation between the values for phenol, HQ, and CC (average = 0.0012 $\pm$ 0.0003 $min^{-1}$) with that for BQ suggests that reaction (reduction) of the hydrophobic *p*-benzoquinone may have three possible origins: (i) scavenging of H• by BQ occurs at the hydrophobic interface while the hydrophillic substrates react in the solution bulk where the concentration of radicals is lower; (ii) the reduction of BQ by H• is more efficient than oxidation of phenol, HQ, or CC; and (iii) because BQ is hydrophobic and therefore more likely to be poised at the bubble/liquid interface, it may undergo pyrolysis in addition to H• atom scavenging. Our data preclude a choice between the three possibilities. From the data illustrated in Figure 11.5b, it is deduced that the rate of formation of the solvent radicals $k_i$ is 2.7 $\pm$ 0.3 x $10^{-5}$ $min^{-1}$.

## 11.7 MECHANISTIC ASPECTS

Following the pathway summarized by equations 11.2-11.4, Scheme 11.10 illustrates the steps in the oxidation (and reduction of BQ) of phenol. Thus, attack of this solute by •OH radicals yields the dihydroxycyclopentadienyl radical[25] (the •OH adduct), by analogy with our observations on xylenols (see Chapter 10), which can subsequently decay to give catechol and hydroquinone; the *p*-benzoquinone is formed subsequent to formation of the semiquinone radical.[26] *p*-Benzoquinone also forms from the sono-oxidation of hydroquinone, which may also be produced from in turn from *p*-benzo-quinone via a reductive process with H• radicals. Further oxidation of HQ, CC, and BQ

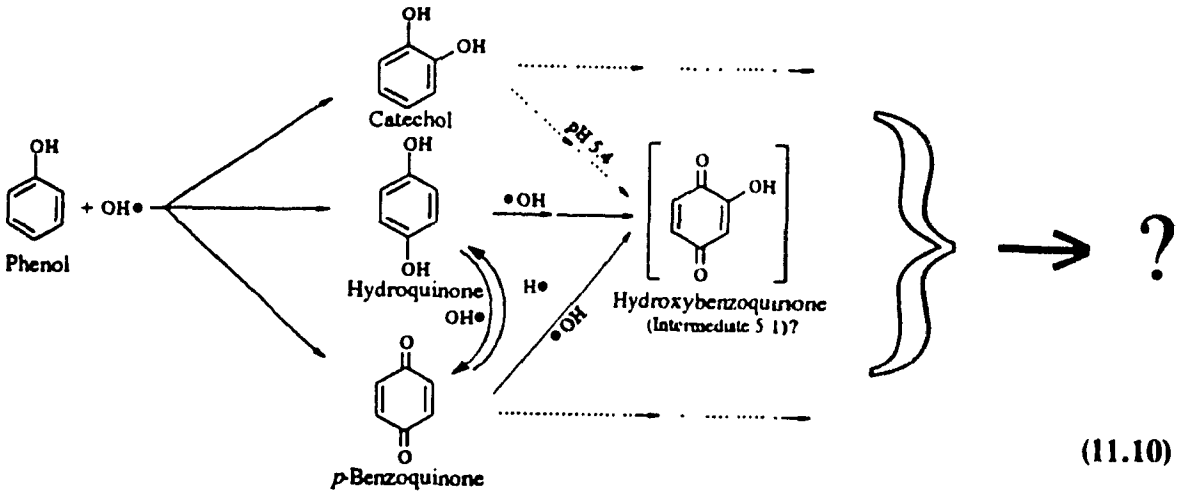


(11.10)

by •OH radicals probably yields hydroxy-p-benzoquinone, whose ultimate immediate fate remains elusive. We can only speculate that the ring will cleave to produce a variety of aliphatics with higher oxygen-to-carbon ratios. The absence of loss of TOC reported here and earlier[22] (though different conditions were used) must indicate that the presence of both an oxidizing and a reducing radical suppresses somewhat, or at least considerably retards the ultimate mineralization of the substrates examined.

## 11.8 CONCLUDING REMARKS

The sonochemical oxidation of phenol was examined in air-equilibrated aqueous media at various pH's and at various insonation powers. Its disappearance follows zero-order kinetics at $[\text{phenol}]_{\text{initial}} \approx 30$ to 70 $\mu$M. Three principal intermediate species formed at pH 3: catechol (CC), hydroquinone (HQ), and *p*-benzoquinone (BQ); at natural pH (5.4-5.7) only catechol and hydroquinone formed. No intermediate species were detected at pH 12 under the conditions used. The sonochemical fate of CC, HQ, and BQ was also examined at pH 3 and at natural pH's. At pH 3, BQ is the major species formed

during insonation of HQ, while HQ is produced during insonation of BQ. In both cases, an additional intermediate formed in trace quantities that has been tentatively identified as hydroxy-*p*-benzoquinone. These same intermediate species have been identified in the heterogeneous photocatalyzed oxidation of phenol in irradiated titania suspensions. The present results confirm the important role of •OH radicals in degradation processes. Although $CO_2$ is the ultimate product in heterogeneous photocatalysis, irradiation of a phenolic aqueous solution by ultrasounds showed no loss of total organic carbon (TOC) after several hours, even though the aromatic substrate and the intermediates had degraded. A simple kinetic model/scheme has been proposed to account for the events in the conversion of the substrates to products. It is argued that the hydrophobic *p*-benzoquinone reacts with •OH and H• radicals at the hydrophobic gas bubble/liquid interface, while the hydrophillic species (phenol, CC, and HQ) react, to a large extent, with the •OH radicals in the solution bulk.

# REFERENCES


1. Ollis, D.F., Pelizzetti, E., Serpone, N., in *"Photocatalysis - Fundamentals and Applications"*, Serpone, N. and Pelizzetti, E., Eds., Wiley-Interscience, New York, **1989**, pp. 603-637.

2. Lur'e, Y.Y., *Russ. J. Phys. Chem.*, **1963**, *37*, 1264.

3. Chen, J.W., Chang, J.A., Smith, G.V., *Chem. Eng. Prog. Symp. Ser.*, **1966**, *67*, 18.

4. Kotronarou, A., Mills, G., Hoffmann, M.R., *J. Phys. Chem.*, **1991**, *95*, 3630.

5. Suslick, K.S., in *"Ultrasound - Its Chemical, Physical, and Biological Effects"*, Suslick, K.S., Ed., VCH Publishers, New York, **1988**, pp. 123-163 and references therein.

6. Margulis, M.A., Dmitrieva, A.F., *Zh. Fiz. Khim.*, **1981**, *55*, 159.

7. Margulis, M.A., Dmitrieva, A.F., *Zh. Fiz. Khim.*, **1982**, *56*, 323; *ibid.*, 875.

8. Fujikawa, S., Akamatsu, T., *J. Fluid Mech.*, **1980**, *97*, 481.

9. Both dihydrogen and dioxygen form by insonation of water in the presence of various metal catalysts and crushed glass from the secondary reactions of the radicals produced (Borgarello, E., Serpone, N., unpublished results, **1984**).

10. Riesz, P., Berdahl, D., Christman, C.L., *Environ. Health Perspect.*, **1985** *64*, 233.

11. Serpone, N., Terzian, R., Minero, C., Pelizzetti, E., *Adv. Chem. Series*, xxx (**1992**) 0000, *in press*.

12. Al-Ekabi, H., Serpone, N., *J. Phys. Chem.*, **1988**, *92*, 5726.

13. Okamoto, K., Yamamoto, Y., Tanaka, H., Tanaka, M., Ataya, A., *Bull. Chem. Soc. Jpn.*, **1985**, *58*, 2015.

14. Okamoto, K., Yamamoto, Y., Tanaka, H., Ataya, A., *Bull. Chem. Soc. Jpn.*, **1985**, *58*, 2023.

15. Augugliaro, V., Palmisano, L., Sclafani, A., Minero, C., Pelizzetti, E., *Toxicol. Environ. Chem.*, **1988**, *16*, 89.

16. (a) Zechmeister, L., Wallcave, L., *J. Am. Chem. Soc.*, **1955**, *77*, 2953.
(b) Zechmeister, L., Magoon, E.F., *J. Am. Chem. Soc.*, **1956**, *78*, 2149.
(c) Currell, D.L., Zechmeister, L., *J. Am. Chem. Soc.*,**1958**, *80*, 207.

17. See for example:
(a) Kitazume, T., *Ultrasonics*, **1990**, *28*, 322.
(b) Ando, T., Kimura, T., *Ultrasonics*, **1990**, *28*, 326.
(c) Fadel, A., *Tetrahedron*, **1991**, *47*, 6265.
(d) Olah, G.A., Wu, A.-H., *Synthesis*, **1991**, *135*, 204.
(e) Ichihara, J., Funabiki, K., Hanafusa, T., *Tetrahedron Lett.*, **1989**, *31*, 1848.
(f) Ranu, B.C., Basu, M.K., *Tetrahedron Lett.*, **1991**, *32*, 3243.
(g) Goldsmith, D., Soria, J.J., *Tetrahedron Lett.*, **1991**, *32*, 2457.
(h) Berthelot, J., Benammar, Y., Lange, C., *Tetrahedron Lett.*, **1991**, *32*, 4135.

18. Toy, M.S., Stringham, R.S., in *"Organic Phototransformations in Nonhomogeneous Media"*, Fox, M.A., Ed., *ACS Symposium Series*, vol. 278, American Chemical Society, Washington, D.C., **1985**, pp. 287-295.

19. Serpone, N., Colarusso, P., to be submitted for publication.

20. Currell, D.L., Wilheim, G., Nagy, S., *J. Am. Chem. Soc.*, **1963**, *85*, 127.

21. Fischer, C.-H., Hart, E., Henglein, A., *J. Phys. Chem.*, **1986**, *90*, 223.

22. Chen, J.W., Smith, G.V., *"Feasibility Studies of Applications of Catalytic Oxidation in Wastewater"*, United States Environmental Protection Agency, Report No. 17020 ECI 11/**1971**.

23. Suslick, K.S., in *"High-Energy Processes In Organometallic Chemistry"*, Suslick, K.S., Ed., American Chemical Society, Washington, D.C., **1987**, chapter 12, p 208.

24. Hart, E., Fischer, C.-H., Henglein, A., *J. Phys. Chem.*, **1990**, *94*, 284.

25. Land, E.J., Ebert, M., *Trans. Faraday Soc.*, **1967**, *63*, 1181.

26. Terzian, R., Serpone, N., Draper, R.B., Fox, M.A., Pelizzetti, E., *Langmuir*, **1991**, *7*, 3081.

# CHAPTER 12

# KINETIC AND MECHANISTIC ASPECTS IN HETEROGENEOUS PHOTOCATALYSIS

## 12.1 KINETIC ASPECTS

### 12.1.1 Reactions in Homogeneous *versus* Heterogeneous Media

In this thesis, the behaviour of xylenols was examined in both heterogeneous and homogeneous media. The pulse radiolysis studies in homogeneous media were carried out to identify the primary organic radicals formed upon reaction of •OH radicals with xylenols. The principal radical intermediates formed are the •OH-adducts (see Chapter 10) which may then eliminate $H_2O$ to form phenoxyl radicals as was shown for 3,4-xylenol. The intermediate products detected in the course of heterogeneous photocatalysis experiments (dihydroxydimethylbenzenes and dimethylbenzoquinones) can be formed from these •OH-adducts. It was therefore of interest to see whether there was a correlation between the rates of degradation of xylenols in heterogeneous media with either the rates of •OH-adduct formation in homogeneous media, or with the rates of decay of the •OH adducts in homogeneous media. The results are illustrated in Figure 12.1. it can be seen that in both cases there is **no clear correlation** between the reactions in the two media; this is not surprising. Reaction rates in heterogeneous media are affected by the amount of interaction each substrate has with the particulate surface (adsorption/desorption equilibria), both in the dark and upon illumination of the surface.

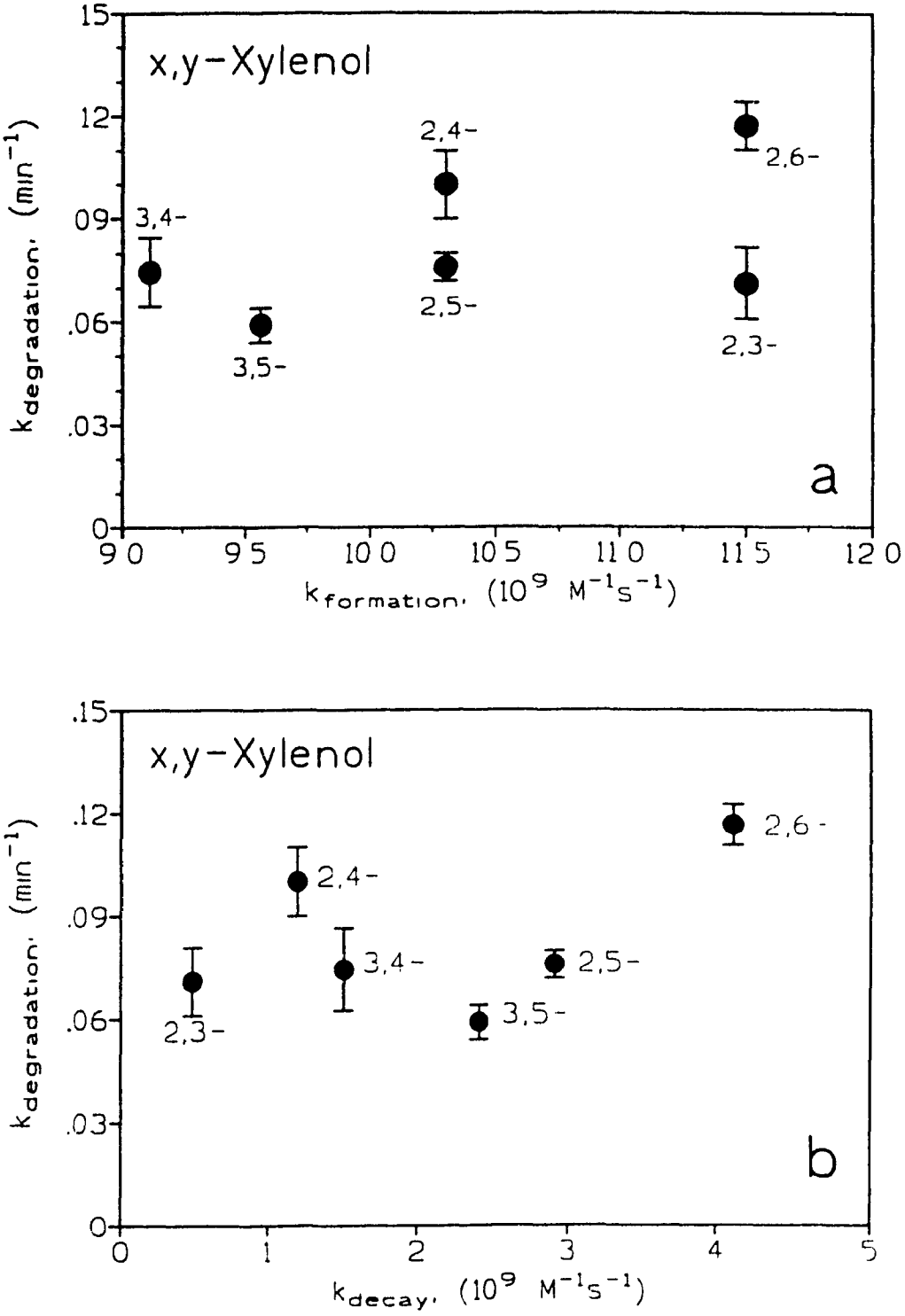


**Figure 12.1** Comparison of the rates of degradation of xylenols in heterogeneous media (conditions as per Table 6.4, Chapter 6) with the rates of a) formation of •OH-adducts in homogeneous solution, and b) decay of •OH-adducts (conditions as per Table 10.4 and text, Chapter 10).

Also, in homogeneous media, •OH-adducts typically decay via second-order kinetics to form dimeric products; in heterogeneous media, only trace quantities of dimeric products have been detected in the case of dichlorophenol.[1]

### 12.1.2 Effect of the Nature of the Substrate in Photocatalytic Reactions

The rates of the $TiO_2$ photocatalyzed degradation of many organic compounds have been examined in this work and elsewhere;[2-4] some of the results obtained are summarized in Table 12.1. It can be seen that under a given set of experimental conditions, the apparent first order rate constants for photodegradation do not seem to vary immensely upon changing the nature of the substrate. For example, under the experimental conditions used by Sabin *et al*,[2] the apparent first order rate constant varied from $2.4 \times 10^{-3}$ $min^{-1}$ (tribromomethane) to $2.1 \times 10^{-1}$ $min^{-1}$ (1,2-dichlorobenzene) with all values (aside from tribromomethane) being in the order of $10^{-1}$-$10^{-2}$ $min^{-1}$. Similar results can also be seen in the work of Matthews[3] where values ranged between $7.9 \times 10^{-2}$ $min^{-1}$ (4-chlorophenol) and $1.6 \times 10^{-1}$ $min^{-1}$ (naphthalene). The results reported in this thesis are also consistent with this observation. This indicates that the nature of the substrate does not play a significant role in determining photodegradation rates and that other factors may be rate-determining.

Following light absorption by $TiO_2$ both electrons and holes are concurrently produced. The holes (surface-bound •OH radicals) are the reactive species in photodegradation reactions. In order to keep the photooxidation process going, accu-

**Table 12.1** Comparison of apparent rate constants of $TiO_2$-photocatalyzed degradation reactions under various experimental conditions.

| Substrate | $k_{app}$, $min^{-1}$ [a] | Experimental Conditions | Ref. |
|---|---|---|---|
| Benzene | $1.4 \times 10^{-1}$ | 450 W Xenon lamp<br>$\lambda > 320$ nm<br>Perkin-Elmer HS-6 round reaction vessel<br>Volume= 2mL<br>[S]= 1 mM<br>$[TiO_2]$= 1g/L (slurry) | 2 |
| Chlorobenzene | $1.3 \times 10^{-1}$ | | |
| 1,2-Dichlorobenzene | $2.1 \times 10^{-1}$ | | |
| Bromobenzene | $1.8 \times 10^{-2}$ | | |
| 1,2-Dichloroethylene | $1.2 \times 10^{-1}$ | | |
| Trichloroethylene | $1.4 \times 10^{-1}$ | | |
| Tetrachloroethylene | $1.2 \times 10^{-1}$ | | |
| Dichloromethane | $1.1 \times 10^{-1}$ | | |
| Trichloromethane | $3.6 \times 10^{-2}$ | | |
| Tribromomethane | $2.4 \times 10^{-3}$ | | |
| 1,1,2,2-Tetrachloroethane | $9.0 \times 10^{-2}$ | | |
| 1,2-Dichloropropane | $1.2 \times 10^{-1}$ | | |
| Bis-(2-chloroethyl)ether | $1.9 \times 10^{-1}$ | | |
| 1,1-Difluoro-1,2,2-trichloroethane | $2.9 \times 10^{-2}$ | | |
| 1,1-Difluoro-1,2-dichloroethane | $4.0 \times 10^{-2}$ | | |
| Salicylic Acid | $9.8 \times 10^{-2}$ | 20 W Black-light lamp<br>Spiral reactor coated with $85\mu g/cm^2$ $TiO_2$<br>Flow rate= 120 $cm^3$/min<br>Vol= 500 $cm^3$<br>[S]= 10 $\mu$M | 3 |
| Phenol | $9.7 \times 10^{-2}$ | | |
| 2-Chlorophenol | $8.4 \times 10^{-2}$ | | |
| 4-Chlorophenol | $7.9 \times 10^{-2}$ | | |
| Benzoic Acid | $1.0 \times 10^{-1}$ | | |
| 2-Naphthol | $8.1 \times 10^{-2}$ | | |
| Naphthalene | $1.6 \times 10^{-1}$ | | |
| Fluorescein | $1.1 \times 10^{-1}$ | | |
| Salicylic Acid | $5.2 \times 10^{-2}$ | Same as above<br>[S]= 100 $\mu$M | 3 |
| Phenol | $4.1 \times 10^{-2}$ | | |
| 2-Naphthol | $4.0 \times 10^{-2}$ | | |
| 2-Fluorophenol | $1.0 \times 10^{-1}$ | 1500 W Xe lamp (AM1 simulated sunlight)<br>$\lambda > 310$ nm<br>Pyrex reaction vessel<br>Volume= 5 mL<br>$[TiO_2]$= 50 mg/L (slurry)<br>[S]= 200 $\mu$M | 4 |
| 3-Fluorophenol | $7.4 \times 10^{-2}$ | | |
| 4-Fluorophenol | $1.1 \times 10^{-1}$ | | |
| 2,4-Difluorophenol | $1.3 \times 10^{-1}$ | | |
| 3,4-Difluorophenol | $1.2 \times 10^{-1}$ | | |
| 3-Fluorocatechol | $5.9 \times 10^{-2}$ | | |
| Hydroquinone | $7.4 \times 10^{-2}$ | | |
| Catechol | $7.4 \times 10^{-2}$ | | |

| Substrate | $k_{app}$, $min^{-1}$ [a] | Experimental Conditions | Ref. |
|---|---|---|---|
| 2-Fluorophenol<br>3-Fluorophenol<br>4-Fluorophenol<br>2,4-Difluorophenol<br>3,4-Difluorophenol<br>Hydroquinone | $1.7 \times 10^{-1}$<br>$1.3 \times 10^{-1}$<br>$1.6 \times 10^{-1}$<br>$2.4 \times 10^{-1}$<br>$1.6 \times 10^{-1}$<br>$1.6 \times 10^{-1}$ | Same as above<br>$[TiO_2]$= 0.1 g/L | 4 |
| o-Cresol<br>m-Cresol<br>p-Cresol | $1.1 \times 10^{-4}$<br>$4.0 \times 10^{-3}$<br>$1.2 \times 10^{-4}$ | 900 W Hg/Xe lamp<br>$\lambda > 220$ nm<br>Pyrex reaction vessel<br>Volume= 50 mL<br>$[TiO_2]$= 2g/L (slurry)<br>[S] $\approx$ 185 $\mu$M | This work |
| 2,3-Xylenol<br>2,4-Xylenol<br>2,5-Xylenol<br>2,6-Xylenol<br>3,4-Xylenol<br>3,5-Xylenol | $7.9 \times 10^{-2}$<br>$1.1 \times 10^{-1}$<br>$7.5 \times 10^{-2}$<br>$1.2 \times 10^{-1}$<br>$7.0 \times 10^{-2}$<br>$5.4 \times 10^{-2}$ | Same as above<br>[S] $\approx$ 165 $\mu$M | This work |
| 2,3,5-Trimethylphenol | $1.4 \times 10^{-1}$ | Same as above<br>[S]= 159 $\mu$M | This work |

a) Apparent first order rate constant for substrate disappearance.

mulation of the electrons is to be avoided since it would increase the electron/hole recombination rate. The scavenging of the electrons would therefore be the rate-limiting factor in these reactions. It has been suggested by Gerisher and Heller[5] that the rate of electron transfer from the catalyst particles to oxygen may be rate-determining in photocatalytic processes. The results obtained in this work and elsewhere are consistent with this notion.

## 12.2 MECHANISTIC ASPECTS

Based on the evidence gathered in this work and elsewhere, a mechanism (Figure 12.2) has been proposed for the photo-oxidative degradation of methylated phenols on irradiated $TiO_2$ particles. Since evidence to date indicates that the reaction is a surface reaction (see discussion in Chapter 2), it is presumed that the phenols will chemisorb onto the semiconductor surface (see below). Phenols are known to react with titanium compounds to form titanium phenoxides. The amount of chemisorption is believed to be small as dark adsorption is typically $< 10$ % for methylated phenols. Upon irradiation, electron/hole pairs are formed. In competition with recombination in the bulk, both charge carriers rapidly migrate to the surface where they are both ultimately trapped by intrinsic traps [($Ti^{IV}$-$O^{2-}$-$Ti^{IV}$) for the hole and (-$Ti^{IV}$-) for the electron].[6] Hole trapping on the surface may occur for hydroxylated and/or hydrated anatase $TiO_2$ particles [pathway (b)] to yield surface-bound •OH radicals. These have been detected using prereduced anatase $TiO_2$ powders in aqueous solutions (pH 4 and 7) at ambient conditions by Jaeger and Bard[7] and by Harbour *et al*;[8] these results have since been confirmed by other workers.[6,9-13] A low-temperature (77 K) ESR study by Anpo *et al* identified the •OH radical (no spin traps);[14] however, this was recently disputed by Howe and Grätzel[6] who found no evidence for •OH species, even at 4.2 K, but inferred that the ESR signal seen by Anpo *et al.*[14] is attributable to the O • radical anion resulting from trapping positive holes at lattice oxide ions (-$O^{2-}$-). They further postulated[6] that the •OH radical identified by spin trapping methods is not the primary product of hole trapping, but originates as a transient intermediate of photo-oxidation.

Formation of surface-bound •OH radicals via pathway (b) is consistent with these

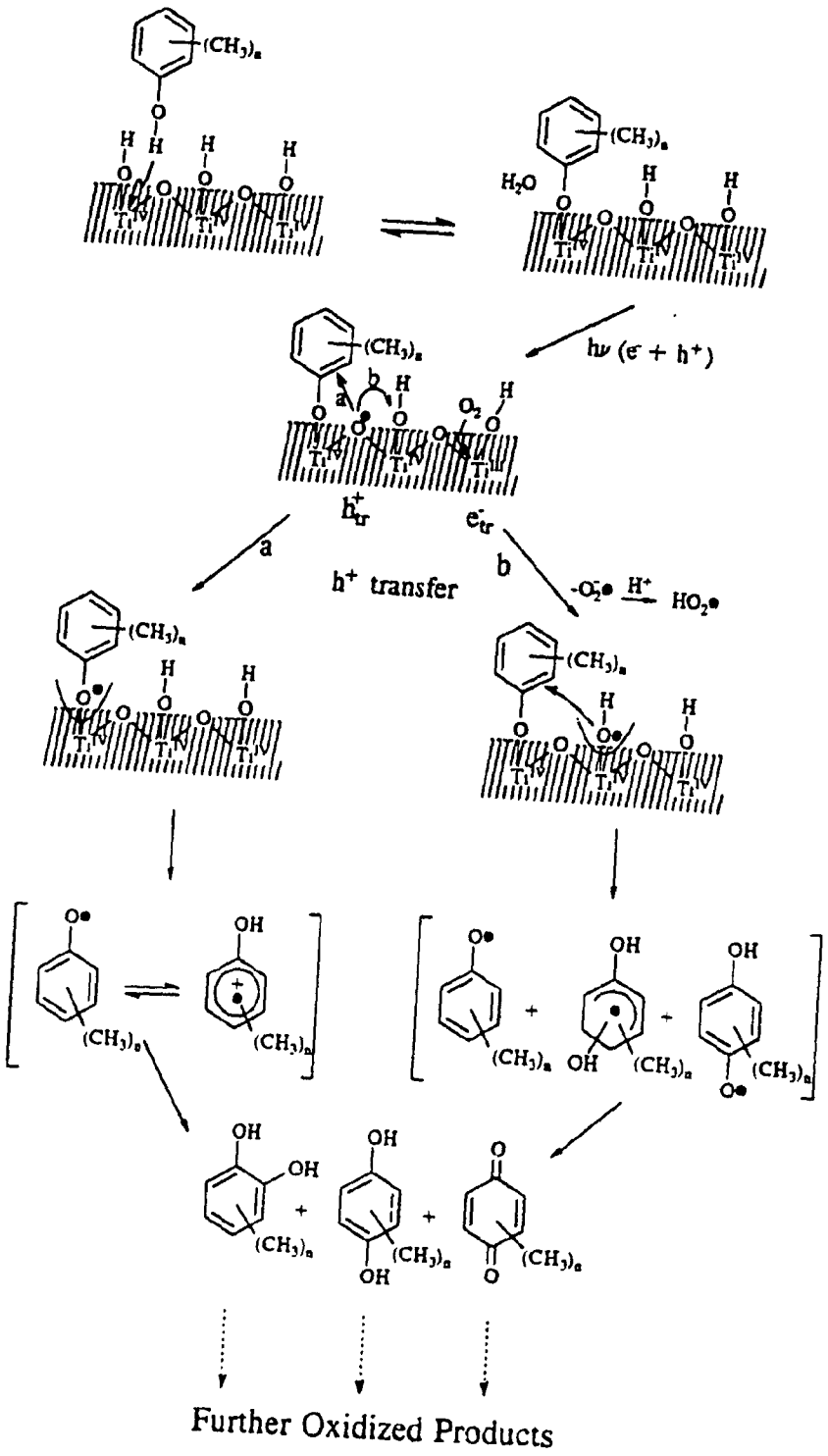


**Figure 12.2** Proposed mechanism for the photo-oxidation of methylated phenols.

observations. The •OH radicals formed are unlikely to diffuse away from the surface as was demonstrated by pulse radiolysis experiments.[15] These surface-bound •OH radicals may react with the organic substrates to form first the •OH-adducts and subsequently the phenoxyl radicals, as evidenced in homogeneous media by the pulse radiolysis studies on the xylenols reported here and by Land and Ebert's work on phenol.[16] In principle, the surface-trapped hole can also react directly with the phenolic substrate [pathway (a)]; the cation radicals formed may further react with water to form hydroxylated compounds as in pathway (b). The two pathways cannot be distinguished on the basis of product analysis alone; however, at room temperature, formation of surface-bound hydroxyl radicals should predominate simply on the basis of the relative concentration of OH groups on $TiO_2$ *versus* the possible few test molecules of the organic substrates. Pathway (b) is believed to be the dominant pathway. The distinction between the two pathways (a) and (b) of Figure 12.2 may in fact be a moot point following the recent work of Lawless, Serpone and Meisel[15] that noted the indistinguishability of the trapped hole as $\{Ti^{IV}\text{-}O^{-}\bullet\text{-}Ti^{IV}\}\text{-}OH^{-}$ and as $\{Ti^{IV}\text{-}O^{2-}\text{-}Ti^{IV}\}\text{-}\bullet OH$.

Electrons can be scavenged by pre-adsorbed molecular oxygen to give the superoxide radical anion $(O_2^{-}\bullet)_{ads}$.[6] This is consistent with the fact that no photodegradation of 4-chlorophenol occurs in the absence of $O_2$.[17] It should be noted that based on the results reported in Chapter 9 for pentabromophenol, reaction of the electron with phenols to also form phenoxyl radicals cannot be ruled out; it is, however, unlikely to be the major reaction pathway.

Hydroxylated compounds formed via both pathways (a) and (b) also would react in a similar manner producing compounds with increasingly higher oxygen-to-carbon ratios until the final reaction product, $CO_2$, is formed.

# REFERENCES


1. Pelizzetti, E., in: *Proceedings of the Solar Energy Meeting IPS-9*, Beijing, China, *In press*, **1992**.

2. Sabin, F., Türk, T., Vogler, A., *J. Photochem. Photobiol. A: Chem.*, **1992**, *63*, 99.

3. Matthews, R.W., *J. Phys. Chem.*, **1987**, *91*, 3328.

4. Minero, C., Aliberti, C., Pelizzetti, E., Terzian, R., Serpone, N., *Langmuir*, **1991**, *7*, 928.

5. Gerischer, H., Heller, A., *J. Phys. Chem.*, **1991**, *95*, 5261.

6. Howe, R.F., Grätzel, M., *J. Phys. Chem.*, **1987**, *91*, 3906.

7. Jaeger, C.D., Bard, A.J., *J. Phys. Chem.*, **1979**, *83*, 3146.

8. Harbour, J.R., Tromp, J., Hair, M.L., *Can. J. Chem.*, **1985**, *63*, 204.

9. Avudaithai, M., Kutty, T.R.N., *Mat. Res. Bull.*, **1988**, *23*, 1675.

10. Volz, H.G., Kaempf, G., Fitzky, H.G., Klaeren, A., *ACS Symp. Ser.*, **1981**, *151*, 163.

11. Grätzel, M., Howe, R.F., *J. Phys. Chem.*, **1990**, *94*, 2566.

12. Maldotti, A., Amadelli, R., Bartocci, C., Carassiti, V., *J. Photochem. Photobiol. A: Chem.*, **1990**, *53*, 263.

13. Howe, R.F., *Adv. Coll. Interfac. Sci.*, **1982**, *18*, 1.

14. Anpo, M., Shima, T., Kubokawa, Y., *Chem. Lett.*, **1985**, 1799.

15. Lawless, D., Serpone, N., and Meisel, D., *J. Phys. Chem.*, **1991**, *95*, 5166.

16. Land, E.J., Ebert, M. *Trans. Faraday Soc.* **1967**, *63*, 1181.

17. Barbeni, M., Pramauro, E., Pelizzetti, E., Borgarello, E., Grätzel, M., Serpone, N. *Nouv. J. Chim.* **1984**, *8*, 547.

# CHAPTER 13

# FINAL CONCLUSIONS

## 13.1 CONCLUDING REMARKS

Titanium dioxide, irradiated by ultraviolet/visible light, has been used to mediate the photocatalyzed degradation of several methylated creosote phenolics. These included: *ortho*-, *meta*-, and *para*-cresol, 2,3-, 2,4-, 2,5-, 2,6-, 3,4- and 3,5-xylenol as well as 2,3,5-trimethylphenol. In addition, the photocatalyzed mineralization of methylhydroquinone and 4-methylcatechol, two intermediates detected in the photodegradation of cresols, was examined. A practical case study was also carried out on a commercial sample of coal tar creosote. In an attempt to gain a better understanding of the primary intermediates formed in heterogeneous photocatalysis, pulse radiolysis was used to identify the organic radicals formed upon reaction of •OH radicals with creosote phenolics. The compounds chosen were the six isomers of xylenol as well as a series of pentahalogeneted phenols (F, Cl and Br). Finally, the sonochemical oxidation of phenol, a model compound used in photocatalysis, was carried out and the process was compared to $TiO_2$-mediated photo-oxidation.

The total photomineralization of cresols to carbon dioxide and water occurs in air-equilibrated aqueous $TiO_2$ suspensions. Two major hydroxylated aromatic intermediate species have been identified by high performance liquid chromatography (HPLC): 4-methylcatechol and methylhydroquinone. Photochemical efficiencies (lower limits of

quantum yields; 365 nm) of compound disappearance are, respectively, 0.0096, 0.0076, and 0.0104 for *o*-, *m*-, and *p*-cresol. The effect of such parameters as pH, initial cresol concentration, $TiO_2$ concentration, oxygen concentration and radiant power levels on the degradation of *m*-cresol was examined in detail. The reaction rates increased with increasing pH. Also, oxygen led to an increase of the reaction rate. The rate of photo-oxidation of *m*-cresol was increased linearly with increasing light intensity in the intensity region examined (from 0 to 36 $mW/cm^2$).

The photocatalyzed mineralization of methylhydroquinone (MHQ) and 4-methyl-catechol (4-MCC) was examined in air-equilibrated, irradiated aqueous suspensions of $TiO_2$ at pH 3. The temporal course of the degradation was followed by HPLC, gas chromatography (for $CO_2$ evolution), and also by diffuse reflectance spectroscopy for 4-MCC. Total disappearance of MHQ occurred in $\approx$ 1 hr via apparent first-order kinetics, followed by the concomitant stoichiometric evolution of $CO_2$ which is complete after $\approx$ 1 hr of irradiation. 4-Methylcatechol is strongly adsorbed ($\approx$ 53%) to the catalyst's surface, and its disappearance is complete within $\approx$ 20 min of irradiation; this was confirmed by diffuse reflectance spectra of the catalyst powder. Quantitative amounts of $CO_2$ were also detected.

The disappearance of 2,3-, 2,4-, 2,5-, 2,6-, 3,4- and 3,5-xylenol in air-equilibrated, irradiated $TiO_2$ suspensions takes place in $<$ 1 hr at pH 3. In the presence of excess molecular oxygen, the degradation of 3,4-xylenol is faster ($\leq$ 0.5 hr) and complete mineralization to $CO_2$ and $H_2O$ takes place in $\approx$ 1 hr. The photochemical efficiencies for the disappearance of xylenols at 365 nm were: 0.0060 (3,4-xylenol),

0.0067 (2,3-xylenol), 0.0067 (3,5-xylenol), 0.0074 (2,5-xylenol), 0.012 (2,4-xylenol), and 0.015 (2,6-xylenol). These results are comparable to those obtained for cresol under nearly identical experimental conditions.

The effect of various experimental factors such as pH, temperature, photocatalyst concentration, substrate concentration, and light intensity, was examined in some detail for 3,4-xylenol. The rate of the photocatalyzed reaction increased as a function of pH and temperature. The activation energy for the photodegradation of 3,4-xylenol was $E_a = 2.1 \pm 0.2$ Kcal/mol; this value is comparable to values reported in the literature for other phenols. Concentration dependence experiments (varying [$TiO_2$] or [3,4-xylenol]) indicate the reaction follows saturation-type kinetics. Finally, the reaction rate was directly proportional to the light intensity (I) at low light fluxes, proportional to $I^{1/2}$ at intermediate fluxes, and independent of I at higher fluxes. This result is consistent with both theoretical predictions and experimental observations by others.

The major intermediates have been identified in the photodegradation of xylenols: these are either dihydroxydimethylbenzenes or dimethylbenzoquinones; other intermediates also form but were not identified under our experimental conditions.

The disappearance of 2,3,5-trimethylphenol in air-equilibrated, irradiated $TiO_2$ suspensions takes place in $< 45$ min at pH 3. In excess molecular oxygen, the degradation of 2,3,5-TMP is faster ($\leq 20$ min) and complete mineralization to $CO_2$ and $H_2O$ takes place in $\approx 1$ hr. The major aromatic intermediates formed during the photodegradation of 2,3,5-TMP were 2,3,5-trimethylhydroquinone, 2,3,5-trimethylbenzoquinone, and 3,5,6-trimethylcatechol; other intermediates also formed but were not

identified under our experimental conditions.

The present thesis adds other examples (methylated phenols) to the classes of environmental organic contaminants that may be present in wastewaters and which can be degraded effectively by the photocatalytic method employed herein. This work also completes the survey of the water soluble phenolic components of creosote.

The photocatalyzed mineralization of creosote using heterogeneous photocatalysis was carried out in aqueous media. $TiO_2$ was used as the photocatalyst and total mineralization was demonstrated by the quantitative analysis of $CO_2$, the final product. The photodegradation process was monitored both in solution (for water soluble compounds) and on the photocatalyst surface (for water insoluble compounds). This study illustrates the practicality of HETEROGENEOUS PHOTOCATALYSIS in the decontamination of typical multicomponent samples such as one is likely to encounter in polluted aquifers.

The optical and kinetic characteristics of the transients formed by the reaction of OH• and $N_3$• radicals with pentabromo- (PBP-OH), pentachloro- (PCP-OH), and penta-fluorophenol (PFP-OH) were examined by pulse radiolysis techniques in buffered (pH 8) aqueous media. The principal products from the reaction of OH• with PBP-O and PCP-O$^-$ are: (i) the corresponding pentahalophenoxyl radicals {ca. 75% (PBP-O•) and ca. 77% (PCP-O•)}, (ii) the •OH-adducts, dihydroxypentahalocyclohexadienyl radical anions, HO•-PXP-O$^-$ ($\approx$ 18% for X = Br, $\approx$ 8% for X = Cl), and (iii) the semiquinone anion radicals, bromanil anion radical (ca. 7%) and chloranil anion radical (ca. 15%). Their kinetics of formation via electron transfer and •OH addition were assessed. Oxidation of PCP-O and PBP-O$^-$ by $N_3$• radicals also yields the respective

phenoxyl species: PBP-O•, $k_{ET}$ = 6.1 ± 0.9 x $10^9$ $M^{-1}s^{-1}$; PCP-O•, $k_{ET}$ = 3.3 ± 0.6 x $10^9$ $M^{-1}s^{-1}$. The reaction of OH• with PFP-O⁻ anion gave exclusively the dihydroxypentafluorocyclohexadienyl radical, HO•-PFP-O⁻, $k_{ADD}$ = 4.6 ± 0.9 x $10^9$ $M^{-1}s^{-1}$. Solvated electrons react with PBP-O⁻ ($k_e$ = 2.6 x $10^{10}$ $M^{-1}s^{-1}$) to give a highly reactive dianionic electron adduct, which following loss of $Br^-$ and reaction with $H_2O$ yields a mixture of isomeric tetrabromophenoxyl radicals. It is concluded that reaction of the electron with halogenated phenols in heterogeneous media cannot be ruled out on the basis of these observations. Photoreductions of halophenols and haloaromatics in general, can also lead to those intermediates observed under photo-oxidative conditions.

2,6- and 3,4-Xylenol react with $N_3$• radicals to form the corresponding dimethylphenoxyl species, 2,6-dimethylphenoxyl radical ($k_f$= 2.8 ± 0.6 x $10^9$ $M^{-1}s^{-1}$ and the 3,4-dimethylphenoxyl radical ($k_f$= 4.1 ± 0.6 x $10^9$ $M^{-1}s^{-1}$) respectively; H• reacts with 2,6-xylenol to form the hydroxy-2,6-dimethylcyclohexadienyl radical (H•-adduct) with $k_f$= 1.1 ± 0.3 x $10^9$ $M^{-1}s^{-1}$.

Reaction of •OH radicals with 2,3-, 2,4-, 2,5-, 2,6- and 3,5-xylenol in buffered aqueous media (pH 4) have been examined. They yield exclusively the •OH-adducts (dihydroxydimethylcyclohexadienyl radicals) as the initial products with $k_{add}$ ranging from 9.6 x $10^9$ to 1.2 x $10^{10}$ $M^{-1}s^{-1}$. Subsequent $H_2O$ elimination from the •OH-adducts to yield phenoxyl or benzyl type radicals has not been ruled out. 3,4-Xylenol reacts with •OH to form both an •OH-adduct and a phenoxyl radical. At pH ≤ 8, the 3,4-phenoxyl radical is formed via $H_2O$ elimination from the •OH-adduct; by contrast, at pH ≥ 9, both radicals appear to form concurrently. It is proposed that at pH ≥ 8, phenoxyl

radicals are formed via either water elimination as for lower pHs or via an inner sphere electron transfer from the xylenol to •OH in the •OH-adduct. The mechanism of the reaction of 3,4-xylenol with •OH is more consistent with the behaviour of phenol and cresol than with the behaviour of methylated benzenes. Similar behaviour by the other isomers of xylenol has not been ruled out.

In heterogeneous media ($TiO_2$ dispersions), photo-oxidations may well proceed via pathways analogous to those with •OH radicals even though analysis of intermediate products along the various stages of oxidation would suggest •OH additions to aromatic rings.

The rates of photodegradation of xylenols in heterogeneous media were compared with both the rates of •OH-adduct formation and •OH-adduct disappearance in homogeneous media. No clear correlation was evident.

The sonochemical oxidation of phenol was examined in air-equilibrated aqueous media at various pH's and at various insonation powers. Its disappearance follows zero-order kinetics at $[\text{phenol}]_{\text{initial}} \approx 30$ to 70 $\mu$M. Three principal intermediate species formed at pH 3: catechol, hydroquinone, and *p*-benzoquinone; at natural pH (5.4-5.7) only catechol and hydroquinone formed. No intermediate species were detected at pH 12 under the conditions used. The sonochemical fate of the three intermediates was also examined at pH 3 and at natural pH's. At pH 3, *p*-benzoquinone is the major species formed during insonation of hydroquinone, while hydroquinone is produced during insonation of benzoquinone. In both cases, an additional intermediate formed in trace quantities that was tentatively identified as hydroxy-*p*-benzoquinone. These same

intermediate species have been identified in the heterogeneous photocatalyzed oxidation of phenol in irradiated titania suspensions. The present results confirm the important role of •OH radicals in degradation processes. Although $CO_2$ is the ultimate product in heterogeneous photocatalysis, irradiation of a phenolic aqueous solution by ultrasounds showed no loss of total organic carbon (TOC) after several hours, even though the aromatic substrate and the intermediates had degraded.

The work reported is additional evidence that heterogeneous photocatalysis provides an efficient method to totally mineralize the phenolic and non-phenolic (mostly PAH's) components of creosote to $CO_2$ and $H_2O$ and that the technique has potential for practical applications in water decontamination as was illustrated for creosote contaminated water. The intermediates formed are typically hydroxylation products; these can be obtained from either the •OH adducts or the phenoxyl radicals formed upon reaction of •OH radicals with phenols in homogeneous media. It is however believed that the major reaction pathway in heterogeneous media is •OH-addition. Sono-oxidation may provide an alternative method to photo-oxidation in cases where solutions are not optically clear enough to allow passage of light; the method did not however lead to total mineralization of phenol in aerated solution under the conditions used.

# APPENDIX A

# KINETIC DATA OBTAINED IN THE PULSE RADIOLYTIC STUDY OF PENTAHALOPHENOLS

The kinetic data presented in this appendix were obtained during the course of the pulse radiolytic studies on pentahalophenols presented in Chapter 9; these include the data from concentration dependence experiments that were carried out.

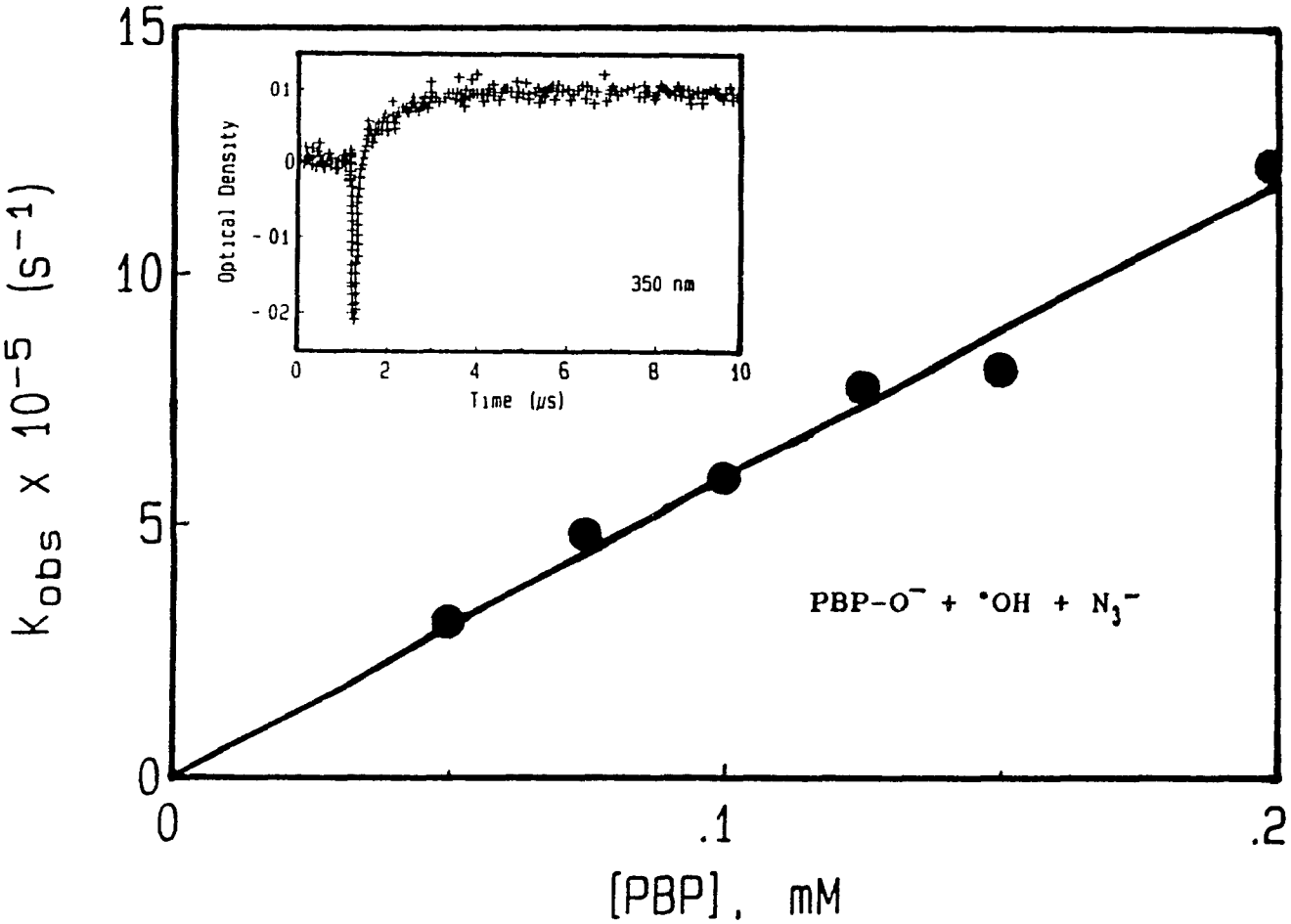


**Figure A1** Plot of $k_{obs}$ *versus* [PBP-O$^-$] as measured at 350 nm for the $N_3$• oxidation of PBP-O$^-$ at constant [•OH] (=1.88 x $10^{-6}$ M). Inset shows the increase in the optical density at 350 nm upon irradiation of 2 x $10^{-4}$ M PBP-O$^-$ in a $N_2O$-saturated solution at pH 8 and containing 0.01 M $NaN_3$.

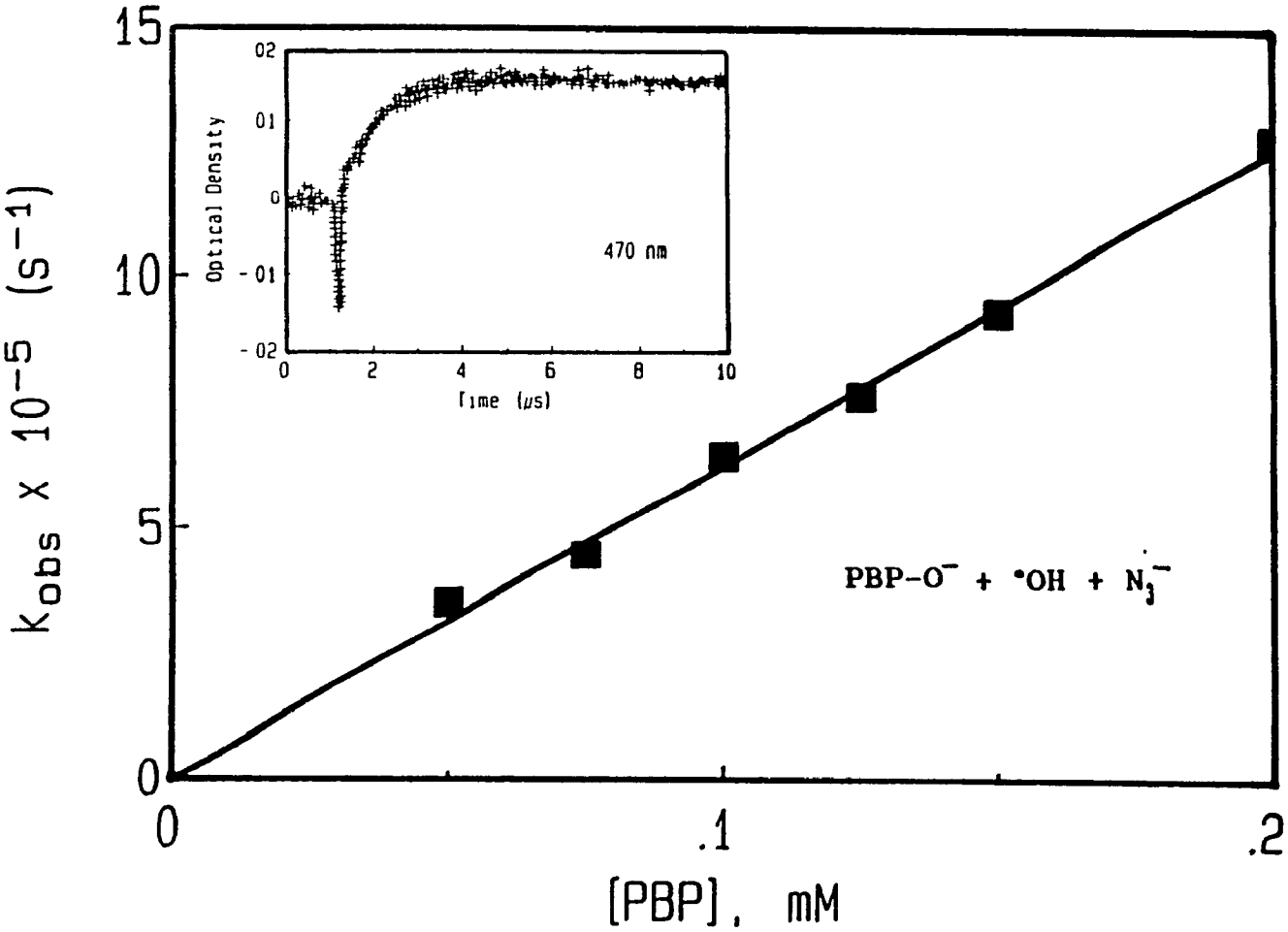


**Figure A2** Plot of $k_{obs}$ *versus* [PBP-O$^-$] as measured at 470 nm for the $N_3$• oxidation of PBP-O$^-$ at constant [•OH] (=1.88 x $10^{-6}$ M). Inset shows the increase in the optical density at 470 nm upon irradiation of 2 x $10^{-4}$ M PBP-O$^-$ in a $N_2O$-saturated solution at pH 8 and containing 0.01 M $NaN_3$.

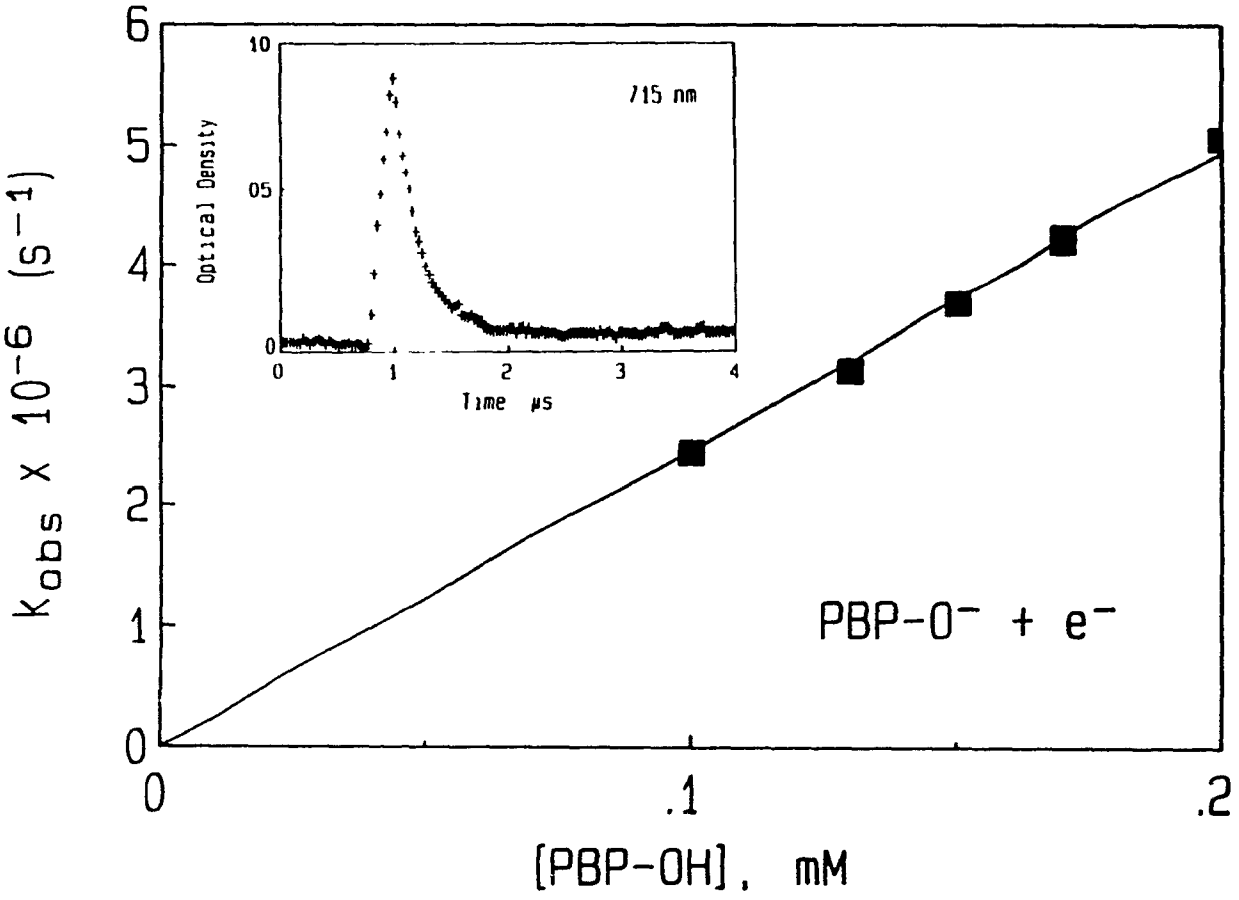


**Figure A3** Plot of $k_{obs}$ *versus* [PBP-O$^-$] as measured at 715 nm for the $e^-_{(aq)}$ addition to PBP-O$^-$ at constant [$e^-_{(aq)}$] (=2.2 x $10^{-6}$ M). Inset shows the decay in the optical density at 715 nm upon irradiation of 2 x $10^{-4}$ M PBP-O$^-$, 0.2 M *tert*-butanol, in a $N_2$-saturated aqueous solution at pH 8.

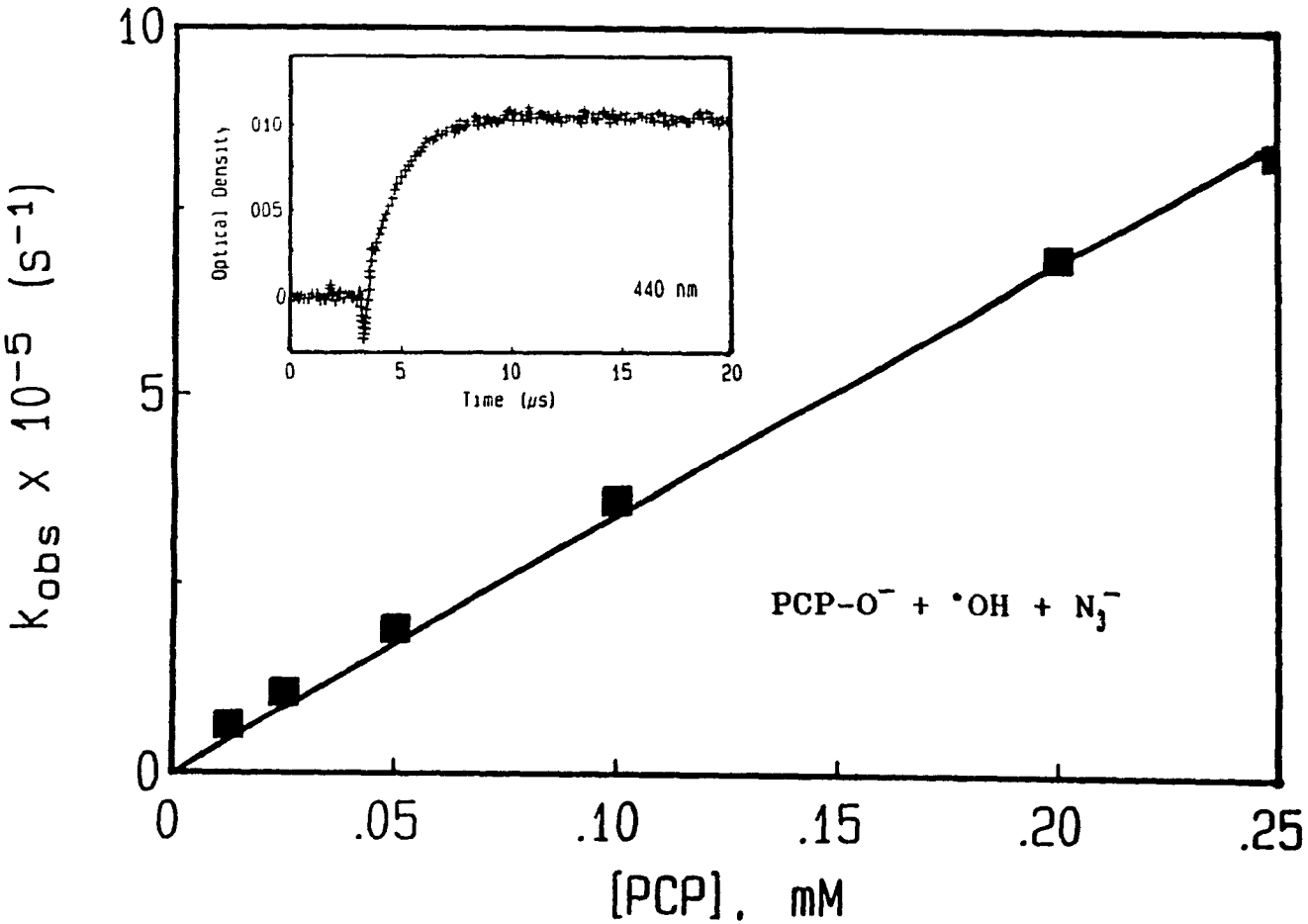


**Figure A4** Plot of $k_{obs}$ *versus* [PCP-O$^-$] as measured at 440 nm for the $N_3$• oxidation of PCP-O$^-$ at constant [•OH] (=1.14 x $10^{-6}$ M). Inset shows the increase in the optical density at 440 nm upon irradiation of 2.5 x $10^{-4}$ M PCP-O$^-$ in a $N_2O$-saturated solution at pH 8 and containing 0.01 M $NaN_3$.

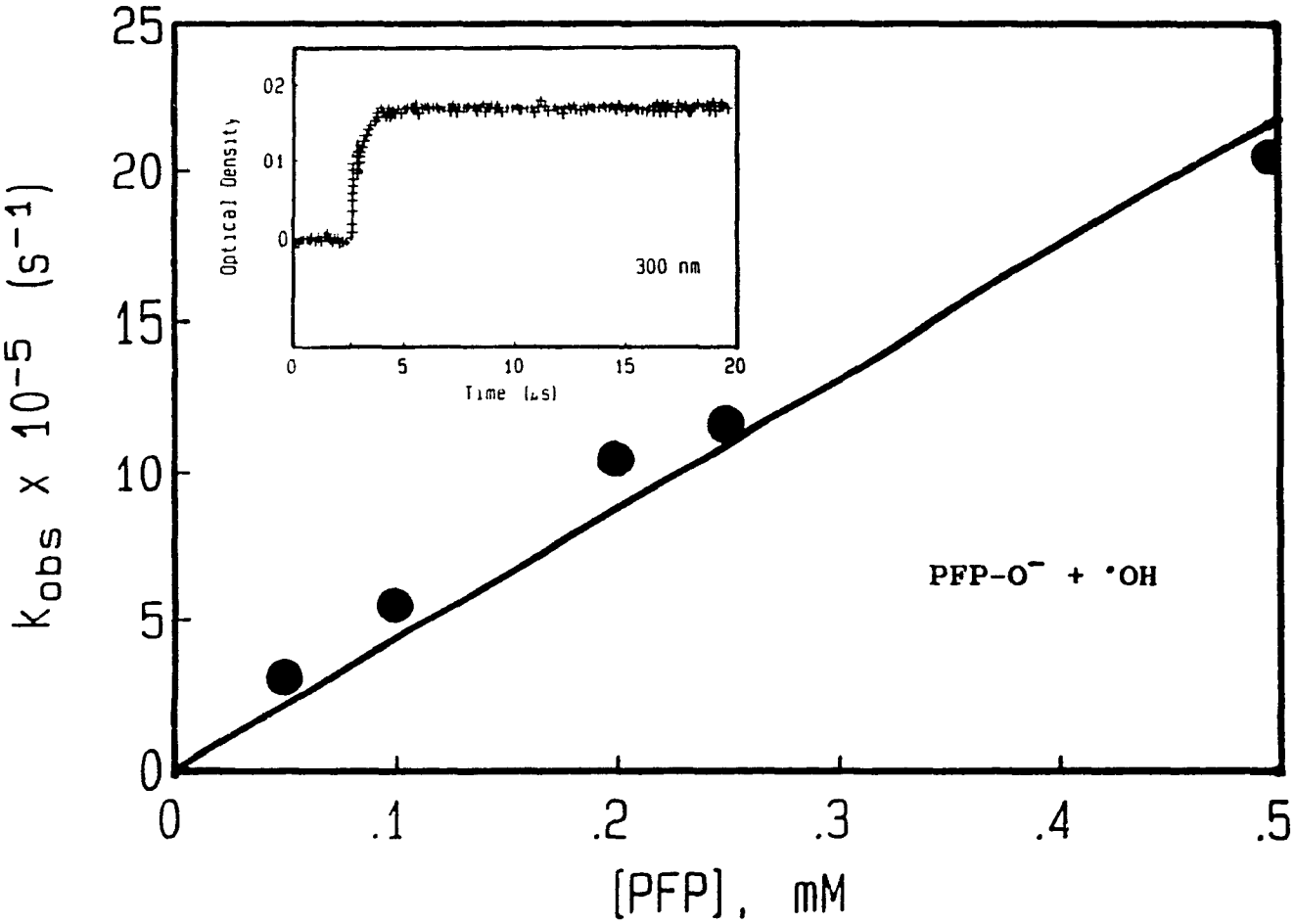


**Figure A5** Plot of $k_{obs}$, *versus* [PFP-O⁻] as measured at 300 nm for the •OH oxidation of PFP-O⁻ at constant [•OH] (=1.52 x $10^{-6}$ M). Inset shows the increase in the optical density at 300 nm upon irradiation of 5 x $10^{-4}$ M PFP-O⁻ in a $N_2O$-saturated solution at pH 8.

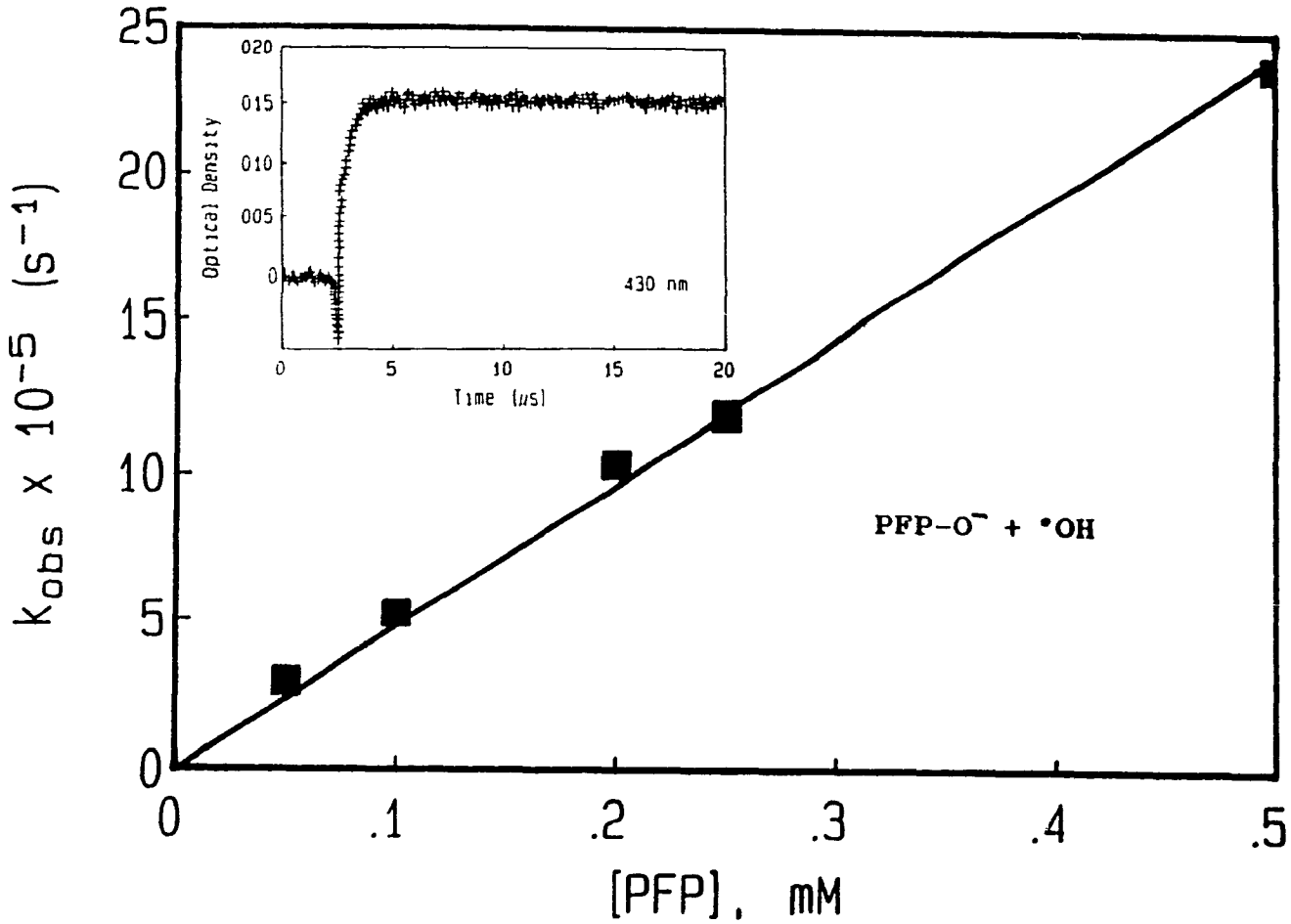


**Figure A6** Plot of $k_{obs}$ *versus* [PFP-O⁻] as measured at 430 nm for the •OH oxidation of PFP-O⁻ at constant [•OH] (=1.83 x $10^{-6}$ M). Inset shows the increase in the optical density at 430 nm upon irradiation of 5 x $10^{-4}$ M PFP-O⁻ in a $N_2O$-saturated solution at pH 8.

# APPENDIX B

# KINETIC AND SPECTRAL DATA OBTAINED IN THE PULSE RADIOLYTIC STUDY OF XYLENOLS

The kinetic and spectral data presented in this appendix were obtained during the course of the pulse radiolytic studies on xylenols presented in Chapter 10; these include time-resolved absorption spectra for the dihydroxydimethylcyclohexadienyl radicals as well as the data from all concentration dependence experiments that were carried out.

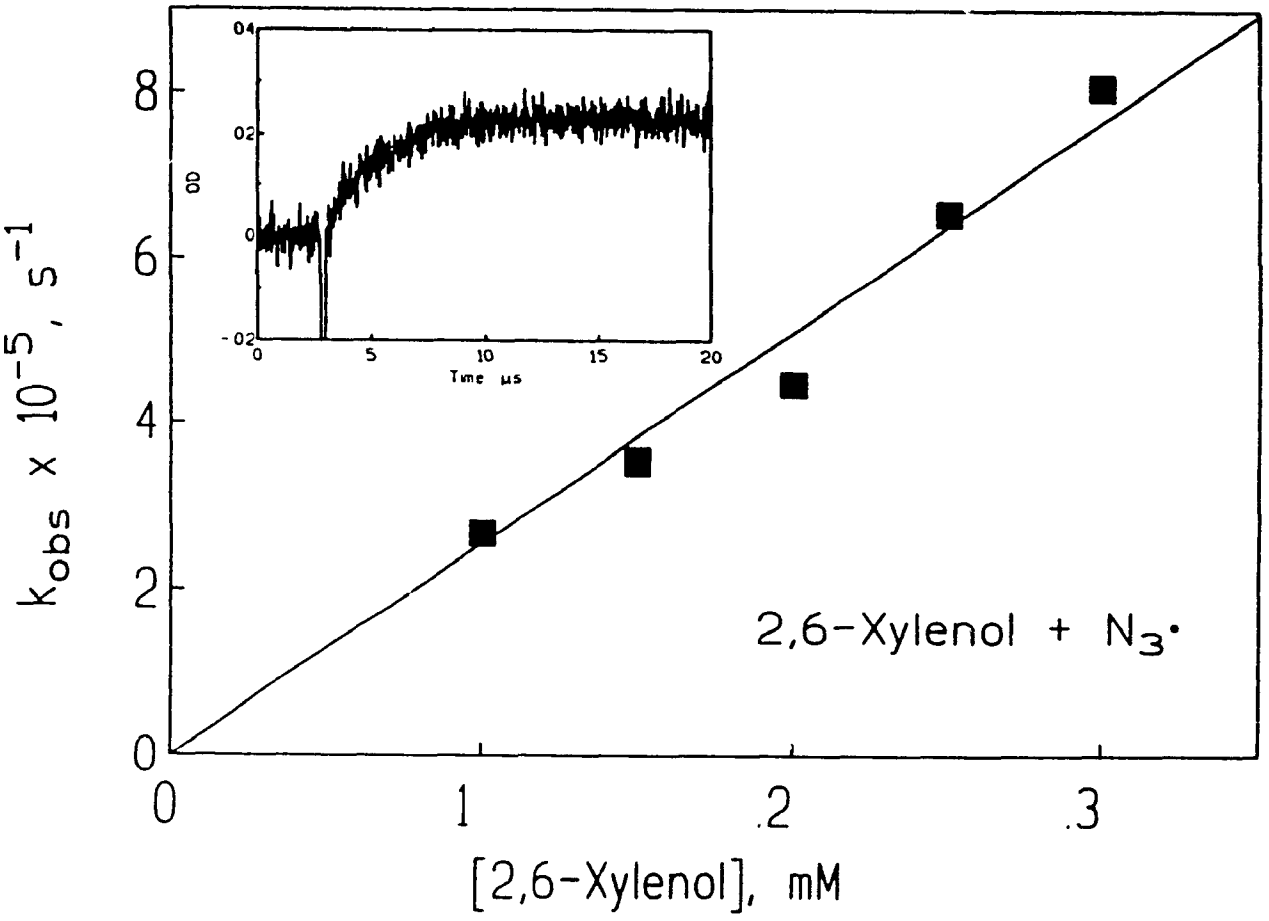


**Figure B1** Plot of [2,6-Xylenol] *versus* $k_{obs}$ as measured at 375 nm for the $N_3$• oxidation of 2,6-Xylenol at constant dose ([OH•] = 3.34 x $10^{-6}$ M); Inset shows the increase in optical density at 375 nm upon irradiation of 2 x $10^{-4}$ M 2,6-Xylenol at pH 5.8 in a 0.01 M $NaN_3$ aqueous solution; the solution was $N_2O$-saturated.

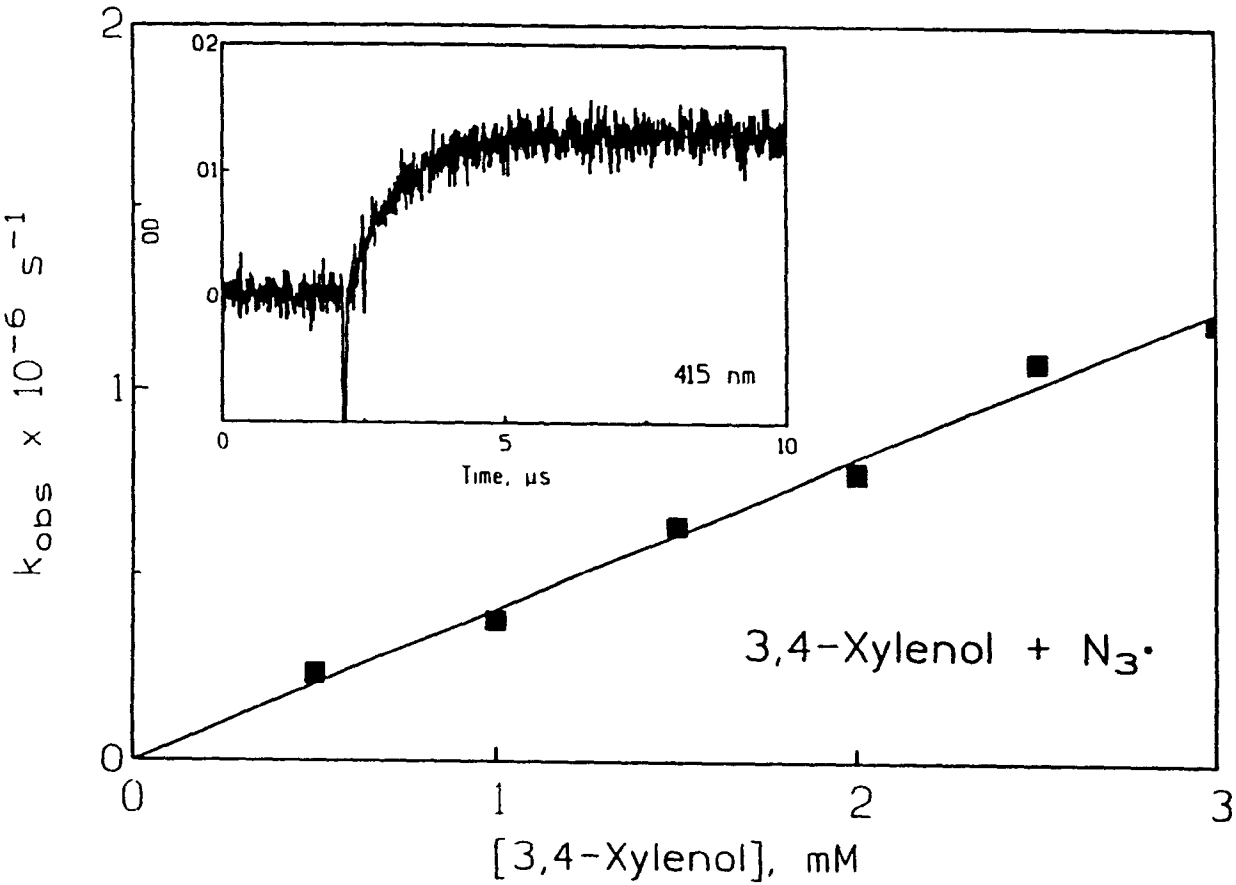


**Figure B2** Plot of [3,4-Xylenol] *versus* $k_{obs}$ as measured at 415 nm for the $N_3$• oxidation of 3,4-Xylenol at constant dose ([OH•]= 1.68 x $10^{-6}$ M); Inset shows the increase in optical density at 415 nm upon irradiation of 3 x $10^{-4}$ M 3,4-Xylenol at pH 5.8 in a 0.01 M $NaN_3$ aqueous solution; the solution was $N_2O$-saturated.

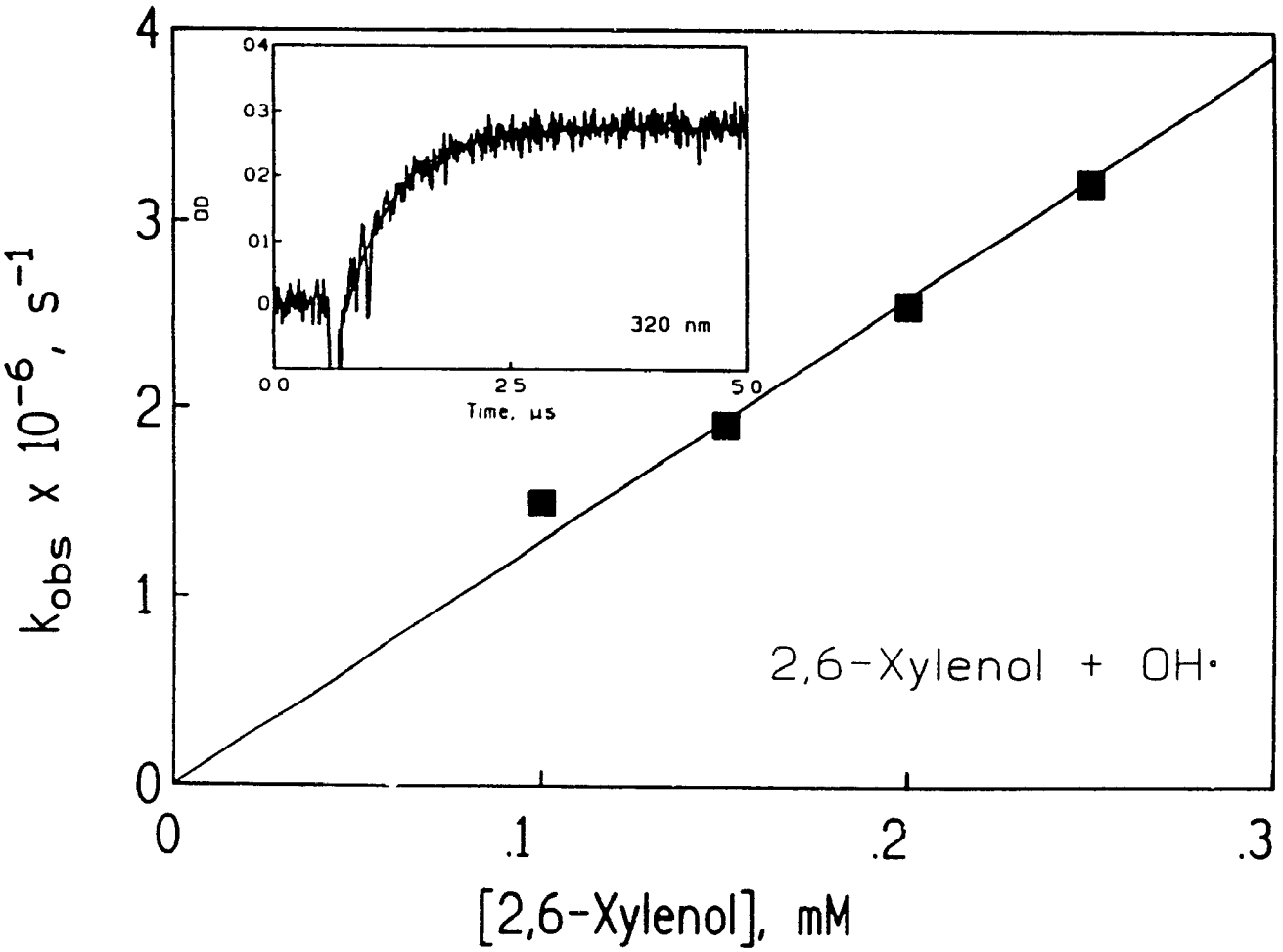


**Figure B3** Plot of [2,6-Xylenol] *versus* $k_{obs}$ as measured at 320 nm for the OH• oxidation of 2,6-Xylenol at constant dose ([OH•]= 4.22 x $10^{-6}$ M); Inset shows the increase in optical density at 320 nm upon irradiation of a 1.5 x $10^{-4}$ M aqueous solution of 2,6-Xylenol buffered at pH 4. The solution was $N_2O$-saturated.

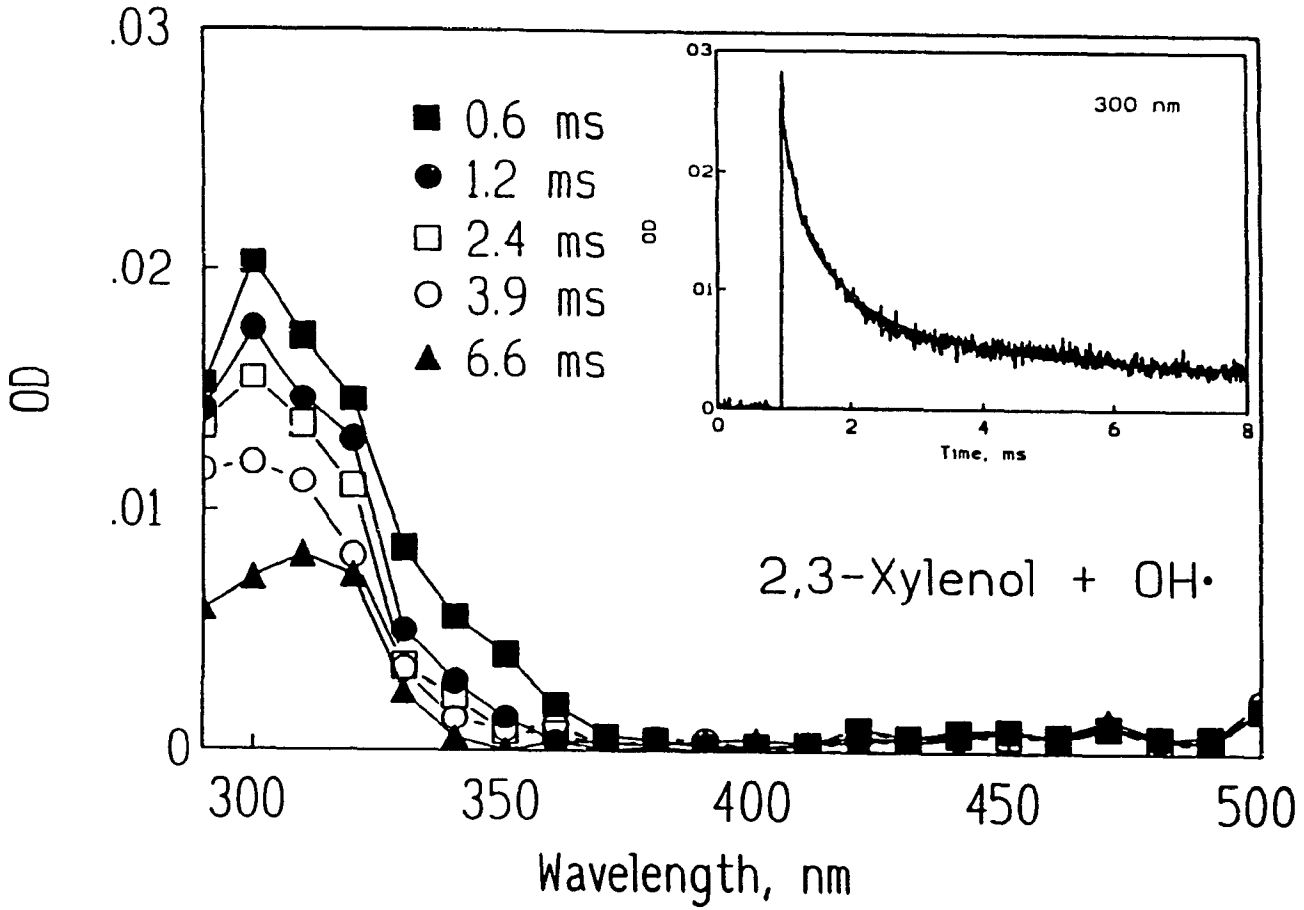


**Figure B4** Transient absorption spectra of the reaction product between 2,3-Xylenol and OH• monitored at 0.6, 1.2, 2.4, 3.9 and 6.6 ms following irradiation of a 2.5 x $10^{-4}$ M aqueous 2,3-Xylenol solution buffered at pH 4. The solution was $N_2O$-saturated; [•OH]= 4.87 x $10^{-6}$ M. The inset shows the decay of the optical density at 300 nm.

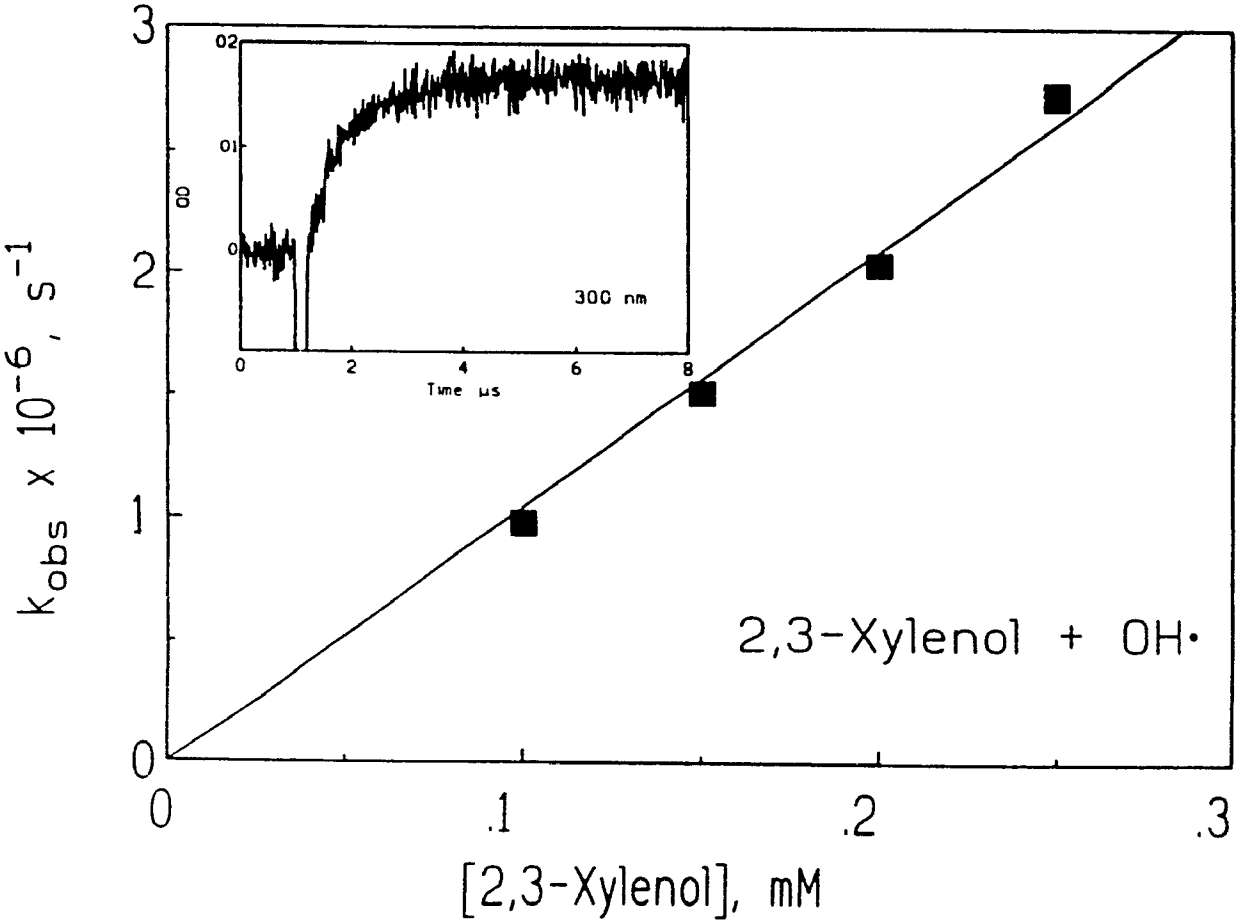


**Figure B5** Plot of [2,3-Xylenol] *versus* $k_{obs}$ as measured at 300 nm for the OH• oxidation of 2,3-Xylenol at constant dose ([OH•]= 2.5 x $10^{-6}$ M); Inset shows the increase in optical density at 300 nm upon irradiation of a 1.5 x $10^{-4}$ M aqueous solution of 2,3-Xylenol buffered at pH 4. The solution was $N_2O$-saturated.

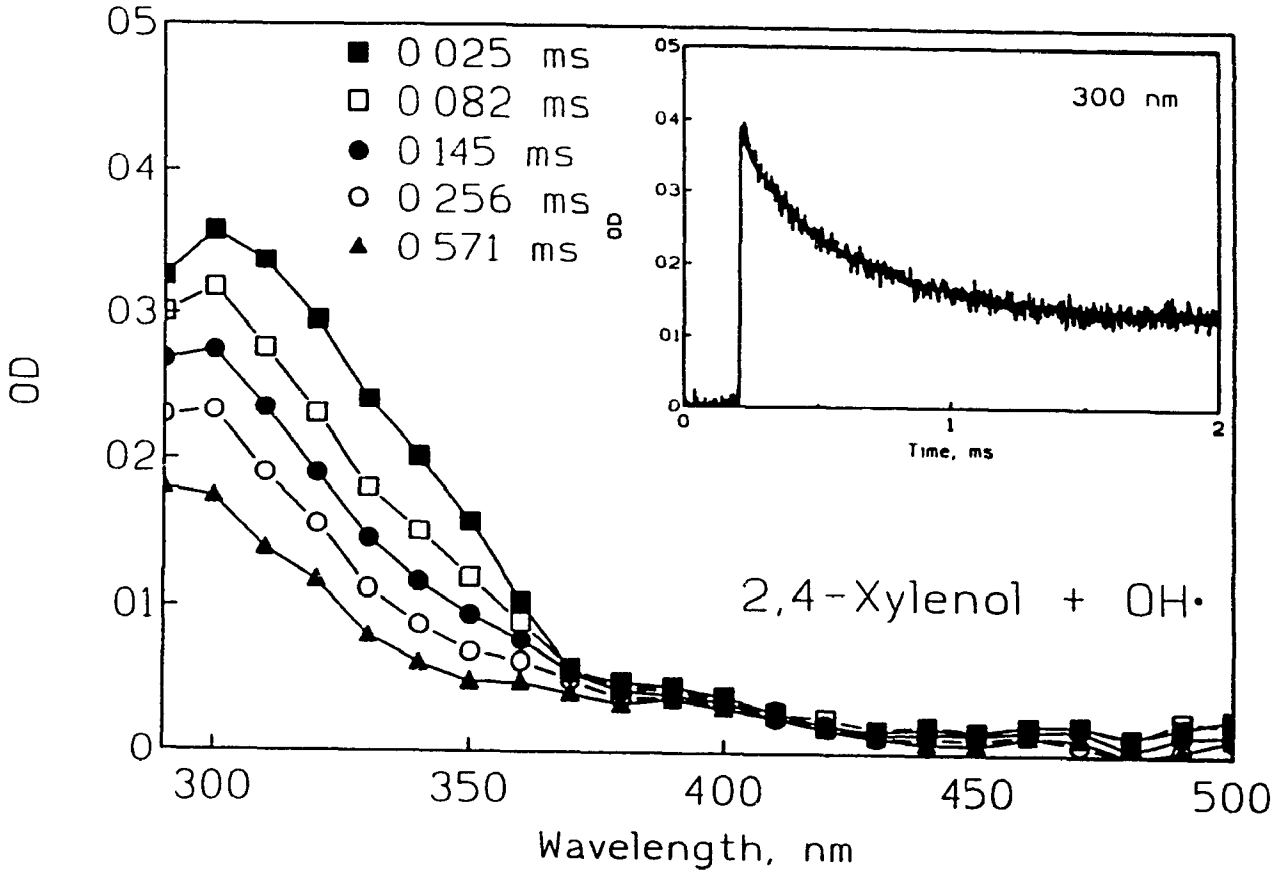


**Figure B6** Transient absorption spectra of the reaction product between 2,4-Xylenol and OH• monitored at 0.025, 0.082, 0.145, 0.256 and 0.571 ms following irradiation of a 2.5 x $10^{-4}$ M aqueous 2,4-Xylenol solution buffered at pH 4. The solution was $N_2O$-saturated; [•OH]= 5.16 x $10^{-6}$ M. The inset shows the decay of the optical density at 300 nm.

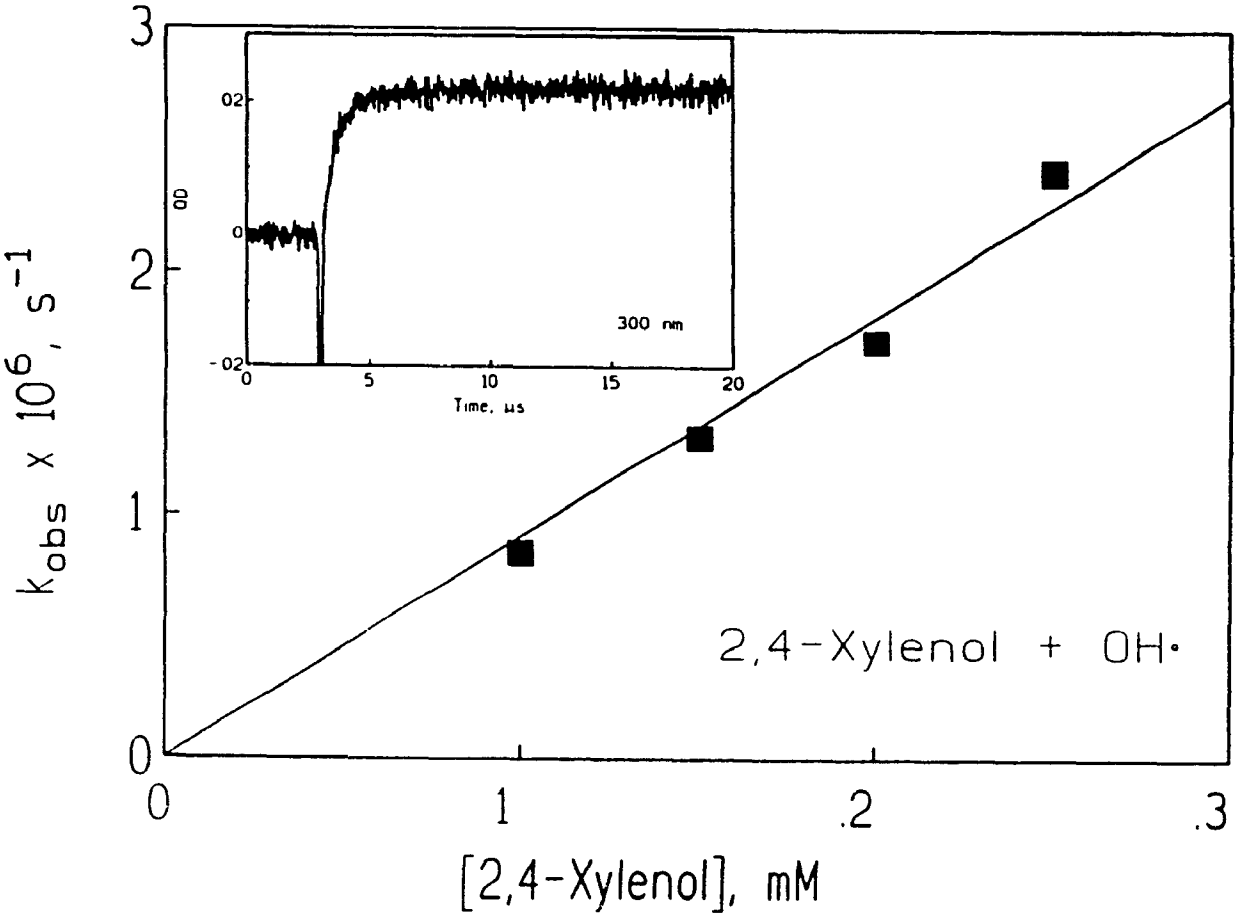


**Figure B7** Plot of [2,4-Xylenol] *versus* $k_{obs}$ as measured at 300 nm for the OH• oxidation of 2,4-Xylenol at constant dose ([OH•]= 2.69 x $10^{-6}$ M); Inset shows the increase in optical density at 300 nm upon irradiation of a 2 x $10^{-4}$ M aqueous solution of 2,4-Xylenol buffered at pH 4. The solution was $N_2O$-saturated.

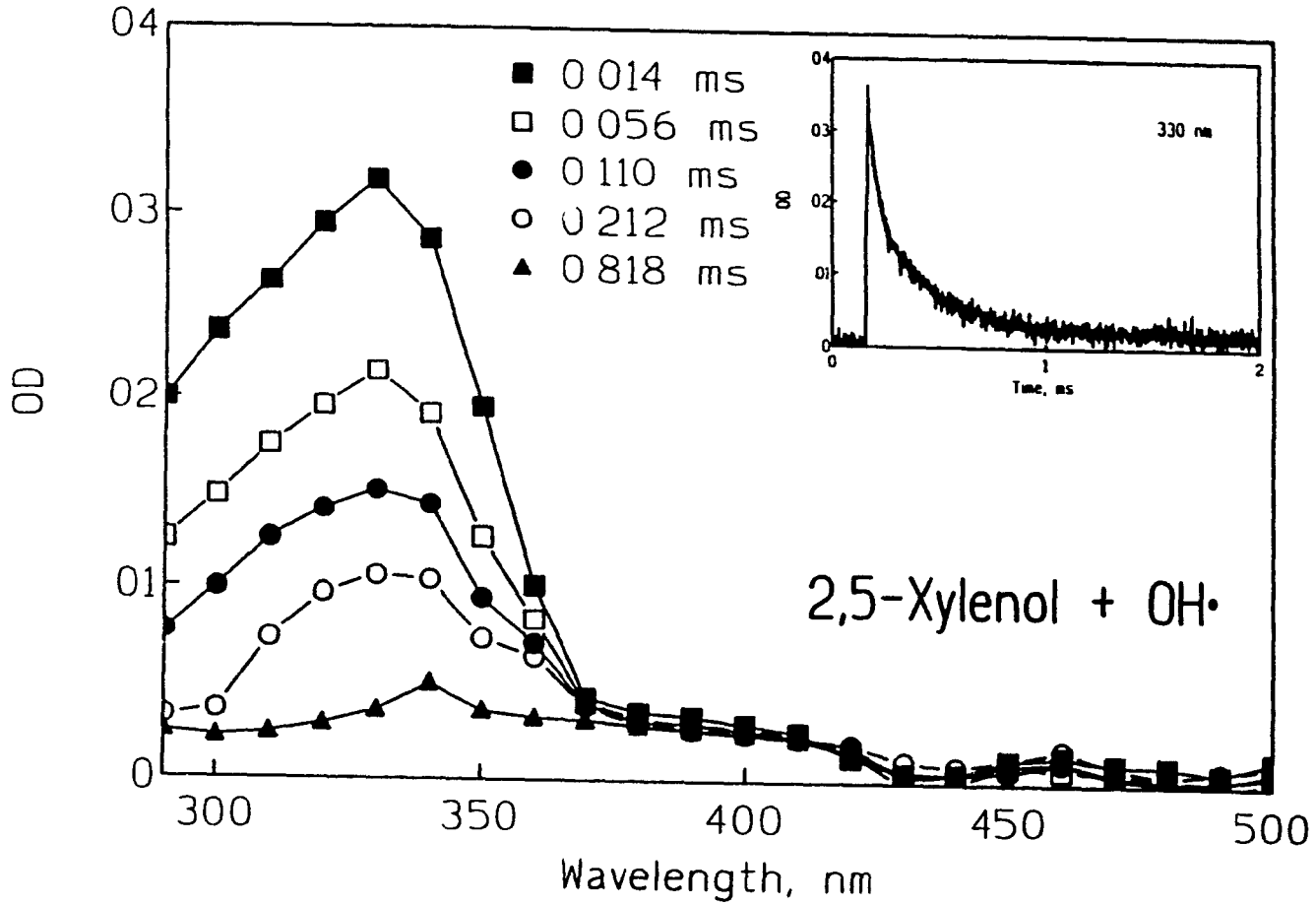


**Figure B8** Transient absorption spectra of the reaction product between 2,5-Xylenol and OH• monitored at 0.014, 0.056, 0.11, 0.212 and 0.818 ms following irradiation of a 3 x $10^{-4}$ M aqueous 2,5-Xylenol solution buffered at pH 4. The solution was $N_2O$-saturated; [•OH]= 5.45 x $10^{-6}$ M. The inset shows the decay of the optical density at 330 nm.

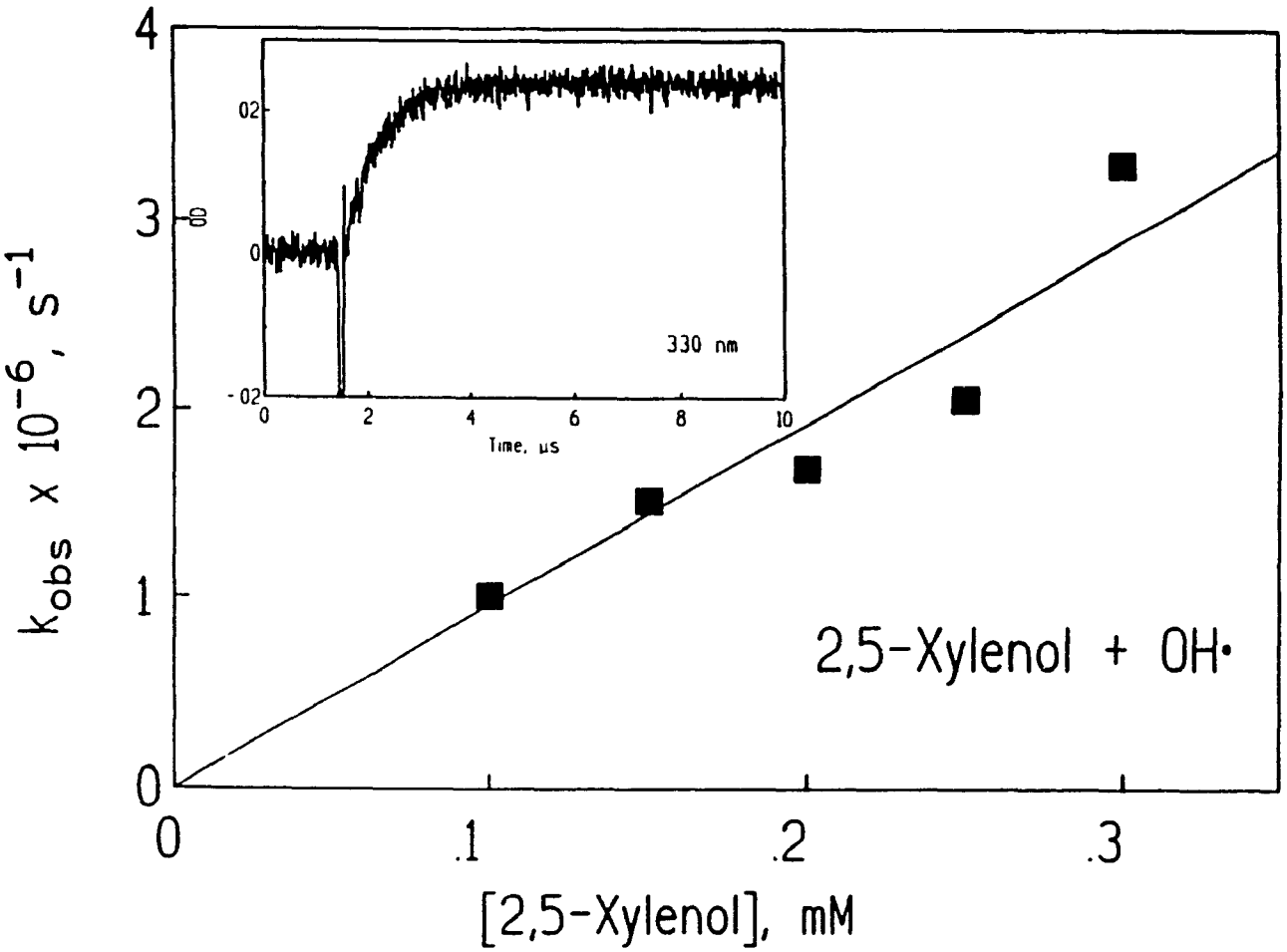


**Figure B9** Plot of [2,5-Xylenol] *versus* $k_{obs}$ as measured at 330 nm for the OH• oxidation of 2,5-Xylenol at constant dose ([OH•]= 3 x $10^{-6}$ M); Inset shows the increase in optical density at 330 nm upon irradiation of a 1.5 x $10^{-4}$ M aqueous solution of 2,4-Xylenol buffered at pH 4. The solution was $N_2O$-saturated.

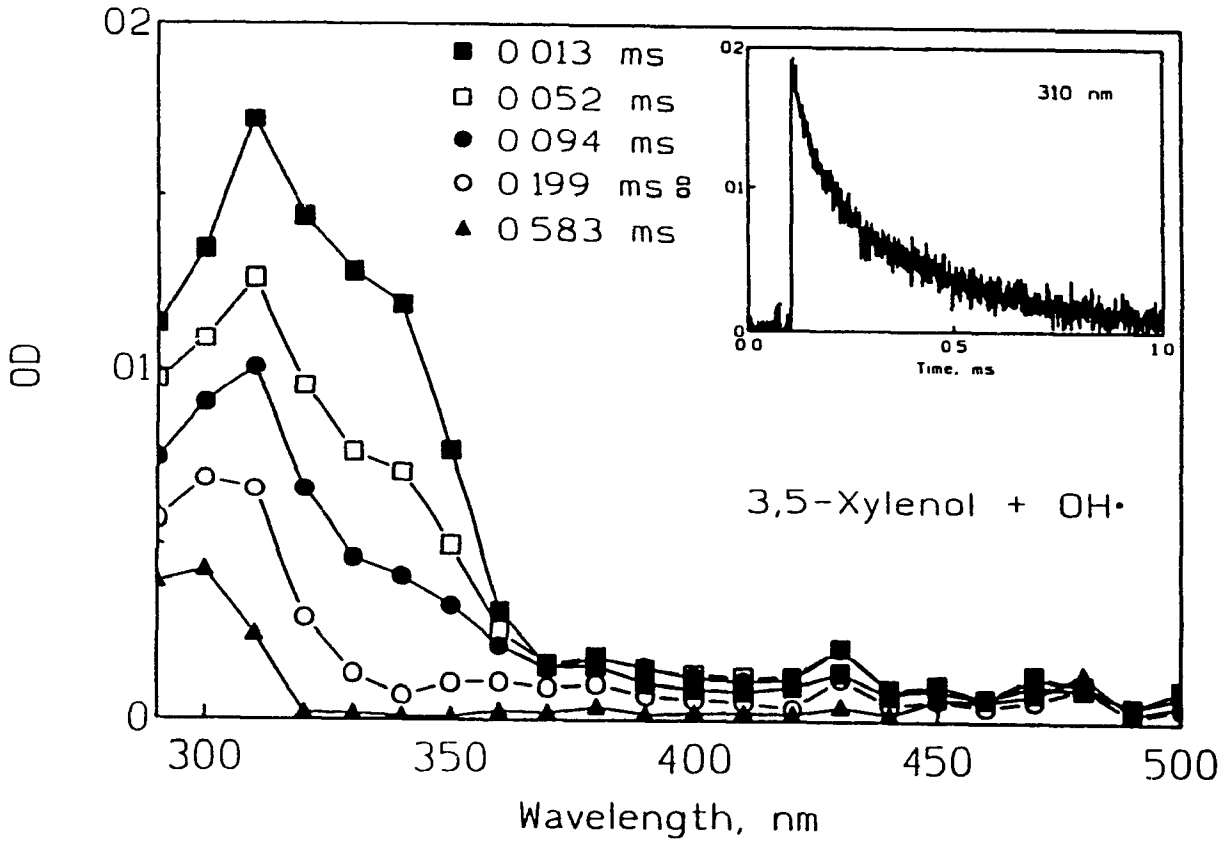


**Figure B10** Transient absorption spectra of the reaction product between 3,5-Xylenol and OH• monitored at 0.013, 0.052, 0.094, 0.119 and 0.583 ms following irradiation of a 3 x $10^{-4}$ M aqueous 3,5-Xylenol solution buffered at pH 4. The solution was $N_2O$-saturated; [•OH]= 2.93 x $10^{-6}$ M. The inset shows the decay of the optical density at 310 nm.

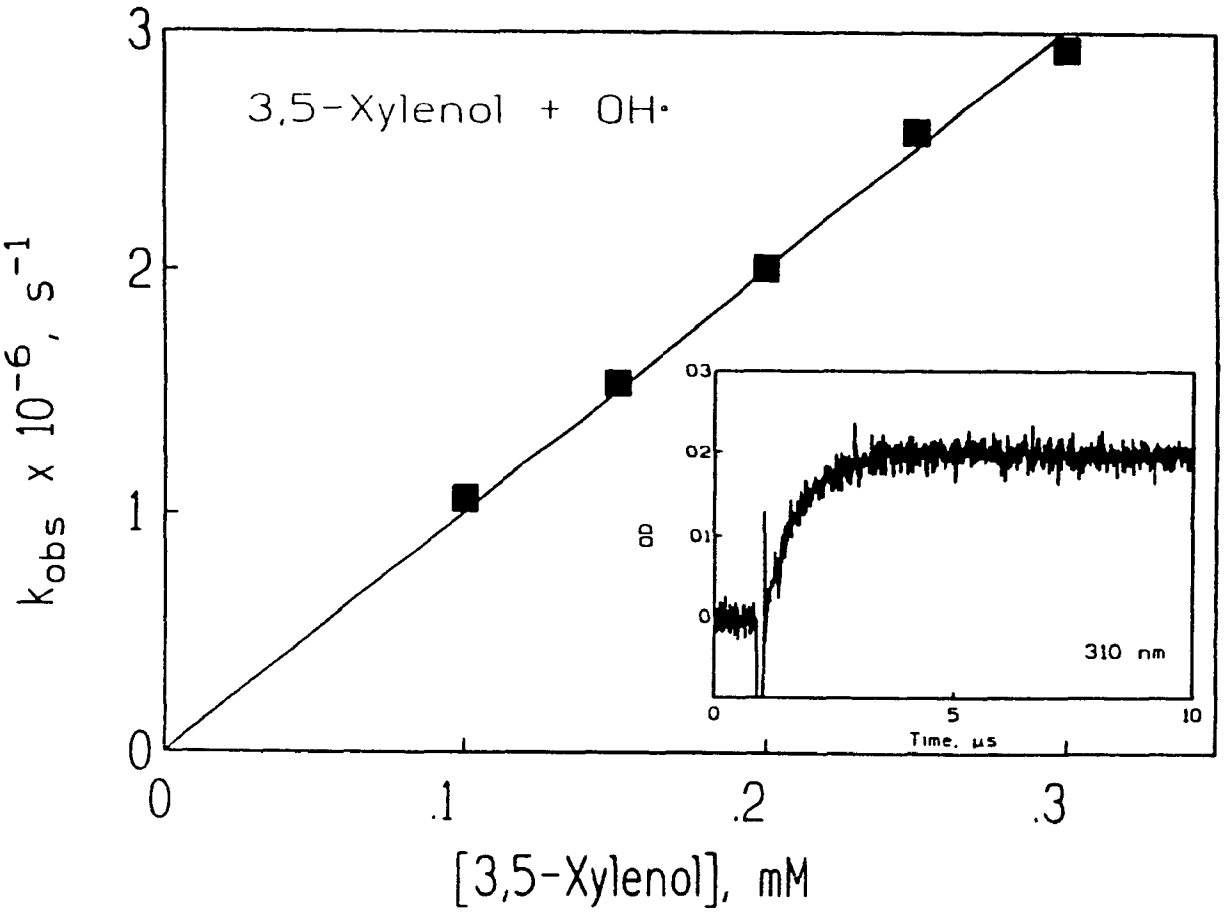


**Figure B11** Plot of [3,5-Xylenol] *versus* $k_{obs}$ as measured at 310 nm for the OH• oxidation of 3,5-Xylenol at constant dose ([OH•] = 2.8 x $10^{-6}$ M); Inset shows the increase in optical density at 310 nm upon irradiation of a 1.5 x $10^{-4}$ M aqueous solution of 3,5-Xylenol buffered at pH 4. The solution was $N_2O$-saturated.

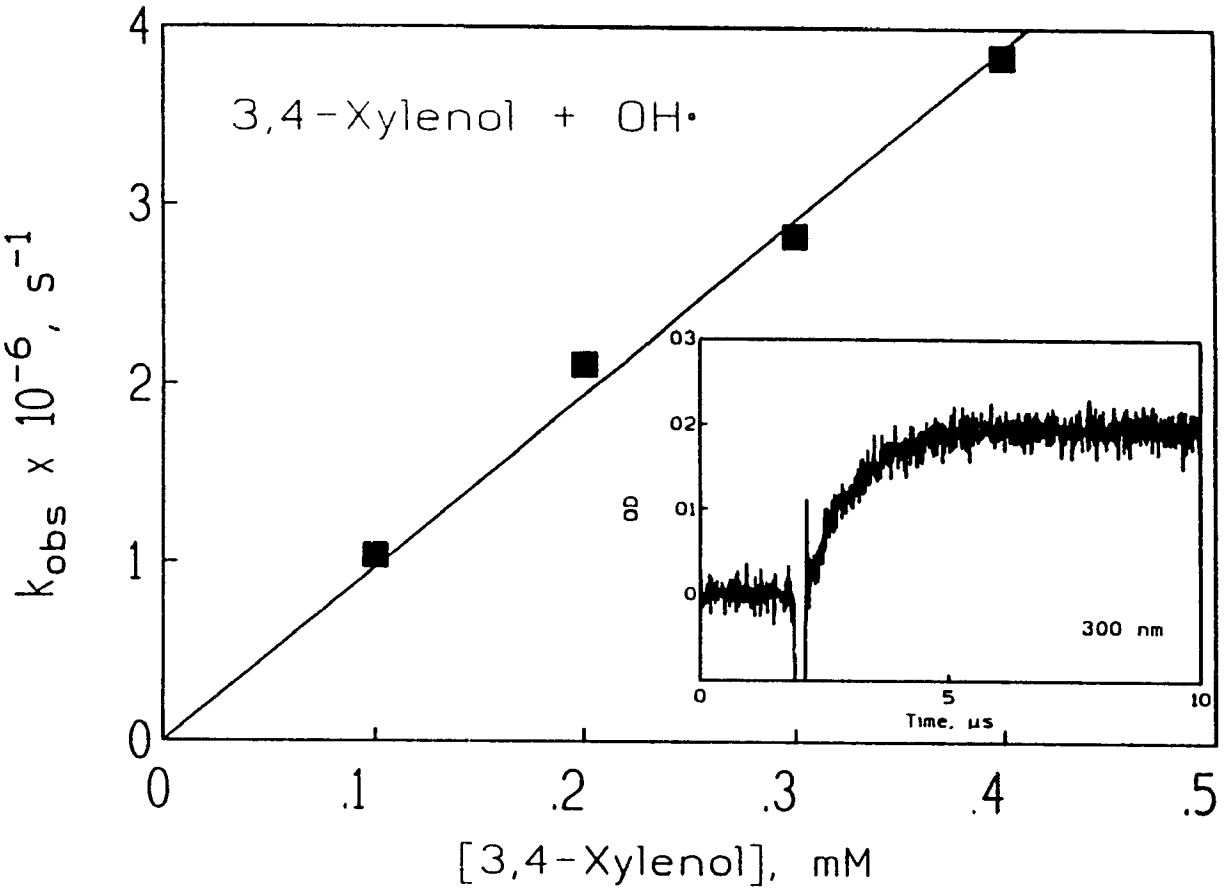


**Figure B12** Plot of [3,4-Xylenol] *versus* $k_{obs}$ as measured at 300 nm for the OH• oxidation of 3,4-Xylenol at constant dose ([OH•]= 2.72 x $10^{-6}$ M); Inset shows the increase in optical density at 300 nm upon irradiation of a 1 x $10^{-4}$ M aqueous solution of 3,4-Xylenol buffered at pH 4. The solution was $N_2O$-saturated.

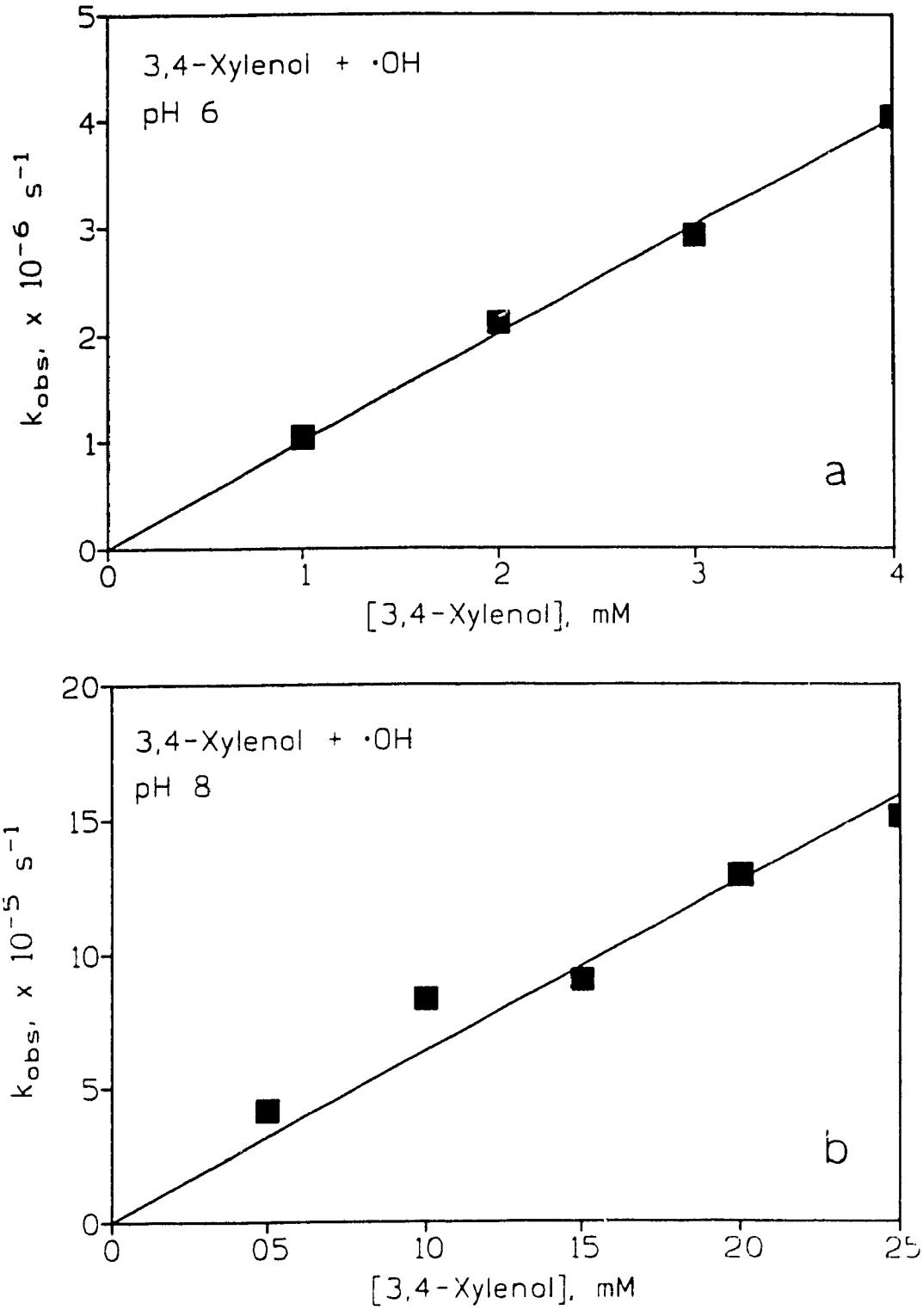


**Figure B13** a) Plot of [3,4-Xylenol] *versus* $k_{obs}$ as measured at 300 nm for the OH• oxidation of 3,4-Xylenol at constant dose ([•OH]= 1.83 x $10^{-6}$ M) at pH 6; b) Plot of [3,4-Xylenol] vs $k_{obs}$ as measured at 300 nm for the •OH oxidation of 3,4-Xylenol at constant dose ([•OH]= 1.62 x $10^{-6}$ M) at pH 8.

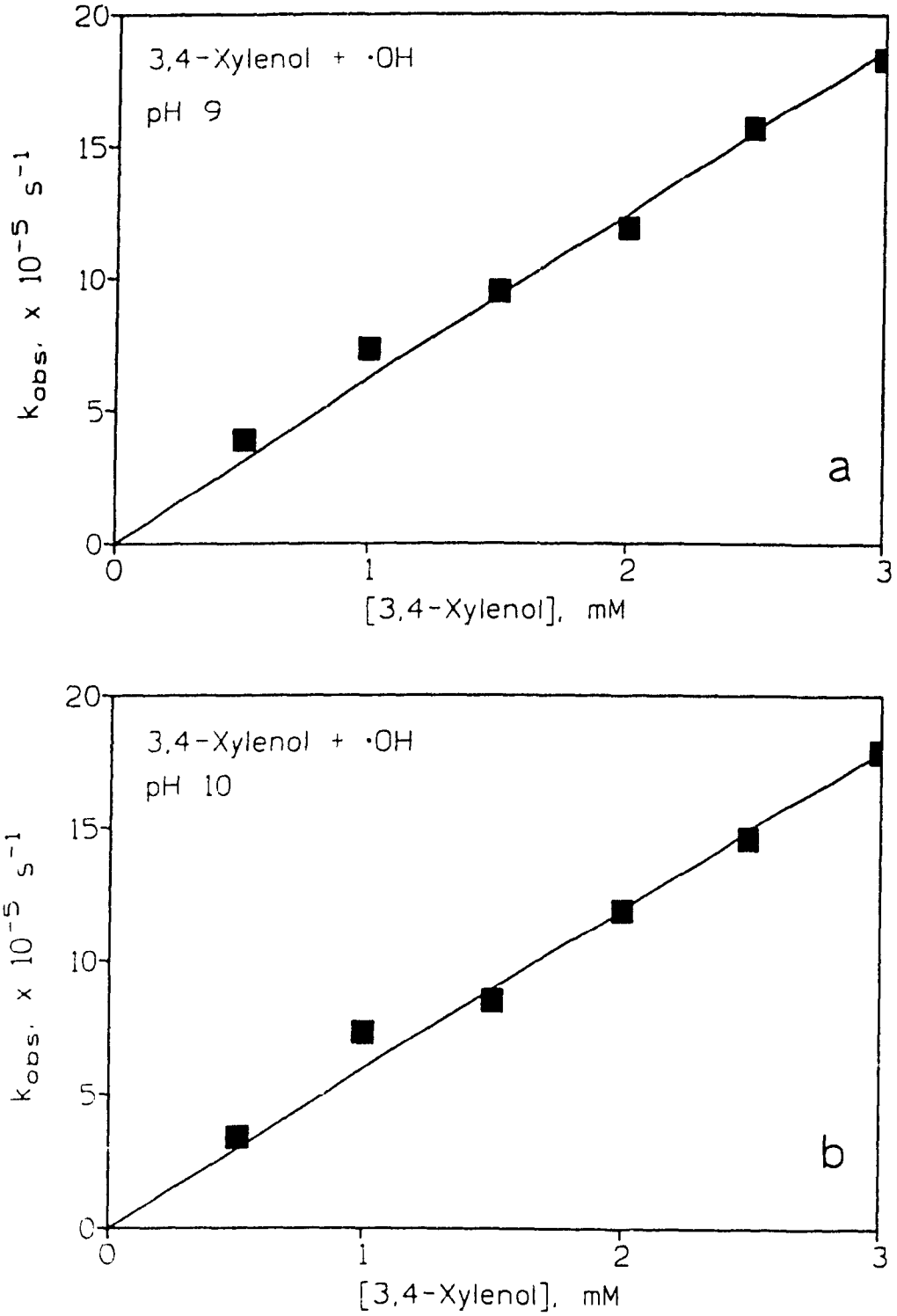


**Figure B14** a) Plot of [3,4-Xylenol] *versus* $k_{obs}$ as measured at 300 nm for the OH• oxidation of 3,4-Xylenol at constant dose ([OH•]= 1.90 x $10^{-6}$ M) at pH 9; b) Plot of [3,4-Xylenol] vs $k_{obs}$ as measured at 300 nm for the OH• oxidation of 3,4-Xylenol at constant dose ([OH•]= 1.42 x $10^{-6}$ M) at pH 10.

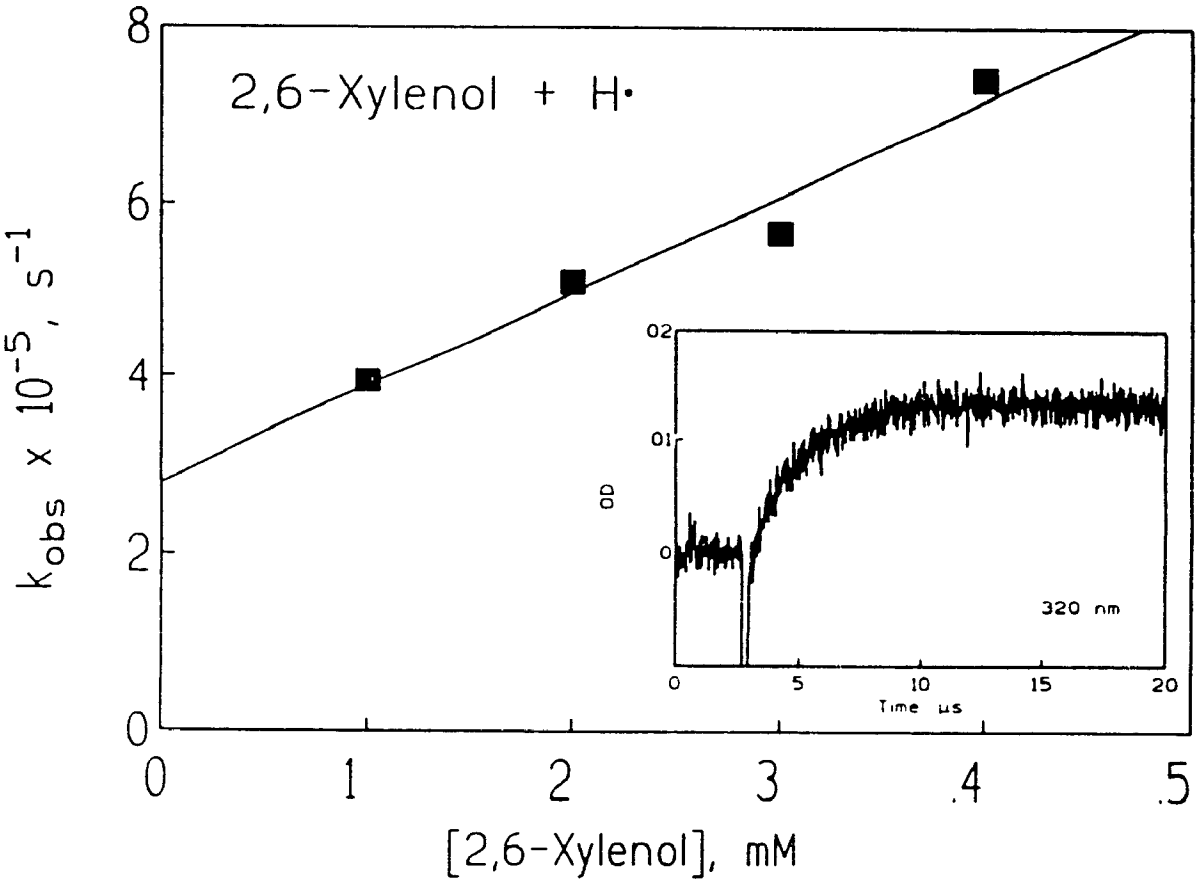


**Figure B15** Plot of [2,6-Xylenol] *versus* $k_{obs}$ as measured at 320 nm for the reaction of 2,6-Xylenol with H• at constant dose ([H•] = 2.19 x $10^{-6}$ M); Inset shows the increase in optical density at 320 nm upon irradiation of 2 x $10^{-4}$ M 2,6-Xylenol at pH 1 (buffered) in a 0.2 M *tert*-butyl alcohol aqueous solution; the solution was $N_2$-saturated.